THE UNIVERSITY *of* EDINBURGH

The effects of diesel exhaust particles on the kidney and renal vasculature

Souzana Angel

A thesis submitted for the degree

Doctor of Philosophy

The University of Edinburgh

2024

Contents

Declaration

I declare that this thesis has been composed solely by myself and that it has not been submitted, in whole or in part, in any previous application for a degree. Except where states otherwise by reference or acknowledgement, the work presented is entirely my own.

Parts of this work have been published in the Analytical and Bioanalytical Chemistry journal.

Souzana Angel

Acknowledgements

First, I would like to express my deepest gratitude to my primary supervisor, Dr Mark Miller, for his unwavering support and guidance throughout the most challenging moments of my PhD. Your willingness to have Zoom calls after working hours to discuss my thesis, along with the time and effort you dedicated to providing feedback and advice, have been invaluable. I am also deeply appreciative of your help in securing additional funding and the extension that allowed me to complete the thesis write-up. Thank you to my co-supervisors Dr Neeraj Dhaun (Bean) and Dr Alicja Czopek for their advice on experimental design. The financial support from the British Heart Foundation, the College of Medicine and Veterinary Medicine, REA3 and Prof Robert Semple made this PhD project possible and I am truly appreciative of their contribution.

I extend my gratitude to Dr Rob Hunter (The University of Edinburgh) and Prof Holly Shiels (The University of Manchester) for examining this work and for being understanding throughout the process, making the viva a truly enjoyable and constructive experience.

The critical contributions of Dr Lorna Eades and Dr Gavin Sim in performing the ICP-MS gold measurements and Dr Petra Krystek's advice and shared expertise in ICP-MS are greatly appreciated. I am also thankful to Prof Rodger Duffin for teaching me how to collect and process BALF samples, Dr Emanuel Jeldes for conducting the cell differentials for the chronic exposure study and Dr Kirsten Wilson for performing the urine creatinine measurements. The support of the LF2 staff has

been crucial, especially Chris Ratcliffe, for diligently managing morning checks for my mice, particularly during the intense angiotensin II study. A special mention goes to Will Mungall for his exceptional training, patience and bringing positivity to long and stressful days in the animal unit. I am thankful to the BDD group, but particularly Lorraine Bruce for always being there to help, Joss for all his advice and guidance on the angiotensin II study and Rachel for her encouraging pre-viva conversations that helped calm my nerves.

Finally, and most importantly, I want to express my deepest gratitude to my family and friends. I dedicate this work to my beautiful mama, Vanya, who passed away during my PhD. Thank you for instilling in me the importance of education, hard work, perseverance, integrity and humility. Your unwavering support and countless sacrifices have given me the opportunities I have today. I know you are watching over me, proud of this achievement, with a smile on your face. I love and miss you tremendously and think of you every single day!

I am forever grateful to my dad, Sammy, for his endless love and support, which have been my anchor throughout this experience. Your wisdom, advice and guidance during difficult and stressful times have shown me the high road and kept me moving forward-I love you so so much!

To my fiancé, Anton, I am beyond grateful for the unwavering support, patience and encouragement you have shown me throughout this long and challenging journey. You moved countries and cities, changed jobs and made countless sacrifices so we could be together while I pursued my education and career. I appreciate all the time you spent driving me to and from the lab, especially on weekends and late evenings, the delicious meals you made when I was so busy I would forget to eat and the way you always believed in me, even when I doubted myself. I love you and will always be grateful to you!

A special thanks goes to my best friend, Dina, who, despite the distance over the

last 11 years, has been my biggest cheerleader. Your encouragement, belief in me and willingness to jump on a call any time of day and listen when things were tough (which was often!) have been a constant source of strength. I am so lucky to know you and call you my friend.

Abstract

Exposure to ambient air pollution is associated with increased morbidity and mortality, contributing to an estimated 7–9 million premature deaths annually worldwide. While its effects on the respiratory system are well documented, epidemiological studies have also linked air pollution to diseases in extra-pulmonary organs, including the kidneys. Air pollution comprises a complex mix of gases, liquids and particulate matter (PM), with ultrafine particles (≤0.1 µm) posing significant risks due to their large surface area-to-mass ratio, capacity to carry surface chemicals and ability to reach remote organs. Diesel exhaust particles (DEP) are a major source of ultrafine PM in urban settings. I hypothesise that nanoparticles in diesel exhaust can reach and sequester in the kidney, compromising renal function through inflammation, oxidative stress and promoting renal vascular dysfunction.

Particles can exert extra-pulmonary effects by entering the bloodstream and sequestering in distant organs. To investigate this pathway in the kidneys, mice were administered gold nanoparticles of various sizes (2, 3–4, 7–8, 14 and 40 nm) via pulmonary instillation/inhalation twice weekly for four weeks. Gold nanoparticles were chosen as they can be synthesised in broadly the same size as particles in diesel exhaust, gold is largely inert and there are a number of sensitive techniques to detect it. Using inductively coupled plasma mass spectrometry, gold was detected in the blood, urine and kidney in a size-dependent manner, with a statistical significance cutoff of <7 nm.

The renal effects of acute exposure to DEP were investigated. Mice instilled with

a single dose of reference material DEP (SRM 2975, NIST) exhibited pulmonary inflammation, evidenced by an increased total cell count (TCC) in the bronchoalveolar lavage fluid (BALF), primarily due to neutrophil infiltration. However, systemic inflammation was minimal, with only slight elevation in a few markers. DEP exposure did not upregulate kidney injury molecule-1 (*KIM-1*; early marker of kidney injury) or tumour necrosis factor alpha (*TNF-α*) expression in renal tissue. These results suggest that the dose and/or length of exposure may have been insufficient to induce renal effects.

To further investigate, mice were exposed to DEP for four consecutive weeks (twice weekly), which resulted in pulmonary inflammation, evidenced by elevated BALF TCC, but had no impact on markers of systemic inflammation. Prolonged exposure did not affect kidney function, as indicated by unchanged mRNA expression of injury and inflammation markers in renal tissue, no changes in urinary excretion of KIM-1 and unaltered kidney morphology in histological assessments. The effect of DEP on renal vascular function was assessed *in vitro* using wire myography. Renal artery sections from healthy mice were exposed to DEP, either alone or with superoxide dismutase (SOD), in the myograph bath. DEP did not change the vascular reactivity to the adrenergic-dependent vasoconstrictor phenylephrine (PE) but caused a rightward shift in the dose-response curve of the endothelial-dependent vasodilator acetylcholine (ACh). A significant increase in the endothelial-independent vasodilator sodium nitroprusside (SNP) EC_{50} was noted following DEP addition, which was not reversed by the addition of SOD. To assess *ex vivo* effects, vascular reactivity of renal artery rings from mice chronically exposed to DEP was tested. While no overall changes were observed between the DEP and control groups, the ACh EC_{50} in the DEP group was significantly lower with a leftward shift in dose-response curve, indicating potential DEP-induced vascular hypersensitivity.

Given the limited effects of DEP in healthy mice, a mouse model of hypertension-induced kidney injury was utilised. Mice were fed a high-salt diet (3% Na^+) and implanted with osmotic minipumps delivering exogenous angiotensin II

(500 ng/kg/min), while receiving DEP twice weekly. The study was terminated after two weeks due to mice suffering spontaneous aortic ruptures. DEP exposure did not induce systemic inflammation or alter renal mRNA expression of genes associated with kidney injury, inflammation or fibrosis. However, there was a trend towards increased renal transcript levels of the angiotensin receptor and oxidative stress-related genes (*SOD3* and endothelial nitric oxide synthase-*eNOS*) in mice exposed to the combination of angiotensin II, a high-salt diet and DEP.

In summary, despite nanoparticles having the ability to reach the kidney and to induce pulmonary inflammation, limited effects of DEP were seen in healthy mice. In a model of kidney injury DEP showed indications of oxidative stress and inflammation. Future studies should consider longer exposure periods of DEP, different sources of air pollution and other models of susceptibility to kidney injury. These results underscore the potential for air pollution to exacerbate underlying health conditions, emphasising the importance of stringent air quality regulations and targeted public health interventions.

Covid-19 impact statement

Since all research presented in this thesis was conducted in a laboratory, it was significantly impacted by the Covid-19 pandemic. Five months into my PhD, the first lockdown began and I lost access to the lab for the next six months. Even after regaining access, strict regulations within our institute caused further delays over the next year. Limited lab occupancy restricted access to equipment, while social distancing rules made training on new procedures and animal work with chronic exposure protocols (which were the priority at this point), very challenging. Delays in consumable deliveries and coordinating multi-departmental work further hindered progress. As a result, some of the experiments and assays originally planned could not be performed in the available time. This thesis was written after the end of the funding period around full time employment.

Lay abstract

Air pollution is a major health concern, causing an estimated 7–9 million early deaths each year globally. While its harmful effects on the lungs are well-known, recent studies have also linked exposure to air pollution to diseases in other organs, including the kidneys. Air pollution is made up of a mix of gases, liquids and tiny particles. Among these, ultrafine particles (nanoparticles ≤0.0001 millimetre) are especially dangerous because they can carry harmful chemicals on their surface and once inhaled can reach various organs in the body. In cities, diesel exhaust is a major source of these ultrafine particles. I hypothesise that particles from diesel exhaust can travel to the kidneys and cause damage by triggering inflammation and cellular stress.

To test this, I used gold nanoparticles of various sizes that are similar in size to diesel exhaust particles and the mouse as a model. Gold is safe to use in experiments and reliable methods exist to detect it in the body. I exposed mice to these gold nanoparticles through their lungs twice weekly for four weeks. At the end of the experiment, a sensitive technique was used to measure the concentration of gold in the blood, urine and kidneys of the mice. Gold, especially smaller particles, was found in all tissues, showing that inhaled nanoparticles can reach and accumulate in the kidney.

Next, I studied the effects of short-term exposure to diesel exhaust particles (DEP) on the kidneys. Mice exposed to a single dose of DEP showed inflammation in the lungs, but no significant inflammation throughout the body. There was no increase in markers of kidney injury or inflammation in the kidney tissue. This suggests that a

single exposure might not be sufficient to cause substantial kidney damage.

Next, I investigated the effects of long-term exposure to DEP on function of the kidney and the artery delivering blood to the kidney. Mice were exposed to DEP twice weekly for four consecutive weeks. This prolonged exposure caused lung inflammation but no inflammation throughout the body and did not affect kidney function at the molecular or structural level. I also tested whether DEP could affect the ability of the arteries leading to the kidney ("renal arteries") to contract and relax, which would control the delivery of blood to the kidney. I isolated kidney arteries from healthy mice and directly exposed the vessels to DEP. Results showed that when DEP was present vessels were less able to relax. I then tested how vessels from mice chronically exposed to DEP to the lungs would react. Although there were no major effects of DEP, some arteries became more sensitive in some conditions, suggesting there was a counter response to DEP when it was administered to the lungs.

Given the limited effects of DEP in healthy mice, I used a mouse model of kidney injury caused by high blood pressure. These mice were fed a high-salt diet and received a hormone called angiotensin II through small pumps, while also being exposed to DEP twice weekly. Despite these conditions, DEP exposure did not cause widespread inflammation or changes in kidney genes related to injury, inflammation or scarring. However, there was a tendency for increased levels of genes related to cellular stress in the kidneys of mice exposed to the combination of a high-salt diet, angiotensin II and DEP.

In summary, while nanoparticles from diesel exhaust can reach the kidneys and cause lung inflammation, they did not cause kidney damage in healthy mice. However, there were signs that DEP may cause cellular stress in mice with pre-existing kidney damage. Future studies should explore longer exposure to DEP, different types of air pollution and other models of kidney disease. This study highlights the potential for air pollution to worsen underlying health conditions and underscores the need for strict air quality regulations to protect public health.

Abbreviations

AAA	Abdominal aortic aneurysm
AAP	Ambient air pollution
ACE	Angiotensin-converting enzyme
ACh	Acetylcholine
AD	Adenine
ADH	Antidiuretic hormone
AKI	Acute kidney injury
ANOVA	Analysis of variance
Ang II	Angiotensin II
APC	Allophycocyanin
ARB	Angiotensin receptor blocker
ATN	Acute tubular necrosis
$AT1_AR$	Angiotensin-II receptor type 1A
AT1R	Angiotensin-II receptor type 1
AQP2	Aquaporin-2
Au	Gold
BALF	Bronchoalveolar lavage fluid
BAPN	β-aminopropionitrile
BP	Blood pressure
BSA	Bovine serum albumin
BUN	Blood urea nitrogen

CCL17 (TARC)	Chemokine (C-C) ligand 17 (thymus and activation-regulated chemokine)
CCL22 (MDC)	Chemokine (C-C) ligand 22 (macrophage-derived chemokine)
CD	Cell differentials
CD	Collecting duct
cDNA	Complementary deoxyribonucleic acid
CDNP	Combustion derived nanoparticles
CH_4	Methane
CKD	Chronic kidney disease
CNS	Central nervous system
CO	Carbon monoxide
CO_2	Carbon dioxide
COPD	Chronic obstructive pulmonary disease
CP	Cysplatin
Ct	Cycle threshold
CVD	Cardiovascular disease
CXCL1 (KC)	CXC motif chemokine ligand 1 (keratinocyte chemoattractant)
Cys-C	Cystatin C
D1R	Dopamine 1 receptor
D_{ae}	Aerodynamic diameter
DBP	Diastolic blood pressure
DCT	Distal convoluted tubule
DEP(s)	Diesel exhaust particles
ECM	Extracellular matrix
ENaC	Epithelial sodium channel
eGFR	Estimated glomerular filtration rate
eNOS	Endothelial nitric oxide synthase
ELISA	Enzyme linked immunosorbent assay
EPR	Electron paramagnetic resonance

ESRD	End stage renal disease
GAPDH	Glyceraldehyde 3-phosphate dehydrogenase
G-CSF	Granulocyte colony-stimulating factor
GM-CSF	Granulocyte-macrophage colony-stimulating factor
GRK4	G protein coupled receptor kinase 4
GSH	Glutathione
H_2O_2	Hydrogen peroxide
H&E	Haematoxylin and eosin
HCl	Hydrochloric acid
HNO_3	Nitric acid
HRV	Heart rate variability
ICP-MS	Inductively coupled plasma mass spectrometry
IFN-γ	Interferon-gamma
IHC	Immunohistochemical
IL	Interleukin
IRI	Ischaemia reperfusion injury
it	Instillation
JG	Juxtaglomerular
KIM-1	Kidney injury molecule-1
KPSS	High potassium physiological salt solution
LOD	Limit of detection
MR	Minerallocorticoid receptor
mRNA	Messenger ribonucleic acid
NaCl	Sodium chloride
NADPH	Nicotinamide adenine dinucleotide phosphate hydrogen
NAG	N-acetyl-β-D-glucosaminidase
NCC	Sodium-chloride cotransporter
NCD	Non-communicable diseases
NGAL	Neutrophil gelatinase-associated lipocalin

NH_3	Ammonia
NIST	National institute of standards and technology
NO	Nitric oxide
NO_2	Nitrogen dioxide
NO_2^-	Nitrite
NO_3^-	Nitrate
NO_x	Nitrogen oxides
NPs	Nanoparticles
O_2^-	Superoxide
O_3	Ozone
OS	Oxidative stress
PAH	Polycyclic aromatic hydrocarbons
PC	Protein corona
PCT	Proximal convoluted tubule
PE	Phenylephrine
PM	Particulate matter
$PM_{2.5}$	PM with D_{ae} <2.5 µm
PM_{10}	PM with D_{ae} <10 µm
ppm	Parts per million
PSS	Physiological salt solution
PVAT	Perivascular adipose tissue
RAAS	Renin-angiotensin-aldosterone system
RBF	Renal blood flow
Rh	Rhodium
ROS	Reactive oxygen species
RT-qPCR	Quantitative reverse transcription polymerase chain reaction
SA-PE	Streptavidin-phycoerythrin
SBP	Systolic blood pressure
SNP	Sodium nitroprusside

SO_2	Sulphur dioxide
SOD	Superoxide dismutase
SRM	Standard reference material
STOs	Secondary target organs
SVOCs	Semi-volatile organic compounds
TAA	Thoracic aortic aneurysm
TAC	Total antioxidant capacity
TCC	Total cell count
TEM	Transmission electron microscopy
TGF-β	Transforming growth factor beta
TNF-α	Tumour necrosis factor alpha
TRPA1	Transient receptor potential cation channel, member A1
UFPs	Ultrafine particles
VOCs	Volatile organic compounds
WT	Wild type

List of Figures

List of Tables

Chapter 1

Introduction

1.1 Kidney disease

1.1.1 Acute kidney injury

One of the primary functions of the kidneys is the filtration and excretion of nitrogenous waste products. Elevated levels of blood urea nitrogen (BUN) and creatinine are indicative of impaired renal function, reflecting reduced clearance of these metabolites. Acute kidney injury (AKI) is defined by a sudden decline in renal function within 48 h, resulting in the accumulation of nitrogenous waste [1–3]. AKI is associated with increased morbidity and mortality, affecting approximately 13.3 million individuals and contributing to an estimated 1.7 million deaths globally [4–6]. The incidence of AKI is notably high among hospitalised patients, estimated to affect ~20% of adults and >25% of children-incidence exceeding 50% in intensive care settings [7–9].

Aetiology of AKI

The aetiologies of AKI are multifaceted and can be broadly categorised into pre-renal, renal (intrinsic) and post-renal causes, each involving distinct pathophysiological mechanisms that lead to compromised renal function (summarised in Figure 1.1) [2, 3]. Pre-renal azotemia, characterised by elevated nitrogenous waste in the blood, occurs due to reduced renal perfusion resulting in decreased glomerular filtration rate (GFR) without direct damage to the renal parenchyma. Given that the kidneys receive ~25% of cardiac output, any disruption in systemic blood volume or isolated renal circulation can significantly impact renal perfusion and function [10]. Aetiologies of pre-renal AKI include: (1) hypovolemia, which may result from haemorrhage, burns, diuresis or dehydration (secondary to vomiting, diarrhea, excessive sweating), (2) decreased cardiac output, commonly associated with congestive heart failure or other states of reduced cardiac output such as pericardial tamponade, (3) reduced vascular resistance (peripheral vasodilation), occurring in conditions, such as sepsis, anaphylaxis or as an adverse effect of vasodilatory medications, and (4) renal vasoconstriction, induced by vasoconstrictive medications, anaesthesia or conditions such as hypercalcemia [2, 11].

Post-renal AKI occurs due to acute obstruction of urinary flow, leading to increased intratubular pressure and a consequent reduction in GFR. This obstruction may also impair renal blood flow and initiate inflammatory processes that further decrease GFR. The obstruction can occur at any point in the urinary tract-from the renal tubules to the urethra. Obstructions above the urethra typically need to affect both kidneys to cause significant renal impairment, although patients with pre-existing renal insufficiency may develop AKI with obstruction of only one kidney. Clinically, post-renal AKI may manifest as anuria (complete absence of urine production), oliguria (low urine output), polyuria (excessive urine output), nocturia (excessive urination at night) or nonoliguric AKI [1, 12].

The aetiologies of intrinsic AKI encompass a range of insults affecting the four major structures of the kidney: (1) the renal tubules, (2) the glomeruli, (3) the interstitium and (4) the intra-renal blood vessels. AKI due to damage to the tubular epithelial cells of the renal tubules is termed acute tubular necrosis (ATN), which is the most prevalent form of renal AKI. The primary aetiologies of ATN are ischaemia and nephrotoxicity from various exogenous compounds. Glomerular damage leading to AKI is most commonly attributed to acute glomerulonephritis, characterised by inflammation of the glomerulus. Interstitial damage-induced AKI occurs due to interstitial nephritis, often resulting from allergic reactions to medications (commonly antibiotics) or bacterial infections. Vascular damage causing AKI arises from injury to intra-renal vessels, leading to reduced GFR. Such vascular damage can be induced by conditions like malignant hypertension, renal artery stenosis, atheroembolic disease and pre-eclampsia.

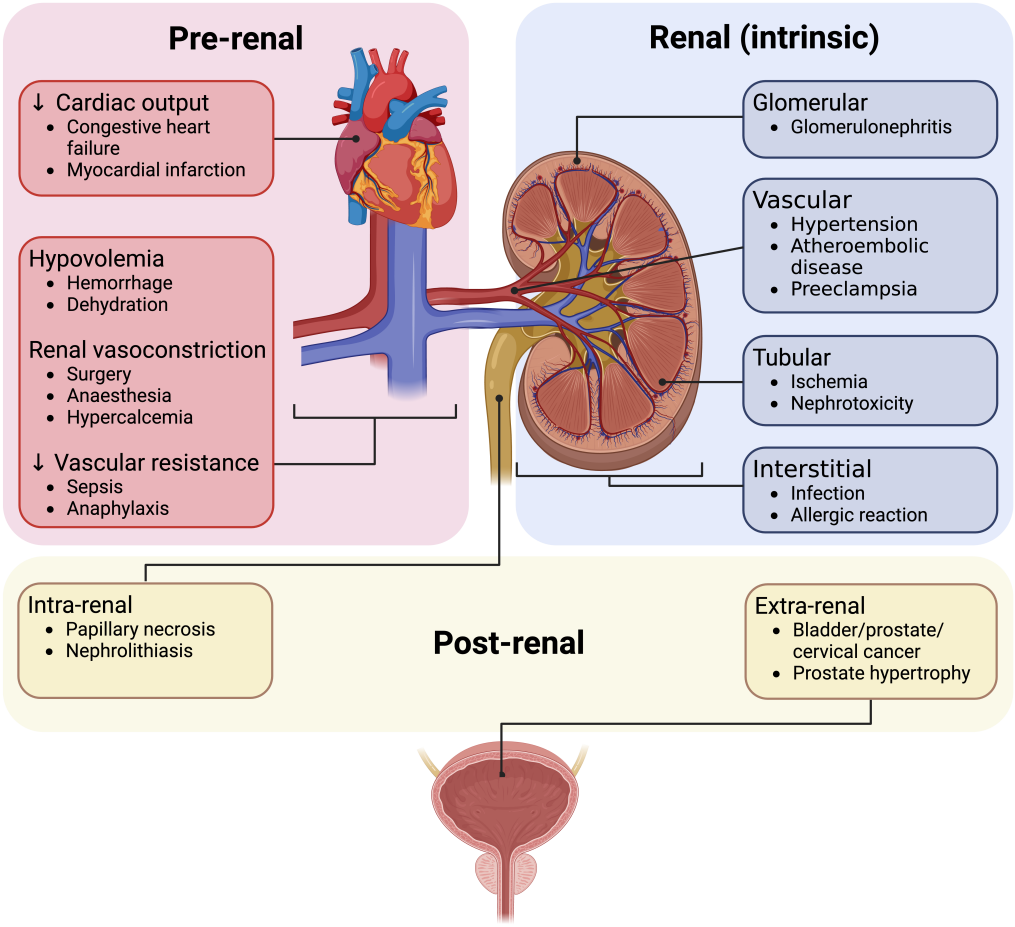

Figure 1.1: Aetiology of acute kidney injury. Schematic diagram illustrating the three main categories of acute kidney injury (AKI)-pre-renal, renal (intrinsic) and post-renal and examples of underlying causes for each. ↓-decrease. Figure created by the author using BioRender.

1.1.2 Chronic kidney disease

Chronic kidney disease (CKD) is defined as a sustained decline in renal function, characterised by an estimated glomerular filtration rate (eGFR) below 60 mL/min/1.73 m^2 for at least 3 months, regardless of the cause [13, 14]. CKD presents a significant global health challenge, affecting over 13% of the population worldwide [15] and 25–35% of individuals over 65 [16]. In 2016 it was ranked as the 13^{th} leading cause of death globally [17], with projections placing it as the 5^{th} leading cause by 2040 [18]. The 2012 Kidney Disease Improving Global Outcomes (KDIGO) guidelines classify CKD into 5 stages based on eGFR and albuminuria [19]. The most common primary diseases leading to CKD and ultimately end stage renal disease (ESRD) are type 2 diabetes (30–

50%) and hypertension (27%) [20], with rising CKD prevalence partly attributed to the ageing population but also the increasing incidence of these risk factors [21]. The burden of CKD is compounded by its strong association with cardiovascular disease (CVD), with CKD patients facing significantly higher risks of CVD, including heart failure [22], peripheral vascular disease [23] and stroke [24]. As CKD progresses, the prevalence of CVD increases [25], with cardiovascular mortality rates in dialysis patients significantly increasing compared to the general population [26, 27]. This association is partly due to the high prevalence of hypertension in CKD patients, which affects 70–80% of stage 1 CKD patients and >95% in stages 4 and 5 before dialysis initiation [28, 29]. The renin-angiotensin-aldosterone system plays a crucial role in blood pressure regulation.

1.1.3 The AKI-CKD interplay

Historically, AKI and CKD were primarily differentiated by the duration of renal function decline. However, emerging evidence suggests a closer interrelationship, with each condition potentially exacerbating the other [30]. AKI is increasingly recognised as an independent risk factor for both the initiation and acceleration of CKD progression. Contrary to earlier beliefs that AKI survivors do not experience long-term consequences, it is now well-established that these individuals have a heightened risk of developing CKD and ESRD [31]. AKI induces a cascade of detrimental effects, including reduced renal function, heightened inflammatory responses (such as neutrophil and macrophage infiltration), tubular cell loss and the activation of fibrotic pathways [32]. In cases of severe or repeated injury, maladaptive repair mechanisms can occur, characterised by chronic inflammation, sustained reduction in renal function and structural changes, such as interstitial fibrosis and permanent cell cycle arrest in tubular cells [33, 34]. These processes set the stage for CKD development. Conversely, CKD is also recognised as a risk factor for AKI [35]. The chronic dysfunction inherent to CKD increases the kidney's vulnerability to even mild insults progressing into AKI episodes. Additionally, the impaired regenerative capacity in CKD patients hinders recovery from AKI, leading to further renal function decline and accelerating CKD progression [36].

1.1.4 The renin-angiotensin-aldosterone system

The renin-angiotensin-aldosterone system (RAAS) is a sequential hormonal pathway essential for regulating blood volume and blood pressure (BP) via the release of angiotensin II and aldosterone (Figure 1.2). Juxtaglomerular (JG) cells, specialised smooth muscle cells surrounding the afferent arteriole in the glomerular corpuscle, function as high-pressure baroreceptors that detect changes in BP. When blood volume or BP decreases, these cells synthesise prorenin, which is cleaved into the active enzyme renin and released from secretory granules.

In the liver, renin cleaves the inactive angiotensinogen to form angiotensin I, which is then converted by angiotensin-converting enzyme (ACE) in the lungs into angiotensin II (Ang II). Ang II restores blood volume and BP through multiple mechanisms. It acts as a vasoconstrictor by binding to angiotensin II receptor type 1 (AT1R), initiating a signalling cascade that increases intracellular calcium, leading to vascular constriction and elevated BP.

Ang II also maintains GFR under conditions of renal hypoperfusion by constricting efferent arterioles, and to a lesser extent afferent arterioles. This increases the filtration fraction (proportion of blood filtered across the glomerulus), enhancing water and salt reabsorption due to the more concentrated blood exiting the glomerulus.

In the kidneys, Ang II directly stimulates sodium and water reabsorption by increasing the activity of the sodium-hydrogen exchanger (Na^+/H^+ antiporter) on the apical surface of proximal convoluted tubule (PCT) epithelial cells, driven by sodium-potassium ATPase. Ang II also induces aldosterone release from the adrenal cortex. Binding of aldosterone to the intracellular mineralocorticoid receptors (MR) upregulates the sodium-chloride cotransporter (NCC) in the distal convoluted tubule (DCT) and the epithelial sodium channel (ENaC) in the collecting duct (CD), therefore enhancing sodium reabsorption.

Furthermore, Ang II promotes the release of antidiuretic hormone (ADH/arginine vasopressin) from the posterior pituitary gland. ADH binds to V receptors on principal

cells in the late distal tubule and CD, leading to the phosphorylation and insertion of aquaporin-2 (AQP2) into the apical membrane, facilitating water reabsorption. Ang II also stimulates thirst through its action on the hypothalamus [37].

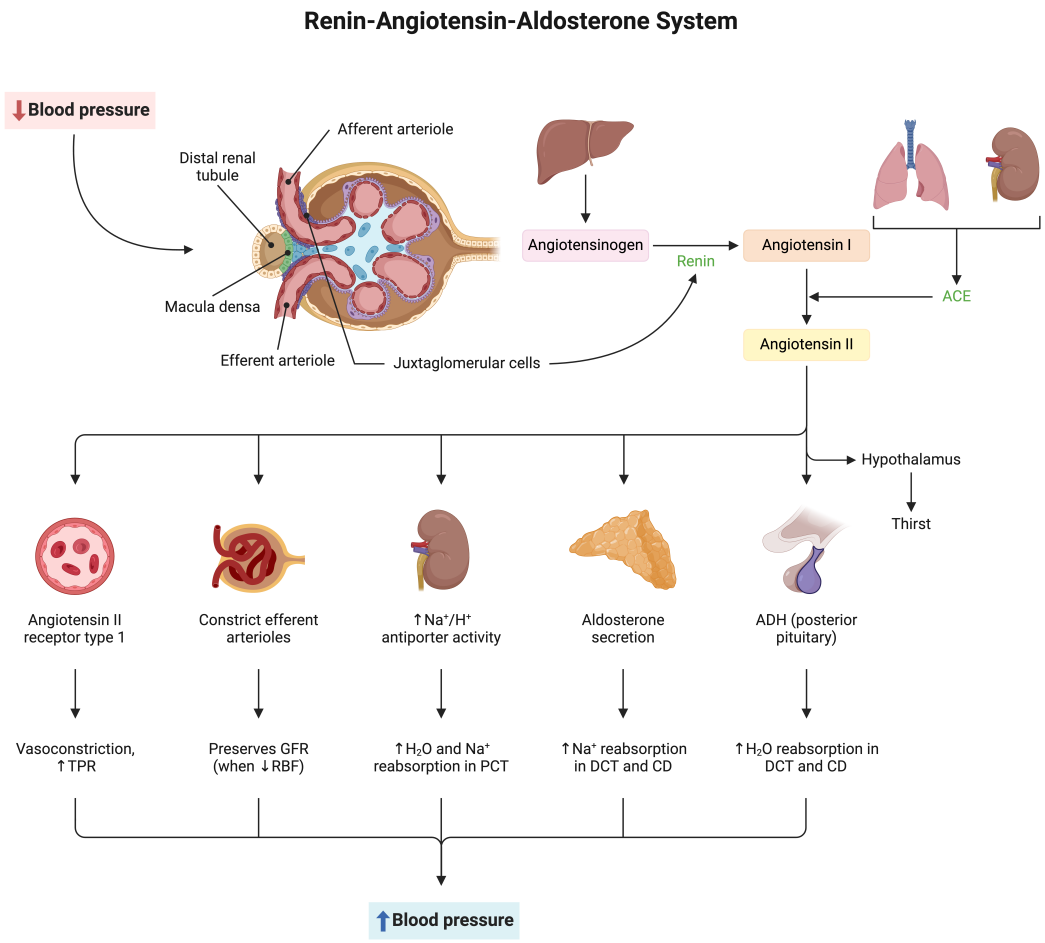

Figure 1.2: Diagram of the renin-angiotensin-aldosterone system and the hypertensive effects of angiotensin II. Juxtaglomerular cells surrounding the afferent arterioles of the glomerulus detect decrease in blood pressure or volume and initiate a cascade leading to the release of angiotensin II (Ang II). Ang II elevates blood pressure through multiple mechanisms: promoting antidiuretic hormone release from the posterior pituitary, stimulating aldosterone secretion from the adrenal gland, constricting afferent arterioles, inducing global vasoconstriction and directly enhancing sodium reabsorption in the renal tubules. ACE-angiotensin-converting enzyme, ADH-antidiuretic hormone, PCT-proximal convoluted tubule, DCT-distal convoluted tubule, CD-collecting duct, GFR-glomerular filtration rate, RBF-renal blood flow, TPR-total peripheral resistance, ↑-increase, ↓-decrease. Figure created by the author using BioRender.

1.1.5 Angiotensin, salt and hypertension

Hypertension is characterised by a systolic pressure of ≥140 mmHg and/or a diastolic pressure of ≥90 mmHg [38]. It is the leading preventable risk factor for CVD and all-cause mortality globally. In 2010 it was estimated that nearly 1.4 billion people, representing >30% of the global adult population, were affected by hypertension, with approximately 10.5 million deaths attributed to the condition [39, 40]. The prevalence of essential hypertension continues to rise due to increasing lifestyle-related risk factors, including poor diet (high in sodium and/or low in potassium) and insufficient physical activity [41].

The relationship between sodium intake and hypertension

Maintenance of osmotic pressure and water homeostasis in the extracellular space relies on the precise regulation of sodium balance. More than 85% of daily sodium intake comes from salt (sodium chloride, NaCl) consumption and ~90% of this sodium is excreted by the kidneys [42, 43]. Historically, prior to the discovery of salt's preservative properties, daily salt intake was <0.25 g/day (0.1 g/day of sodium). Currently, the global average salt intake has increased to 9–12 g/day (3.5–5.5 g/day of sodium), exceeding the World Health Organization recommendation of <5 g salt per day [38, 44]. This shift towards a high-salt diet is driven largely by the increased production and consumption of processed foods [38] and is estimated to contribute to 1.89 million deaths annually [45]. The elevated salt intake imposes a significant challenge on the kidneys' ability to excrete the excess sodium.

Data from animal studies, observational studies and clinical trials demonstrate a causal relationship between excessive salt consumption and hypertension [46–52]. Long-term high-salt diets (8 weeks) in rats have been shown to induce hypertension, promoting renal injury through increased inflammatory cell infiltration, extracellular matrix formation and reduced cell survival [48, 49].

Epidemiological studies suggest that hypertension prevalence increases with age only when accompanied by high salt intake. For instance, the Yanomamo and Xingu

Indians of Brazil and rural populations in Kenya and Papua New Guinea consume diets very low in salt (from <1 to 3 g/day), resulting in a hypertension prevalence of <5% [53]. Elevated BP was observed when members of these populations migrated to Westernised societies and adopted high-salt diets. A study involving >100,000 participants from 18 countries reported a positive association between high salt intake and BP, which was even more pronounced in the elderly, those with hypertension and individuals consuming low-potassium diets [50].

Clinical trials have shown that reducing salt intake can lower BP. A meta-analysis of 34 clinical trials demonstrated that reducing salt consumption to 4.4 g/day decreased systolic and diastolic BP by 4.2 and 2.1 mmHg, respectively, with a stronger effect observed in hypertensive individuals [51]. Similar results were observed in the TONE study, where reduced salt intake in hypertensive, elderly individuals (n=681) resulted in a reduction of systolic and diastolic BP by 4.3 and 2.0 mmHg, respectively [52].

1.2 Atmospheric pollution

1.2.1 Historical evidence for the relationship between air pollution and human health

Our understanding of the adverse health effects of exposure to air pollution has been growing over the last >60 years. The realisation that air pollution can have significant effects on human morbidity and mortality was substantiated by several major incidents in the first half of the 20$^{\text{th}}$ century [54]. In December of 1930 a thick and almost motionless fog covered the Meuse Valley in Belgium, forming a toxic cloud of pollutants from chimney exhaust, which resulted in a total of 60 deaths between December 4 and 5 [55]. In October 1948 another environmental disaster took place in Donora, Pennsylvania, in which industrial pollutants from a local smelting plant started to accumulate in the air above Donora. This resulted in 20 sudden deaths, 400 people were hospitalised and an estimated 5,000–7,000 individuals (of 14,000 residents) became ill [56, 57]. In the UK, the most notable such environmental disaster was the Great Smog in London in December 1952 [58]. In the 1930s and 1940s London above ground

transport comprised mainly of emission-free trams. However, these were replaced by diesel buses (the last tram stopped operating just 5 months before the smog) and by December 1952 there were 8,000 buses running, adding their fumes to the winter fog. This, combined with the smoke from indoor heating (coal burning) during this particularly cold winter and the windless conditions, formed a thick, dusty, smoky layer over the city [58–60]. It was estimated that as a result in the weeks following the smog >4,000 people died and thousands more suffered lifelong health problems. Recent studies suggest that the number of fatalities is much greater-around 12,000 [61].

These tragic events had two important consequences. First, they prompted environmental research and promoted public awareness of the effects of air pollution on human health. Second, they lead to introduction of governmental regulations, such as the Clean Air Act (1956) in the UK and the Clean Air Act (1963) and Air Quality Act (1967) in the USA, which aim to reduce the levels of pollutants and extent of toxicity [62]. Introduction of this legislature in the UK has significantly reduced particulate air pollution-in London particulate concentration is now closer to 20–30 $\mu g/m^3$ compared to the 300 $\mu g/m^3$ 70 years ago (and upward of 3,000 $\mu g/m^3$ in December 1952) [58, 63, 64]. Nevertheless, air pollution remains a major public health concern. Exposure to ambient (outdoor) air pollution (AAP) is associated with increased morbidity (4.2% of global disability-adjusted life years) and mortality, contributing to 7–9 million premature deaths per year globally (7.6% of total global deaths) (the combined cost of life due to ambient and indoor air pollution reached 9 million deaths per year worldwide) [65–67]. AAP has been estimated to reduce global life expectancy by ~1 year and up to ~1.2–1.9 years in heavily polluted countries in Asia and Africa. These values are even higher in some countries in the Middle East and North Africa, like Afghanistan, Sudan and Egypt, where reduction in AAP would have increased life expectancy by 2.3, 2.2 and 2 years, respectively [68]. AAP also poses an enormous economic burden equating to about 1–3 trillion US dollars per year worldwide-a cost projected to reach 18–25 trillion US dollars by 2060 [69, 70]. A recent report placed air pollution as the 5^{th} risk factor for all cause disease, preceding

traditional risk factors, such as poor diet and sedentary lifestyle [65]. Notably, global reduction of air pollution to levels within the World Health Organization Air Quality Guidelines [71] is expected to increase life expectancy to a similar magnitude as eradicating both lung and breast cancer (~0.6 years) [72].

1.2.2 Components of atmospheric pollution

Air pollution is a complex cocktail of gases, liquids and particles (Table 1.1) and their concentrations in the atmosphere depend on geographic location, meteorological conditions, seasonality, topography, diurnal/seasonal cycles in solar radiation and temperature [73]. Atmospheric pollutants may have a natural (volcanic eruptions, wildfires, etc.) or anthropogenic (agriculture, burning of fossil fuels for transport, industry and electricity generation, etc.) origin and are categorised as primary or secondary. Primary pollutants are those directly emitted into the atmosphere, such as particulate matter (PM), sulphur dioxide (SO_2), nitrogen oxides (NO_x, including nitrogen monoxide (NO) and nitrogen dioxide (NO_2)), ammonia (NH_3), carbon monoxide (CO), methane (CH_4), volatile organic compounds (VOCs), including benzene, and certain metals and polycyclic aromatic hydrocarbons (PAH). Secondary pollutants result from chemical and photochemical reactions of primary pollutants, therefore their levels are much harder to control [74]. Tropospheric (ground-level) ozone (O_3) is a key secondary pollutant and is formed by the interaction of NO_x and organic compounds in the presence of sunlight [75]. Some pollutants are not particularly dangerous at ambient levels (such as CH_4 and carbon dioxide (CO_2)) or even completely harmless, like sodium chloride (NaCl). Others, however, have a high toxicity level and can cause significant health problems (O_3, PAH, CO) [74]. Nevertheless, epidemiological studies suggest that PM is the component that tends to show the strongest association with adverse human health effects [76, 77].

Table 1.1: Components of air pollution

	Pollutant	**Sources**	**Health Effects**
Particulate Matter	PM_{10}	Dust from erosion	Lung cancer, CVD [73, 78]
	$PM_{2.5}$	Combustion of fuels	
	UFP		
Gas	CO	Incomplete combustion of carbonaceous fuels (wood, petrol, coal, natural gas)	Difficulty breathing, exhaustion, dizziness, can be deadly at high levels [79, 80]
	NO_x (NO, NO_2)	High temperature combustion of fuels for heating, transportation, industry and power generation	Asthma and other respiratory conditions, long term-respiratory and CVD mortality, cancers [81, 82]
	O_3	Smog. Formed from photochemical reactions with pollutants, such as VOCs, CO and NO_x emitted from vehicles and industry	Difficulty breathing, triggers asthma, reduces lung function, COPD, CVD and cancers [81, 83–85]
	SO_2	Combustion of fossil fuels for domestic heating, industries and power generation	Asthma and respiratory diseases [86, 87]

Continues on next page

Continuation of Table 1.1

	Pollutant	**Sources**	**Health Effects**
	CO_2	Outdoor-burning of fossil, oil and gas, deforestation. Indoor-CO_2 respired into ambient air (as a bi-product of human metabolism)	Metabolic stress, increased respiratory rate and brain blood flow (CO_2 >10,000), headaches, dizziness (CO_2 >50,000 ppm), sweating, confusion (CO_2 >100,000 ppm) [88, 89]
VOCs/SVOCs	Benzene	Vehicle exhaust, industrial emissions, tobacco smoke	Headaches, lassitude, weakness, CNS depression, cardiac arrhythmia, leukaemia [90, 91]
	PAH	Incomplete combustion-vehicle exhaust, power plants; volcanoes, forest fires	Various cancers (lung, skin and others), CVD, oxidative stress [92, 93]

Table 1.1: Components of air pollution. D_{ae}-aerodynamic diameter, PM-particulate matter, PM_{10}-PM with D_{ae} 2.5-10 µm, $PM_{2.5}$-PM with D_{ae} <2.5 µm, UFPs-ultrafine particles (D_{ae} <0.1 µm), VOCs-volatile organic compounds, SVOCs-semi-volatile organic compounds, CO-carbon monoxide, NO_x-nitrogen oxides, NO-nitrogen monoxide, NO_2-nitrogen dioxide, O_3-ozone, SO_2-sulphur dioxide, CO_2-carbon dioxide, PAH-polycyclic aromatic hydrocarbons, CVD-cardiovascular disease, COPD-chronic obstructive pulmonary disease, ppm-parts per million, CNS-central nervous system.

1.2.3 Particulate matter

Due to the complex and continually changing composition of air pollution, with its constituents all interacting with each other, it is difficult to determine the health effects of individual pollutants. Although accounting for ~2% of air pollutant mass (the remaining 98% consist of gases or vapour-phase components, such as CO, NO_2, NO, O_3, SO_2, VOCs, etc.), PM, especially ultrafine particles (UFPs), has attracted significant attention as playing a key role in air pollution-associated morbidity and mortality [73, 77].

PM originates from both natural (e.g. wildfires and windblown dust) and anthropogenic activities (e.g. road dust, tire wear emissions, construction and agriculture) [54]. These particles are a result of fuel combustion or can be formed in the atmosphere by chemical reactions between different pollutants and are composed of inorganic components (sulphates, nitrates, trace metals, chlorides, ammonium), elemental and organic carbon, crystal materials, biological components (bacteria, pollens, spores) and VOCs [54, 94] (Figure 1.3A). Environmental PM is categorised based on particle aerodynamic diameter-coarse (PM_{10}, particle diameter ≤10 µm), fine ($PM_{2.5}$, diameter ≤2.5 µm) and ultrafine particles ($PM_{0.1}$, diameter ≤0.1 µm), also termed nanoparticles (NPs) (Figure 1.3B). While PM_{10} preferentially deposits in the upper airways, $PM_{2.5}$ and NPs can reach the alveoli of the lungs. Small NPs are able to penetrate the alveolar-capillary membrane and enter the systemic circulation [95, 96]. Although most studies showing association between air pollution and disease focus on particle mass measurement (expressed as micrograms per cubic metre-µg/m^3), other particle characteristics may influence their activity. Chemical composition, charge, solubility, surface area, size and particle count-all these metrics could determine particle toxicity [73, 97]. In fact, the high surface area-to-mass ratio of the small UFPs, their high capacity to carry surface chemicals and their ability to potentially reach remote organs suggest that they may induce greater toxicity compared to other sources of PM [73, 98, 99].

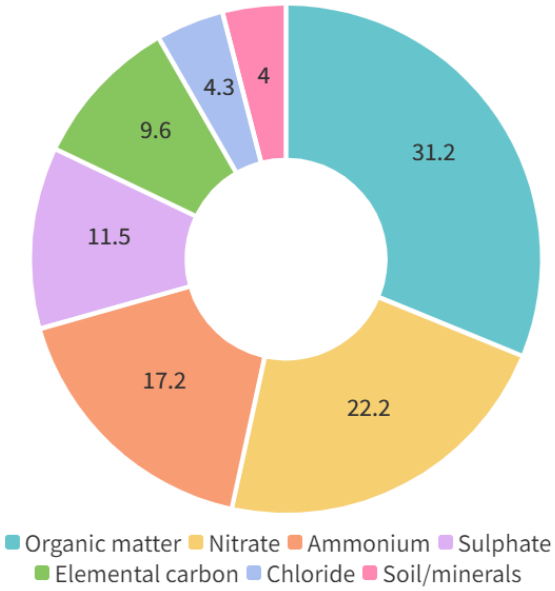

(A) $PM_{2.5}$ composition

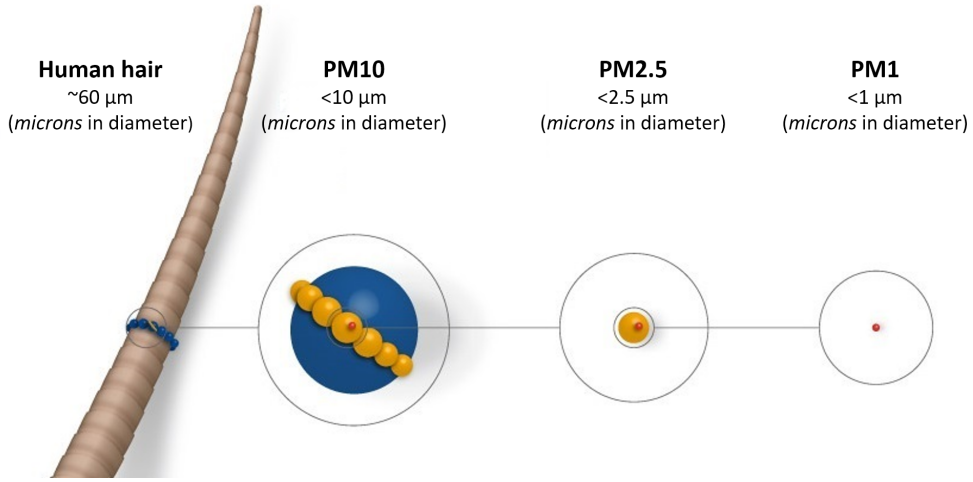

(B) PM size comparison

Figure 1.3: Particulate matter composition and size comparison. (**A**) Pie chart of the various constituents of particulate matter (PM). These values are based on $PM_{2.5}$ collected during winter campaigns in London (North Kensington) and proportions may vary between locations (figure adapted from [100]). (**B**) Diagram comparing size of particulate matter to human hair (figure adapted from [101]).

In the last few decades a great focus has been placed on traffic pollution. Nowadays, many individuals spend a significant amount of time in motor vehicles and in high traffic areas, increasing their exposure to the pollutants in traffic fumes. Additionally, a substantial number of people, especially of low socioeconomic background, live near high volume roads (as many as 40% of the residents in California), making them even

more susceptible to the adverse effects of vehicle emissions [102]. While combustion of both petrol and diesel in vehicle engines produces combustion-derived nanoparticles (CDNP), diesel produces more particles per unit fuel than petrol does [103]. Upon combustion in automobiles diesel gives rise to low solubility nanoparticles with a carbon core and a complex chemical structure, containing sulphate, nitrate, metals and other trace elements. Singlet nanoparticles are 5–20 nm but are usually found in agglomerates of 60–100 nm [97]. As the main source of ultrafine PM in urban environments, diesel exhaust particles (DEPs) have become the model particle for studying the adverse effects of air pollution and are therefore the focus of the work described in this thesis.

1.2.4 Particulate matter and disease

Numerous studies have established a strong association between exposure to AAP and deleterious health effects. Observational epidemiological studies have linked AAP exposure to increased risk of miscarriages [104], worse semen quality [105], reduced foetal growth [106, 107] and adverse pregnancy outcomes [108, 109]. Air pollution potentially impairs cognitive function, increasing the risk of dementia [110]. AAP has been associated with a number of malignancies, including childhood astrocytoma and leukaemia [111], colorectal [81, 112], gastric [113] and bladder cancer [114, 115]. Although AAP is known to be particularly damaging to the lungs and airways, contributing to 280,000 lung cancer deaths and >800,000 chronic obstructive pulmonary disease (COPD) deaths, it has been estimated that over half of the deaths associated with AAP are due to CVD-mainly ischaemic heart disease and stroke [66] (Figure 1.4). The increased risk of cardiovascular morbidity and mortality may be in part due to pollution exacerbating common CVD risk factors, such as diabetes and metabolic syndrome [99]. Controlled exposure studies on humans have demonstrated that short-term acute exposure to diesel exhaust (1–2 h) can have multiple detrimental effects on the cardiovascular system, including impaired vascular tone regulation (impaired vessel relaxation) [116], arterial stiffness [117], increased thrombogenicity and platelet-neutrophil and platelet-monocyte aggregates [118]. Studies suggest that these adverse vascular and pro-thrombotic effects are

predominantly mediated by particulates in diesel exhaust [119, 120]. Animal models have replicated the detrimental effects of air pollution on cardiovascular health, extending them to other cardiovascular conditions (e.g. atherosclerosis and cardiac hypertrophy) and providing a number of plausible biological mechanisms for epidemiological associations [121, 122].

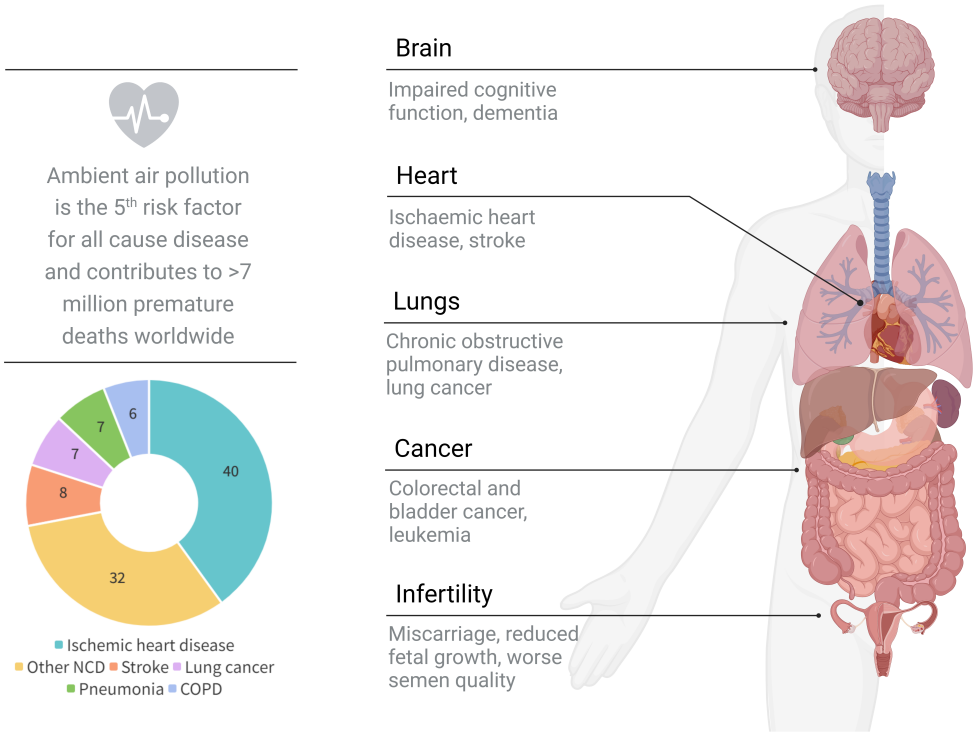

Figure 1.4: Systemic effects of chronic exposure to air pollution. Schematic diagram of the various adverse health effects throughout the body resulting from prolonged exposure to ambient air pollution. Pie chart demonstrates the most common causes of mortality (as %) due to outdoor pollution (chart adapted from [66]). NCD-non-communicable diseases, COPD-chronic obstructive pulmonary disease. Figure created by the author using BioRender.

1.2.5 Mechanisms for the systemic effects of inhaled particulate matter

Although there is substantial evidence suggesting a causal relationship between PM exposure and morbidity, especially cardiorespiratory disease, the precise underlying mechanisms remain to be fully established. Furthermore, the pathways linking inhalation of pollutants to effects on specific organ systems needs to be

ascertained. Induction of inflammation and oxidative stress (OS) are two key pathways involved in the detrimental effects of PM in the lung and in different facets of PM-induced dysfunction in systemic organs [99]. Inhaled particles activate alveolar neutrophils and macrophages to induce pulmonary inflammation and this process is further triggered by PM-derived OS. Oxygen derived free radicals, such as superoxide (O_2^-) and hydroxyl free radicals drive OS and impair cellular function. In fact, in the absence of biological tissue DEP has the capacity to produce O_2^- [123] and metals on the surface of DEP assist in the generation of hydroxyl free radicals [124, 125]. When in contact with cells DEP can promote OS via a number of cellular mechanism, including nicotinamide adenine dinucleotide phosphate (NADPH) oxidase and mitochondrial dysfunction [126, 127]. Therefore, inflammation and OS likely act synergistically to amplify each other's effects [99].

At present three main hypotheses have been proposed for potential pathways linking particle inhalation and their detrimental systemic effects (Figure 1.5) [99, 128]. The classical ('inflammation') theory is that inhaled pollutants are taken up by alveolar macrophages, leading to these cells' activation, therefore inducing pulmonary inflammation. Inflammatory cytokines then 'spill-over' into the circulation to cause systemic inflammation and OS [99, 129]. Although there are inconsistencies between different inflammatory biomarkers and between studies, OS and inflammation play a key role in multiple stages of the mode of action of inhaled PM. Therefore, even if they are not the sole underlying cause, these pathways represent an important mediator in amplifying the signal from PM [99].

The second hypothesis postulates that particles can activate alveoli sensory receptors which in turn stimulate sensory efferent neurons. This activation of the central nervous system leads to changes in autonomic balance (towards increase in sympathetic and decrease in parasympathetic activity) or neuroendocrine activity to ultimately indirectly affect other organs [130, 131]. Studies in rodents have demonstrated that DEP-driven cardiac effects (increased blood pressure, arrhythmia and myocardial injury) can be attenuated by blocking the alveolar sensory receptor

TRPA1 (transient receptor potential cation channel, member A1) or the beta adrenergic receptors [121, 132]. The role of this pathway in mediating non-cardiac aspects of the cardiovascular system could be explained by activation of the central nervous system (such as the hypothalamic-pituitary-adrenal axis) and subsequent endocrine release [133, 134].

The third hypothesis ('translocation') is that the small size of the nanoparticle fraction of PM allows these molecules to cross over the alveolar membrane, enter the pulmonary circulation and be carried by the blood to harm other organs. Furthermore, chemicals in PM (e.g. metals or polyaromatic hydrocarbons) may leach from the particles' surface, gain access to the circulation to directly interact with systems throughout the body. The technical limitations of visualising these small particles and detecting their low levels in the circulation challenges proving this hypothesis [99]. Nevertheless, animal studies have shown translocation of NPs to the heart, liver [135], olfactory bulb [136] and studies in humans have detected PM in the brain [137]. Our group has previously investigated this pathway in mice by using gold nanoparticles of various sizes and showed that particles with a primary size <30 nm entered the circulation and preferentially deposited in inflammation-rich vascular lesions compared to arteries without disease [138].

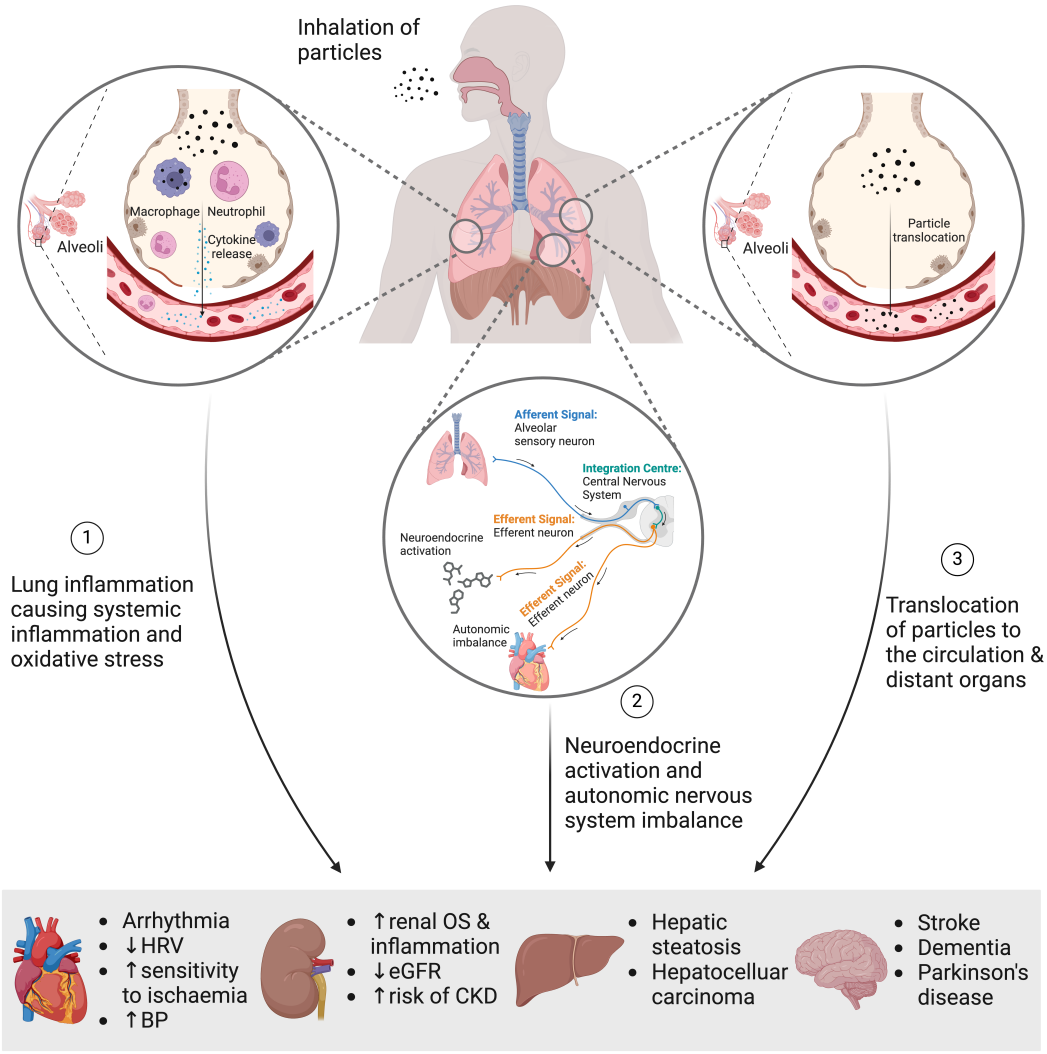

Figure 1.5: Schematic representation of the biological mechanisms for the systemic effects of inhaled particles. Several hypotheses have been proposed for the pathways by which inhaled particles exert systemic effects. The three main ones are: (**1**) inflammation-particles cause lung inflammation and the 'spill-over' of cytokines and inflammatory mediators results in systemic inflammation, (**2**) neuroendocrine activation-particles activate alveolar sensory neurons which through efferent neuron stimulation induce autonomic imbalance (towards increase in sympathetic and decrease in parasympathetic activity) or neuroendocrine activity which can ultimately alter function of organs throughout the body, and (**3**) translocation-particles cross the lung epithelial barrier, enter the circulation where they promote systemic inflammation and oxidative stress and can thus reach distant organs and systems to directly exert adverse effects. Black dots represent particles, blue dots represent cytokines and inflammatory mediators; ↑-increase, ↓-decrease, HRV-heart rate variability, BP-blood pressure, OS-oxidative stress, eGFR-estimated glomerular filtration rate, CKD-chronic kidney disease. Figure created by the author using BioRender.

1.3 Air pollution and kidney disease

It is now well established that AAP and especially PM is associated with increased cardiorespiratory morbidity and mortality. However, it has recently become evident that PM has effects throughout the body, including the kidney. This section provides a brief overview of the evidence from epidemiological and animal studies.

1.3.1 Epidemiological studies

In the last decade a number of epidemiological studies have examined the relationship between exposure to AAP and the incidence of CKD, as well as other adverse renal outcomes, such as progression to ESRD, changes in eGFR, proteinuria and albuminuria. A summary of the main findings from the epidemiological papers discussed in this section is presented in Table 1.2.

Exposure to increasing concentrations of $PM_{2.5}$ has been strongly linked to increased risk of CKD [139–141]. A recent study involving ~2.2 million US veterans demonstrated a linear relationship between increase in $PM_{2.5}$ concentrations and the risk of CKD and progression to ESRD [139]. Long-term exposure to increasing $PM_{2.5}$ concentrations was strongly associated with an increase in the incidence of an eGFR ≤60 mL/min/1.73 m^2 (representing a ≥50% reduction of normal kidney function, therefore used to define CKD) and decline in renal function, represented by an eGFR decline ≥30% [139]. The negative association between $PM_{2.5}$ concentration and decline in eGFR over time has further been shown in other studies where for each 2.1 µg/m^3 increase in $PM_{2.5}$ a reduction in GFR of 1.87 mL/min/1.73 m^2 was estimated and an additional reduction of 0.6 mL/min/1.73 m^2 each consecutive year [140, 142]. Furthermore, an increase of 1 µg/m^3 in $PM_{2.5}$ concentration has shown strong association with a higher urinary albumin-to-creatinine ratio [140]. The association between increasing $PM_{2.5}$ concentration and these adverse renal effects has largely remained statistically significant even after adjusting for demographics, socioeconomic status, age, gender, race and other CKD risk factors, such as diagnosis of diabetes or hypertension [140, 141]. Interestingly, in some studies this correlation was not

observed in diabetics or individuals taking angiotensin receptor blockers [142].

Collectively, these studies, while few in number, demonstrate a relatively consistent relationship between exposure to higher concentrations of $PM_{2.5}$ and increased risk of CKD progression to ESRD. It is interesting that associations were observed at the modest levels of pollution (all studies exhibited a mean $PM_{2.5}$ of 10–12 $\mu g/m^3$) which is below UK guidelines for $PM_{2.5}$ (<25 $\mu g/m^3$) and are not necessarily representative of other countries, especially those with developing economies.

Recently, several studies have examined AAP exposure and kidney disease in Taiwan-a region with higher levels of pollution. In a recent nationwide Taiwanese study $PM_{2.5}$ concentrations were divided into levels by quartiles (Q) and results showed that compared to individuals exposed to Q1 (<29.5 $\mu g/m^3$), those from Q2 (29.5–33.3 $\mu g/m^3$), Q3 (33.3–41.2 $\mu g/m^3$) and Q4 (>41.2 $\mu g/m^3$) exhibited an increase in CKD risk of 1.33, 1.55 and 1.74-fold, respectively. Furthermore, individuals from Q3 and Q4 had a 1.52 and 1.69-fold increased risk of developing ESRD, respectively [143]. These observations are in line with those made by Bowe *et al.* in the USA cohort [139]. Estimates suggest that for every 10 $\mu g/m^3$ increase in $PM_{2.5}$ concentration CKD risk increases by 6% [144]-this correlation has been noted in other studies [145, 146]. A strong association between increase in particle concentration and decline in eGFR has been observed with conflicting results on the particulate size elucidating this effect with some suggesting it's only larger particulates (mainly PM_{10} but not $PM_{2.5}$) [145] and others suggesting particles as small as $PM_{2.5}$ could trigger this [146]. In one study, the adverse renal outcomes associated with PM_{10} exposure were much more predominant among women and associations with $PM_{2.5-10}$ were limited to females [145]. Interestingly, in a number of studies the PM-induced decline in eGFR was measured in 'low risk' individuals (normotensive, non-diabetic subjects with normal weight, an eGFR ≥60 mL/min/1.73 m^2 and <65 years) but not in subjects who were hypertensive, diabetic, overweight, with an eGFR <60 mL/min/1.73 m^2 and >65 years [145, 146].

Table 1.2: Summary of epidemiological studies

Study	**Cohort**	**Pollutant & Means of Measurement**	**Renal Outcomes**
Bowe *et al.* [139]	n=2,482,737 (all US veterans), mostly white men, median age ~62 years, median follow-up of 8.52 years	$PM_{2.5}$, data from the US EPA AQS (using ground-based air monitoring stations across the USA) & NASA space-borne satellite sensors	Increasing $PM_{2.5}$ levels associated with an increase in incident rate of eGFR <60 mL/min/1.73 m^2, CKD, eGFR decline ≥30% (from baseline) and ESRD
Blum *et al.* [140]	n=10,997, median follow-up=17.7 years, baseline mean participant age=63, baseline eGFR=86 mL/min/1.73 m^2	$PM_{2.5}$, data from the US EPA AQS (using ground-based air monitoring stations)	Each 1 µg/m^3 higher annual average $PM_{2.5}$ was associated with higher UACR and significantly higher risk of incident CKD
Bragg-Gresham *et al.* [141]	n=1.1 million people (≥65 years old), 40% male, diverse ethnic backgrounds, both rural and urban status	$PM_{2.5}$, median county level $PM_{2.5}$=12.2 µg/m^3, measurements obtained from the US EPA AQS and NASA MODIS data	Median county-levels CKD prevalence=16% (ranging 0%–60%), $PM_{2.5}$ concentration positively associated with CKD diagnosis

Continues on next page

Continuation of Table 1.2

Study	**Cohort**	**Pollutant & Means of Measurement**	**Renal Outcomes**
Mehta *et al.* [142]	n=669 (all male, mostly white), from Boston area, MA, age at entry=21–80 years (mean age=73.5 years), at baseline-most were former smokers and used anti-hypertensive medication	$PM_{2.5}$, concentration measurements obtained from NASA MAIAC and MODIS data (using satellite based models), mean 1-year average $PM_{2.5}$=11.4 µg/m^3 at first visit and 10.5 µg/m^3 over all visits	1-year $PM_{2.5}$ exposure associated with reduced eGFR and higher rate of decline in eGFR over time (not observed for individuals on ARBs and less apparent in diabetics)
Lin *et al.* [143]	n=161,970 Taiwan citizens (43.8% males), average age ~40 years, a retrospective study	$PM_{2.5}$, $PM_{2.5}$ levels organised in quartiles (lowest-Q1, highest-Q4), data collected 1998–2011 using TAQMD data obtained from an air quality monitor closest to the clinic where the patients received medications for URI	An increase in risk of CKD and ESRD with increasing $PM_{2.5}$ concentration-compared to individuals in Q1 (<29.5 µg/m^3), those in Q4 (>41.2 µg/m^3) had a 1.74-fold increased risk of CKD and 1.69-fold increased risk of developing ESRD

Continues on next page

Continuation of Table 1.2

Study	**Cohort**	**Pollutant & Means of Measurement**	**Renal Outcomes**
Chan *et al.* [144]	n=100,629 Taiwan citizens (52% males), mean age ~39 years (all ≥20 years old), followed up 3–13 years (mean=6.5 years)	$PM_{2.5}$, concentrations estimated at each participant's address using NASA MODIS data and validated using ground monitoring stations	Increase in $PM_{2.5}$ associated with increased risk of developing CKD. Every 10 µg/m^3 increase in $PM_{2.5}$ was associated with a 6% increased risk of developing CKD
Yang *et al.* [145]	n=21,656 (all reside in New Taipei City, Taiwan), 30–97 years old (mean age ~54 years), female:male=2:1	PM_{10}, $PM_{2.5-10}$, $PM_{2.5}$ and $PM_{2.5Absorbance}$. PM collected in 20 sampling sites over 3 14-day periods. PM levels measured using LUR models, which combined PM absorbance data (from impactors), land use data, traffic related information and each participant's residential address	CKD association with $PM_{2.5-10}$ and PM_{10} was stronger in individuals <65 years of age (vs older), normotensive (vs hypertensive), with normal weight (vs overweight) and stronger for (PM_{10}) or limited to ($PM_{2.5-10}$) women. $PM_{2.5}$ and $PM_{2.5Absorbance}$ were not associated with CKD prevalence or eGFR decline

Continues on next page

Continuation of Table 1.2

Study	**Cohort**	**Pollutant & Means of Measurement**	**Renal Outcomes**
Chen *et al.* [146]	n=8,479, all >65 years old and residents of Taipei city, Taiwan, equal gender distribution, mean age=74.2 years	PM_{10}, $PM_{2.5–10}$, $PM_{2.5}$ and $PM_{2.5Absorbance}$. PM levels measured using LUR models as described in Yang *et al.* [145]	1-year exposure to PM_{10}, $PM_{2.5–10}$ and $PM_{2.5Absorbance}$-lower eGFR in people with baseline eGFR ≤60 mL/min/1.73 m^3, but not in those with eGFR >60 mL/min/1.73 m^3. A 1-year exposure to traffic pollution associated with increased CKD prevalence

Table 1.2: Summary of epidemiological studies. Summary of main findings of epidemiological studies discussed in Section 1.3.1. n-number of participants, $PM_{2.5}$-particulate matter with aerodynamic diameter <2.5 µm, $PM_{2.5–10}$-particulate matter with aerodynamic diameter 2.5–10 µm, PM_{10}-particulate matter with aerodynamic diameter <10 µm, EPA-Environmental Protection Agency, AQS-Air Quality System, NASA-National Aeronautics and Space Administration, eGFR-estimated glomerular filtration rate, CKD-chronic kidney disease, ESRD-end stage renal disease, UACR-urinary albumin-to-creatinine ratio, MODIS-moderate resolution imaging spectroradiometer, MA-Massachusetts, MAIAC-multi-angle implementation of atmospheric correction, ARB-angiotensin receptor blocker, TAQMD-Taiwan Air Quality-Monitoring Database, URI-upper respiratory infections, LUR-land use regression.

1.3.2 Animal studies

Mechanistic studies have used animal models of renal injury to further investigate the relationship between air pollution and kidney disease. In one such study, histological analysis revealed that acute $PM_{2.5}$ exposure did not result in visible kidney injury, but rather lead to renal damage at the molecular level (increase in uric acid, renal kidney injury molecule-1 (KIM-1) and serum cystatin C (Cys-C) [147]. Data suggest that AKI was a result of $PM_{2.5}$-induced renal inflammatory response and OS and the renin-angiotensin system (RAS) was likely to be a key upstream pathway inducing these changes [147]. This was in line with the finding from another study where *sub-chronic* $PM_{2.5}$ exposure (in whole body chambers with a particle cutoff size of 2.5 µm for 5 h/day, 4 days/week for 8 consecutive weeks) significantly increased the RAS proteins angiotensin-converting enzyme (ACE) and angiotensin II receptor 1 (AT1R), induced OS and substantially compromised renal function (elevated KIM-1, Cys-C and plasma creatinine) [148].

Exposure to $PM_{2.5}$ has also been associated with hypertension-a major risk factor for the development of kidney disease and specifically impaired Na^+ excretion (natriuresis) [149]. Activation of the dopamine 1 receptor (D1R) induces natriuresis, while its hyper-phosphorylation by the G protein coupled receptor kinase 4 (GRK4) halts the process. Lu *et al.* demonstrated that chronic exposure to $PM_{2.5}$ significantly increased systolic and diastolic blood pressure (SBP, DBP) and decreased basal natriuresis levels in male Sprague-Dawley rats [149]. The authors suggest that $PM_{2.5}$-induced reactive oxygen species (ROS) generation drives expression of GRK4 through an increase in its transcription factor c-Myc. The subsequent hyper-phosphorylation of D1R and its lower expression result in impaired natriuresis and therefore hypertension [149]. Similar observations were made in offspring of rats exposed to $PM_{2.5}$ during pregnancy [150].

A few studies have investigated the renal effects of acute and chronic DEP exposures in rodent models of cisplatin (CP)-induced AKI. In all studies, CP administration was associated with renal injury (increased serum urea and creatinine,

urine output and N-acetyl-β-D-glucosaminidase (NAG) activity, induced OS through decrease in glutathione (GSH) and superoxide dismutase (SOD) [151, 152]. A study by Ali *et al.* showed that *acute* DEP exposure alone significantly affected only NAG, interleukin-6 (IL-6) and total antioxidant capacity (TAC) but concomitant CP+DEP treatment did not aggravate CP-induced changes [151]. These results were not in agreeance with data from another study using a similar protocol, which showed that while DEP alone largely did not affect renal parameters (except GSH), concomitant CP+DEP significantly exacerbated CP-induced changes [152]. On the other hand, *chronic* exposure to DEP alone had no adverse renal effects while concomitant CP+DEP treatment exacerbated the effects of CP alone on urea, urine albumin, KIM-1, neutrophil gelatinase-associated lipocalin (NGAL) and 8-isoprostane [153]. DEP did not raise SBP compared to saline, while CP did so substantially [153]. Histological assessment of cortical tissue in all studies revealed acute tubular necrosis with eosinophilic material, interstitial oedema and congestion in both CP and CP+DEP groups, while renal architecture of saline and DEP groups was preserved [151–153].

Studies have also investigated the potential exacerbating renal effects of prolonged DEP exposure on rodent models of CKD (induced by an adenine (AD)-supplemented diet). Similarly to CP, AD treatment lead to renal injury by ROS generation and increased DNA damage in addition to the previously mentioned renal parameters [154]. Although DEP alone induced only ROS generation, it significantly aggravated the AD-induced changes in lipid peroxidation, ROS generation, catalase and DNA damage [154]. These results conflict with those from another study where DEP had no effect on kidney function and AD+DEP did not exacerbate AD-driven renal changes [155]. Further histological evaluation of kidney sections suggested an increase in injury and fibrosis in both DEP and AD mice-changes the authors suggested to be exacerbated in the concomitant group (although no quantification was performed) [154]. In the same study SBP increased with both DEP and AD alone compared to saline and was further elevated in the AD+DEP group compared to

either treatment alone [154]. These observations are not in line with those from another study, where haemodynamic analysis indicated an increase in baseline SBP and DBP with AD treatment but not with DEP. Here, phenylephrine administration produced a dose-dependent increase in SBP and DBP and treatment with DEP and AD either alone or combined significantly decreased phenylephrine action. Furthermore, baseline renal blood flow (RBF) was decreased by both DEP and AD compared to control. This effect was further amplified in AD+DEP treatment. Phenylephrine caused a dose-dependent reduction in RBF which remained unchanged in AD group. Treatment with DEP prevented this phenylephrine-induced reduction in RBF-an effect amplified in AD+DEP group [155]. A summary of the main findings from the animal studies discussed in this section is presented in Table 1.3.

However, despite these interesting observations, data on the topic are limited and many questions remain, such as: What are the properties of the PM responsible for these effects? What is the precise characterisation of the renal injury (e.g. glomerular and/or tubulointerstitial injury, reversibility, time course)? And what are the roles of key mechanisms (e.g. OS, changes in the renal vasculature, particle translocation)?

Table 1.3: Summary of animal studies

Study	Study Design	Treatment Group	Renal Outcomes
Ali *et al.* [151]	Rats-male Wistar (7–8 ws, n=6) DEP-SRM 2975, 1 *it* (day 5 post-CP), 0.5 mg/kg AKI-CP, 1 *ip*, 6 mg/kg	DEP	⇑ uNAG; ↑ pIL-6, pCRP ⇓ TAC
		CP	⇑ pUrea, pIL-6, pCRP, pNGAL, uNAG; ↑ pCreat ⇓ $Creat_{Clearance}$, rGSH, rSOD, rCAT, TAC
		CP+DEP	↑ pIL-6, rPlatinum ↓ $Creat_{Clearance}$
Nemmar *et al.* [152]	Rats-Male Wistar (10–12 ws) DEP-SRM 2975, 1 *it* (day 6 post-CP), 0.5 mg/kg AKI-CP, 1 *ip*, 6 mg/kg	DEP	No change in parameters measured
		CP	⇑ sUrea, sCreat, uVol, uProt, uNAG; ⇓ rGSH, uOsmolarity
		CP+DEP	No change in parameters measured
Nemmar *et al.* [152]	Rats-Male Wistar (10–12 ws, n=6–8) DEP-SRM 2975, 1 *it* (day 6 post-CP), 1 mg/kg AKI-CP, 1 *ip*, 6 mg/kg	DEP	⇓ rGSH
		CP	⇑ sUrea, sCreat, uVol, uProt, uNAG ⇓ rGSH, rSOD, uOsmolarity
		CP+DEP	⇑ sUrea, sCreat, uNAG ⇓ rGSH

Continues on next page

Continuation of Table 1.3

Study	**Study Design**	**Treatment Group**	**Renal Outcomes**
Nemmar *et al.* [153]	Rats-male Wistar (10–12 ws) DEP-SRM 2975, *it* every 2nd day for 8 days (total *it*=5), 0.5 mg/kg AKI-CP, 1 *ip* (1 h before 3rd *it*), 6 mg/kg	DEP	No change in parameters measured
		CP	⇑ pUrea, pCreat, rKIM-1, r8-Iso, uAlbumin, bSBP; ↑ uGGT ⇓ $Creat_{Clearance}$
		CP+DEP	⇑ pUrea, rNGAL, r8-Iso, rtNO, uAlbumin, uGGT, bSBP
Nemmar *et al.* [154]	Mice-male TO (n=6–8) DEP-SRM 2975, *it* every 4th day for 4 ws, 0.5 mg/kg CKD-AD diet (0.25% w/w), 4 ws	DEP	⇑ rROS, bSBP
		AD	⇑ pUrea, pCreat, rROS, rLP, DNA damage, bSBP ⇓ $Creat_{Clearance}$, rCAT
		AD+DEP	⇑ rTNF-α, rROS, rLP, DNA damage, bSBP ⇓ rCAT
Al-Suleimani *et al.* [155]	Rats-male Wistar (n=4–7) DEP-SRM 2975, *it* every 2nd day for 4 ws, 0.5 mg/kg CKD-AD diet (0.75% w/w), 4 ws	DEP	↑ sCreat
		AD	⇑ pUrea, sCreat, bSBP, bDBP Histology-casts, tubular necrosis, dilatation
		AD+DEP	Histology-tubular dilatation, necrosis and casts

Continues on next page

Continuation of Table 1.3

Study	**Study Design**	**Treatment Group**	**Renal Outcomes**
Zhang *et al.* [147]	Mice-BALB/c (6–8 ws) $PM_{2.5}$ collected using filters in China. *it* on days 0 and 2, 10 mg/mL in 50 µL saline. Mice culled on day 3, 7 or 14	$PM_{2.5}$	⇑ sCysC, sUA, rH_2O_2; mRNA: rKIM-1 (day 3 & 7), rHO-1, rNOX-4, rNF-κB, rTNF-α ; protein: rNOX-4, TNF-α (day 7), r-p65 (day 7), ACE, rAT1R (day 3 & 7) ⇓ rGSH-PX, rSOD mRNA
Aztatzi-Aguilar *et al.* [148]	Rats-male Sprague-Dawley $PM_{2.5}$-collected in Mexico. Sub-chronic exposure in WBC (2.5 L/min airflow)-5 h/day, 4 days/week, 8 weeks	$PM_{2.5}$	⇑ MBP, DBP, H_2O con., UFR, pCreat, haematuria, uβ-2M, uCys-C, rRANTES, Col dep; mRNA: rB1R; protein: rAT1R, rACE, rB1R, γ-GCLc, rKIM-1, rTGF-β ⇓ eGFR, rIL-6, rIL-1β, rTNF-α, rIL-4, rIL-10, rIFN-γ, rIL-17a, rMIP-2; mRNA: rAT1R, rACE, rKLK-1 rSOD-2, rHO-1, rCol3α1; protein: rKLK-1, Nrf-2, rS0D-2, rHO-1 Histology: tubular lesions, tissue structural alterations, intertubular immune cell infiltration

Continues on next page

Continuation of Table 1.3

Study	**Study Design**	**Treatment Group**	**Renal Outcomes**
Lu *et al.* [149]	Rats-Sprague-Dawley (8–10 ws) $PM_{2.5}$ (ambient) collected in China. *it* every 3rd day for 8 ws, low or high dose-$PM_{2.5}$-L-3 µg or $PM_{2.5}$-H-30 µg in 25 µL PBS	$PM_{2.5}$-L & $PM_{2.5}$-H	⇑ SBP, DBP, phos-D1R, GRK4 mRNA, GRK4 protein ⇓ uVol, $uNa^{+}{}_{Excretion}$; UFR and $uNa^{+}{}_{Excretion}$ post-fenoldopam (D1-like receptor agonist) treatment, D1R protein

Table 1.3: Summary of animal studies. Summary of animal studies discussed in Section 1.3.2. Differences in renal outcomes based on the following comparisons: 'DEP'=DEP vs Control, 'CP'=CP vs Control, 'AD'=AD vs Control, 'CP+DEP'=CP+DEP vs CP, 'AD+DEP'=AD+DEP vs AD. ⇑-significant increase, ↑-trend towards increase but no statistics shown, ⇓-significant decrease, ↓-trend towards decrease but no statistics shown, ws-weeks, *n*=number of animals/group, *it*-intratracheal instillation, *ip*-intraperitoneal injection, u-urinary, p-plasma, s-serum, r-renal, t-total, b-baseline, con-consumption, dep-deposition, phos-phosphorylated, DEP-diesel exhaust particles, SRM-standard reference material, $PM_{2.5}$-particulate matter with diameter <2.5 µm, AKI-acute kidney injury, CKD-chronic kidney disease, CP-cisplatin, AD-adenine, WBC-whole-body chamber, NAG-N-acetyl-β-D-glucosaminidase, IL-interleukin, CRP-C reactive protein, TAC-total antioxidant capacity, NGAL-neutrophil gelatinase-associated lipocalin, Creat-creatinine, GSH-glutathione, SOD-superoxide dismutase, CAT-catalase, Vol-volume, Prot-protein, KIM-1-kidney injury molecule-1, 8-Iso-8-isoprostane, SBP-systolic blood pressure, GGT-γ-glutamyl transpeptidase, NO-nitric oxide, ROS-reactive oxygen species, LP-lipid peroxidation, TNF-α-tumour necrosis factor-α, DBP-diastolic blood pressure, Cys-C-cystatin C, UA-uric acid, H_20_2-hydrogen peroxide, HO-1-heme oxygenase 1, NOX-4-NADPH oxidase 4, NFκB-nuclear factor κ B, ACE-angiotensin-converting enzyme, AT1R-angiotensin receptor type I, GSH-PX-GSH peroxidase, MBP-mean blood pressure, UFR-urinary flow rate, β-2M-β 2 microglobulin, B1R-bradykinin receptor type-I, γ-GCLc-γ-glutamyl cysteine ligase, TGF-β-transforming growth factor β, eGFR-estimated glomerular filtration rate, IFN-γ-interferon γ, MIP-2-macrophage inflammatory protein-2, KLK-1-kallikrein 1, Col3α1-pro-α 1 chain of type III collagen, Nrf-2-nuclear factor erythroid 2-related factor 2, D1R-dopamine D1 receptor, GRK4-G-protein coupled receptor kinase type 4.

1.4 Hypothesis and aims

The overarching hypothesis explored in this thesis is:

Particles in diesel exhaust can reach and accumulate in the kidney, where they promote injury and inflammation at both morphological and molecular levels and induce vascular dysfunction. These effects are exacerbated in a mouse model of hypertension-induced kidney injury.

The first aim of this thesis was to determine whether inhaled nanoparticles in diesel exhaust, considered highly harmful, can translocate from the lungs to the bloodstream, reach and sequester in the kidneys, thus cause detrimental effects. Gold nanoparticles were selected due to their inert nature and safety for exposure studies, ability to be synthesised in sizes similar to particles in diesel exhaust, low background levels in tissues and the availability of sensitive techniques for quantification. Additionally, the capacity of translocated DEP to impair vascular function was assessed by *in vitro* application of DEP on renal arteries from healthy mice. These questions are addressed in Chapter 3.

The renal effects of pulmonary DEP exposure were studied in healthy mice across two main investigations. Chapter 4 explores the impact of acute DEP exposure on markers of renal injury and inflammation. Chapter 5 examines a model of chronic DEP exposure, reflecting real-life scenario more accurately. This study evaluated the effects of prolonged exposure on kidney inflammation and injury markers, as well as the impact of DEP on vascular function *in vivo*.

Chapter 6 investigates whether DEP exposure exacerbates kidney damage in mice with pre-existing renal injury. Unlike most studies in the field, which use cisplatin or adenine, this study employed a model of hypertension-induced injury through continuous administration of angiotensin II combined with a high-salt diet. This approach was chosen as hypertension is a more relevant and common cause of kidney disease in humans than exposure to cisplatin or adenine.

Chapter 2

Materials and methods

2.1 Animal source and breeding

All animal studies were performed in line with the United Kingdom Home Office regulations and conformed to the Animals Scientific Procedures Act (1986). Animal procedures were performed under project licence P1D9E2AD5, held by Prof Matthew Bailey. Male C57BL/6J mice, aged 8–10 weeks were purchased from Charles River Laboratories (Tranent, UK) and allowed at least a week between transportation and start of any experiment to equilibrate with their environment. Mice were housed in groups of up to 5 per cage and maintained under the following controlled conditions: temperature of 21°C ± 1°C in stock holding rooms and 24°C ± 1°C in procedural rooms, humidity of 55% ± 10% and a 12 h light-dark cycle (lights on 7 AM to 7 PM).

2.2 Particle administration

2.2.1 DEP administration

The diesel exhaust particles (DEP) used in this study were Standard Reference Material (SRM 2975), collected from industrial forklift engine exhausts and obtained from the National Institute of Standards and Technology (NIST, Gaithersburg, MD, USA). DEP was suspended in sterile saline (0.9% NaCl) at a dose of 1 mg/mL. To minimise aggregation, particle suspensions were always vortexed, then sonicated for 15 min and mixed thoroughly again prior to administration. DEP was delivered to the lungs of mice using the instillation/oropharyngeal aspiration method. Mice were anaesthetised with isoflurane (Merial)-4% for induction and 2–3% for short-term maintenance, inside an anaesthesia induction chamber. Following assessment of the level of anaesthesia using the hind limb reflex test mice were taken out of the chamber, placed supine with extended neck on an angled board, held by their front teeth. The tongue was gently pulled out using forceps and DEP was administered at the relevant dose (35 µg or 50 µg, diluted in 35 µL or 50 µL of saline, respectively) by placing the suspension at the base of the tongue. The tongue was held out to prevent swallowing and then the mouse's nose was briefly covered to encourage the animal to

inhale the droplet via the oropharynx. Figure 2.1 shows a schematic representation of the procedure.

The DEP exposure protocols for the studies in this thesis were developed based on a review of previous study designs. Research in rats suggests a timeline in which pulmonary inflammation is mild at 2 h post-exposure, peaks at 6 h and remains elevated at 24 h [122, 156]. Based on the proposed pathway of DEP particles-entering the lungs, translocating to the circulation and eventually reaching distant organs-a delay in the onset of systemic inflammation relative to pulmonary inflammation was anticipated. Dose selection was based on previous studies in mice, both within and outside our group, which used 35 µg and 50 µg DEP (or an equivalent dose in rats) [122, 156, 157]. Based on this, two acute exposure protocols were designed, discussed in Chapter 4: a single 35 µg instillation with mice culled at 18 h and a single 50 µg exposure with mice culled at 6 h or 16 h post-exposure. These findings, along with the aim of maximising the permitted dose under the project licence, informed the experimental design used in the chronic exposure study, discussed in Chapter 5, and the DEP exposure study in a hypertensive mouse model, discussed in Chapter 6, which involved repeated exposures to 50 µg DEP with mice culled at 18 h post-final exposure.

Figure 2.1: Schematic representation of pulmonary instillation procedure. Mice were anaesthetised, assessed for level of anaesthesia using the hind limb reflex test and were then placed supine with extended neck on an angled board, held by their front teeth. The tongue was gently pulled out using forceps and DEP/saline was administered by placing the suspension at the base of the tongue. As the tongue was held out, the mouse's nose was briefly covered to ensure the droplet would enter the lungs. Figure created by the author using BioRender.

2.2.2 Gold nanoparticles administration

Healthy male adult C57BL/6J mice were subjected to repeated pulmonary exposure (680 µg in total, 50 µL of 1.7 mg/mL, twice weekly for 4 consecutive weeks) of gold nanoparticles (one of the following sizes: 2, 3–4, 7–8, 14 and 40 nm) or their particle-free dispersant as a control. Particle sizes were chosen to reflect glomerular pore size (~4–6 nm) [158]. Particles were purchased from NanoPartz™ (Loveland,CO, USA)-2 and 40 nm and PlasmaChem GmbH (Germany)-3–4, 7–8 and 14 nm. Prior to each instillation particles were sonicated for 5 min then vortexed for 2 min. Instillation procedure was carried out as previously described in Section 2.2.1.

2.3 Measurement of pulmonary inflammation from bronchoalveolar lavage fluid

2.3.1 Collection of BALF

To collect BALF, lungs were lavaged with 0.8 mL of sterile saline (0.9% NaCl) three times (primary lavage kept separate, secondary and tertiary lavages were combined, now referred to as secondary lavage) and both were kept on ice until processed. BALF was centrifuged at 3,000 rpm for 5 min-primary lavage supernatant was aliquoted and stored at -80°C for future analysis. The secondary lavage supernatant was discarded. Cell pellet from primary lavage was gently resuspended in 500 µL of 1% bovine serum albumin (BSA; Sigma)-this suspension was combined with secondary lavage cells by gentle pipetting. Cells were kept on ice until further processing.

2.3.2 BALF total cell count

For each sample, 50 µL of cell suspension was mixed with 50 µL lysis buffer and 50 µL stabilising buffer (ChemoMetec A/S, Denmark). The sample was drawn up into a NucleoCassette™ (ChemoMetec A/S, Denmark) and the BALF total cell count (TCC) was determined using a NucleoCounter™ (ChemoMetec A/S, Denmark).

2.3.3 BALF cell differential counts

For each sample a glass slide was inserted into a slide clip (holder) ensuring that the frosted upper part of the slide was face up. A filter card (with the absorbent surface touching the slide) was put onto the slide and the cytofunnel was positioned onto the filter paper making sure that all holes are aligned.

Based on the total cell count, for each sample the volume required to achieve 40,000 cells was calculated and was combined with 1% BSA+saline to reach a final volume of 300 µL. This cell suspension was then gently mixed, pipetted into the cytofunnel and centrifuged at 300 rpm for 3 min at medium acceleration. Slides were left to dry for 5–10 min before staining with Diff-Quik (Raymond A Lamb. London, UK).

For each stage of the staining, slides were placed in the appropriate solution for 30 dips, then drained before moving to the next solution. Steps were as follows: 100% methanol (for fixing cells), red stain (Eosin G in phosphate buffer), blue stain (Thiazine dye in phosphate buffer) and distilled water. BALF cell differential counts were conducted by manually enumerating and classifying approximately 200 cells per sample into their respective cell types. Data for each cell type are presented as (1) percentage of total number of cells counted manually and (2) the absolute number of cells from each cell type in the lung lavage by referring back to the original total cell count obtained by the nucleocounter. Macrophages were identified as large, circular cells with single-lobed nuclei, neutrophils were identified as smaller cells with multi-lobed nuclei, eosinophils were identified as larger cells with a two-lobed nucleus (lobes connected by a thread) and red cytoplasmic granules and lymphocytes were identified as smaller cells with large, single-lobed nuclei surrounded by a minimal amount of cytoplasm. A schematic representation of BALF processing is presented in Figure 2.2.

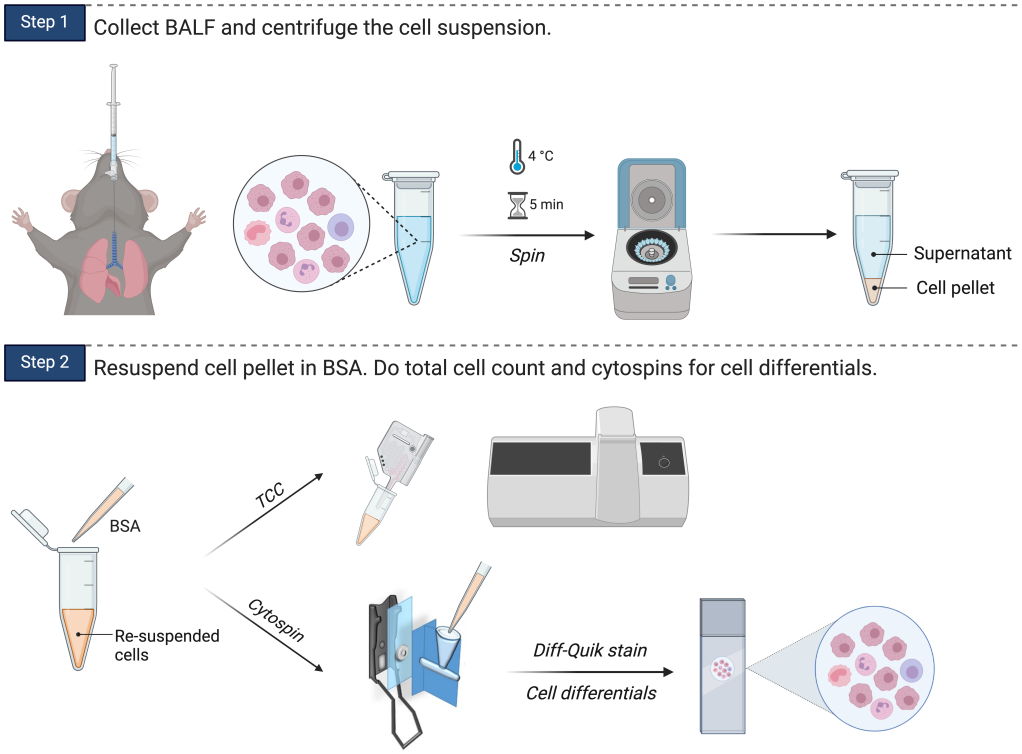

Figure 2.2: Diagram of BALF collection and processing protocol for total cell count and differential analysis. Lungs were lavaged with sterile 0.9% NaCl three times. BALF was centrifuged and cells resuspended with 1% BSA. TCC was determined using a nucleocounter. For each sample, a total number of 40,000 cells were suspended in 1% BSA+saline, pipetted into a cytofunnel and centrifuged. Slides were air-dried before being stained with Diff-Quik, followed by cell differential analysis. BALF-bronchoalveolar lavage fluid, BSA-bovine serum albumin, TCC-total cell count. Figure created by the author using BioRender.

2.4 Circulating cytokines measurement

2.4.1 Measurement of plasma IL-6 levels by ELISA

Mice were culled by terminal anaesthesia with intraperitoneal *ip* injection of Dolethal (100 µL, 200 mg/mL; Vetoquinol UK Ltd). Following assessment of mouse consciousness using the hind limb reflex test, blood was collected by cardiac puncture (syringe was pre-coated with citrate 3.8%), placed in an EDTA-coated tube (BD K2EDTA Microtainer) and kept on ice. Within 30 min of collection, blood was centrifuged at 2,000 × g for 5 min at 4°C, plasma was separated, placed in a fresh Eppendorf tube and stored at -80°C until further processing.

Circulating levels of IL-6 were measured in plasma using a commercial enzyme-linked immunosorbent assay (ELISA) kit (Quantikine™ ELISA, R&D Duoset Systems, Patricell Ltd, Nottingham, UK) following manufacturer's instructions. Briefly, an 8-point standard was prepared by making serial dilutions (1:2 in Calibrator Diluent) from the stock standard provided (500 pg/mL). The final point of the standard was used as a blank (Calibrator Diluent only). A control sample provided in the kit was also included. The control sample and each standard were run in technical duplicates. Due to low plasma volumes available, samples were run in singles.

The microplate strips were loaded by adding 50 µL Assay Diluent and 50 µL of sample, standard or control to each well. Plate was mixed gently and left to incubate for 2 h at room temperature on a plate shaker (for continuous gentle mixing). Plate was then washed by aspirating each well and filling it with 400 µL Wash Buffer-this process was repeated four times. After the last aspiration 100 µL of mouse IL-6 conjugate were pipetted into each well and incubated for 2 h at room temperature. The aspiration/wash step was repeated five times as described before, followed by addition of a Substrate Solution (100 µL/well) and incubation for 30 min at room temperature, protected from light. Finally, the reaction was stopped by adding a Stop Solution (100 µL) and gently tapping the plate to ensure thorough mixing.

The optical intensity of each well was immediately determined, using a microplate reader (OPTImax Tunable Microplate Reader, Molecular Devices, CA) set to 450 nm and corrected by subtracting the 570 nm readings. This step corrects for the optical imperfections in the plate and is essential as readings made directly at 450 nm without corrections may be higher and less accurate. Using the GraphPad Prism software the corrected absorbance measurements were plotted against the known concentrations of the standards. The standard curve produced was then used to interpolate the concentrations of the samples.

2.4.2 Measurement of circulating cytokines using a multiplex assay

Mice were culled by terminal anaesthesia with an *ip* injection of Dolethal (100 µL, 200 mg/mL; Vetoquinol UK Ltd). Following assessment of mouse consciousness using the hind limb reflex test, blood was collected by cardiac puncture (syringe was precoated with citrate 3.8%), placed in an EDTA-coated tube (BD K2EDTA Microtainer) and kept on ice. Within 30 min of collection, blood was centrifuged for 20 min at 1,000 × g, plasma was separated, placed in a fresh Eppendorf tube and stored at -80°C until further processing.

Cytokine levels were measured in plasma using the LEGENDplex™ Multi-Analyte Flow Assay Kit (Mouse Macrophage/Microglia Panel (13-plex), Biolegend®). This is a bead-based assay which combines sandwich ELISA and flow cytometry and allows for the simultaneous quantification of multiple cytokines and chemokines. The panel included the following cytokines: CXC motif chemokine ligand 1 (keratinocyte chemoattractant)-CXCL1 (KC), free active transforming growth factor beta-TGF-β1, IL-18, IL-23, chemokine ligand 22 (macrophage-derived chemokine)-CCL22 (MDC), IL-10, IL-12p70, IL-6, tumour necrosis factor alpha (TNF-α), granulocyte colony-stimulating factor (G-CSF), chemokine ligand 17 (thymus and activation-regulated chemokine)-CCL17 (TARC), IL-12p40 and IL-1β.

Assay principle

Each bead set is conjugated to a specific antibody on its surface and forms the capture beads for that particular analyte. When the sample is mixed and incubated with a selected panel of capture beads, each analyte binds to its specific capture beads. After washing, a cocktail of biotinylated antibodies is added and each detection antibody binds to its specific analyte, forming the capture bead-analyte-detection antibody sandwich. Streptavidin-phycoerythrin (SA-PE) is then added and it binds to the biotinylated detection antibodies which provides fluorescent signal intensity proportional to the amount of bound analytes.

The individual beads are distinguished by size and varying levels of internal

allophycocyanin (APC) fluorescence intensity. APC is an intensely bright phycobiliprotein isolated from red algae that exhibits far-red fluorescence with high quantum yields. Beads are then acquired on a conventional flow cytometer. A schematic diagram illustrating the assay principle is presented in Figure 2.3.

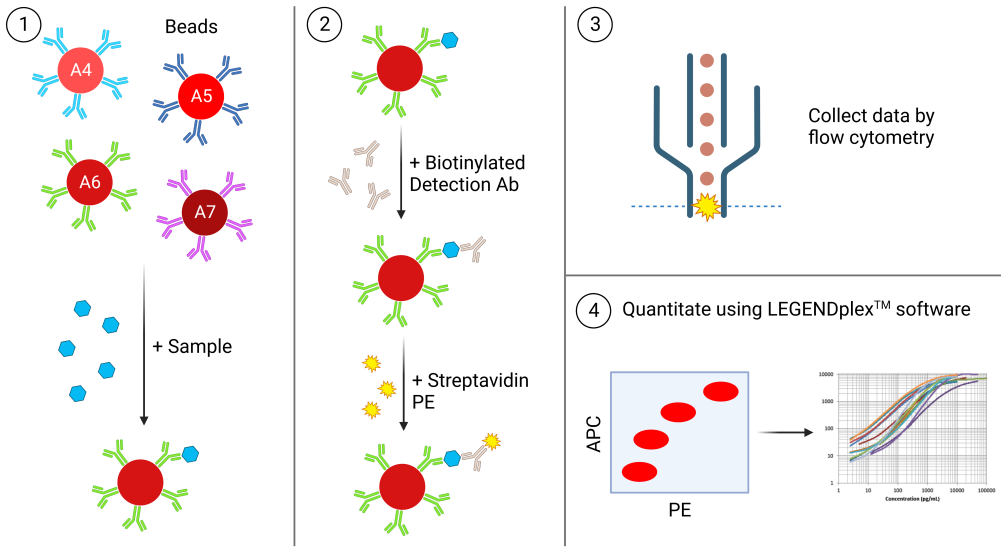

Figure 2.3: Principle of multiplex assay. Ab-antibody, Streptavidin-PE-streptavidin-phycoerythrin. Figure created by the author using BioRender.

Assay protocol

Plasma samples were diluted 2-fold with Assay Buffer (as per manufacturer's instructions) and run in singles. An 8-point standard curve was generated by making 1:4 serial dilutions from the stock standard provided (10,000 pg/mL). The final point of the standard was used as a blank (Assay Buffer only). Each standard was run in technical duplicates.

Standards and diluted plasma samples were loaded onto a V-bottom 96-well plate-components shown in Table 2.1 (beads were the last component to be added to each well and were vortexed for 30 sec prior to loading; bottle was shaken intermittently to mix them and avoid settling). The samples and beads were mixed for 2 h at room temperature on a plate shaker (800 rpm), protected from light. Following incubation,

the plate was centrifuged (1,100 rpm) for 5 min and supernatant discarded. The plate was washed by dispensing 200 µL Wash Buffer into each well, incubating it for 1 min, centrifuging again for 5 min and finally discarding the Wash Buffer. This wash step was repeated twice. Samples were then incubated with Detection Antibodies (12.5 µL/well) for 1 h at room temperature on a plate shaker (800 rpm), protected from light. The SA-PE was then added directly (12.5 µL/well) and allowed to incubate with the samples for 30 min at room temperature on a plate shaker (800 rpm), protected from light. The plate was centrifuged, supernatant discarded and plate washed as previously described, forming a bead pellet at the bottom of the plate at the end. Finally, beads were resuspended by adding 150 µL Wash Buffer and gentle pipetting. Samples were read on a flow cytometer and run by Shonna Johnston.

Reagent	**Standard Wells (µL)**	**Sample Wells (µL)**
Matrix C	37.5	-
Assay Buffer	-	37.5
Standard	25	-
Plasma (diluted)	-	25
Beads	12.5	12.5

Table 2.1: Reagents used in beads-based multi-analyte flow assay. All reagents were provided in Biolegend's LEGENDplex™ Mouse Macrophage/Microglia Panel (13-plex) assay kit.

Data analysis

Data were analysed using BioLegend's LEGENDplex™ Data Analysis cloud-based software. The software automatically finds and gates the beads based on forward and side scatter profile, followed by internal APC fluorescence. It then applies a 5-parameter curve fitting algorithm to generate a standard curve for each analyte. Samples are then automatically quantified based on these curves.

2.5 Measuring mRNA levels in renal tissue by RT-qPCR

2.5.1 Tissue harvest

Mice were culled by terminal anaesthesia with an *ip* injection of Dolethal (100 µL, 200 mg/mL; Vetoquinol UK Ltd). Kidneys were dissected and the capsule removed. Each kidney was cut longitudinally and one half further cut in two. A quarter from each kidney was placed in 1 mL of RNA*later*™ solution (Thermo Fisher, MA, USA) and kept at 4°C for 24 h, then stored at -80°C long-term.

2.5.2 RNA extraction

Immediately prior to RNA extraction mouse kidneys were split into cortex and medulla, placed in 700 µL of QIAzol™ and homogenised using the TissueLyserII homogeniser (Qiagen) (2 × 60 sec, 30 Hz frequency). RNA was isolated using the RNeasy Plus Universal Kit (Qiagen) following manufacturer's instructions and RNA concentration was quantified using a spectrophotometer (NanoDrop, ND-1000).

2.5.3 Reverse transcription and quantitative polymerase chain reaction

cDNA was synthesised using the High-Capacity RNA-to-cDNA™ kit (Applied Biosystems, CA, USA). For each RT reaction an RNA extract volume corresponding to 2,000 ng of diluted RNA was mixed with 1 µL of the 20 × enzyme mix and 10 µL of the 2 × RT buffer to obtain a total reaction volume of 20 µL. Negative controls were also included, where RT enzyme or RNA were replaced with an equal volume of water. Samples were reverse transcribed on a Veriti 96-well Thermal Cycler (Applied Biosystems, USA) using cycling conditions outlined in Table 2.2. The cDNA product was stored at -20°C long-term.

Step	Temperature (°C)	Time (min)
1	37	60
2	95	5
3	4	∞

Table 2.2: Cycling conditions used for reverse transcription reaction.

The cDNA generated from the RT reaction was amplified and quantified using quantitative polymerase chain reaction (qPCR). An 8-point standard curve was constructed by pooling an equal volume from each cDNA sample and performing a 1:4 dilution (with nuclease-free water) for the first point and serial 1:2 dilutions for points 2–7. The final point of the standard was used as a blank (nuclease-free water only). The remaining cDNA was diluted 1:40 (2.5 ng/µL) to fit middle of standard curve. For each reaction (run in technical triplicates) 2 µL of diluted cDNA (or standard) were added to 8 µL of master mix (components listed in Table 2.3). Negative controls, as described above, were also added. Reactions were run on a Roche LightCycler 480 instrument (Roche Diagnostics Ltd., Basel, Switzerland)-specific cycling conditions outlined in Table 2.4. Quantification data for each gene of interest and reference gene were accepted if standard curve was adequate (efficiency=1.7–2.1, error<0.4) and results were normalised against the average Cp value of the housekeeping gene glyceraldehyde 3-phosphate dehydrogenase (GAPDH). Primer sequences for RT-qPCR are presented in Table 2.5.

Reagent	Volume/reaction (µL)	
	EG	**Qiagen**
PowerUP™ SYBR® Green Master Mix	5	5
Primer	-	1
Forward primer	0.6	-
Reverse primer	0.6	-
Nuclease-free H_2O	1.8	2
Total	**8**	**8**

Table 2.3: Master mix components for qPCR. Composition of qPCR master mix depended on the source of primers-Eurofins Genomics (EG) or Qiagen (QuantiTect).

Step	Temperature (°C)	Time	№ Cycles
UDG activation	50	2 min	1
Dual lock DNA polymerase	95	2 min	1
Denaturation/	95	15 sec	40
amplification	60	1 min	
Melt curve	95	15 sec	1
	60	1 min	
	95	∞	

Table 2.4: Cycling conditions used for qPCR reaction. UDG-uracil-DNA glycosylase.

Protein	**Gene**	**Primer sequence/Catalogue number**
GAPDH	*Gapdh*	F 5'-ACT GGC ATG GCC TTC CG-3' R 5'-CAG GCG GCA CGT CAG ATC-3'
KIM-1	*Havcr1*	F 5'-AAA CCA GAG ATT CCC ACA CG-3' R 5'-GTC GTG GGT CTT CCT GTA GC-3'
Renin	*Ren1*	F 5'-GGG AGG CAG GGC CTA CAC-3' R 5'-CTC TCC TGT TGG GAT ACT GTA GCA-3'
TNF-α	*Tnf*	F 5'-CAC AAG ATG CTG GGA CAG TGA-3' R 5'-TCC TTG ATG GTG GTG CAT GA-3'
$AT1_AR$	*Agtr1a*	QT00261464
COL1A1	*Col1a1*	QT00162204
eNOS	*Nos3*	QT00152754
SOD3	*Sod3*	QT00246169

Table 2.5: Primer sequences for qPCR protocol. Primers were purchased either from Eurofins Genomics or Qiagen (QuantiTect). F-forward primer, R-reverse primer.

2.6 Histology

Dissected mouse kidneys were place in 10% formalin for 24 h at room temperature before being transferred to 70% ethanol long-term. Samples were dehydrated by being passed up an ethanol gradient (70%, 80%, 95% and 100%) and xylene before embedding in paraffin blocks. Sections of fixed kidneys were cut (5 µm), stained with haematoxylin and eosin (H&E) and assessed for morphological abnormalities using light microscopy (examined and photographed using a Nikon eclipse Ci microscope).

2.6.1 Haematoxylin and eosin staining

Kidney sections were deparaffinised in xylene (2 × 5 min) and passed down an ethanol gradient (100%, 95%, 80%, 70% for 20 sec each) for rehydration. After staining for 5 min with Harris modified Haematoxylin, sections were sequentially placed in acid alcohol (10 sec), Scott's Tap Water Substitute (30 sec) and eosin (10 sec) with rinsing under tap water after each step. Slides were then taken back up the ethanol gradient and xylene and mounted with DPX.

2.7 Osmotic minipump implantation

2.7.1 Minipump preparation

Minipump preparation was carried out using aseptic techniques to prevent contamination of both the solution and minipump. Using a syringe and blunt-tipped filling tubes osmotic minipumps (Alzet® model 2004, Charles River Laboratories) were filled with angiotensin II (Angiotensin II human, Sigma Aldrich, Dorset, UK) at the desired dose of 500 ng/kg/min. This was done slowly to prevent the introduction of bubbles as this can affect pumping rates. Minipumps were then placed in sterile saline and kept at 37°C for 40 h for "priming" as per manufacturer's instructions. This step is essential as all minipumps have a start-up gradient during which they soak up fluid and come to temperature, therefore priming allows immediate pumping when implanted into the animal.

2.7.2 Minipump implantation surgery

Osmotic minipumps were implanted subcutaneously (*s/c*) into male C57BL/6J mice under isoflurane anaesthesia (Merial)-4% for induction (in a chamber) and 2–3% for maintenance during the procedure (using a nose cone adaptation). Prior to surgery animals received a Vetergesic analgesic injection (*s/c*, 0.3 mg/mL; Ceva, UK) along with a *s/c* injection of 0.5 mL 0.9% sterile saline to minimise post-operative pain and aid recovery. Hair from the lower cervical area was shaved and cleaned with iodine (Vetersept®). A small incision was made in the nape of the neck and a small pocket (*s/c*) was created using tissue-separating scissors. The minipump was placed in the pocket and the incision closed using a 5-0 absorbable suture (Ethicon). A schematic diagram of the procedure is presented in Figure 2.4.

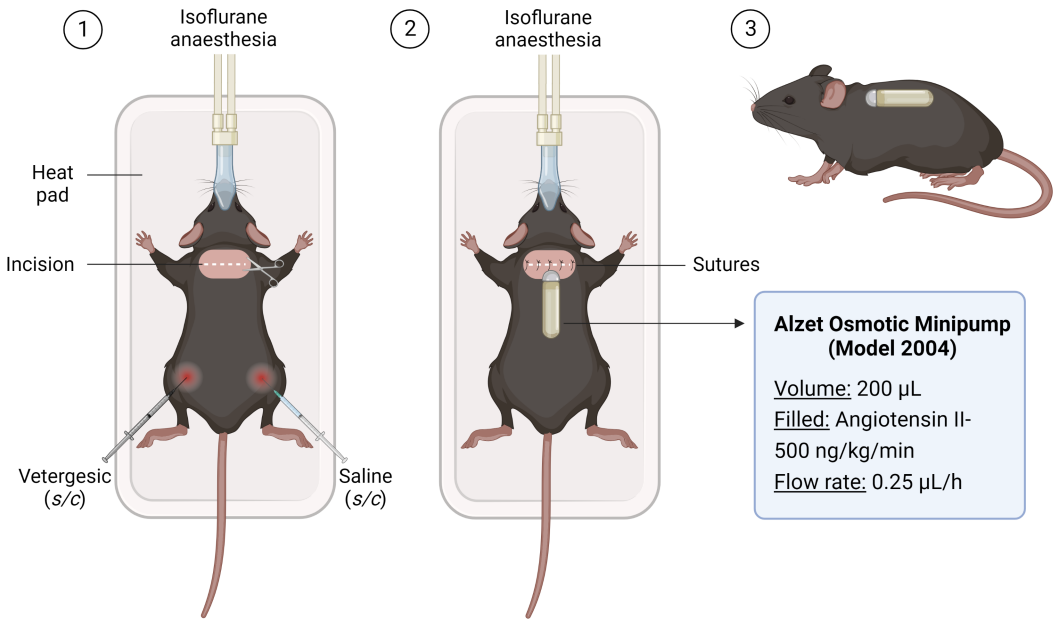

Figure 2.4: Osmotic minipump implantation procedure. *s/c*-subcutaneous injection. Figure created by the author using BioRender.

2.8 Urine measurements

2.8.1 Metabolic cage protocol

Mice were individually housed and placed in metabolic cages for urine collection for 16–20 h. This time period always encompassed the 7 PM–7 AM time period, when the animals were active. Metabolic cage experimental designs are outlined in the methods sections of the relevant chapters.

2.8.2 Urinary KIM-1 measurement

Levels of urinary KIM-1 were measured using a commercial enzyme-linked immunosorbent assay (ELISA) kit (Mouse TIM-1/KIM-1/HAVCR Quantikine® ELISA, R&D Duoset Systems; Patricell Ltd, Nottingham, UK) following manufacturer's instructions. Briefly, the stock standard provided (5,000 pg/mL) was first diluted 10-fold to achieve a concentration of 500 pg/mL, which served as the 1st point of the 8-point standard prepared by making serial dilutions (1:2). The final point of the standard was used as a blank (Calibrator Diluent only). A control sample provided in the kit was also included. Urine samples require at least a 15-fold dilution (as per manufacturer's recommendations), therefore preliminary tests were conducted to estimate the appropriate level of dilution to ensure the optical density measurements fell within the assay's detection range. Based on the results, samples were diluted 1:40. Each standard, control and experimental sample was run in technical duplicates. All dilutions were performed using the Calibrator Diluent solution provided.

The microplate strips were loaded by adding 50 µL Assay Diluent and 50 µL of sample, standard or control to each well. Plate was mixed gently and left to incubate for 2 h at room temperature on a plate shaker (for continuous gentle mixing). Plate was then washed by aspirating each well and filling it with 400 µL Wash Buffer-this process was repeated a total of five times. After the last aspiration 100 µL of cold mouse TIM-1 conjugate were pipetted into each well and incubated for 1 h at 2–8 °C without shaking. The aspiration/wash step was repeated five times as described before,

followed by addition of a Substrate Solution (100 µL/well) and incubation for 30 min at room temperature, protected from light. Finally, the reaction was stopped by adding a Stop Solution (100 µL) and gently tapping the plate to ensure thorough mixing.

The optical intensity of each well was immediately determined, using a microplate reader (OPTImax Tunable Microplate Reader, Molecular Devices, CA) set to 450 nm and corrected by subtracting the 570 nm readings. This step corrects for the optical imperfections in the plate and is essential as readings made directly at 450 nm without corrections may be higher and less accurate. Each sample was further adjusted by subtracting the average reading of the blank samples. Using the GraphPad Prism software the final absorbance measurements were plotted against the known concentrations of the standards to generate a four parameter logistic (4-PL) curve-fit. The standard curve produced was then used to interpolate the concentration of each sample and the resulting values were multiplied by the dilution factor to produce the final estimated concentration. Urinary KIM-1 levels were normalised to urinary creatinine.

2.8.3 Urinary creatinine measurement

Urine creatinine measurements were performed by Kirsten Wilson from the Centre for Reproductive Health at The University of Edinburgh. Briefly, creatinine measurements were determined using a creatininase/creatinase enzymatic method as described by Börner *et al.* [159] making use of a commercial kit (Creatinine enzymatic colorimetric assay, Sentinel Diagnostics via Alpha Laboratories Ltd., Eastleigh, UK) adapted for use on either a Cobas Fara or Mira analyser (Roche Diagnostics Ltd, Welwyn Garden City, UK). Within run precision was CV <3% while intra-batch precision was CV <5%.

Assay principle

When the sample is combined with the Enzymatic Creatinine Liquid reagents the creatinine is converted by three enzymes in a sequential cascade: creatininase, creatinase and sarcosine oxidase. First, creatininase catalyses the conversion of

creatinine to creatine. Creatine is then enzymatically converted by creatinase into sarcosine and urea. Sarcosine oxidase then converts sarcosine to glycine, formaldehyde and hydrogen peroxide (H_2O_2). The resulting H_2O_2 reacts with 4-aminoantipyrine and N-ethyl-N-sulfopropyl-m-toluidine, catalysed by peroxidase, to form a quinoneimine dye. The intensity of the dye's colour, measured at 546 nm, allows for the quantification of creatinine in the sample. A schematic diagram of the assay principle is presented in Figure 2.5.

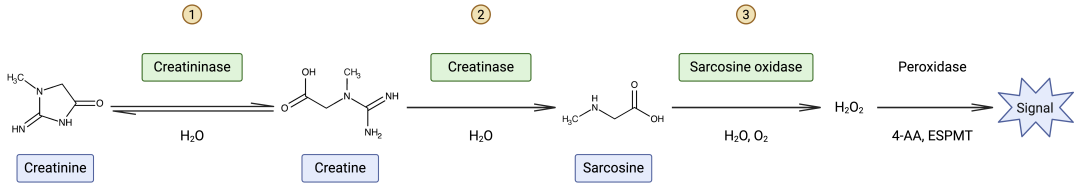

Figure 2.5: Urine creatinine measurement assay principle. Creatinine in urine samples is converted by three enzymes in a sequential cascade: creatininase, creatinase and sarcosine oxidase. In the final step, hydrogen peroxide (H_2O_2) reacts with 4-aminoantipyrine (4-AA) and N-ethyl-N-sulfopropyl-m-toluidine (ESPMT), catalysed by peroxidase, to form a quinoneimine dye, the intensity of which is measured to quantify creatinine. Figure created by the author using BioRender.

2.9 Assessment of vascular function: wire myography

To assess vascular function under isometric experimental conditions, wire myography was performed on renal arteries. In this study, the wire myograph 610 M system of Danish Myo Technology (DMT) was used.

2.9.1 Renal artery isolation and mounting

Mice were culled by an *ip* injection of Dolethal (100 µL, 200 mg/mL; Vetoquinol UK Ltd) and the kidneys, with the intact vasculature connected to the abdominal aorta, were isolated and placed in ice-cold physiological salt solution (PSS, components listed in Table 2.6). Both kidneys and the top and bottom ends of the abdominal aorta were pinned down on a silicone-coated petri dish containing ice-cold PSS and vessels were cleaned of perivascular adipose tissue (PVAT).

The wire myograph consists of 4 baths and each bath has gas supply and aspirators to remove solutions. Each bath was filled with 6 mL of PSS, warmed to 37°C and supplied with gas of 95% O_2 and 5% CO_2. Perfusing the vessels with this gas mixture intends to mimic the O_2 and CO_2 concentrations in human arterial blood. Dissected renal arteries were transferred to the baths and cut into rings of 1–2 mm in length. Under a microscope each renal artery was mounted onto a myograph by passing a fine 40 µm wide stainless steel wire through the vessel lumen, trying not to touch the inner vessel wall. The wire ends were stabilised by the screws and baths returned to the myograph.

Reagent	**PSS**	**KPSS**
NaCl	119.0 mM	3.2 mM
KCl	3.7 mM	125.0 mM
$MgSO_4$	1.2 mM	1.2 mM
$NaHCO_3$	25.0 mM	25.0 mM
KH_2PO_4	1.2 mM	1.2 mM
EDTA	27.0 µM	27.0 µM
D-Glucose	5.5 mM	5.5 mM
$CaCl_2$	2.5 mM	2.5 mM

Table 2.6: Reagents for preparing PSS and KPSS solutions used in wire myography. PSS-physiological salt solution, KPSS-high potassium physiological salt solution.

2.9.2 Normalisation of vascular tension

Normalisation of vascular tension is a key step in the wire myography protocol which aims to determine the internal vessel circumference which produces the maximal isometric contractility. Vascular reactivity depends on the initial vessel tension, hence normalisation is an essential step for the accurate comparison of drug

effects and reproducibility of results.

Normalisation was performed using the DMT Normalisation Module on LabChart (AD Instrumentals), which involves testing the length/tension relationship for each vessel. Vessel length was determined using a scale incorporated in the microscope eyepiece. To set the vessel tension, the micrometer dial, separating the myograph jaws, was turned in increments of 2 mN each time. For every increase in force, the distance between the jaws was measured until the vessel reached a maximum of 13.3 kPa, which corresponds to an intramural pressure of 100 mmHg. The length/tension graph produced was used to determine the optimal internal circumference (IC_1) for each vessel to produce maximal vascular reactivity. The jaws were then adjusted to correspond to the IC_1, at which the vessels remained for the rest of the experiment. Vessels were left to equilibrate for 30 min.

2.9.3 Vascular reactivity protocol

Viability of renal arteries was tested by bathing vessels in 6 mL of a high potassium PSS (KPSS, components listed in Table 2.6) to induce a maximal contractile response through cell depolarisation. Once the concentration response curve peaked and plateaued, the baths were emptied, the vessels washed three times with warmed PSS and left to equilibrate for 20 min. This process was repeated three times.

To assess vascular reactivity, vessels were treated with the adrenergic-dependent vascular contraction agent phenylephrine (PE; Sigma), the endothelial-dependent vasodilator acetylcholine (ACh; Sigma) and the endothelial-independent vasodilator sodium nitroprusside (SNP; Sigma) and dose response curves were generated for each (10^{-9}, 3×10^{-9}, 10^{-8}, 3×10^{-8}, 10^{-7}, 3×10^{-7}, 10^{-6}, 3×10^{-6} and 10^{-5} M). Following each drug administration, vessels were washed with PSS until they reached baseline tension and left for 20 min before the next treatment. For vasodilation, arteries were preconstricted by PE incubation at a dose that would induce ~80% of the maximal contraction. The mechanism of action of each drug is presented in Figure 2.6.

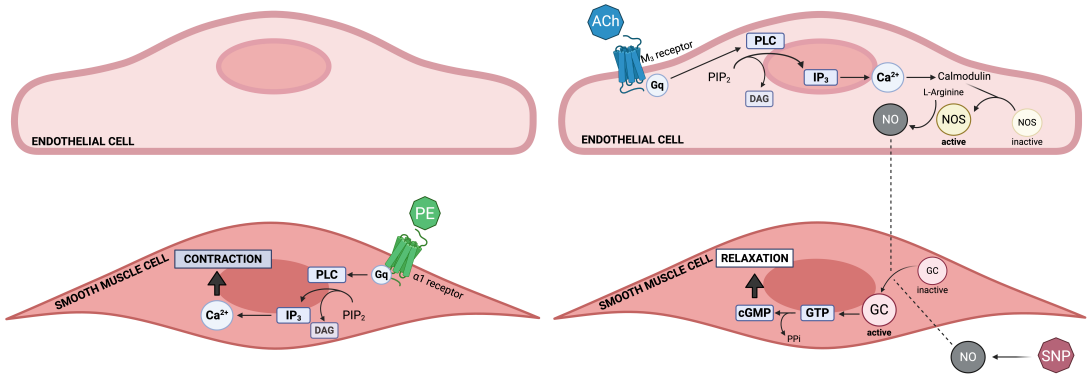

(A) **(B)**

Figure 2.6: Mechanism of action of vasoactive drugs used in wire myography. Signalling pathways of the endothelium-independent vasoconstrictor phenylephrine (PE), the endothelium-dependent vasodilator acetylcholine (ACh) and the endothelium-independent vasodilator sodium nitroprusside (SNP).(**A**) PE acts on alpha-1 (α-1) receptors on vascular smooth muscle cells (VSMC), triggering a signalling cascade that increases intracellular calcium (Ca^{2+}), leading to constriction. (**B**) ACh binds to muscarinic 3 (M3) receptors on endothelial cells, triggering a signalling cascade that increases intracellular Ca^{2+}, leading to nitric oxide (NO) synthesis. NO then acts on VSMC, causing relaxation. SNP acts as a NO donor to cause relaxation. PLC-phospholipase C, PIP_2-phosphatidylinositol 4,5-bisphosphate, DAG-diacylglycerol, IP_3-inositol triphosphate, NOS-nitric oxide synthase, GC-guanylyl cyclase, GTP-guanosine-5'-triphosphate, cGMP-cyclic guanosine monophosphate. Figure created by the author using BioRender.

2.9.4 The effects of *in vitro* DEP application on vascular function

One way in which DEP may exert its effects is by producing superoxides and other oxygen-derived free radicals [160]. In this experiment the direct effect of DEP on vascular reactivity and whether DEP-induced vascular changes could be reversed by superoxide dismutase (SOD) were assessed *ex vivo* in mouse renal artery grafts using wire myography.

Healthy, untreated mice were culled and renal artery was isolated as described in Section 2.9.1. Arteries were mounted on a wire myograph and vascular tone was normalised as previously detailed in Section 2.9.2. Vessel viability was confirmed by KPSS administration followed by treatment with PE, ACh and SNP (Section 2.9.3). Arteries were pretreated with either DEP alone or combined DEP+SOD before each drug administration. For this, a fresh suspension of DEP (SRM 2975, NIST) was prepared each day (2 mg/mL stock solution) in PSS, vortexed and sonicated to ensure

particle dispersion and added to the myograph bath at a concentration of 30 µg/mL. SOD (Sigma) was dissolved in PSS (5,000 U/mL stock solution) and added to the myograph bath at a concentration of 100 U/mL. A ≥20 min period was allowed between DEP/DEP+SOD administration and addition of any vasoactive agent. A ≥30 min washout period was ensured before treatment with subsequent drugs. Vessels in the control group were not pretreated with DEP/DEP+SOD. A diagram with the protocol details is presented in Figure 2.7.

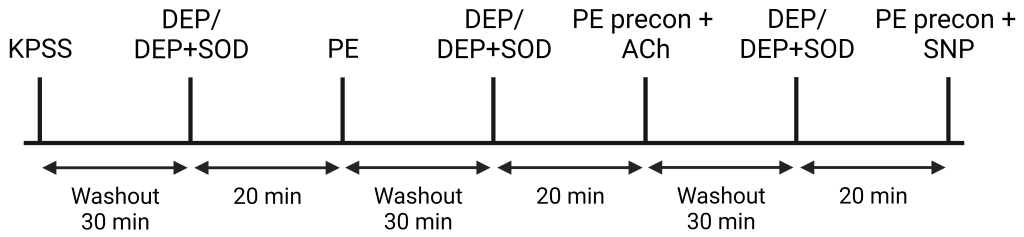

Figure 2.7: Timeline of myography protocol for assessing the direct effects of DEP on the renal vasculature. Renal arteries from healthy mice were isolated, mounted on a wire myograph and treated with phenylephrine (PE), acetylcholine (ACh) and sodium nitroprusside (SNP) to assess vascular function. Vessels were pretreated with diesel exhaust particles alone (DEP, SRM 2975, 30 µg/mL) or in combination with superoxide dismutase (SOD, 100 U/mL). KPSS-high potassium physiological salt solution, PE precon-preconstriction with the PE dose that induced ~80% of the maximal contraction.

2.9.5 Wire myography data analysis

Data were visualised and collected using the LabChart 7 pro software (v.7.3.2) and analysed using LabChart Reader 8 (v.8.1.22). For vasoconstriction, the maximum force for each dose was collected and recorded-for KPSS in mN and for PE as percentage of the maximum KPSS-induced response. For vasodilation, the minimal force for each dose was collected and expressed as percentage of the tension induced by PE preconstriction. A diagram of the analysis process is presented in Figure 2.8.

For each treatment a dose response curve was synthesised in GraphPad Prism 9. A non-linear regression in the logarithmic equation of the dose versus the response was performed, which allowed for the calculation of the logEC_{50}-the concentration of the

vasoactive compound required to induce 50% of the maximum response.

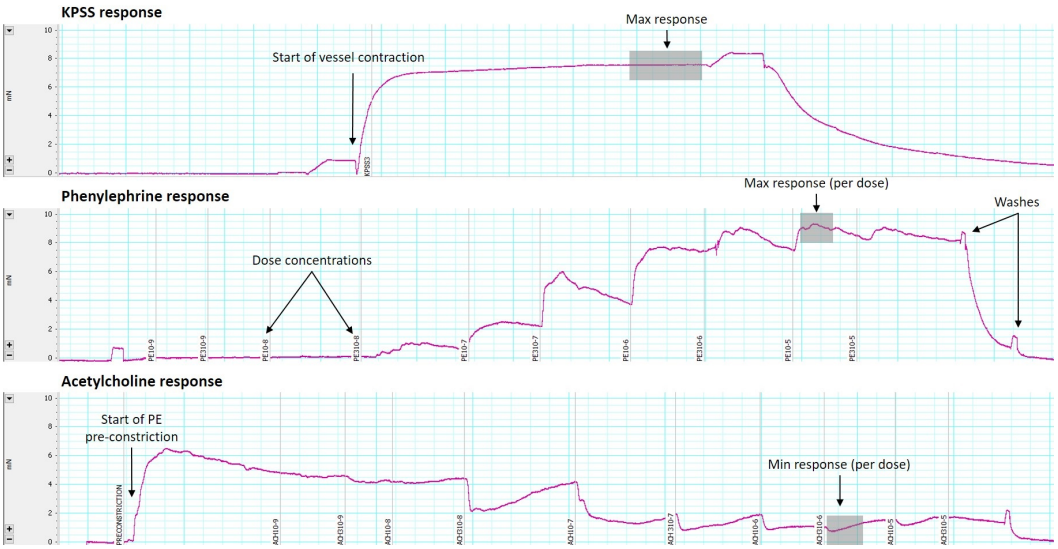

Figure 2.8: Exemplars of wire myography vasoreactivity data from LabChart.

2.10 Analysis of gold concentration in tissues using inductively coupled plasma mass spectrometry

All sample digestion and measurement of gold (Au) concentration using inductively coupled plasma mass spectrometry (ICP-MS) were performed by Dr Gavin Sim and Dr Lorna Eades from the School of Chemistry at The University of Edinburgh. All chemicals used for sample pretreatment and mass spectrometry were of analytical grade or of high purity. Nitric acid (HNO_3) and hydrochloric acid (HCl) of ≥99.9999% purity were purchased from Thermo Fisher Scientific (UK), L-cysteine (Acros Organics, NJ, USA) and deionised (DI) water 18.2 MΩ produced with an Arium II system (Sartorius, Germany). The calibration standard solution of gold and the solution of the element rhodium (Rh), used as internal standard, were prepared using single-element stock solutions with a concentration of 1,000 mg/mL (both PlasmaCAL grade, SPE Science, France). For quality control aspects on the relevant ultra-trace level, two reference samples-"SERONorm™ Trace Elements in Whole blood L-1" and "SERONorm™ Trace Elements in Urine L-2" (both supplied by AB Scientific, UK), were included into the

analytical procedure. Although the gold concentrations were not certified in these samples, they were used as reference matrices for additional control experiments.

Sample preparation

Blood (~500 mg) or whole kidneys (~200 mg) were placed in disposable borosilicate tubes and digested in 2 mL aqua regia (1:3 ratio of concentrated HNO_3-to-concentrated HCl) at 80°C for 1 h on a block heater type (BT5D, Grant Instruments, UK). Following digestion, 8 mL of ultrapure water was added to reach a final volume of 10 mL. For each digestion batch, two reagent blanks were also added. Urine samples were directly diluted by a factor of 10 in 2% (v/v) aqua regia (aqua regia diluted in DI water), left for 30 min and centrifuged for 5 min at 1,400 rpm to remove debris. To further stabilise the gold during analysis and aid washout, immediately before analysis all pretreated samples (blood, kidney and urine) were further diluted by a factor of 10 in a solution of 0.01% w/v L-cysteine in 1% v/v HCl (HCl diluted in DI water). Schematic diagram of the tissue processing procedure is presented in Figure 2.9.

Sample analysis

Gold content in all samples was analysed using a multi quadrupole inductively coupled plasma mass spectrometer (multiquad-ICP-MS type 8900, Agilent, USA). Instrumental setup and methodological settings are outlined in Table 2.7. Two external calibration curves were applied for gold of the interference-free isotope ^{197}Au were performed-a micro-calibration at the start of analysis (0.001–0.5 ng/mL Au) and a macro-calibration at the end (0.01–2 ng/mL Au). Further online addition and correction with an internal standard (200 ng/mL Rh with the measured isotope ^{103}Rh) and the correction for the chemical blank were also applied. As gold is a challenging element to analyse due to the potential memory effect of the ICP-MS system, a thorough washout protocol was designed and tested prior to analysis. The protocol included the following optimisation steps: (1) comparing background Au concentrations when employing new single-use digestion tubes versus used and cleaned tubes, and (2) testing different solutions and acids to reduce background Au

concentration in blank and washout solutions. Based on this optimisation: (1) new, single-use digestion tubes were used to maintain Au background concentration low and reliable, and (2) sample dilution in 0.01% L-cysteine w/v in 1% v/v HCl, introducing a blank check after every three samples and a refined washout protocol were applied during the measurement series of the pretreated blood, kidney and urine samples. Implementing these changes reduced background inter-sample carry over to 0.03 ng/mL Au for samples which were <1 ng/mL Au. For samples reporting >1 ng/mL Au in digest, analysis was repeated to ensure carry over did not affect the data. The methodological limit of detection (LOD) and limit of quantification (LOQ) were determined under reproducibility circumstances and in the blank (LOB) as well as in the three matrices of interest-blood, kidney and urine. Due to Au concentration being reported as "< value" on the certificate, SERONorm™ samples were used to (1) check for blanks and (2) establish the trueness by spike recovery using a spiked concentration of 0.5 ng/mL Au. Selected samples were run in duplicates and triplicates in order to establish the inter- and intra-batch analysis variation. A schematic diagram of the protocol is presented in Figure 2.9.

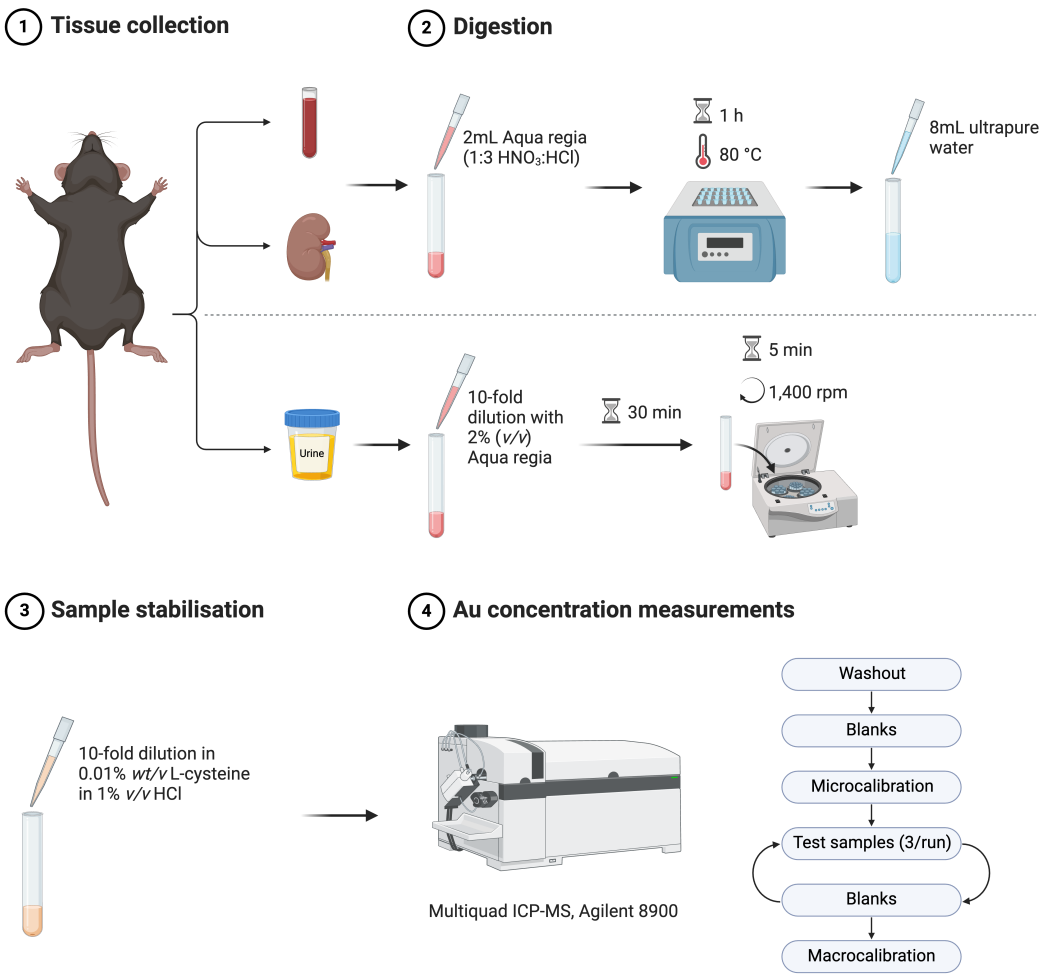

Figure 2.9: Protocol for gold concentration measurements using ICP-MS. Healthy mice were administered gold (Au) nanoparticles via pulmonary instillation (*it*) twice weekly for 4 consecutive weeks. Mice were culled ~18 h after last *it* and whole blood, kidneys and urine were collected. Tissues were digested, stabilised and Au concentration measured using multi quadrupole inductively coupled plasma mass spectrometer (ICP-MS). w-weight, v-volume. Figure created by the author using BioRender.

Parameter	**Settings**
Nebuliser	Micro-mist nebuliser by peristaltic pump at a rate of ~1.0 mL/min
Spray chamber	Scott double pass (quartz)
Sampler and skimmer cone	Nickel
Take up time	1.5 min
Washout time	2 min
RF power	1550 W
RF matching voltage	1.8 V
Plasma gas flow	15 L/min Ar
Auxiliary gas flow	0.9 L/min Ar
Nebuliser gas flow	1.03 L/min Ar
Measured isotope (internal standard isotope)	^{197}Au (^{103}Rh)
Operation mode	Single quad mode
Methodological settings	Fully quantitation mode with 1 point per mass unit and integration time of 0.1 ms, number of replicates=3

Table 2.7: ICP-MS instrumental setup and methodological settings.

2.11 Statistical analysis

Statistical analysis and graph generation were conducted using GraphPad Prism 10 (GraphPad Software, California, USA). Data are presented as Mean ± SEM. Outliers were identified using Grubbs' test and excluded if $p<0.05$. Comparisons between two groups were performed using an unpaired Student's *t*-test, with Welch's correction applied when significant differences in variance were detected by an F-test. For comparisons involving three or more groups, ordinary One-way ANOVA was used, followed by Dunnett's multiple comparisons test (for comparisons to a control) or Tukey's *post hoc* test (for comparisons among all groups). Two-way ANOVA with Tukey's multiple comparisons test was employed to analyse the effects of two independent factors simultaneously. Statistical significance was defined as $p<0.05$ and statistical tests used are stated in the figure legends of each results chapter.

Chapter 3

Particle translocation to the kidney and its impact on renal vascular function

3.1 Introduction

Ambient air pollution is the largest environmental risk factor, responsible for approximately 7 million premature deaths each year globally-a number estimated to have increased by 66% in the last two decades [161, 162]. The detrimental effects of air pollution go beyond the respiratory system-in fact, studies have shown a clear correlation between exposure to air pollution and diseases in all major organs of the body [163]. Epidemiological studies have also linked pollution to kidney disease [164, 165] (further detailed in Table 1.2), the mechanisms, however, remain unclear. Air pollution is a complex mixture of various toxic components, however, particulate matter is especially damaging to human health. As particles originate from different sources, their composition and size vary. Nevertheless, the small, ultrafine particles have shown the strongest association with disease. Their high surface area-to-mass ratio suggests they may carry harmful substances to the body and their small size (≤100 nm) allows them to reach deep into the alveoli and potentially cross from the lungs to the circulation (translocate) and reach distant organs [166]. This translocation hypothesis is a riveting explanation for the detrimental effects of air pollution all throughout the body.

Tracing nano-sized particulates in the body is challenging for a number of reasons: they are extremely small in size, levels of particles that pass the alveolar-capillary barrier are low and get diluted even further into the blood and tissues. Furthermore, particles, such as those in diesel exhaust, are carbon-based, making them problematic to trace in cells naturally high in carbon. To get around this, our group has previously used gold nanoparticles as a model to track particle movement in the body [138]. Gold nanoparticles can be obtained in broadly the same sizes as particles in diesel exhaust, gold is inert, making it safe for exposure studies, background gold levels in biological tissues are extremely low and there are a number of sensitive and reliable techniques to detect them. Our group has previously shown gold nanoparticles present in blood of adult volunteers as early as 15 min after inhalation (and in most at 24 h) and was detectable in blood and urine 3 months

after exposure. Studies in rodents revealed a size-dependent translocation, with different size thresholds for particle detection in blood (30–100 nm) and in urine (10–30 nm). These observations suggested that intermediate-sized particles may sequester in the kidney. Particles in diesel exhaust have a primary size of 10–80 nm, therefore, the translocation and accumulation of combustion-derived particles in the kidney may be a key pathway through which pollution could induce kidney disease.

3.1.1 Hypothesis and aims

The hypotheses explored in this chapter are:

1. **Nano-sized particles found in air pollution have the capacity to cross the alveolar-capillary barrier, be carried in the circulation to distant organs and sequester in the kidney.**
2. **Nanoparticle translocation into the circulation leads to vascular dysfunction in renal arteries.**

Aims:

1. Investigate particle translocation following exposure using gold nanoparticles by establishing gold concentration in tissues.
2. Assess the impact of *in vitro* DEP application on vascular function in renal arteries as a proof-of-concept for the effects of nanoparticle translocation to the circulation. Evaluate the capacity of SOD to attenuate these effects.

3.1.2 Study design

In addressing the aims of this chapter, two studies were designed.

To explore particle translocation, gold nanoparticles of various sizes were administered to the lungs of healthy mice twice weekly for 4 consecutive weeks and mice were culled ~18 h after the last instillation. Blood, kidneys and urine were collected, digested and concentration of gold in each matrix was measured using ICP-MS. A diagram of the study design is presented in Figure 3.1.

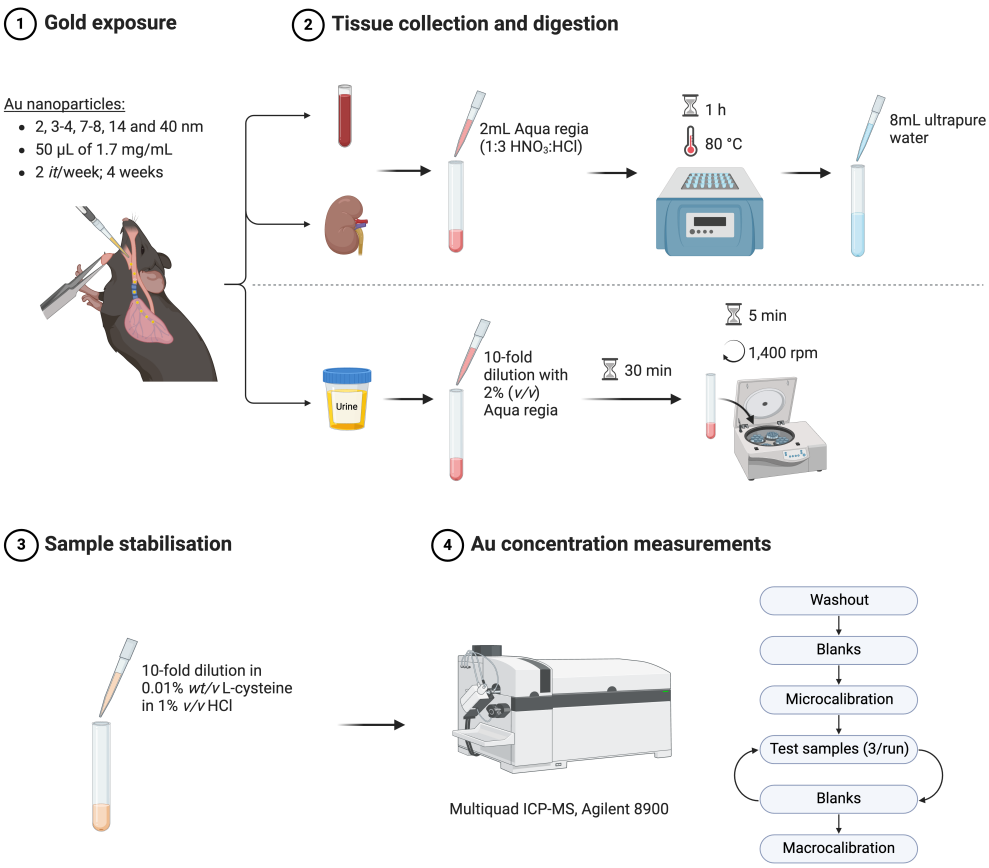

Figure 3.1: Study design for gold nanoparticles translocation experiment. Healthy mice were administered gold (Au) nanoparticles (50 µL of 1.7 mg/mL, total of 680 µg) of various sizes (2, 3–4, 7–8, 14 and 40 nm diameter) via pulmonary instillation (*it*) twice weekly for 4 consecutive weeks. Mice were culled ~18 h after last *it* and whole blood, kidneys and urine were collected. Tissues were digested and Au concentration measured using multi quadrupole inductively coupled plasma mass spectrometer. Figure created by the author using BioRender.

To investigate the impact of nanoparticle translocation to the blood on vascular function, a proof-of-concept experiment was conducted by directly applying DEP to isolated renal arteries, followed by vascular function assessment using wire myography. Renal arteries from healthy mice were tested for their responsiveness to phenylephrine (PE)-an adrenergic receptor agonist, acetylcholine (ACh)-an endothelium-dependent vasodilator and sodium nitroprusside (SNP)-an endothelium-independent vasodilator. The potential of superoxide dismutase (SOD) to mitigate DEP-induced vascular effects was also evaluated.

3.2 Methods

Each procedure performed in this chapter is detailed in the main Materials and Methods chapter. All animal experiments in this chapter were performed on healthy, adult, male C57BL/6J mice, aged 8–10 weeks at the start of each study and maintained under controlled conditions, further detailed in Section 2.1.

3.2.1 Gold nanoparticles administration

Mice were split into 6 groups and administered gold nanoparticles of various sizes (2, 3–4, 7–8, 14 and 40 nm-citrate coated) or citrate (vehicle) directly to the lungs using the instillation/inhalation method (detailed in Section 2.2.2). Particles were diluted to a final concentration of 1.7 mg/mL and were sonicated and vortexed immediately prior to administration to minimise aggregation. Briefly, mice were placed under transient isoflurane anaesthesia and, following assessment of anaesthesia level, were placed supine on an angled board. Nanoparticle suspension was gently positioned at the base of the tongue as to be inhaled as the anaesthesia wore off. Particles were administered at a maximum frequency of once every 72 h. Mice were culled ~18 h after the last 8^{th} instillation by terminal anaesthesia with *ip* injection of Dolethal. After assessment of mouse consciousness, blood was collected by cardiac puncture, kidneys were isolated with the capsule removed and urine was collected from the bladder. All tissues were stored at -80°C until further processing.

3.2.2 ICP-MS

All sample digestion and measurement of gold (Au) concentration using inductively coupled plasma mass spectrometry (ICP-MS) were performed by Dr Gavin Sim and Dr Lorna Eades from the School of Chemistry at The University of Edinburgh. Blood or whole kidneys were placed in disposable borosilicate tubes and digested in 2 mL aqua regia at 80°C for 1 h on a block heater. Following digestion, 8 mL of ultrapure water was added to reach a final volume of 10 mL. For each digestion batch, two reagent blanks were also added. Urine samples were directly diluted with 2% (v/v) aqua regia

by a factor of 10, left for 30 min and centrifuged for 5 min at 1,400 rpm to remove debris. To further stabilise the gold during analysis and aid washout, immediately prior to analysis all samples were further diluted by a factor of 10 with a solution of 0.01% L-cysteine in 1% v/v HCl. Gold concentration in all samples was measured using a multi quadrupole inductively coupled plasma mass spectrometer (see Section 2.10).

3.2.3 Assessment of vascular function following *in vitro* application of DEP: wire myography

To assess vascular function under isometric experimental conditions, wire myography was performed on renal arteries. In this study, the wire myograph 610 M system of Danish Myo Technology (DMT) was used.

Renal artery isolation and mounting

Healthy, untreated mice were culled by an *ip* injection of Dolethal and the kidneys with the intact vasculature connected to the abdominal aorta were isolated and placed in ice-cold PSS. Both kidneys and the top and bottom ends of the abdominal aorta were pinned down on a silicone-coated petri dish containing ice-cold PSS and vessels were cleaned of PVAT.

The wire myograph consists of 4 baths and each bath has gas supply and aspirators to remove solutions. Each bath was filled with 6 mL of PSS, warmed to 37°C and supplied with gas of 95% O_2 and 5% CO_2. Dissected renal arteries were transferred to the baths and cut into rings of 1–2 mm in length. Under a microscope each renal artery was mounted onto a myograph by passing a fine 40 µm wide stainless steel wire through the vessel lumen. The wire ends were stabilised by the screws and baths returned to the myograph.

Normalisation of vascular tension

Normalisation of vascular tension is a key step in the wire myography protocol which aims to determine the internal vessel circumference which produces the

maximal isometric contractility. Vascular reactivity depends on the initial vessel tension, hence normalisation is an essential step for the accurate comparison of drug effects and reproducibility of results.

Normalisation was performed using the DMT Normalisation Module on LabChart, which involves testing the length/tension relationship for each vessel. Vessel length was determined using a scale incorporated in the microscope eyepiece. To set the vessel tension, the micrometer dial, separating the myograph jaws, was turned in increments of 2 mN each time. For every increase in force, the distance between the jaws was measured until the vessel reached a maximum of 13.3 kPa, which corresponds to an intramural pressure of 100 mmHg. The length/tension graph produced was used to determine the optimal internal circumference (IC_1) for each vessel to produce maximal vascular reactivity. The jaws were then adjusted to correspond to the IC_1, at which the vessels remained for the rest of the experiment. Vessels were left to equilibrate for 30 min.

Vascular reactivity protocol

Viability of renal arteries was tested by bathing vessels in high potassium PSS (KPSS) to induce a maximal contractile response. Once the concentration response curve peaked and plateaued, baths were emptied, the vessels washed three times with warm PSS and left to equilibrate for 20 min. This process was repeated three times.

To assess vascular reactivity, vessels were treated with the adrenergic-dependent vascular contraction agent phenylephrine (PE), the endothelial-dependent vasodilator acetylcholine (ACh) and the endothelial-independent vasodilator sodium nitroprusside (SNP). For vasodilation, arteries were preconstricted by PE incubation at a dose that would induce ~80% of the maximal contraction. Prior to administration of each drug, arteries were pretreated with either DEP alone or combined DEP+SOD (vessels in the control group were pretreated with equal volume of PSS). For this, a fresh suspension of DEP in PSS was prepared each day, vortexed and sonicated to ensure particle dispersion and added to the myograph bath at a concentration of 30 µg/mL [123]. SOD was

dissolved in PSS and added to the myograph bath at a concentration of 100 U/mL. A ≥20 min period was allowed between DEP/DEP+SOD administration and addition of any vaso-active agent. Following each drug administration vessels were washed with PSS until they reached baseline tension and left for ≥30 min washout period before treatment with subsequent drugs. A diagram with the protocol details is presented in Figure 2.7.

3.3 Results

3.3.1 Inhaled gold nanoparticles translocate and sequester in the kidney

Gold was detected in whole blood in a size-dependent manner (Figure 3.2A)-the smaller the particle size administered, the greater the gold concentration in the blood (2 nm $p \leq 0.0001$, 3–4 nm $p \leq 0.001$). Although concentrations were lower, a similar dependency was observed in the urine ($p \leq 0.0001$) (Figure 3.2C). Gold nanoparticles were also detected in the kidney (2 nm $p \leq 0.0001$, 3–4 nm $p \leq 0.01$) (Figure 3.2B). In all tissues, gold concentration from groups administered 2 nm and 3–4 nm-sized particles was significantly higher compared to that in vehicle-treated control animals (Figure 3.2).

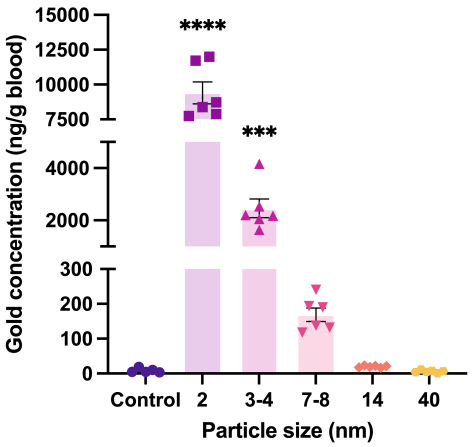

(A) Blood

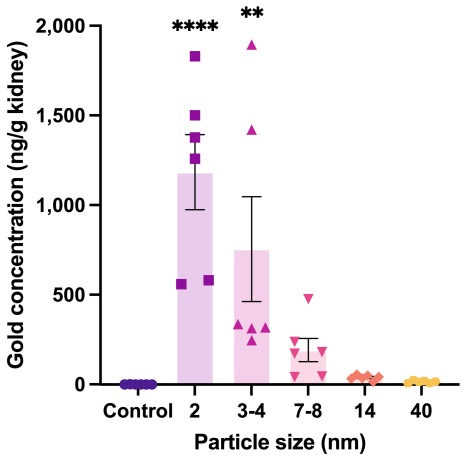

(B) Kidney

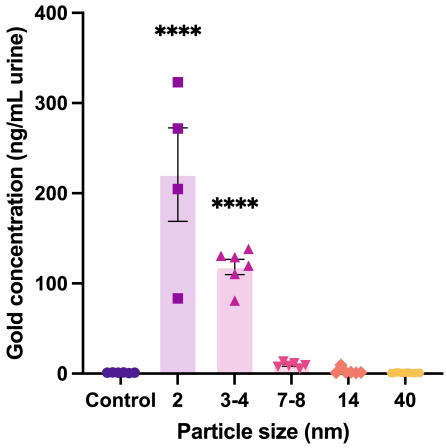

(C) Urine

Figure 3.2: Gold nanoparticles concentration in mouse tissues following pulmonary instillation. Mice were instilled with gold nanoparticles of various sizes (2 instillations/week for 4 consecutive weeks, 50 µL, 1.7 mg/mL) and gold concentration was measured in (**A**) blood, (**B**) kidney and (**C**) urine using ICP-MS (each dot represents an animal). Data presented as Mean ± SEM (n=6 except control blood n=5 and 2 nm urine n=4). **$p \leq 0.01$, ***$p \leq 0.001$, ****$p \leq 0.0001$ compared to control (ordinary One-way ANOVA with Dunnett's multiple comparisons test).

3.3.2 *In vitro* application of DEP impairs nitric oxide-dependent vasodilation in renal arteries

After confirming that inhaled nanoparticles can be transported via the circulation to the kidney and accumulate there (Section 3.3.1), we sought to examine the effects of these translocated particles on vascular function. In this proof-of-concept experiment, DEP was directly applied to isolated vessels to simulate translocation.

To investigate the effects of *in vitro* application of DEP on vascular function, renal artery grafts from healthy mice were assessed for their reactivity to phenylephrine (PE)-an adrenergic receptor agonist, acetylcholine (ACh)-an endothelium-dependent vasodilator and sodium nitroprusside (SNP)-an endothelium-independent vasodilator. The potential of SOD to reverse DEP-induced vascular effects was also evaluated. Renal artery vasoconstriction in response to high potassium physiological salt solution (KPSS) was measured at the start of the protocol as a marker of vessel viability post-mounting, with no significant difference in maximal constriction observed across all groups (Figure 3.3).

Dose-response curves were generated for each vasoactive drug and non-linear regression was used to calculate EC_{50} values (the concentration required to induce 50% maximal response) to assess vessel sensitivity. These curves and graphs with EC_{50} values are presented in Figure 3.4, with statistical analysis results summarised in Table 3.1.

Dose-response curves for PE showed no differences among the three groups and EC_{50} values were similar across treatments (Figure 3.4A and 3.4B). Although DEP treatment did not significantly alter vessel response to ACh (Figure 3.4C), a rightward shift in the dose-response curve and a slightly higher mean EC_{50} were observed in the DEP group compared to controls, though this was not statistically significant (p=0.5733; Figure 3.4D). Dose-response curve for SNP suggested a DEP-induced slight impairment in vasodilation at SNP concentrations of 10 nM and 30 nM, similar to the observations in the DEP+SOD group at 30 nM and 100 nM (Figure 3.4E). DEP administration significantly increased SNP EC_{50} compared to

control (p=0.0173; Figure 3.4F).

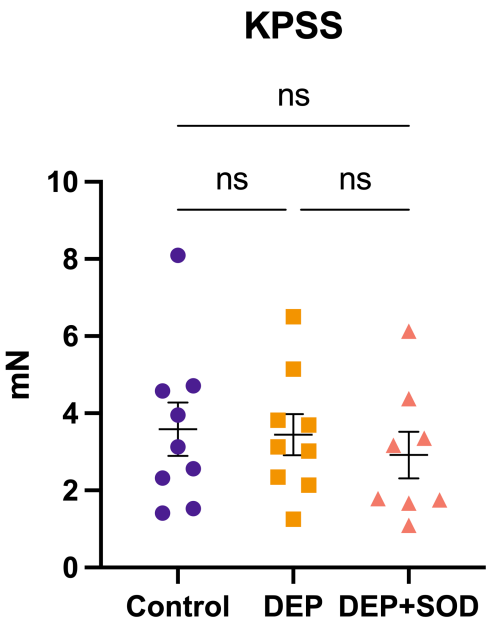

Figure 3.3: Assessment of renal arteries constriction by KPSS prior to treatment with DEP/DEP+SOD *in vitro*. Renal arteries from healthy, untreated mice were isolated and mounted on a wire myograph. Vessel viability was assessed by measuring constriction in response to potassium-induced depolarisation (KPSS-high potassium physiological salt solution). Measurements were made prior to treatment with DE/DEP+SOD. Each dot represents an animal. Data presented as Mean ± SEM; ns-not significant (ordinary One-way ANOVA followed by Tukey's multiple comparisons test).

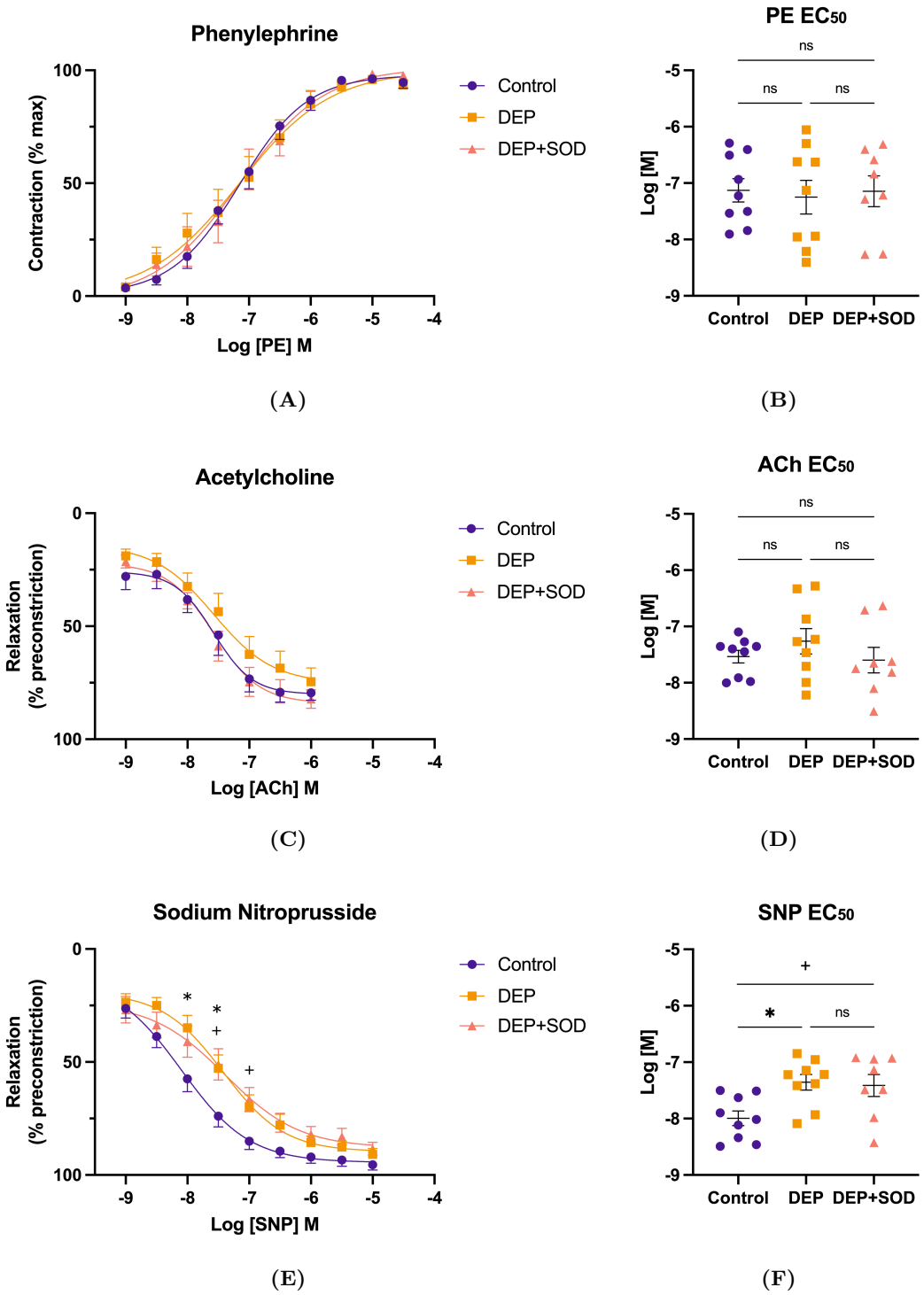

Figure 3.4: Effects of *in vitro* DEP application on renal artery vascular function. Renal arteries from healthy, untreated mice were isolated and vascular reactivity assessed by wire myography following treatment with phenylephrine (PE), acetylcholine (ACh) or sodium nitroprusside (SNP). Prior to each drug administration, vessels were treated with diesel exhaust particles alone (DEP, 30 µg/mL) or combined with superoxide dismutase (SOD, 100 U/mL). Untreated mice served as control. Each dot represents an animal. Data presented as Mean ± SEM. Comparisons control vs DEP are indicated by * and comparisons control vs DEP+SOD are indicated by $^{+}$; ns-not significant, $^{*/+}p \leq 0.05$ (Two-way ANOVA with Tukey's multiple comparisons test for dose-response curves and ordinary One-way ANOVA followed by Tukey's multiple comparisons test for calculation of EC_{50} values).

Drug	Source of Variation	% of total variation	P value	P value summary	EC_{50} P value	
PE	Drug dose × Treatment	0.3765	0.9564	ns	Con/DEP	0.9395
	Drug dose	82.96	<0.0001	****	Con/DEP+SOD	0.9989
	Treatment	0.005153	0.9924	ns	DEP/DEP+SOD	0.9572
ACh	Drug dose × Treatment	0.4788	0.9605	ns	Con/DEP	0.5733
	Drug dose	63.91	<0.0001	****	Con/DEP+SOD	0.9722
	Treatment	2.062	0.3236	ns	DEP/DEP+SOD	0.4573
SNP	Drug dose × Treatment	1.645	0.0006	***	Con/DEP	0.0173
	Drug dose	74.24	<0.0001	****	Con/DEP+SOD	0.0370
	Treatment	3.891	0.0458	*	DEP/DEP+SOD	0.9649

Table 3.1: Statistical analysis summary of the effects of DEP on renal artery vascular function *in vitro*. Renal arteries from healthy mice were isolated and treated with phenylephrine (PE), acetylcholine (ACh) or sodium nitroprusside (SNP) to assess vascular function using wire myography (Figure 3.4). Prior to each drug administration, vessels were treated with diesel exhaust particles (DEP) alone or in combination with superoxide dismutase (SOD). Untreated mice served as control (Con). Table summarises results from statistical analysis for dose-response curves (Two-way ANOVA with Tukey's multiple comparisons test) and EC_{50} values (ordinary One-way ANOVA followed by Tukey's multiple comparisons test). Text in red indicates statistical significance; ns-not significant, $^{*}p \leq 0.05$, $^{***}p \leq 0.001$, $^{****}p \leq 0.0001$.

3.4 Discussion

3.4.1 Particle translocation as a mechanism for the extrapulmonary effects of DEP

Several pathways have been proposed to elucidate the adverse extra-pulmonary health impacts attributed to air pollution (detailed in Section 1.2.5). These include (1) the activation of pulmonary macrophages following particle ingestion, leading to the subsequent release of inflammatory mediators into the circulation and (2) stimulation of alveolar sensory receptors by particulate matter and the subsequent activation of the central nervous system-this neuronal response modulates systemic organs through neural connections and altered release of neuroendocrine signals. The hypothesis that particles, particularly fine particles, could permeate the air-blood barrier and directly interact with systemic organs was introduced in the early 21st century. Significant progress has been made in this area through the demonstration of particle translocation and accumulation into the circulation and secondary target organs (STOs) using various labelled particles. Several factors can affect the distribution of particles in biological systems, such as size, with smaller particles exhibiting a higher propensity for translocation [167–171]. Surface charge can also influence distribution, however, conflicting findings have been reported in different studies regarding the relationship between particle charge and their translocation to specific organs [168, 170, 172]. Upon introduction into physiological fluids, nanoparticles adsorb proteins, resulting in the formation of a protein corona (PC) [173]. This PC has the capability to alter particle identity and influence its activity and destination within the body-the PC formation itself depends on particle size and surface modifications [174]. While only small concentrations of nanoparticles enter the circulation and systemic organs (e.g. <1% of inhaled gold nanoparticles translocated from the lung into the circulation [175] and accumulation of 20 nm iridium particles in STOs estimated at 1–2% of the deposited dose at 24 h after administration [171]), adverse effects could potentially arise from prolonged accumulation (such as cumulative exposure to air pollution over a lifetime) or if particles aggregate in more

susceptible tissue areas, such as those affected by disease [138].

Several studies in rodents have shown the movement of particles to the kidney, using different types of particles (such as gold or radiolabeled iridium) and administered through intratracheal instillation or inhalation/ventilation, mostly falling within the size range of 15–200 nm [171, 176–178]. Our study aimed to expand upon these previous findings by concentrating on the primary (single) size of particles within the range of renal pore sizes. In the kidney, the glomerulus acts as a specialised filtration unit responsible for removing waste products, including nanoparticles, from the blood. Different methods have yielded various estimates of pore size, but most studies indicate that the majority of pores have a median diameter of ~4–6 nm, with a smaller subset having diameters up to ~14 nm [179–181]. The glomerular filtration apparatus is generally considered to have a cutoff size of 6–8 nm [182, 183]. While our study did not aim to directly measure pore size, our results align with existing estimates of glomerular pore size, as evidenced by the higher excretion of sub-7 nm particles and the lower excretion of larger particles (14 nm, with almost no detectable 40 nm particles) in urine samples. This inverse relationship between particle size and their concentration in the kidney is consistent with findings reported by other research groups. For instance, analysis of rat renal tissue following exposure to gold nanoparticles showed a higher proportion of 1.4 nm compared to 18 nm particles 24 h post-administration. Interestingly, accumulation in the kidney was more significant when particles were administered intravenously compared to intratracheally [169]. Studies indicate that NP translocation to STOs peaks at 7 days post-exposure [178], with particles still detectable in the kidneys up to 6 months later [184]. While size is an important determinant in glomerular filtration, other aspects are also crucial, including molecular shape, charge and glomerular permeability, influenced by factors such as inflammation or disease.

As mostly smaller nanoparticles were translocated to the circulation (2 and 3–4 nm), our findings showed a similar size dependency for the kidney and the urine. Although excretion to the urine is a potential mechanism for particle clearance from

the blood, nanoparticles still accumulate in the kidney. These results suggest that nanoparticles may penetrate into renal tissue as opposed to accumulation only of those too large to pass through the glomerulus. To further explore this phenomenon, analysis of renal tissue with transmission electron microscopy (TEM) and Raman spectroscopy could be employed to examine whether nanoparticles exhibit preferential deposition within specific renal regions and whether such deposition is size-dependent. Previous investigations conducted by our group have demonstrated the deposition of gold nanoparticles within sites of vascular pathology in ApoE$^{-/-}$ mice [138]. Future studies could extend this to the kidney, wherein animals with pre-existing renal injury could be administered gold nanoparticles of varying sizes, with subsequent evaluation of particle translocation using the aforementioned methodologies.

3.4.2 The effects of *in vitro* application of DEP on vascular function of mouse renal artery

The conventional pathway for the extrapulmonary effects of particulate matter in air pollution holds that inhaled particles trigger a local inflammatory response in the lungs, which then leads to the release of inflammatory cytokines into the systemic circulation (Section 1.2.5). In contrast, using gold nanoparticles, our study demonstrated that inhaled nano-sized particles can cross the alveolar-capillary barrier and travel through the bloodstream to reach distant organs like the kidneys, where they may exert direct harmful effects (Section 3.3.1). If DEP enters the circulation, does it have the capacity to directly impair renal artery function? To address this question, we conducted a proof-of-concept experiment in which isolated mouse renal arteries were incubated with the well-characterised DEP SRM 2975 and vascular reactivity to PE, ACh and SNP was evaluated using wire myography. The capacity of SOD in counteracting DEP-induced changes was assessed by co-incubating SOD with DEP.

Our results indicated that *in vitro* application of DEP did not alter renal artery sensitivity to PE. However, DEP caused a rightward shift in the ACh

concentration-response curve and a trend toward elevated EC_{50} compared to controls, though these changes did not reach statistical significance. Co-incubation with SOD showed a partial reversal of these effects. In contrast, DEP significantly reduced SNP-induced vasorelaxation, as demonstrated by a marked rightward shift in the dose-response curve and a significantly increased EC_{50}. This inhibitory effect on SNP-induced relaxation was not reversed by SOD. These findings suggest that DEP can directly impair renal artery function, potentially through disruption of the NO signalling pathway, without requiring prior interaction with lung tissue and independent of lung-mediated inflammatory responses.

The large surface area of nanoparticles in diesel exhaust allows for significant free radical generation, particularly oxygen-centred radicals such as O_2^-, as well-documented in previous studies [123, 185]. Prior research in our group used electron paramagnetic resonance (EPR) to demonstrate that a 60 min incubation of DEP suspension (10 µg/mL) significantly increased EPR signal intensity, indicating elevated free radical production compared to controls. This effect was notably diminished with co-incubation of SOD, suggesting that the free radicals generated were primarily O_2^- [123]. O_2^- readily reacts with NO, reducing its bioavailability while forming the cytotoxic compound peroxynitrite [186]. Furthermore, the study showed that NO concentrations from the NO donor 2-(N,N-diethylamino)-diazenolate-2-oxide (DEA/NO) were significantly lower in the presence of DEP, supporting the notion that DEP scavenges NO. These findings collectively indicate that DEP exposure induces the generation of oxygen-centred free radicals, which deplete NO and contribute to the inhibition of NO-mediated vascular relaxation [123]. The DEP-induced impairment of renal artery vascular function *in vitro* observed in the current study may be attributed to this mechanism.

Previous research in female wild type (WT) mice demonstrated that *in vitro* treatment of aortas with a lower dose of DEP (10 µg/mL) did not affect PE-induced constriction [187]. However, a higher DEP dose (100 µg/mL) significantly reduced contractility, as indicated by a decreased maximal response (E_{max}) without altering

EC_{50}. While DEP had no impact on SNP sensitivity, Hansen *et al.* observed a leftward shift in the ACh dose-response curve for both DEP doses, with no significant changes in EC_{50} but a significant increase in maximal relaxation only at the higher dose [187]. In rats, DEP incubation of thoracic aortas significantly impaired endothelium-dependent relaxation and modestly reduced SNP-induced relaxation at DEP doses as low as 10 µg/mL [123]. These findings have been corroborated in human studies, where diesel exhaust inhalation for 1 h during intermittent exercise significantly attenuated the increase in forearm blood flow in response to ACh and SNP infusions at 2 and 6 h post-exposure [116].

In this experiment a high concentration of DEP was used and its relevance to the vascular effects following pulmonary DEP exposure in mice has yet to be determined. However, the *in vitro* effects observed may not fully capture the extent of DEP's impact, as this model does not account for the heightened effects of free radicals, intensified by OS and compromised defences typically associated with DEP-induced inflammation *in vivo*. Nevertheless, the consistency of *in vitro* findings with those observed in human exposure studies [116, 185] indicates that these *in vitro* methods provide a useful preliminary assessment of the vascular effects of DEP *in vivo*.

3.4.3 Chapter summary

In this study, gold nanoparticles were employed as a model for ultrafine particles to explore the translocation pathway as an underlying mechanism for the adverse systemic health effects associated with particulate matter exposure. Having identified the kidney as a potential target for nanoparticle accumulation, our investigation shifted towards assessing the impact of diesel exhaust particles on renal vascular function in healthy mice *in vitro*. In summary, the main findings of this chapter are:

- Gold was detected in whole blood, urine and kidney in a size-dependent manner with a cutoff particle diameter of <7 nm.
- *In vitro* application of DEP to renal arteries from healthy mice had no effect on sensitivity to PE. DEP reduced sensitivity to ACh-induced vasorelaxation, with a minor but non-significant increase in EC_{50} values. DEP significantly impaired endothelium-independent vasodilation and increased EC_{50} values. Co-incubation with SOD did not affect SNP-induced changes but reversed the DEP-induced impairment in ACh sensitivity.

Chapter 4

The effects of acute DEP exposure on the kidney

4.1 Introduction

Results from Chapter 3 demonstrated the potential of inhaled nanoparticles to cross the alveolar-capillary barrier, enter the circulation and sequester in the kidney. Furthermore, the capacity of translocated DEP to cause vascular impairment was demonstrated by applying DEP directly to renal arteries of healthy mice *in vitro*. Next, we aimed to investigate the impact of nanoparticles on renal injury and inflammation in healthy mice following a single DEP exposure.

4.1.1 Hypothesis and aims

The hypothesis explored in this chapter is:

Acute exposure to DEP induces kidney damage through effects on renal inflammation and markers of kidney injury.

Aims:

1. Evaluate pulmonary and systemic inflammation following acute DEP exposure.
2. Determine the effects of acute pulmonary DEP exposure on markers of kidney injury and inflammation.

4.1.2 Study design

To examine the effects of acute DEP exposure on markers of kidney injury, two experiments were performed. In the first one, mice were given a single dose of DEP (35 µg), culled ~18 h later and tissues collected. BALF was collected for pulmonary inflammation measurements, blood was collected for analysis of systemic inflammation and kidneys were harvested to quantify markers indicative of renal injury and inflammation (see Figure 4.1A). In the second experiment mice were administered a higher dose of DEP-50 µg and culled either 6 h or 16 h after instillation. Tissues were collected and analysed for markers of pulmonary, systemic and renal inflammation and kidney injury (see Section 4.2 for methodological details).

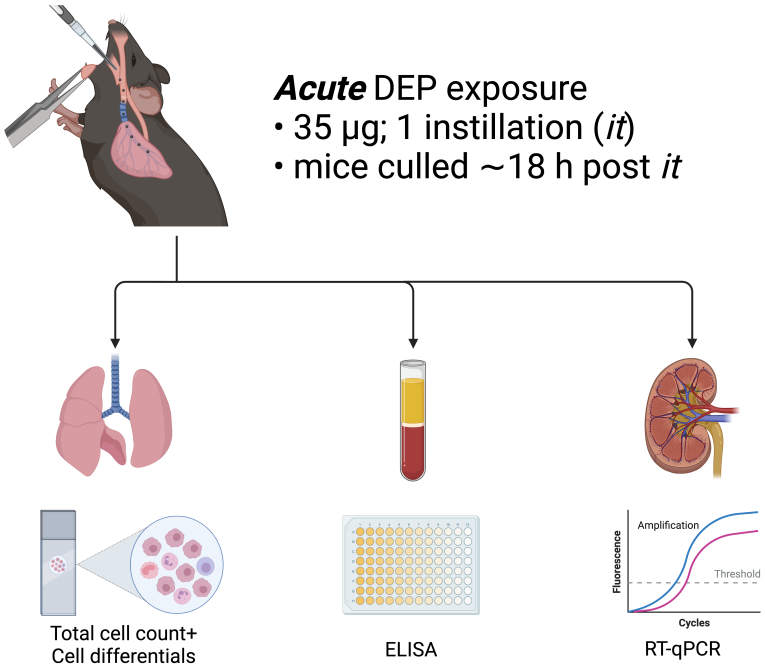

(A)

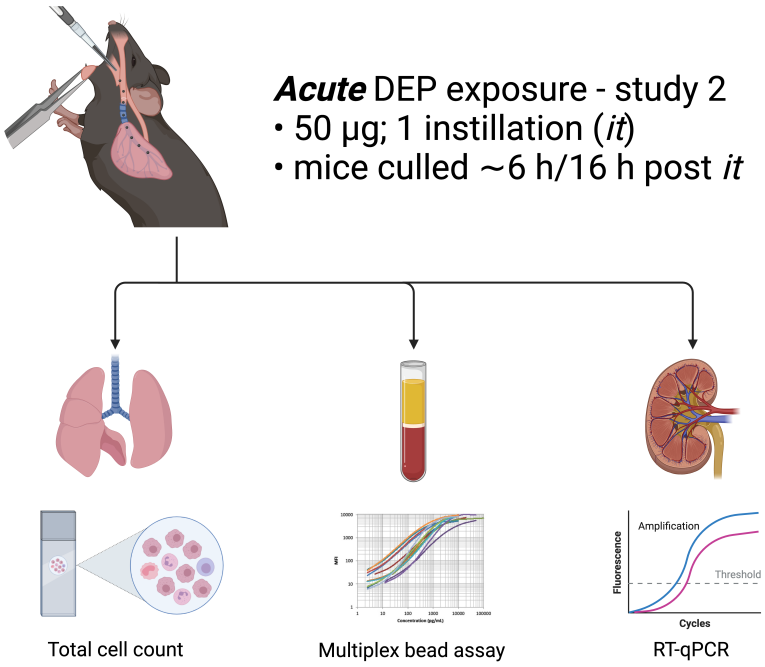

(B)

Figure 4.1: Study designs for acute DEP exposure experiments. Healthy mice were administered either (**A**) a single dose of diesel exhaust particles (DEP, 35 µg) and culled ~18 h after exposure or (**B**) a single dose of DEP (50 µg) and culled ~6 h or 16 h after exposure. Tissues were collected for measurement of DEP-induced effects on markers of pulmonary, systemic and renal inflammation and injury. Figure created by the author using BioRender.

4.2 Methods

Each procedure performed in this chapter is detailed in the main Materials and Methods chapter. All animal experiments in this chapter were performed on healthy, adult, male C57BL/6J mice, aged 8–10 weeks at the start of each study and maintained under controlled conditions, further detailed in Section 2.1.

4.2.1 DEP administration

DEP (SRM 2975, NIST) was suspended in sterile saline (0.9% NaCl) at a concentration of 1 mg/mL and was always sonicated and vortexed prior to administration to avoid particle aggregation. Mice were administered DEP at a single dose of either 35 µg or 50 µg using the instillation/aspiration method. Briefly, mice were placed under transient isoflurane anaesthesia and following assessment of anaesthesia level, were placed supine on an angled board. DEP suspension was gently positioned at the base of the tongue as to be inhaled as the anaesthesia wore off. Control group received sterile saline. This procedure is detailed in Section 2.2.1.

4.2.2 BALF measurements

BALF collection

To assess pulmonary inflammation in mice following DEP exposure, BALF was collected by lavaging the lungs three times with 0.9% NaCl. Primary lavage was kept separate, secondary and tertiary lavages were combined, now referred to as secondary lavage. BALF was centrifuged, cell pellet from primary lavage was resuspended in 1% BSA and combined with suspension from secondary lavage by gentle pipetting (see Section 2.3.1).

Total cell count

For each sample, 50 µL of cell suspension was mixed with equal volumes of lysis buffer and stabilising buffer, sample was drawn up a NucleoCassette™ and total cell count was established using a NucleoCounter™ (see Section 2.3.2).

Cell differential counts

For each sample, a glass slide was inserted into a metal cassette, a filter card placed on top of the slide and finally a cytofunnel on top of the filter card.

Based on the total cell count, for each sample the volume corresponding to 40,000 cells was mixed with 1% BSA to reach a final volume of 300 µL. This suspension was pipetted into the cytofunnels, cassettes were centrifuged, slides were left to dry, followed by Diff-Quik staining.

Immune cells from BALF were stained using the Diff-Quik method by dipping the slides into each solution for 30 sec before moving to the next one. Steps were as follows: 100% methanol (for fixing cells), red stain (Eosin G in phosphate buffer), blue stain (Thiazine dye in phosphate buffer) and distilled water. BALF cell differential counts were conducted by manually enumerating and classifying approximately 200 cells per sample into their respective cell types. Data for each cell type are presented as (1) percentage of total number of cells counted manually and (2) the absolute number of cells from each cell type in the lung lavage by referring back to the original total cell count obtained by the nucleocounter. A detailed description of this protocol is outlined in Section 2.3.3 and a diagram of BALF processing is presented in Figure 2.2.

4.2.3 Measurement of plasma IL-6 levels

Mice were culled ~18 h after DEP exposure by terminal anaesthesia with *ip* injection of Dolethal. After assessment of mouse consciousness, blood was collected by cardiac puncture (syringe was pre-coated with citrate 3.8%). Blood was placed in an EDTA-coated tube, centrifuged, plasma was separated and kept at -80°C for further analysis.

Systemic levels of IL-6 were measured using a commercial ELISA kit, following manufacturer's instructions. Briefly, an 8-point standard was prepared by making serial dilutions from the stock standard provided (500 pg/mL)-the final point being blank. A control sample provided in the kit was also included. Control sample and standards were run in technical duplicates, test samples were run in singles due to low plasma

volumes available. Each well was loaded with 50 µL of sample, control or standard, thoroughly mixed with an equal volume of Assay Diluent, and left to incubate for 2 h on a plate shaker. The plate was washed, conjugate added and incubated for 2 h. Plate was washed again, Substrate Solution added and incubated for 30 min at room temperature, protected from light. Reaction was terminated by adding a Stop Solution and the optical intensity of each well was immediately determined using a microplate reader. This procedure is detailed in Section 2.4.1.

4.2.4 Measuring mRNA levels in renal tissue by RT-qPCR

Tissue harvest

Mice were culled ~6 h, 16 h or 18 h after DEP exposure by terminal anaesthesia with *ip* injection of Dolethal. Kidneys were dissected and the capsule removed. The left kidney was cut longitudinally and one half further cut horizontally into two. A quarter of each kidney was placed in RNA*later*™ solution for 24 h at 4°C, then stored at -80°C for further processing.

RNA extraction

Immediately prior to RNA extraction the quarter of mouse kidney was split into cortex and medulla, placed in QIAzol™ lysis reagent and homogenised using a tissue lyser. RNA was isolated using a commercial kit following manufacturer's instructions and RNA concentration was quantified using a spectrophotometer (see Section 2.5.2).

RT-qPCR

cDNA was synthesised using a commercial kit and following manufacturer's instructions. Briefly, for each RT reaction an RNA extract volume corresponding to 2,000 ng of diluted RNA was mixed with enzyme mix and RT buffer. Negative controls were also included, where RT enzyme or RNA were replaced with an equal volume of water. Samples were reverse transcribed on a Thermal Cycler and the cDNA generated was stored at -20°C until further processing.

The cDNA generated from the RT reaction was amplified and quantified using qPCR. An 8-point standard curve was constructed by pooling an equal volume from each cDNA sample and performing a 1:4 dilution for the first point and serial 1:2 dilutions for points 2–7. The final point of the standard was used as a blank (nuclease-free water only). The remaining cDNA was diluted 1:40 (2.5 ng/µL) to fall within the middle of the standard curve. For each reaction (run in technical triplicates) cDNA was mixed with master mix. Negative controls, as described above, were also added. Reactions were run on a LightCycler instrument and quantification data were accepted if standard curve was satisfactory. Results were normalised against the average Cp value of the housekeeping gene GAPDH. Further details on the RT-qPCR protocol, master mix components, cycling conditions and primer sequences are outlined in Section 2.5.3.

4.2.5 Measurement of circulating cytokines using a multiplex assay

Mice were culled by terminal anaesthesia with an *ip* injection of Dolethal. Following assessment of mouse consciousness using the hind limb reflex test, blood was collected by cardiac puncture (syringe was pre-coated with citrate 3.8%), placed in an EDTA-coated tube and kept on ice. Within 30 min of collection, blood was centrifuged for 20 min at 1,000 × g, plasma was separated, placed in a fresh Eppendorf tube and stored at -80°C until further processing.

Cytokine levels were measured in plasma using the LEGENDplex™ Multi-Analyte Flow Assay Kit (Mouse Macrophage/Microglia Panel (13-plex); Biolegend®). Plasma samples were diluted 2-fold with Assay Buffer and run in singles. An 8-point standard curve was generated by making 1:4 serial dilutions from the stock standard provided (10,000 pg/mL). The final point of the standard was used as a blank (Assay Buffer only). Each standard was run in technical duplicates.

Samples were mixed with beads and either matrix C (for standards) or Assay Buffer (for plasma samples) and loaded onto a V-bottom 96-well plate. The samples and beads were mixed for 2 h at room temperature on a plate shaker, protected from light. Following incubation, the plate was centrifuged for 5 min and supernatant

discarded. The plate was washed by dispensing 200 µL Wash Buffer into each well, incubating it for 1 min, centrifuging again for 5 min and finally discarding the Wash Buffer. This wash step was repeated twice. Samples were then incubated with Detection Antibodies for 1 h at room temperature on a plate shaker, protected from light. Streptavidin-phycoerythrin (SA-PE) was then added directly and allowed to incubate with the samples for 30 min at room temperature on a plate shaker, protected from light. The plate was centrifuged, supernatant discarded and plate washed as previously described, forming a bead pellet at the bottom of the plate at the end. Finally, the beads were resuspended in Wash Buffer by gentle pipetting. Samples were then read on a flow cytometer. A diagram detailing the underlying assay principle is presented in Figure 2.3 and a more comprehensive procedural outline is provided in Section 2.4.2.

4.3 Results

4.3.1 Acute DEP exposure induces pulmonary inflammation through increase in BALF total cell count and neutrophil infiltration

Compared to controls, administration of a single dose of DEP produced a significant increase in total number of cells counted in BALF 18 h after instillation (Figure 4.2A). Performing differential analysis indicated this increase to be mainly due to a substantial rise in the number of neutrophils, as opposed to other inflammatory cell types, such as macrophages and lymphocytes (Figure 4.2B and 4.2C). Pulmonary cells identified as neutrophils rose from 1.1% in control animals to 11.5% in DEP-treated mice (Figure 4.2B). A representative image from cytospins of BALF cells is presented in Figure 4.2D which shows neutrophil infiltration following DEP exposure. Diesel particle accumulation on the surface of or within macrophages of the DEP group is highlighted in the enlarged inset.

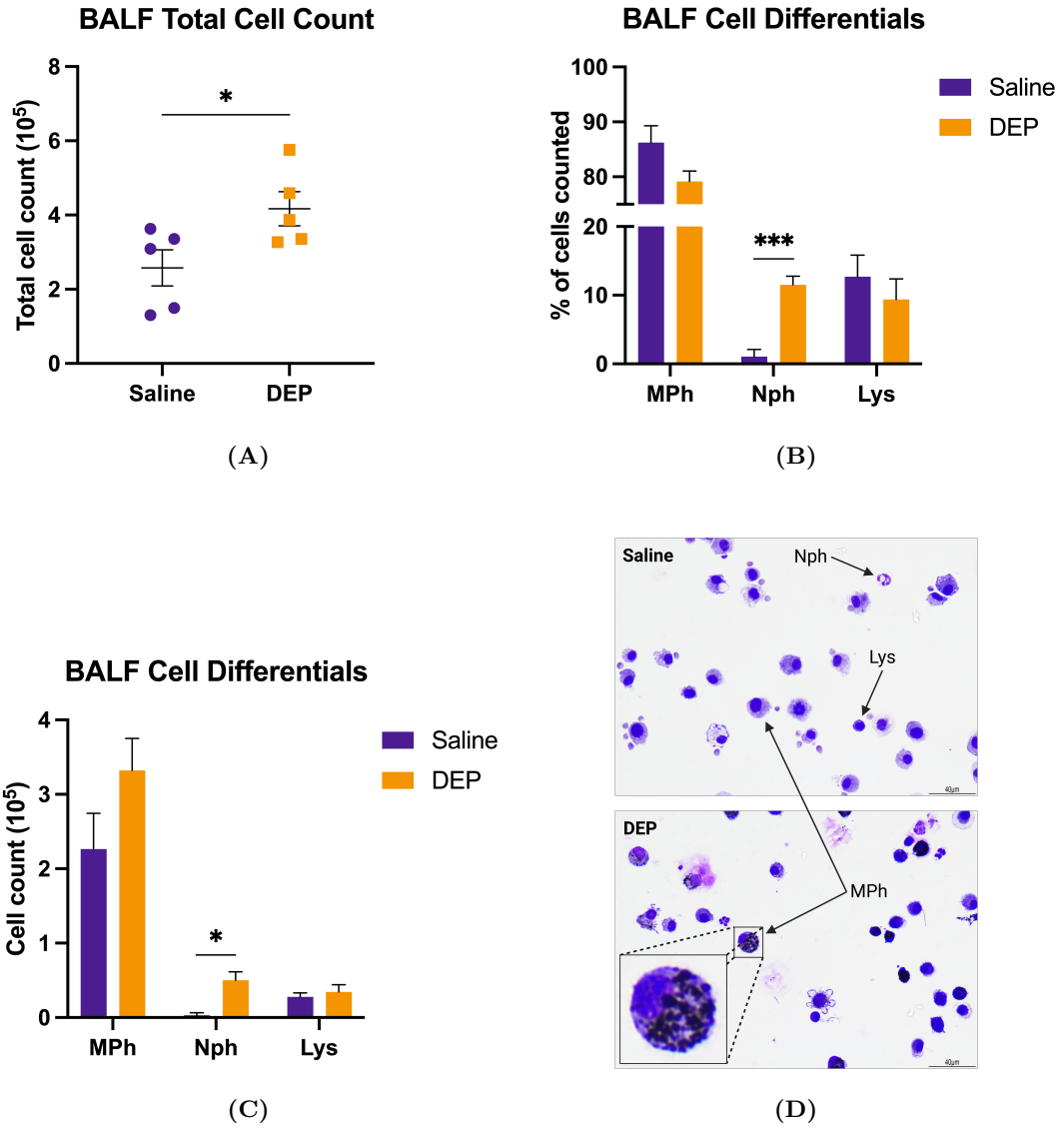

Figure 4.2: Effects of acute pulmonary DEP exposure on lung inflammation. Mice were administered a single dose of diesel exhaust particles (DEP, 35 µg) or saline (control) by pulmonary instillation. Mice were culled ~18 h after exposure, bronchoalveolar lavage fluid (BALF) collected and analysed for (**A**) total cell count and (**B**) cell differentials for each cell type presented as percentage of manually counted cells or (**C**) presented as the total number of each cell type by referring back to the original total cell count from the nucleocounter (n=5 mice/group). (**D**) Representative images of BALF inflammatory cells following Diff-Quik staining. Scale bar 40 µm. Inset highlights accumulation of DEP particles within and on the surface of macrophages. Data presented as Mean ± SEM; *p ≤0.05, ***p ≤0.001 (unpaired Student's t-test; Welch's correction was used where the t-test indicated significant difference in the variance of the two groups being compared). MPh-macrophages, Nph-neutrophils, Lys-lymphocytes.

4.3.2 Acute pulmonary DEP exposure does not elevate systemic IL-6 levels

Interleukin-6 (IL-6) levels were measured in mouse plasma as a marker of systemic inflammation (Figure 4.3). Data showed a slight but insignificant increase in plasma IL-6 levels following acute DEP exposure (mean levels 12.1 pg/mL and 15.6 pg/mL in control and DEP groups, respectively; p=0.6248).

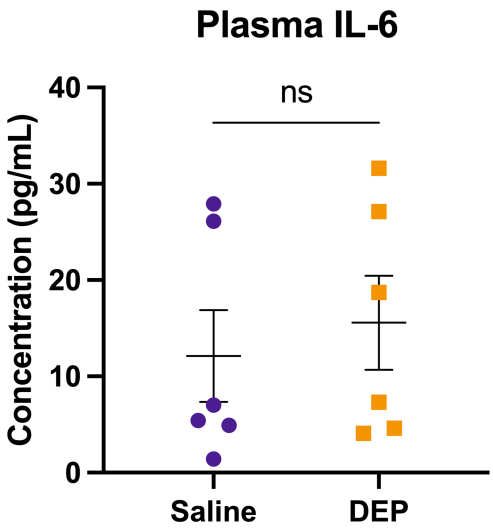

Figure 4.3: Effects of acute pulmonary DEP exposure on levels of circulating IL-6. Mice were administered a single dose of diesel exhaust particles (DEP, 35 µg) or saline (control) by pulmonary instillation. Mice were culled ~18 h after exposure, blood collected and plasma IL-6 levels measured using a commercial ELISA kit. Each dot represents an animal. Data presented as Mean ± SEM; ns-not significant (unpaired Student's t-test).

4.3.3 Acute DEP exposure does not induce *KIM-1* and *TNF-α* expression in the kidney

The effect of acute DEP exposure on kidney injury and inflammation was assessed through the quantification of kidney injury molecule-1 (*KIM-1*) and tumour necrosis factor-alpha (*TNF-α*) mRNA within renal tissue (Figure 4.4). *KIM-1* and *TNF-α* mRNA levels in both control and DEP-treated mice were significantly higher in the medulla compared to the cortex. Nevertheless, although treatment did not induce changes in renal *TNF-α* expression (Figure 4.4B), exposure to DEP resulted in a statistically significant reduction in *KIM-1* expression within both the cortex (p=0.0006) and the medulla (p=0.0172; Figure 4.4A). Raw cycle threshold (Ct) values for each gene and treatment group are presented in Table 4.1.

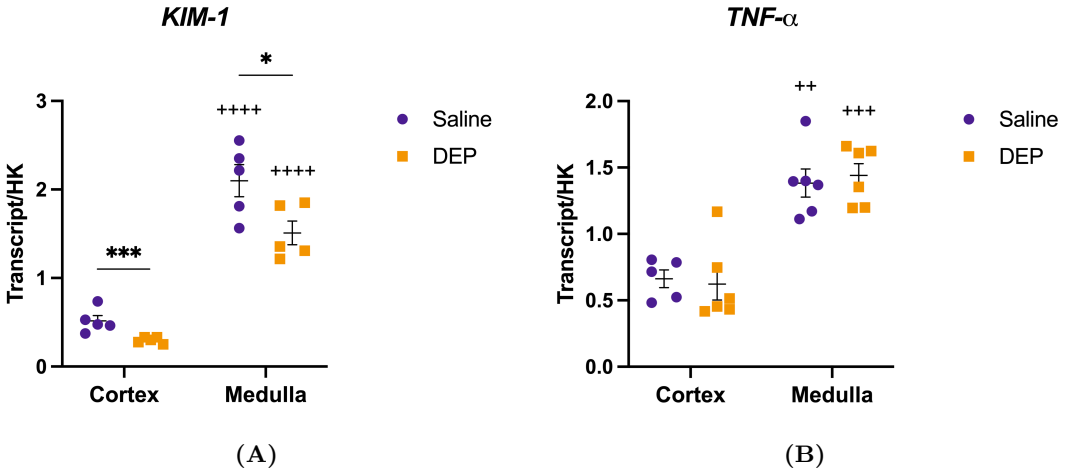

Figure 4.4: Effects of acute pulmonary DEP exposure on transcript levels of biomarkers of kidney injury and inflammation. Mice were administered a single dose of diesel exhaust particles (DEP, 35 µg) or saline (control) by pulmonary instillation. Mice were culled ~18 h after exposure, kidneys collected and renal mRNA levels of (**A**) kidney injury molecule-1 (*KIM-1*) and (**B**) tomour necrosis factor-alpha (*TNF-α*) were measured by RT-qPCR (each dot indicates an animal). Results are normalised to the housekeeping (HK) gene glyceraldehyde 3-phosphate dehydrogenase (GAPDH) and data presented as Mean ± SEM. Comparisons between treatment groups within the same kidney region are indicated by *, whereas comparisons between kidney regions within the same treatment group are indicated by $^{+}$; $^{*}/^{+}p \leq 0.05$, $^{**}/^{++}p \leq 0.01$, $^{***}/^{+++}p \leq 0.001$, $^{****}/^{++++}p \leq 0.0001$ (Two-way ANOVA with a mixed-effects model fitted on log-transformed data).

		Saline	DEP
GAPDH	Cortex	20.98 ± 0.15	20.69 ± 0.16
	Medulla	22.06 ± 0.11	22.16 ± 0.11
KIM-1	Cortex	31.23 ± 0.24	31.52 ± 0.16
	Medulla	30.27 ± 0.15	31.04 ± 0.11
TNF-α	Cortex	34.83 ± 0.17	34.70 ± 0.12
	Medulla	34.91 ± 0.06	34.96 ± 0.05

Table 4.1: Raw Ct values of renal transcript levels following acute DEP exposure: study 1. Mice were administered a single dose of diesel exhaust particles (DEP, 35 µg) or saline (control) by pulmonary instillation. Mice were culled ~18 h after exposure, kidneys collected and renal mRNA levels of kidney injury molecule-1 (*KIM-1*) and tomour necrosis factor-alpha (*TNF-α*) were measured by RT-qPCR (glyceraldehyde 3-phosphate dehydrogenase (*GAPDH*) served as housekeeping gene). Raw cycle threshold (Ct) values for each treatment group are presented as Mean ± SEM.

4.3.4 Acute DEP exposure does not increase BALF total cell count within 16 h post exposure

To further examine the effects of acute DEP exposure on inflammation and markers of kidney damage, a follow-up experiment was conducted. Mice were administered a higher dose of 50 µg DEP (or saline) and culled after ~6 h or 16 h later. Results revealed no significant difference in BALF total cell count between the DEP-exposed and control group 6 h after instillation (Figure 4.5). Although a marginal increase in TCC was observed in DEP-treated mice compared to controls at the 16 h mark, this discrepancy did not attain statistical significance (p=0.1058). While in DEP-exposed mice TCC values at 6 h and 16 h post-instillation were comparable, control animals exhibited a significantly lower count at the 16 h time point (p=0.0159).

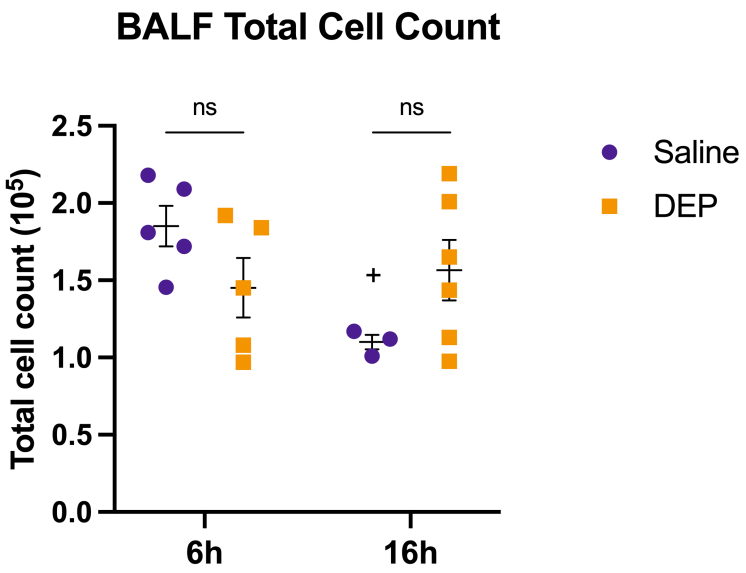

Figure 4.5: Effects of acute pulmonary DEP exposure on BALF total cell count. Mice were administered a single dose of diesel exhaust particles (DEP, 50 µg) or saline (control) by pulmonary instillation and culled ~6 h or 16 h after exposure. Bronchoalveolar lavage fluid (BALF) was collected and total cell count measured. Each dot represents an animal. Data presented as Mean ± SEM; ns-not significant, $^{+}p \leq 0.05$ (comparison between time points within the same treatment group; Two-way ANOVA with a mixed-effects model fitted on log-transformed data).

4.3.5 Acute DEP exposure induces early increases in systemic IL-18 and CCL22 levels

To construct a more comprehensive understanding of the inflammatory state within the systemic circulation after acute DEP exposure, levels of inflammatory markers were quantified in mouse plasma (Figure 4.6). Results revealed concentrations for the pro-inflammatory cytokines IL-23 (Figure 4.6C), IL-12p70 (Figure 4.6E) and IL-1β (Figure 4.6G) to mostly be at the limit of detection (LOD=0.24 pg/mL). No statistically significant disparities were observed either between treatment groups within the same time point or between different time points for the same treatment. At 6 h post exposure, concentrations of both CXCL (KC) (Figure 4.6A) and G-CSF (Figure 4.6F) exhibited similarity between DEP and control groups. However, at 16 h there was a marginal but statistically insignificant increase in these cytokines in DEP-exposed mice compared to controls. At 6 h post exposure a notable rise in levels of the pro-inflammatory cytokine IL-18 and anti-inflammatory cytokine MDC was detected in the DEP group (p=0.0007 and p=0.0017, respectively; Figure 4.6B and Figure 4.6D). A comparable trend was observed at 16 h for both markers, although it did not attain statistical significance. Additionally, there was a substantial increase in MDC levels for DEP 16 h compared to DEP 6 h post-exposure (p=0.0069).

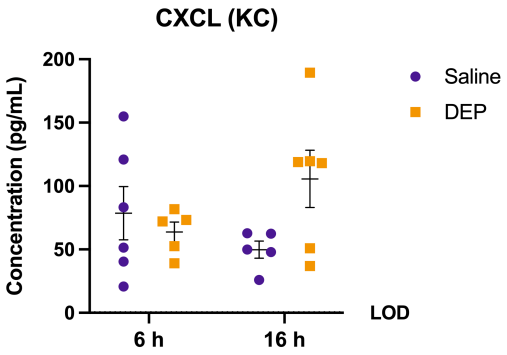
CXCL (KC)
Concentration (pg/mL)
200
150
100
50
0
6 h
16 h
LOD
Saline
DEP

(A)

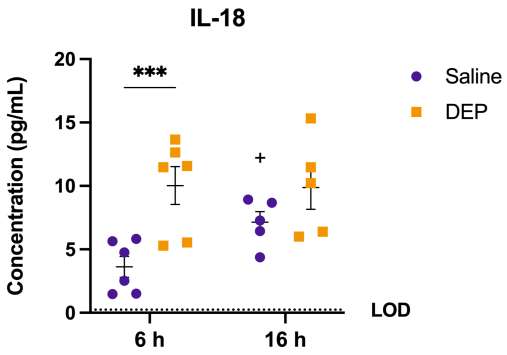
IL-18
Concentration (pg/mL)
20
15
10
5
0
***
+
6 h
16 h
LOD
Saline
DEP

(B)

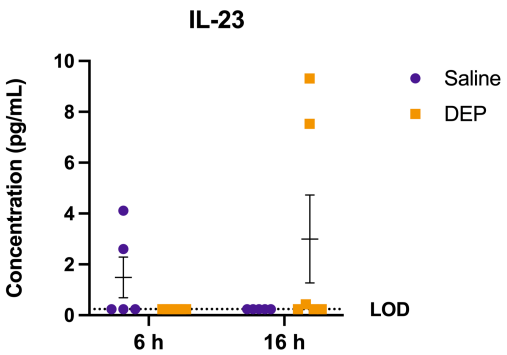
IL-23
Concentration (pg/mL)
10
8
6
4
2
0
6 h
16 h
LOD
Saline
DEP

(C)

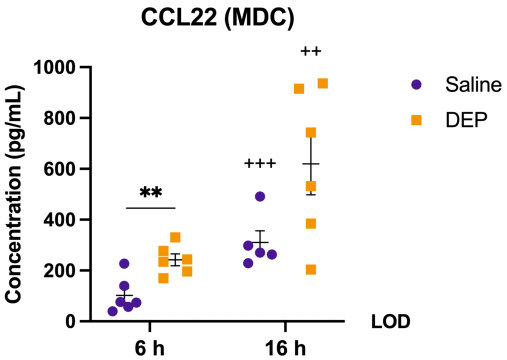
CCL22 (MDC)
Concentration (pg/mL)
1000
800
600
400
200
0
**
+++
++
6 h
16 h
LOD
Saline
DEP

(D)

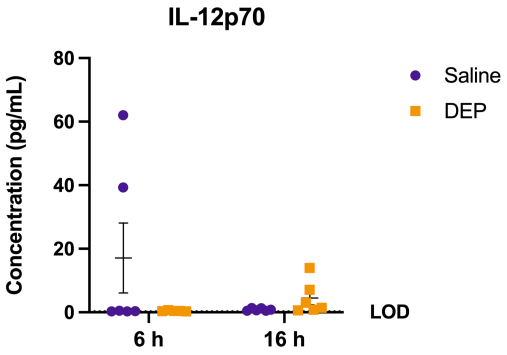
IL-12p70
Concentration (pg/mL)
80
60
40
20
0
6 h
16 h
LOD
Saline
DEP

(E)

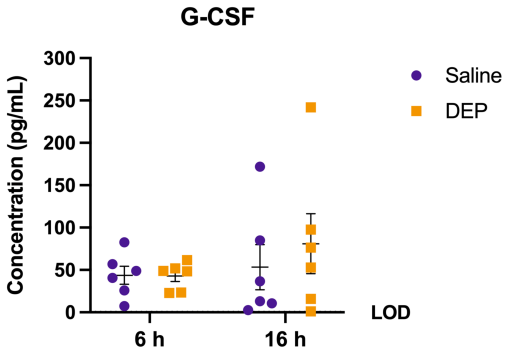
G-CSF
Concentration (pg/mL)
300
250
200
150
100
50
0
6 h
16 h
LOD
Saline
DEP

(F)

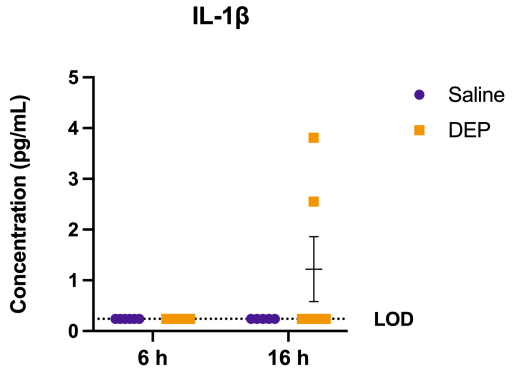

(G)

Figure 4.6: Effects of acute pulmonary DEP exposure on markers of systemic inflammation in mouse plasma. Mice were administered a single dose of diesel exhaust particles (DEP, 50 µg) or saline (control) by pulmonary instillation and culled ~6 h or 16 h after exposure. Blood was collected by cardiac puncture, centrifuged and levels of various markers of systemic inflammation measured in plasma using a multiplex bead assay. Each dot represents an animal. Data presented as Mean ± SEM. Comparisons between treatment groups within the same time point are indicated by *, whereas comparisons between time points within the same treatment group are indicated by $^{+}$; **/^{++}p ≤0.01, ***/^{+++}p ≤0.001 (Two-way ANOVA with a mixed-effects model fitted on log-transformed data). KC-keratinocyte chemoattractant, IL-interleukin, MDC-macrophage-derived chemokine, G-CSF-granulocyte colony-stimulating factor, LOD-limit of detection.

4.3.6 Acute exposure to higher dose of DEP does not upregulate *KIM-1* and *TNF-α* expression in the kidney

KIM-1 mRNA levels in both cortex and medulla exhibited no notable differences between DEP-exposed and control groups at 6 h and 16 h post-instillation (Figures 4.7A and 4.7B). Similar observations were noted for levels of *TNF-α* mRNA when comparing the two treatment groups (Figures 4.7C and 4.7D). Notably, a slight, but significant increase in cortical *TNF-α* mRNA was observed in the saline group at 16 h compared to 6 h (p=0.0317; Figure 4.7C). Additionally, medullary transcript levels for both markers were consistently higher compared to cortical levels. Raw Ct values for each gene and treatment group are presented in Table 4.2.

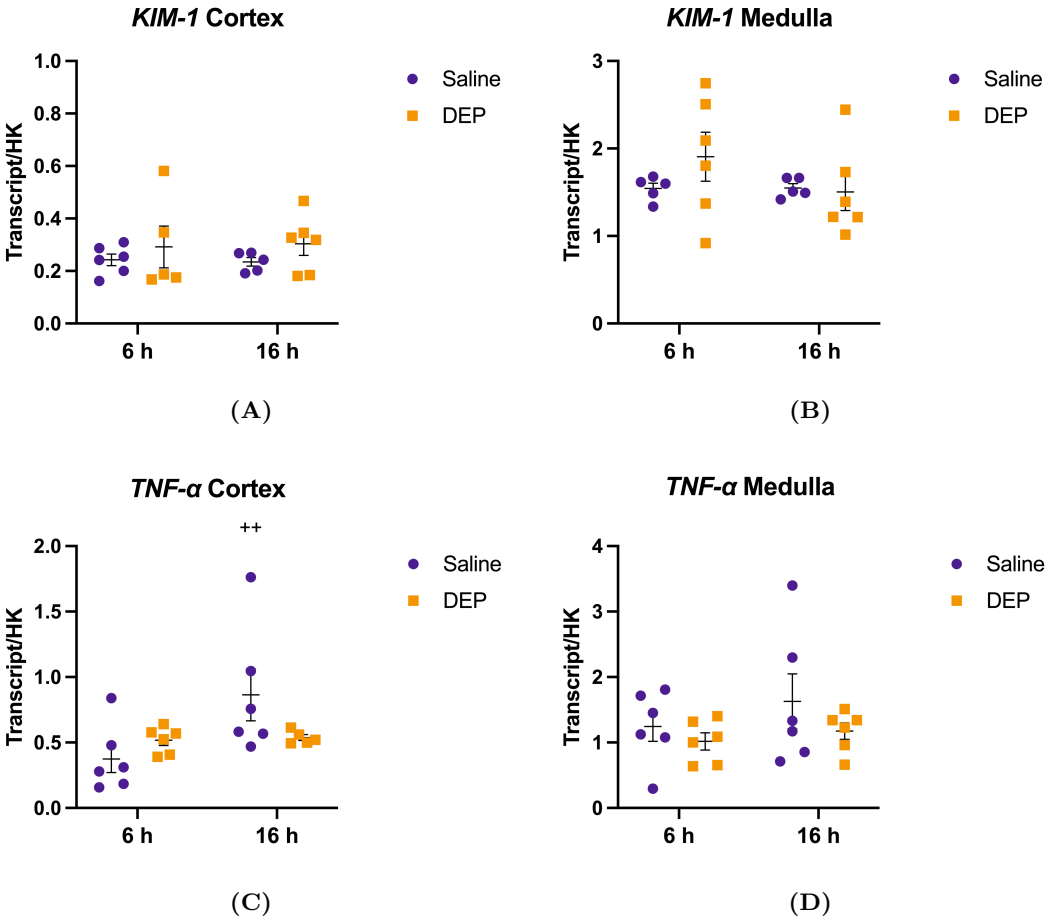

Figure 4.7: Effects of acute DEP exposure on renal *KIM-1* and *TNF-α* expression. Mice were administered a single dose of diesel exhaust particles (DEP, 50 µg) or saline (control) by pulmonary instillation. Mice were culled ~6 h or 16 h after exposure, kidneys collected and renal transcript levels of (**A**, **B**) kidney injury molecule-1 (*KIM-1*) and (**C**, **D**) tumour necrosis factor-alpha (*TNF-α*) were measure in cortex and medulla by RT-qPCR (each dot indicates an animal). Results are normalised to the housekeeping (HK) gene glyceraldehyde 3-phosphate dehydrogenase (*GAPDH*) and data presented as Mean ± SEM; $^{++}p \leq 0.01$ (comparison between time points within the same treatment group; Two-way ANOVA with a mixed-effects model fitted on log-transformed data).

		Saline		DEP	
		6 h	**16 h**	**6 h**	**16 h**
GAPDH	Cortex	18.40 ± 0.18	18.24 ± 0.07	18.26 ± 0.06	18.41 ± 0.08
	Medulla	18.76 ± 0.10	18.47 ± 0.09	18.34 ± 0.04	18.43 ± 0.07
KIM-1	Cortex	30.54 ± 0.24	30.38 ± 0.17	30.29 ± 0.36	30.26 ± 0.19
	Medulla	28.16 ± 0.08	27.75 ± 0.06	27.47 ± 0.23	27.89 ± 0.16
TNF-α	Cortex	33.94 ± 0.45	32.53 ± 0.25	33.13 ± 0.10	33.14 ± 0.10
	Medulla	32.54 ± 0.42	31.91 ± 0.32	32.30 ± 0.19	32.17 ± 0.18

Table 4.2: Raw Ct values of renal transcript levels following acute DEP exposure: study 2. Mice were administered a single dose of diesel exhaust particles (DEP, 50 µg) or saline (control) by pulmonary instillation. Mice were culled ~6 h or 16 h after exposure, kidneys collected and renal transcript levels of kidney injury molecule-1 (*KIM-1*) and tumour necrosis factor-alpha (*TNF-α*) were measured in cortex and medulla by RT-qPCR (glyceraldehyde 3-phosphate dehydrogenase (*GAPDH*) served as housekeeping gene). Raw cycle threshold (Ct) values for each treatment group are presented as Mean ± SEM.

4.4 Discussion

4.4.1 Pulmonary inflammation following acute DEP exposure

After establishing the capacity of ultra-fine gold nanoparticles to translocate to the kidney as a potential mechanism for the extra-pulmonary adverse health effects associated with particulate matter exposure, our subsequent objective was to investigate the renal effects following acute exposure to DEP. In light of our proposed trajectory for particle effects, spanning from the lungs, through the circulation and ultimately to the kidneys, our aim was to quantify inflammation at each of these sites. Our findings reveal that a single administration of DEP at a dose of 35 µg, with BALF collected ~18 h post-instillation, is sufficient to induce pulmonary inflammation, evidenced by an elevation in BALF TCC driven predominantly by neutrophil infiltration into the lungs. These observations align with prior studies. For instance, Tabor *et al.* and Robertson *et al.* demonstrated that intratracheal instillation of rats with 0.5 mg of DEP SRM 2975, the same material used in our investigation, induced a marked increase in BALF TCC and neutrophil count, peaking at 6 h post-exposure but persisting at 24 h post-exposure (BALF collected at 2, 6 and 24 h) [122, 156]. However, in our subsequent experiment, wherein mice were instilled with a slightly higher dose of DEP (50 µg) and BALF was collected at 6 h or 16 h post-treatment, we did not observe a similar time frame for pulmonary inflammation. While in our study DEP did not elicit changes in BALF TCC at either time point, a trend towards increased TCC in the DEP group was noted at 16 h. Nevertheless, due to the limited sample size in the corresponding control group (n=3), the reproducibility and reliability of these findings would benefit from a larger cohort size.

The early-stage neutrophil infiltration induced by DEP in the lungs, as observed in our study, has been corroborated by other groups. Nemmar and colleagues reported neutrophil infiltration in hamsters as early as 1 h post-pulmonary exposure to DEP at doses ranging from 5 to 500 µg [188] and in rats following intravenous administration of DEP at doses of 8, 42 and 212 µg [189]. Notably, while comparable observations were reported in mice for higher doses of DEP (100 µg), such effects were not evident at

lower doses (25 µg) [190]. Interestingly, while neutrophils are the predominant immune cells recruited to the lungs shortly after DEP exposure, studies in mice have indicated a significant increase also in macrophage counts in BALF as early as 24 h post-DEP exposure (15 or 30 µg) [191]. This discrepancy could be due to a difference in the mouse strain and its response to particles or the difference in time of BALF collection.

In addition to their role as regulators of inflammatory responses in the lung following exposure, macrophages serve as the primary cell type responsible for particle clearance *in vivo* [176, 192, 193]. While nano-sized particles swiftly translocate from the alveolar epithelium to the epithelial and septal interstitial spaces, macro-sized particles are engulfed by alveolar macrophages, subsequently transported to the larynx and eventually ingested into the gastrointestinal tract for clearance [176]. This clearance mechanism is thought to be orchestrated by the anti-inflammatory M2 macrophages and is estimated to result in particle half-life in the lung of 60–70 days [194]. In our investigation, we observed presence of DEP in and on the surface of macrophages ~18 h after a single exposure. These findings are supported by rat studies, where staining of BALF cells revealed macrophage phagocytosis of DEP as early as 2 h post-exposure [122, 156].

4.4.2 Systemic inflammatory response to acute DEP exposure

While the effects of DEP on pulmonary inflammation are relatively consistent across studies, the data regarding DEP-induced systemic response vary. In our study, most measured cytokines exhibited no change following DEP exposure. However, exceptions were observed for IL-18 and MDC, which displayed elevated levels at 6 h and 16 h post-exposure, respectively. Controlled human exposure studies have shown inhalation of diesel exhaust (300 µg/m^3 for 1 h) to induce mild systemic inflammation through increased plasma concentrations of TNF-α and IL-6 (24 h later) [185]. Experiments conducted in mice exposed to low-to-moderate doses of DEP (SRM 2975, single instillation of 15 or 30 µg) did not reveal an elevation in plasma IL-6 levels post-treatment in either normo- or hypertensive rodents [191, 195]. Conversely,

when employing a very high DEP dosage of 100 µg (administered on days 1, 3 and 7) and assessing a panel of inflammatory markers, a significant increase in serum IL-1β was observed, while no notable changes were detected in other markers including IL-6, IL-10, IL-12, interferon-gamma (IFN-γ) and granulocyte-macrophage colony-stimulating factor (GM-CSF) [196]. Similarly, investigations in rats have produced diverse outcomes. A single intratracheal instillation with standardised DEP (SRM 2975) at 500 µg induced no changes in plasma IL-6, TNF-α or CRP concentrations. Interestingly, even when administered intravenously (0.5 mg/kg), DEP had no effect on plasma levels of these markers [122]. However, systemic CRP levels were markedly increased one day after instillation with a higher dose (1,000 µg) of $PM_{2.5}$ collected from an urban environment. Conversely, no significant alterations were noted with lower doses (250 µg and 500 µg), although changes were noted for the intermediate dose on day 3 post-exposure [197]. The discrepancies observed may be attributed to various factors including difference in mouse strain, pollutant source and composition (standardised diesel exhaust versus ambient particles), exposure dosage and the duration between exposure and inflammation assessment. These findings underscore the importance of assessing a diverse range of markers to comprehensively evaluate the systemic effects of particle exposure and avoid potential oversights.

4.4.3 Effects of acute DEP exposure on markers of renal damage and inflammation

To study the renal effects of acute DEP exposure, transcript levels of the markers of kidney damage-*KIM-1*, and inflammation-*TNF-α*, were measured in renal tissue. The utility of KIM-1 as a marker for kidney injury was initially elucidated by Ichimura *et al.*, who subsequently identified its significance as a predictor of outcome for chronic kidney disease [198, 199]. KIM-1, a transmembrane protein, is minimally expressed in healthy kidneys but is significantly upregulated in the proximal tubule following injury. In this context, KIM-1 functions as a phagocytic receptor, facilitating the clearance of apoptotic and necrotic cells and thereby preventing the release of harmful cellular contents that could exacerbate inflammation and tissue

damage [200]. Additionally, after proximal tubular injury, the extracellular domain of KIM-1 is cleaved in a metalloproteinase-dependent manner, released into the renal tubule and excreted into the urine [201]. The extent of KIM-1 upregulation in both renal tissue and urine correlates with the severity of renal damage [198, 202]. Elevated levels of KIM-1 have been detected in the urine of patients with various acute and chronic kidney conditions, suggesting its potential as a sensitive and specific marker for AKI diagnosis [203]. Notably, KIM-1 upregulation is believed to precede the increase in serum creatinine-the current standard diagnostic tool for AKI detection alongside reduced urine output, further solidifying it as a marker for early detection of AKI [204, 205]. More recently, KIM-1 has also been proposed as a blood-based marker for kidney injury [206]. The findings of our study revealed that following acute DEP exposure, there was an elevation in the expression of *KIM-1* and *TNF-α* within the medulla relative to the cortex in both control and treated mice. Additionally, while expression levels in the cortex remained relatively consistent across all time points, there was a slight but insignificant increase over time in the medulla. These observations align with our expectations, as *KIM-1* is predominantly expressed (and upon injury-upregulated) in renal proximal tubule cells, particularly within the S3 region of the medulla, in both human [203] and rodent models [207]. However, irrespective of the dosage (35 µg or 50 µg) or time frame (6 h, 16 h or 18 h), acute exposure to DEP did not induce an elevation in the expression of *KIM-1* or *TNF-α* in renal tissue.

Research findings in rodents regarding the effects of acute exposure to diesel particles on markers of kidney damage vary among studies. For instance, a study conducted on Wistar rats, which were administered a single intratracheal instillation of DEP (SRM 2975, 0.5 mg/kg) and sacrificed 24 h later, demonstrated that, compared to the control group, DEP treatment induced a significant increase only in urinary NAG concentration and a decrease in TAC, with no changes observed in other parameters of kidney damage, such as plasma urea and creatinine, or renal GSH, SOD and CAT [151]. In contrast, a study by Nemmar *et al.*, with a similar

experimental setup, found no alterations in any parameters of renal damage measured. Notably, it was only when the dose was doubled (to 1 mg/kg) that a substantial decrease was observed solely in renal GSH, while other parameters including serum urea and creatinine, urinary NAG and protein, and renal SOD remained unaffected [152]. Additionally, another study involving mice exposed to $PM_{2.5}$ (500 µg, collected from an urban environment) on days 0 and 2 and culled on days 3 or 7, revealed $PM_{2.5}$-induced changes in various markers including renal *KIM-1*, *TNF-*α, *NF-*κB, *SOD* and *GSH-PX* mRNA, kidney protein concentrations for TNF-α, ACE and AT1R, and serum cystatin C [147]. The discrepancy between the findings in these studies and our data could be attributed to differences in dose (10-fold difference), source of diesel particles and mouse strain.

4.4.4 Chapter summary

In this study, the effects of acute pulmonary DEP exposure on markers of kidney injury and inflammation were explored in healthy mice. In addition, the impact of single DEP exposure on pulmonary and systemic inflammation was also assessed. In summary, the main findings of this chapter are:

- Pulmonary administration of a single dose of DEP was sufficient to induce pulmonary inflammation evident by a substantial increase in BALF total cell count and neutrophil infiltration to the lung.
- The induction of systemic inflammation by DEP was generally insignificant, as indicated by the marginal elevation observed in only a limited number of inflammatory markers following exposure.
- Acute exposure to DEP did not result in the upregulation of either *KIM-1* or *TNF-*α mRNA in renal tissue.

Chapter 5

The effects of chronic DEP exposure on the kidney and renal vasculature

5.1 Introduction

Results from Chapter 4 demonstrated that a single pulmonary administration of DEP induced local inflammation in the lungs without causing significant systemic inflammation or upregulation of renal damage and inflammation markers. This could suggest that renal effects from DEP exposure may require prolonged accumulation, which may better mimic the chronic exposure to air pollution over many years in the real world. Therefore, this chapter aims to investigate the renal effects of chronic pulmonary DEP exposure in healthy mice, using the maximum dose permitted under the project license. Additional markers of kidney function were evaluated and the impact of DEP on renal vascular function was examined.

5.1.1 Hypothesis and aims

The hypothesis explored in this chapter is:

Prolonged pulmonary DEP exposure induces kidney damage through effects on renal inflammation and markers of kidney injury and promotes renal vascular dysfunction.

Aims:

1. Determine the effects of chronic DEP exposure on pulmonary and systemic inflammation.
2. Examine the impact of prolonged DEP administration on markers of renal function in healthy mice.
3. Assess renal vascular function in healthy mice following chronic pulmonary DEP exposure using wire myography.

5.1.2 Study design

In addressing the aims of this chapter a study was conducted whereby healthy mice were administered DEP or saline by pulmonary instillation (*it*) twice weekly for 4

consecutive weeks. Mice were individually house in metabolic cages for urine collection at 3 time points: at baseline prior to 1st *it*, halfway through the protocol (after 4th *it*) and at the end of the study after the last 8th *it*. Mice were culled ~18 h after last *it* and tissues collected. BALF was collected for pulmonary inflammation measurements, blood for analysis of systemic inflammation, kidneys were harvested to quantify markers indicative of renal injury and inflammation and examine changes in renal morphology, urine was analysed for markers of kidney injury and renal arteries were isolated for analysis of vascular function. A diagram of the study design is presented in Figure 5.1.

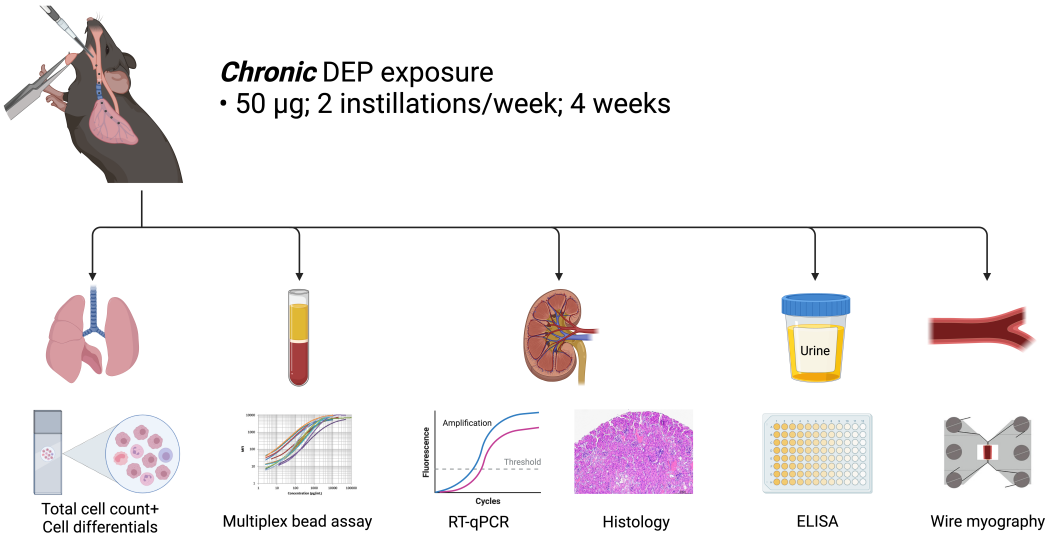

Figure 5.1: Study design for chronic DEP exposure experiment. Healthy mice were exposed to diesel exhaust particles (DEP, 50µg) or saline (control) twice weekly for 4 consecutive weeks by pulmonary instillation (*it*). Mice were culled ~18 h after last *it* and various organs collected for measurement of DEP-induced effects on pulmonary and systemic inflammation, markers of renal injury and vascular function. Figure created by the author using BioRender.

5.2 Methods

Each procedure performed in this chapter is detailed in the main Materials and Methods chapter. All animal experiments in this chapter were performed on healthy, adult, male C57BL/6J mice, aged 8–10 weeks at the start of the study and maintained under controlled conditions, further detailed in Section 2.1.

5.2.1 DEP administration

DEP (SRM 2975, NIST) was suspended in sterile saline (0.9% NaCl) at a concentration of 1 mg/mL and was always sonicated and vortexed prior to administration to avoid particle aggregation. Using the instillation/aspiration method mice were administered DEP twice weekly for 4 consecutive weeks at a dose of 50 µg [157]. Briefly, mice were placed under transient isoflurane anaesthesia and following assessment of anaesthesia level, were placed supine on an angled board. DEP suspension was gently positioned at the base of the tongue as to be inhaled as the anaesthesia wore off. Control group received sterile saline. DEP was administered at a maximum frequency of once every 72 h. This procedure is detailed in Section 2.2.1.

5.2.2 BALF measurements

BALF collection

To assess pulmonary inflammation in mice following chronic DEP exposure, BALF was collected by lavaging the lungs three times with 0.9% NaCl. Primary lavage was kept separate, secondary and tertiary lavages were combined, now referred to as secondary lavage. BALF was centrifuged, cell pellet from primary lavage was resuspended in 1% BSA and combined with suspension from secondary lavage by gentle pipetting (see Section 2.3.1).

Total cell count

For each sample, 50 µL of cell suspension was mixed with equal volumes of lysis buffer and stabilising buffer, sample was drawn up a NucleoCassette™ and total cell

count was established using a NucleoCounter™ (see Section 2.3.2).

Cell differential counts

For each sample, a glass slide was inserted into a metal cassette, a filter card placed on top of the slide and finally a cytofunnel on top of the filter card.

Based on the total cell count, for each sample the volume corresponding to 40,000 cells was mixed with 1% BSA to reach a final volume of 300 µL. This suspension was pipetted into the cytofunnels, cassettes were centrifuged, slides were left to dry, followed by Diff-Quik staining.

Immune cells from BALF were stained using the Diff-Quik method by dipping the slides into methanol, red stain (Eosin G in phosphate buffer), blue stain (Thiazine dye in phosphate buffer) and finally distilled water. BALF cell differential counts were conducted by manually enumerating and classifying approximately 200 cells per sample into their respective cell types-for this experiment cell differential counts were performed by Dr Emanuel Jeldes and Prof Rodger Duffin from the Centre for Inflammation Research at The University of Edinburgh. Data for each cell type are presented as (1) percentage of total number of cells counted manually and (2) the absolute number of cells from each cell type in the lung lavage by referring back to the original total cell count obtained by the nucleocounter. A detailed description of this protocol is outlined in Section 2.3.3 and a diagram of BALF processing is presented in Figure 2.2.

5.2.3 Measurement of circulating cytokines using a multiplex assay

Mice were culled by terminal anaesthesia with an *ip* injection of Dolethal. Following assessment of mouse consciousness using the hind limb reflex test, blood was collected by cardiac puncture (syringe was pre-coated with citrate 3.8%), placed in an EDTA-coated tube and kept on ice. Within 30 min of collection, blood was centrifuged for 20 min at 1,000 × g, plasma was separated, placed in a fresh Eppendorf tube and stored at -80°C until further processing.

Cytokine levels were measured in plasma using the LEGENDplex™ Multi-Analyte Flow Assay Kit (Mouse Macrophage/Microglia Panel (13-plex); Biolegend®). Plasma samples were diluted 2-fold with Assay Buffer and run in singles. An 8-point standard curve was generated by making 1:4 serial dilutions from the stock standard provided (10,000 pg/mL). The final point of the standard was used as a blank (Assay Buffer only). Each standard was run in technical duplicates.

Samples were mixed with beads and either matrix C (for standards) or Assay Buffer (for plasma samples) and loaded onto a V-bottom 96-well plate. The samples and beads were mixed for 2 h at room temperature on a plate shaker, protected from light. Following incubation, the plate was centrifuged for 5 min and supernatant discarded. The plate was washed by dispensing 200 µL Wash Buffer into each well, incubating it for 1 min, centrifuging again for 5 min and finally discarding the Wash Buffer. This wash step was repeated twice. Samples were then incubated with Detection Antibodies for 1 h at room temperature on a plate shaker, protected from light. Streptavidin-phycoerythrin (SA-PE) was then added directly and allowed to incubate with the samples for 30 min at room temperature on a plate shaker, protected from light. The plate was centrifuged, supernatant discarded and plate washed as previously described, forming a bead pellet at the bottom of the plate at the end. Finally, the beads were resuspended in Wash Buffer by gentle pipetting. Samples were then read on a flow cytometer. A diagram detailing the underlying assay principle is presented in Figure 2.3 and a more comprehensive procedural outline is provided in Section 2.4.2.

5.2.4 Measuring mRNA levels in renal tissue by RT-qPCR

Tissue harvest

Mice were culled ~18 h after final 8th instillation by terminal anaesthesia with *ip* injection of Dolethal. Kidneys were dissected and the capsule removed. The left kidney was cut longitudinally and one half further cut horizontally into two. A quarter of each kidney was placed in RNA*later*™ solution for 24 h at 4°C, then stored at -80°C for

further processing.

RNA extraction

Immediately prior to RNA extraction the quarter of mouse kidney was split into cortex and medulla, placed in QIAzol™ lysis reagent and homogenised using a tissue lyser. RNA was isolated using a commercial kit following manufacturer's instructions and RNA concentration was quantified using a spectrophotometer (see Section 2.5.2).

RT-qPCR

cDNA was synthesised using a commercial kit and following manufacturer's instructions. Briefly, for each RT reaction an RNA extract volume corresponding to 2,000 ng of diluted RNA was mixed with enzyme mix and RT buffer. Negative controls were also included, where RT enzyme or RNA were replaced with an equal volume of water. Samples were reverse transcribed on a Thermal Cycler and the cDNA generated was stored at -20°C until further processing.

The cDNA generated from the RT reaction was amplified and quantified using qPCR. An 8-point standard curve was constructed by pooling an equal volume from each cDNA sample and performing a 1:4 dilution for the first point and serial 1:2 dilutions for points 2–7. The final point of the standard was used as a blank (nuclease-free water only). The remaining cDNA was diluted 1:40 (2.5 ng/µL) to fall within the middle of the standard curve. For each reaction (run in technical triplicates) cDNA was mixed with master mix. Negative controls, as described above, were also added. Reactions were run on a LightCycler instrument and quantification data were accepted if standard curve was satisfactory. Results were normalised against the average Cp value of the housekeeping gene GAPDH. Further details on the RT-qPCR protocol, master mix components, cycling conditions and primer sequences are outlined in Section 2.5.3.

5.2.5 Histology

Dissected mouse kidneys were placed in 10% formalin for 24 h at room temperature before being transferred to 70% ethanol long-term. Samples were dehydrated up an

ethanol gradient (70%, 80%, 95% and 100%) and xylene before embedding in paraffin blocks. Sections of fixed kidneys were cut (5 µm), stained with haematoxylin and eosin (H&E) and assessed for morphological abnormalities using light microscopy.

Haematoxylin and eosin staining

Kidney sections were deparaffinised in xylene and passed down an ethanol gradient for rehydration. After staining for 5 min with Harris modified Haematoxylin, sections were sequentially placed in acid alcohol, Scott's Tap Water Substitute and eosin. Slides were then taken back up the ethanol gradient and xylene and mounted with DPX. A more comprehensive staining protocol is detailed in Section 2.6.

5.2.6 Urine measurements

To establish how exposure to diesel exhaust particles affects expression of markers of kidney injury in the urine, mice were placed in metabolic cages for urine collection. Urine was collected at 3 time points: at baseline prior to 1st DEP exposure, after 2 weeks (after 4th instillation) and after 4 weeks of exposure (after 8th instillation). Mice were individually housed in metabolic cages for a length of 16–20 h for each collection. This time period always encompassed the 7 PM–7 AM time period, when the animals were active.

Urinary KIM-1 measurement

Urinary levels of KIM-1 were measured using a commercial ELISA kit, following manufacturer's instructions. Briefly, an 8-point standard was prepared by making serial dilutions from the stock standard provided (500 pg/mL)-the final point being blank. A control sample provided in the kit was also included. Standards, control and experimental samples were run in technical duplicates. Each well was loaded with 50 µL of sample, control or standard thoroughly mixed with an equal volume of Assay Diluent and left to incubate for 2 h at room temperature on a plate shaker. The plate was washed, cold mouse conjugate added and incubated for 1 h at 2–8 °C. Plate was washed again, Substrate Solution added and incubated for 30 min at room

temperature, protected from light. Reaction was terminated by adding a Stop Solution and the optical intensity of each well was immediately determined using a microplate reader. KIM-1 concentration for each sample was normalised to urine creatinine levels. This procedure is detailed in Section 2.8.2.

Urinary creatinine measurement

Urine creatinine measurements were performed by Kirsten Wilson from the Centre for Reproductive Health at The University of Edinburgh. Briefly, creatinine measurements were determined using a creatininase/creatinase enzymatic method as described by Börner *et al.* [159] making use of a commercial kit (Sentinel Diagnostics via Alpha Laboratories Ltd., Eastleigh, UK) adapted for use on either a Cobas Fara or Mira analyser (Roche Diagnostics Ltd, Welwyn Garden City, UK). Within run precision was CV <3% while intra-batch precision was CV <5%. Assay principle is detailed in Section 2.8.3.

5.2.7 Assessment of vascular function: wire myography

To assess vascular function under isometric experimental conditions, wire myography was performed on renal arteries. In this study, the wire myograph 610 M system of Danish Myo Technology (DMT) was used.

Renal artery isolation and mounting

Mice were culled by an *ip* injection of Dolethal and the kidneys with the intact vasculature connected to the abdominal aorta were isolated and placed in ice-cold PSS. Both kidneys and the top and bottom ends of the abdominal aorta were pinned down on a silicone-coated petri dish containing ice-cold PSS and vessels were cleaned of PVAT.

The wire myograph consists of 4 baths and each bath has gas supply and aspirators to remove solutions. Each bath was filled with 6 mL of PSS, warmed to 37°C and supplied with gas of 95% O_2 and 5% CO_2. Dissected renal arteries were transferred to the baths and cut into rings of 1–2 mm in length. Under a microscope each renal artery

was mounted onto a myograph by passing a fine 40 µm wide stainless steel wire through the vessel lumen. The wire ends were stabilised by the screws and baths returned to the myograph (for further details see Section 2.9.1).

Normalisation of vascular tension

Normalisation of vascular tension is a key step in the wire myography protocol which aims to determine the internal vessel circumference which produces the maximal isometric contractility. Vascular reactivity depends on the initial vessel tension, hence normalisation is an essential step for the accurate comparison of drug effects and reproducibility of results.

Normalisation was performed using the DMT Normalisation Module on LabChart (AD Instrumentals), which involves testing the length/tension relationship for each vessel. Vessel length was determined using a scale incorporated in the microscope eyepiece. To set the vessel tension, the micrometer dial, separating the myograph jaws, was turned in increments of 2 mN each time. For every increase in force, the distance between the jaws was measured until the vessel reached a maximum of 13.3 kPa, which corresponds to an intramural pressure of 100 mmHg. The length/tension graph produced was used to determine the optimal internal circumference (IC_1) for each vessel to produce maximal vascular reactivity. The jaws were then adjusted to correspond to the IC_1, at which the vessels remained for the rest of the experiment. Vessels were left to equilibrate for 30 min (for further details see Section 2.9.2).

Vascular reactivity protocol

Viability of renal arteries was tested by bathing vessels in high potassium PSS (KPSS) to induce a maximal contractile response. Once the dose-response curve peaked and plateaued, baths were emptied, the vessels washed three times with warm PSS and left to equilibrate for 20 min. This process was repeated three times.

To assess vascular reactivity, vessels were treated with the adrenergic-dependent vascular contraction agent phenylephrine (PE), the endothelial-dependent vasodilator

acetylcholine (ACh) and the endothelial-independent vasodilator sodium nitroprusside (SNP) and dose-response curves were generated for each. Following each drug administration vessels were washed with PSS, until they reached baseline tension and left for 20 min before the next treatment. For vasodilation, arteries were preconstricted by PE incubation at a dose that would induce ~80% of the maximal contraction (for further details see Section 2.9.3).

5.3 Results

5.3.1 Chronic DEP exposure increases BALF total cell count and induced macrophage and neutrophil infiltration to the lungs

A significant increase in total cell count (TCC) was observed in BALF from mice after chronic pulmonary exposure to DEP compared to controls (p=0.0012, Figure 5.2A). Differential cell analysis revealed a higher percentage of neutrophils in the DEP-exposed group (21%) compared to controls (3.9%), along with a slight reduction in macrophages (74.1% vs 86.7% in controls) and lymphocytes (5.5% vs 9.7% in controls; Figure 5.2B). However, the absolute number of each cell type, calculated based on the TCC, indicated that the increase in BALF TCC following chronic DEP exposure was primarily due to substantial macrophage and neutrophil infiltration (Figure 5.2C).

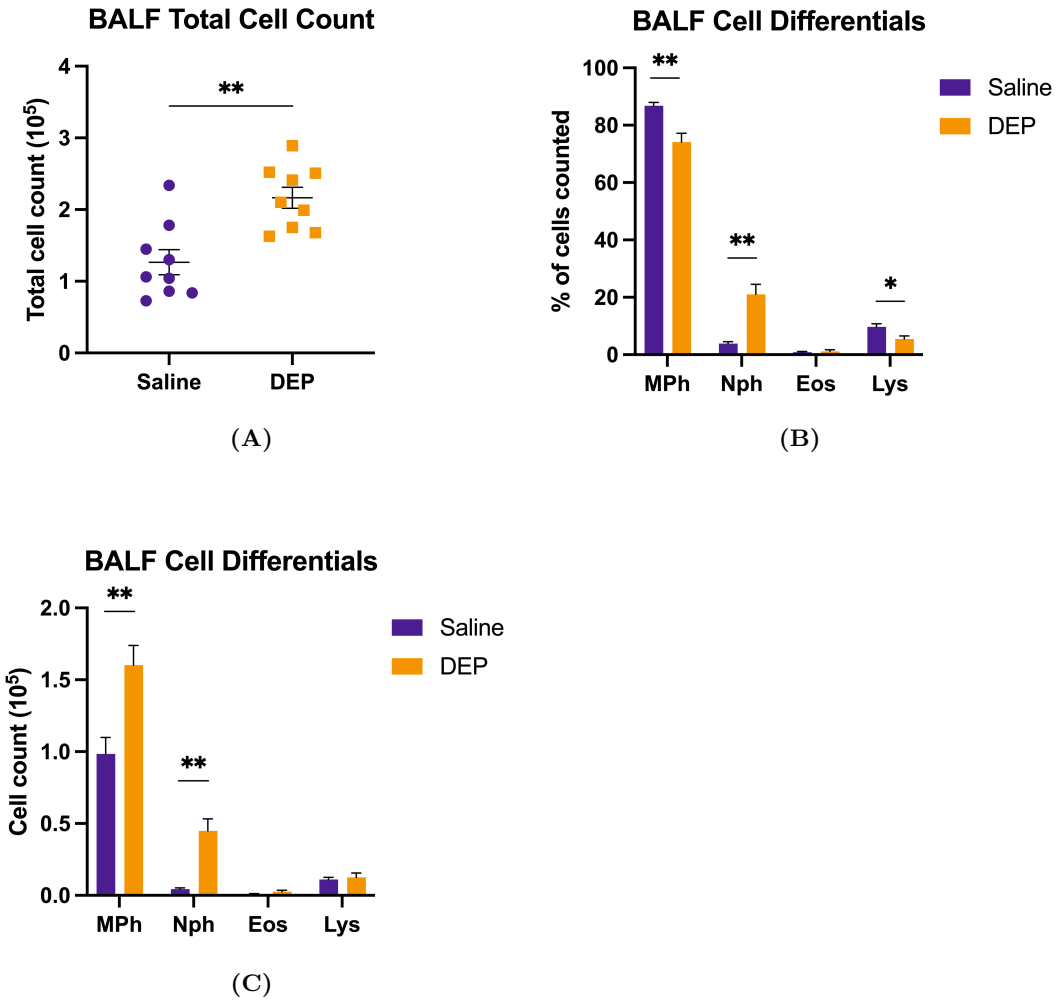

Figure 5.2: Effects of chronic pulmonary DEP exposure on lung inflammation. Mice were administered diesel exhaust particles (DEP, 50 µg) or saline (control) by pulmonary instillation (*it*) twice weekly for 4 consecutive weeks. Mice were culled ~18 h after last *it*, bronchoalveolar lavage fluid (BALF) collected and analysed for (**A**) total cell count and (**B**) cell differentials for each cell type presented as percentage of manually counted cells or (**C**) presented as the total number of each cell type by referring back to the original total cell count from the nucleocounter. Data presented as Mean ± SEM; *p ≤0.05, **p ≤0.01 (unpaired Student's t-test; Welch's correction was used where t-test indicated significant difference in variances of groups being compared). Cell differential counts were performed by Dr Emanuel Jeldes and Prof Rodger Duffin. MPh-macrophages, Nph-neutrophils, Eos-eosinophils, Lys-lymphocytes.

5.3.2 Chronic pulmonary DEP exposure does not induce systemic inflammation in healthy mice

To assess the impact of chronic pulmonary exposure to DEP on systemic inflammation, levels of inflammatory markers were measured in mouse plasma (Figure 5.3). Both the DEP-exposed and control groups showed substantial variability in all markers (Welch's correction was used where the t-test indicated significant difference in the variance of the two groups being compared). Compared to controls, DEP-exposed mice exhibited a slight decrease in plasma levels of CXCL (KC) (mean concentration 186 pg/mL vs 343 pg/mL in control; p=0.2287), CCL22 (MDC) (274 pg/mL vs 479 pg/mL in control; p=0.0834) and G-CSF (52 pg/mL vs 144 pg/mL in control; p=0.1464). While plasma IL-18 levels were similarly low in both groups (mean 12 pg/mL), IL-23 concentrations in the DEP group were slightly lower compared to controls and largely at the limit of detection (LOD=24 pg/mL). IL-12p70 concentration was negligible in both groups (mean <1 pg/mL in DEP and 6 pg/mL in control, with majority of replicates at the LOD) and IL-1β levels were at the LOD.

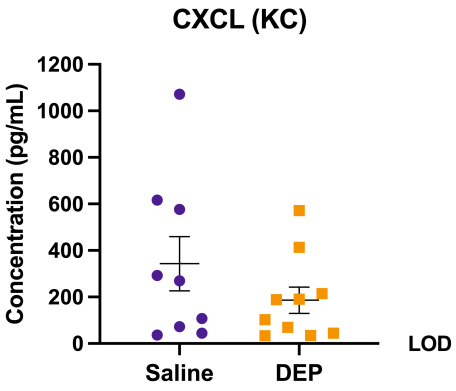
CXCL (KC)
Concentration (pg/mL)
1200
1000
800
600
400
200
0
LOD
Saline
DEP

(A)

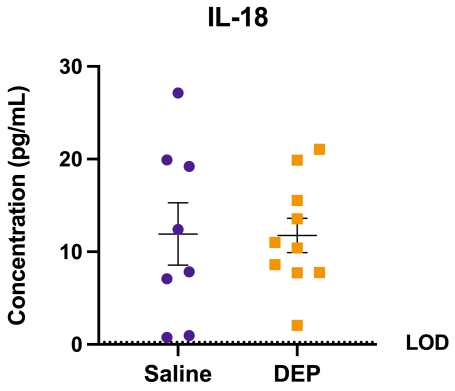
IL-18
Concentration (pg/mL)
30
20
10
0
LOD
Saline
DEP

(B)

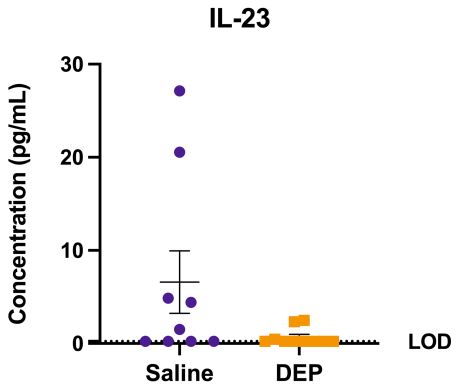
IL-23
Concentration (pg/mL)
30
20
10
0
LOD
Saline
DEP

(C)

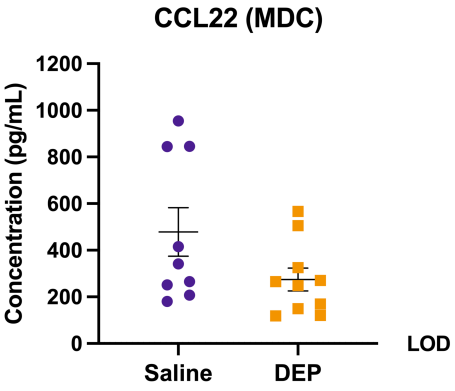
CCL22 (MDC)
Concentration (pg/mL)
1200
1000
800
600
400
200
0
LOD
Saline
DEP

(D)

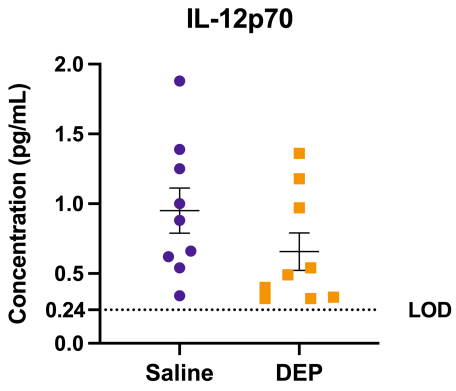
IL-12p70
Concentration (pg/mL)
2.0
1.5
1.0
0.5
0.24
0.0
LOD
Saline
DEP

(E)

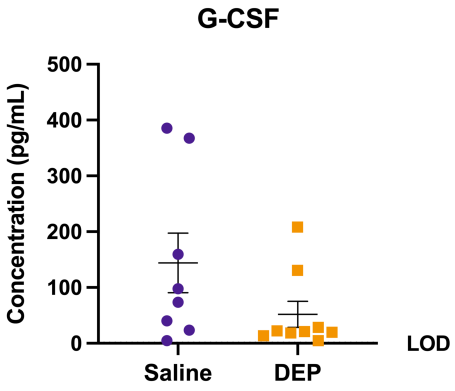
G-CSF
Concentration (pg/mL)
500
400
300
200
100
0
LOD
Saline
DEP

(F)

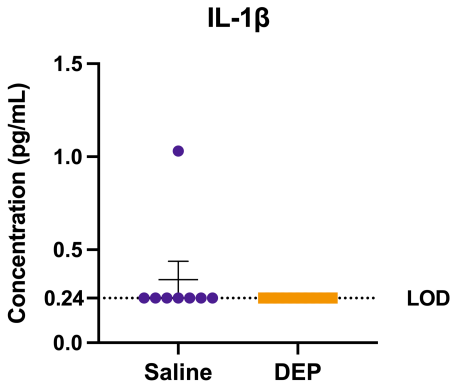

(G)

Figure 5.3: Effects of chronic pulmonary DEP exposure on markers of systemic inflammation in mouse plasma. Mice were administered diesel exhaust particles (DEP, 50 µg) or saline (control) by pulmonary instillation (*it*) twice weekly for 4 consecutive weeks and culled ~18 h after last *it*. Blood was collected by cardiac puncture, centrifuged and levels of various markers of systemic inflammation measured in plasma using a multiplex bead assay. Each dot represents an animal. Data presented as Mean ± SEM (unpaired Student's *t*-test; Welch's correction was used where *t*-test indicated significant difference in variances of groups being compared). KC-keratinocyte chemoattractant, IL-interleukin, MDC-macrophage-derived chemokine, G-CSF-granulocyte colony-stimulating factor, LOD-limit of detection (24 pg/mL).

5.3.3 Chronic pulmonary DEP exposure does not promote kidney injury at the morphological or molecular level in healthy mice

To determine whether the injurious load of prolonged DEP exposure is sufficient to promote detectable renal changes and induce kidney injury, a histological evaluation of renal tissue was conducted on H&E-stained renal sections. Glomeruli were uniformly sized with intact Bowman's capsules. In both groups proximal tubules had larger cuboidal epithelial cells with prominent brush borders, while distal tubules had flatter epithelium, no brush border and larger luminae. H&E staining revealed no gross abnormalities in kidney morphology in DEP-exposed mice compared to controls (Figure 5.4). To look for inflammation in the kidney immunohistochemical (IHC) staining on renal sections was performed for the macrophage marker F4/80 and the T cell marker CD3. Despite lengthy protocol optimisation, staining was weak in relation to the background staining. The staining was deemed not sufficiently reliable to visualise or quantify differences in immune cell infiltration to the kidney between saline- and DEP-treated mice.

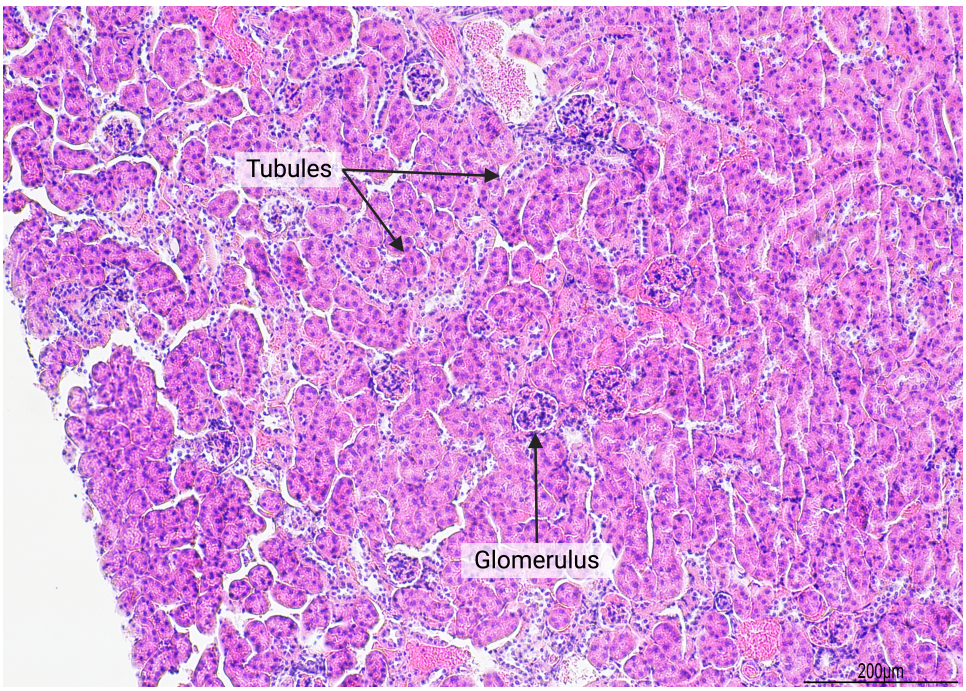

(A) Saline

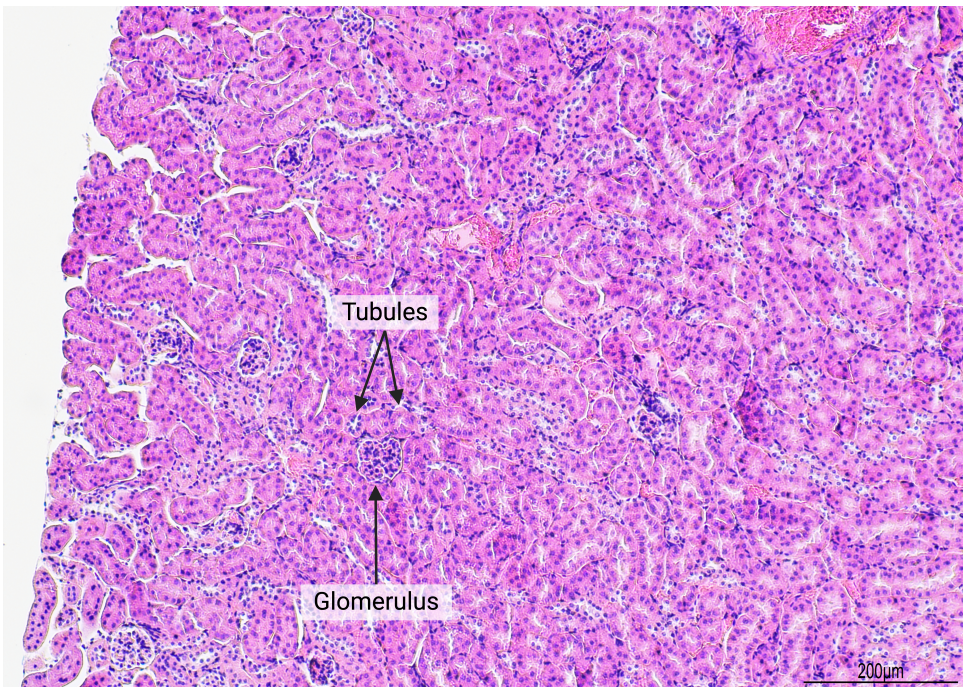

(B) DEP

Figure 5.4: Effects of chronic pulmonary DEP exposure on mouse renal morphology. Mice were administered diesel exhaust particles (DEP, 50 µg) or saline (control) by pulmonary instillation (*it*) twice weekly for 4 consecutive weeks and culled ~18 h after last *it*. Representative light microscopy images of haematoxylin and eosin (H&E)-stained kidney sections (5 µm) from mice treated with (**A**) saline or (**B**) DEP. Scale bar 200 µm.

Given the absence of gross morphological abnormalities from the histological evaluation, more subtle non-histologically detectable injury was assessed by quantifying *KIM-1* and *TNF-α* mRNA levels in renal tissue (Figure 5.5). Chronic DEP exposure did not increase *KIM-1* in either the cortex or medulla (Figure 5.5A). Cortical *TNF-α* transcript levels were similar between groups, while in the medulla *TNF-α* mRNA levels were slightly but insignificantly lower in the DEP group compared to control (p=0.1127; Figure 5.5B). For both groups, *KIM-1* and *TNF-α* transcripts were significantly more abundant in the medulla than in the cortex (p<0.0001). Raw cycle threshold (Ct) values for each gene and treatment group are presented in Table 5.1.

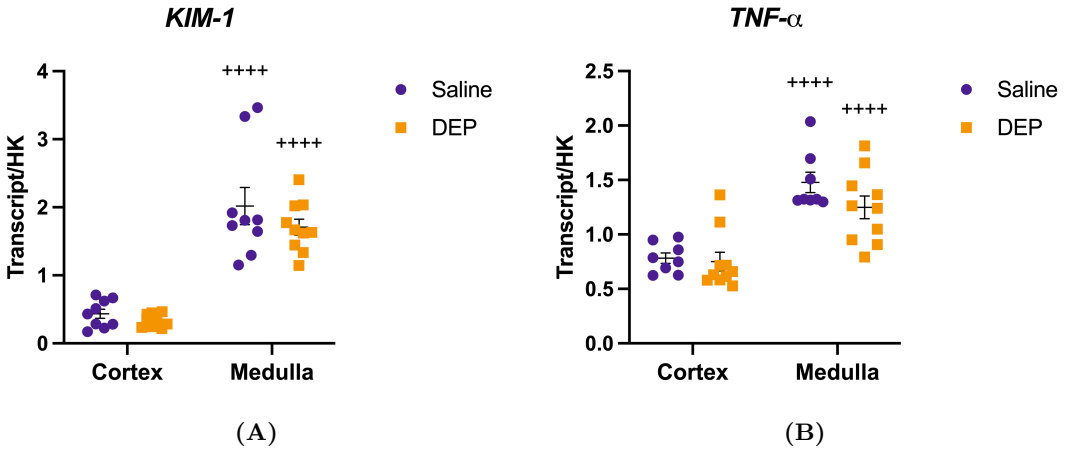

Figure 5.5: Effects of chronic pulmonary DEP exposure on transcript levels of biomarkers of kidney injury and inflammation. Mice were administered diesel exhaust particles (DEP, 50 µg) or saline (control) by pulmonary instillation (*it*) twice weekly for 4 consecutive weeks. Mice were culled ~18 h after last *it*, kidneys collected and renal transcript levels of (**A**) kidney injury molecule-1 (KIM-1) and (**B**) tomour necrosis factor-alpha (TNF-α) were measured by RT-qPCR (each dot indicates an animal). Results are normalised to the housekeeping (HK) gene glyceraldehyde 3-phosphate dehydrogenase (GAPDH) and data presented as Mean ± SEM; $^{++++}p \leq 0.0001$ (comparison between kidney regions within the same treatment group; Two-way ANOVA with a mixed-effects model fitted on log-transformed data).

		Saline	DEP
GAPDH	Cortex	17.87 ± 0.05	18.09 ± 0.10
	Medulla	18.27 ± 0.04	18.31 ± 0.07
KIM-1	Cortex	29.82 ± 0.24	30.31 ± 0.20
	Medulla	27.88 ± 0.18	28.11 ± 0.12
TNF-α	Cortex	32.56 ± 0.10	32.91 ± 0.21
	Medulla	32.06 ± 0.07	32.37 ± 0.17

Table 5.1: Raw Ct values of renal transcript levels following chronic DEP exposure. Mice were administered diesel exhaust particles (DEP, 50 µg) or saline (control) by pulmonary instillation (*it*) twice weekly for 4 consecutive weeks. Mice were culled ~18 h after last *it*, kidneys collected and renal transcript levels of kidney injury molecule-1 (*KIM-1*) and tomour necrosis factor-alpha (*TNF-α*) were measured by RT-qPCR (glyceraldehyde 3-phosphate dehydrogenase (*GAPDH*) served as housekeeping gene). Raw cycle threshold (Ct) values are presented for each treatment group as Mean ± SEM.

KIM-1 is a marker of proximal tubular damage, shown to be significantly upregulated in both renal tissue and urine following kidney injury. Urinary KIM-1 levels were measured in mice chronically exposed to DEP at three time points: baseline-before first exposure (U1), after 2 weeks (U2) and after 4 weeks of exposure (U3) (Figure 5.6). At baseline, urinary KIM-1 (uKIM-1) levels were similar in both groups-approximately 10 ng/mg uCr. In the saline group, uKIM-1 measurements remained stable across all time points. In the DEP group, there was no increase in uKIM-1 after 2 or 4 weeks compared to either baseline or saline concentrations at the corresponding time points.

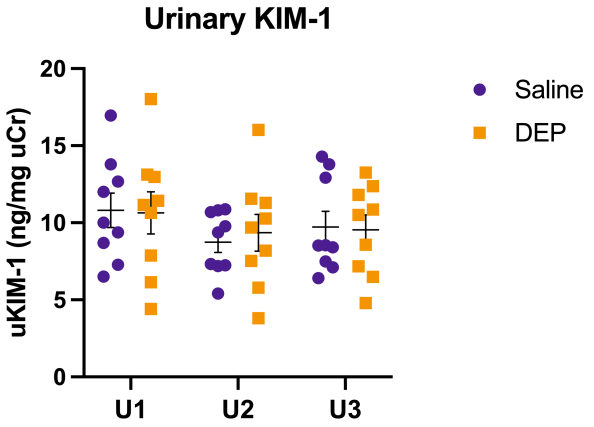

Figure 5.6: Effects of chronic pulmonary DEP exposure on KIM-1 excretion in the urine. Mice were administered diesel exhaust particles (DEP, 50 µg) or saline (control) by pulmonary instillation (*it*) twice weekly for 4 consecutive weeks. Mice were individually housed in metabolic cages (for 16–20 h) for urine collection prior to 1st *it* (U1), after 4th (U2) and after the final 8th *it* (U3). Mice were culled ~18 h after last exposure (immediately following U3 collection) and urinary KIM-1 (uKIM-1) levels were measured (each dot indicates an animal). Results are normalised to urinary creatinine (uCr) and data presented as Mean ± SEM; Two-way ANOVA with a mixed-effects model fitted on log-transformed data followed by Tukey's multiple comparisons test.

5.3.4 Chronic pulmonary DEP exposure may induce hypersensitivity to endothelium-dependent vasodilation in renal arteries

To investigate whether chronic pulmonary DEP exposure alters vascular function, renal artery grafts were assessed for their reactivity to PE, ACh and SNP. Renal artery vasoconstriction in response to KPSS was measured at the start of the experiment as a marker of vessel viability post-mounting. No significant difference in maximal constriction to KPSS was observed between vessels from saline- and DEP-exposed mice (Figure 5.7).

Dose-response curves were generated for each vasoactive drug and non-linear regression was used to calculate EC_{50} values (the concentration required to induce 50% maximal response) to assess vessel sensitivity. These curves and graphs with EC_{50} values are presented in Figure 5.8, with statistical analysis results summarised in Table 5.2.

The response to PE was nearly identical between the saline and DEP groups (p=0.7183; Figure 5.8A), as evidenced by their similar EC_{50} values (p=0.6058; Figure 5.8B). When challenged with ACh from a preconstricted state, renal arteries from DEP-exposed mice exhibited a trend towards increased vasodilation compared to controls, with a significant increase observed only at an ACh concentration of 100 nM (p=0.0457; Figure 5.8C). Although the overall ACh dose-response curves did not differ significantly between treatment groups (p=0.0844), a significant decrease in DEP EC_{50} was observed (p=0.0328; Figure 5.8D), suggesting that chronic DEP exposure may induce vascular hypersensitivity. No significant differences were observed in SNP-induced vasodilation between treatments (Figures 5.8E and 5.8F).

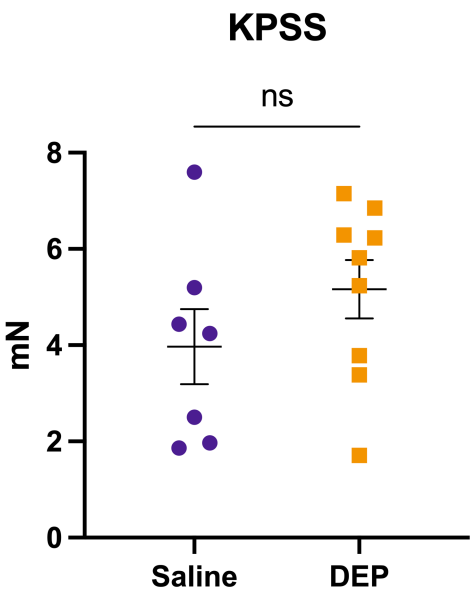

Figure 5.7: Effects of chronic pulmonary DEP exposure on KPSS-induced constriction of renal arteries. Mice were administered diesel exhaust particles (DEP, 50 µg) or saline (control) by pulmonary instillation (*it*) twice weekly for 4 consecutive weeks and culled ~18 h after last *it*. Renal arteries were isolated and mounted on a wire myograph. Vessel viability was assessed by measuring constriction in response to potassium-induced depolarisation (KPSS-high potassium physiological salt solution). Each dot represents an animal. Data presented as Mean ± SEM and analysed by unpaired Student's *t*-test; ns-not significant.

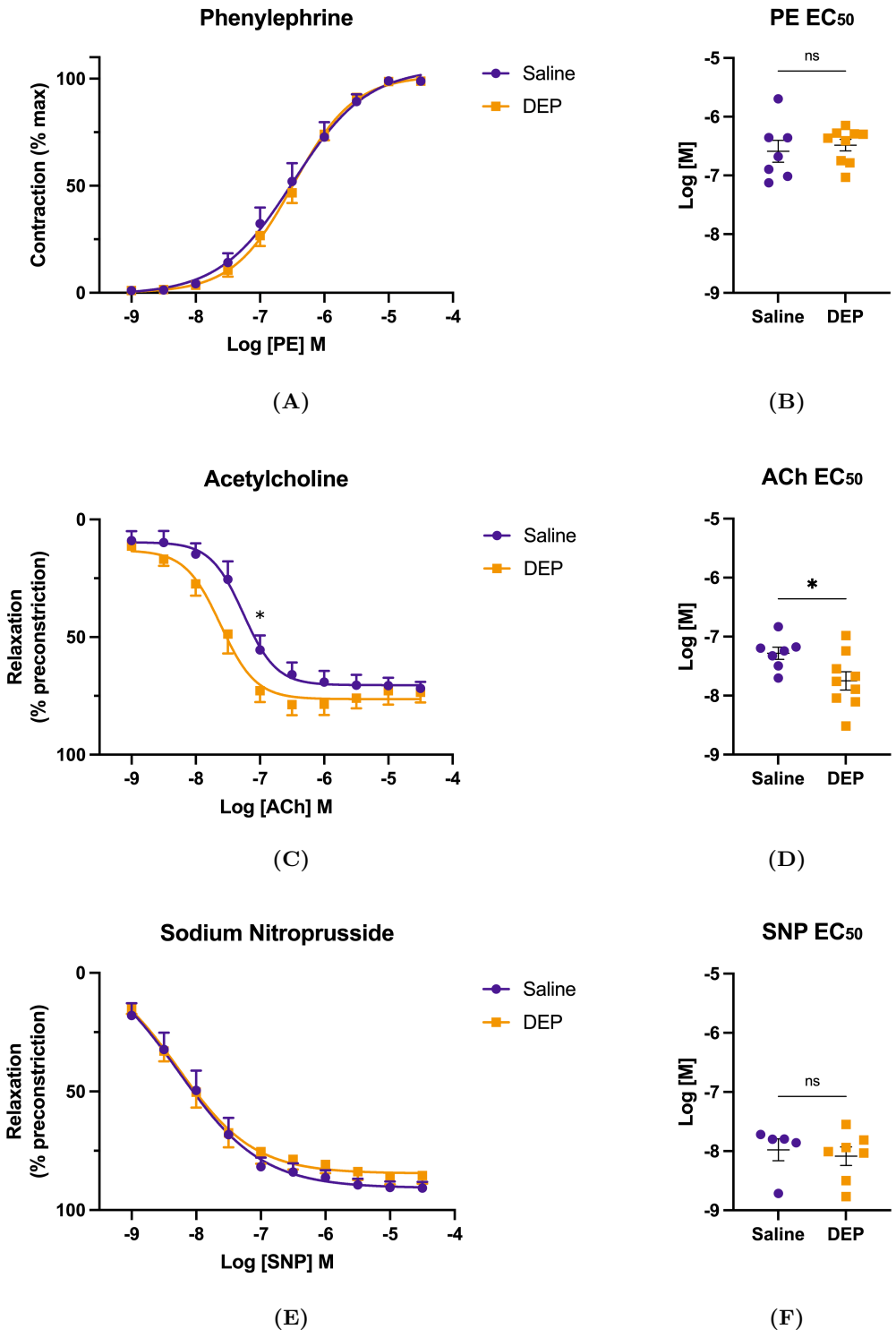

Figure 5.8: Effects of chronic pulmonary DEP exposure on renal artery vascular function *ex vivo*. Mice were administered diesel exhaust particles (DEP, 50 µg) or saline (control) by pulmonary instillation (*it*) twice weekly for 4 consecutive weeks and culled ~18 h after last *it*. Renal arteries were isolated and treated with phenylephrine (PE), acetylcholine (ACh) or sodium nitroprusside (SNP) to assess vascular function using wire myography. Each dot represents an animal. Data presented as Mean ± SEM; ns-not significant; $^*p \leq 0.05$ (dose-response curve analysed by Two-way ANOVA followed by Tukey's multiple comparisons test; EC_{50} values analysed by unpaired Student's *t*-test).

Drug	Source of Variation	% of total variation	P value	P value summary	EC_{50} P value
PE	Drug dose × Treatment	0.09422	0.9154	ns	0.6058
	Drug dose	92.86	<0.0001	****	
	Treatment	0.02185	0.7183	ns	
ACh	Drug dose × Treatment	1.284	0.0647	ns	0.0328
	Drug dose	75.39	<0.0001	****	
	Treatment	2.494	0.0844	ns	
SNP	Drug dose × Treatment	0.2359	0.7799	ns	0.6624
	Drug dose	82.12	<0.0001	****	
	Treatment	0.4199	0.5689	ns	

Table 5.2: Statistical analysis summary of the effects of DEP on renal artery vascular function *ex vivo*. Mice were administered diesel exhaust particles (DEP, 50 µg) or saline (control) by pulmonary instillation (*it*) twice weekly for 4 consecutive weeks and culled ~18 h after last *it*. Renal arteries were isolated and treated with phenylephrine (PE), acetylcholine (ACh) or sodium nitroprusside (SNP) to assess vascular function using wire myography (Figure 5.8). Table summarises results from statistical analysis for dose-response curves (Two-way ANOVA with Tukey's multiple comparisons test) and EC_{50} values (unpaired Students *t*-test). Text in red indicates statistical significance; ns-not significant, ****$p \leq 0.0001$.

5.4 Discussion

Our acute exposure study in Chapter 4 suggests that a longer exposure duration may be necessary to observe DEP-induced effects on renal function in healthy mice, reflecting more accurately the chronic nature of environmental pollution. Consequently, this chapter employs a chronic exposure protocol designed to maximise the duration, frequency and dose of DEP within the limits of the project license. Healthy, male C57BL/6J mice were administered DEP twice weekly for 4 consecutive weeks. Following exposure, tissues were collected for analysis: BALF and plasma to assess pulmonary and systemic inflammation, respectively, kidneys to evaluate injury and inflammation markers and perform histological assessment of renal morphology, urine to assess renal injury and renal arteries to evaluate vascular function using wire myography.

5.4.1 Chronic DEP exposure and pulmonary inflammation

To evaluate pulmonary inflammation following chronic DEP exposure, BALF TCC and cell differential analysis were performed. Prolonged DEP exposure significantly increased BALF TCC, primarily due to neutrophil infiltration, similar to acute exposure. Additionally, macrophage infiltration was also significantly increased. These findings align with previous studies involving DEP and other pollutants.

Miller *et al.* used this chronic exposure protocol in WT mice, administering the same DEP source (SRM 2975) at a slightly lower dose (35 µg). Despite reporting higher absolute cell counts, the impact of DEP on pulmonary inflammation was comparable, with significant increases in BALF TCC due to macrophage infiltration and a smaller contribution from neutrophils. Lymphocyte levels in the control group remained low and were unaffected by DEP treatment [157]. These findings were corroborated by another study, which showed similar inflammatory responses in mice exposed to DEP daily for 7 days at doses equivalent to approximately 120 and 360 µg per mouse [208].

Although acute DEP exposure primarily recruits neutrophils to the lungs, the macrophage recruitment observed in our chronic exposure study has also been reported with shorter protocols and/or lower DEP doses. For instance, Nemmar *et al.* found

that 4 *it* of 15 µg DEP in TO mice over 6 days were sufficient to result in similar BALF TCC and cell differential outcomes [209]. Other studies showed that even shorter protocols with 3 exposures at doses of 10 and 100 µg DEP induced such pulmonary inflammation [210, 211]. However, a dose-dependent response was noted in a study where mice received 5 DEP *it* over 15 days, with significant pulmonary inflammation observed only at the highest dose (120 µg per mouse) and not at lower doses (30 and 60 µg per mouse) [212]. Chronic exposure to $PM_{2.5}$ using whole-body chambers (5 h/day, 4 days/week for 8 weeks, median mass concentration of 375 µg/m^3) also resulted in substantial macrophage infiltration in rat lungs [148].

Histological evaluations consistently showed significant dose-dependent accumulation of particulates within alveoli of DEP exposed mice, primarily within macrophages, with some evidence suggesting dendritic cells may also play a role in particle phagocytosis [157, 208, 210–212]. However, the literature on cytokine levels in BALF following DEP exposure is inconsistent. Among longer exposure studies (7–8 *it*), those with higher doses (120 and 360 µg per mouse) and higher frequency (daily) reported significant increases in BALF inflammatory markers like TNF-α and IL-6 [208], while less frequent and lower dose protocols (twice weekly, 35 µg per mouse) showed no effect [157]. Variability also exists among shorter protocols (4–5 *it*). For instance, while some studies using DEP at doses of 30, 60 and 120 µg per mouse found no significant changes in BALF markers, including IL-5, IL-6, TNF-α and MCP-1, CXCL (KC) was elevated only at the highest dose [212]. Conversely, a protocol involving only 15 µg DEP was sufficient to significantly elevate BALF TNF-α levels, though not IL-6 [209].

5.4.2 Chronic DEP exposure and systemic inflammation

One proposed mechanism for the extrapulmonary effects of inhaled particulates is their uptake by alveolar macrophages and neutrophils, leading to cellular activation, cytokine release and subsequent pulmonary inflammation. These cytokines can then enter the bloodstream, causing systemic inflammation and OS (see Section 1.2.5). After

observing a significant increase in inflammatory cells in the lung following chronic DEP exposure, we next evaluated systemic inflammation. Our findings indicated no significant elevation in macrophage markers in the blood of mice after 4 weeks of DEP exposure.

These findings contrast with previous studies. For example, a single DEP instillation in rats at a similar dose significantly increased plasma TNF-α and IL-6 levels at 24 h post-exposure, though not at 6 h, with plasma CRP levels remaining unchanged [156]. In another study, multiple low-dose DEP exposures (4 *it*, 15 µg per mouse) in TO mice lead to significant increases in plasma TNF-α and CRP, but not IL-6, 48 h after the final instillation [209]. These findings suggest that a 24–48 h period post-exposure may be necessary to observe significant changes in systemic inflammatory markers. Additionally, they highlight the importance of measuring a comprehensive set of markers to capture any potential systemic effects of DEP exposure. Studies involving $PM_{2.5}$ exposure in rodents [149, 213] and humans [214] have consistently demonstrated the potential of these particles to induce systemic inflammation.

5.4.3 Effects of chronic DEP exposure on renal structure, injury and inflammation

The effects of chronic pulmonary exposure to DEP on renal health were evaluated through histological analysis of H&E-stained kidney sections to detect any gross abnormalities. No significant structural or morphological changes were observed in the renal tissue. Consequently, mRNA levels of kidney damage and inflammation markers were assessed. Our results showed no significant changes in the transcript levels of *KIM-1* or *TNF-α* following DEP exposure. Urinary KIM-1 levels were also measured at baseline and after 2 and 4 weeks of exposure, with no significant differences detected between treatment groups and time points.

Previous rodent studies have investigated the effects of chronic air pollution exposure on kidney function. However, variability in pollution sources (e.g.

standardised materials like DEP SRM 2975 vs outdoor $PM_{2.5}$), exposure methods (e.g. instillation vs whole-body chamber exposure) and protocols (e.g. duration, frequency, dose), as well as differences in rodent species and strains, complicate the interpretation and comparison of these findings across the literature.

Nemmar *et al.* utilised the same DEP source as our study to examine its renal effects in both rats and mice. Consistent with our findings, they reported no alterations in kidney damage markers following intratracheal instillation of DEP in Wistar rats (0.5 mg/kg, every 2^{nd} day for 8 days, 5 *it* in total) [153]. Plasma levels of urea, creatinine and creatinine clearance remained unaffected, as did levels of KIM-1, NGAL and 8-isoprostane in kidney homogenates, and albumin and GGT levels in the urine. Histological examination of H&E-stained kidney sections also revealed no changes in renal architecture post-DEP exposure [153]. However, when the same dose was administered to TO mice (every 4^{th} day for 4 weeks, 7 *it* in total), it resulted in different outcomes [154]. While traditional kidney injury markers (plasma urea, creatinine, creatinine clearance and TNF-α and catalase levels in renal homogenates) remained unchanged, DEP exposure significantly increased ROS production in the kidney and lead to renal morphological changes. DEP-treated mice exhibited more necrotic cells, dilated tubules, cast formation and higher scores for renal fibrosis and collagen deposition, as confirmed by Masson's Trichrome and Picrosirius Red staining [154]. Notably, the DEP dose used in both of these studies is equivalent to 12.5–15 µg per mouse, which is over 3 times lower than the dose used in our experiment.

Studies using $PM_{2.5}$ have further investigated the role of particulate pollution in renal disease. Chronic $PM_{2.5}$ exposure has been shown to induce inflammation and OS in the kidney, elevate BP and increase levels of RAAS components, including ACE and AT1R. Prolonged exposure also significantly elevated kidney injury markers, such as KIM-1 and NGAL, and lead to structural changes of the kidney, collagen deposition and fibrosis [147–150, 215]. However, it is important to note that these studies are typically conducted in whole-body exposure chambers with significantly longer exposure protocols, often lasting several hours per day, multiple days per week,

over several months. Additionally, the particles used in these experiments are frequently sourced from highly polluted regions, such as China, Taiwan and Mexico, with exposure concentrations that substantially exceed the WHO's recommended daily $PM_{2.5}$ limit of 15 µg/m^3 [71].

Our findings, along with those from similar studies, suggest that the renal injury observed under these experimental conditions may be too subtle to manifest as significant morphological changes, possibly reflecting early stages of inflammation and OS in the kidney. To investigate this further, I began the optimisation of IHC protocols for detecting the macrophage marker F4/80 and T cell marker CD3 in renal sections, but was unable to complete this work due to time constraints. Completing these stains could provide critical insights into the kidney's early inflammatory response to chronic DEP exposure.

The absence of renal effects following DEP exposure may be due to various factors, such as the experimental design and/or the health condition of the mice. After maximising the dose, exposure duration and frequency permitted under our project license, we further aimed to assessed the impact of chronic DEP exposure on renal function in a mouse model of hypertension, as discussed in detail in Chapter 6.

5.4.4 Impact of chronic pulmonary DEP exposure on renal artery vascular function

To investigate the impact of translocated nanoparticles on vascular function, we evaluated the sensitivity of renal arteries from healthy mice, chronically exposed to DEP, to PE, ACh and SNP using wire myography. Our findings indicated that chronic pulmonary exposure to DEP did not alter renal artery sensitivity to PE-induced vasoconstriction or to vasorelaxation induced by the endothelium-independent NO donor SNP. Although there was no significant overall effect on endothelium-dependent vasorelaxation in response to ACh, DEP exposure resulted in a leftward shift in the ACh dose-response curve and a significant reduction in EC_{50}, indicating a possible DEP-induced hypersensitivity to ACh-mediated

vasorelaxation.

To explore the mechanisms underlying the observed DEP-induced hypersensitivity to endothelium-dependent vasorelaxation, further experiments could be conducted. Among the five muscarinic receptors, the M3 subtype is critical for ACh-mediated vasodilation [216]. ACh binding to the M3 receptor initiates a signalling cascade that enhances NO production via nitric oxide synthase (NOS) [217]. Overexpression of M3 and/or NOS in renal arteries, as determined by Western blot analysis, could suggest their involvement in the DEP-induced hypersensitivity. Additionally, pre-treating vessels with an M3 receptor antagonist, such as 4-DAMP (4-diphenyl-acetoxy-N-methyl-piperidine methiodide) [218], or a NOS inhibitor, such as L-NAME (N^{ω}-Nitro-L-arginine methyl ester) [219], before assessing ACh-induced vasorelaxation could further elucidate their roles. A reduction or abolition of ACh hypersensitivity in DEP exposed mice following pre-treatment with these inhibitors would strongly implicate the M3 receptor and NOS in mediating these effects.

The literature on the effects of DEP on vascular function *ex vivo* is varied, likely due to differences in DEP doses, routes and duration of administration, rodent models and vascular beds studied.

In a study which used a protocol similar to ours (35 µg, 2 *it*/week, 4 weeks) to evaluate the effects of pulmonary DEP exposure on vascular function in WT mouse aortas, no significant changes in vessel responses to PE or SNP were observed between DEP and control mice. However, DEP exposure resulted in a leftward shift in the ACh dose-response curve, aligning with our findings, though it did not reach statistical significance [157]. Another study reported a significant increase in ACh-induced vessel relaxation in WT mice after DEP treatment, demonstrated by a leftward shift in the dose-response curve and a significantly higher maximal response [187]. This study utilised a single dose of DEP (0.5 mg/kg) administered via an *ip* injection, with mice sacrificed 1 h later. The higher dose of DEP reaching the circulation in this model likely accounts for the more pronounced vascular response observed. In this model, DEP had no impact on the sensitivity to SNP or the contractile response to PE [187].

Robertson *et al.* examined vascular function in isolated thoracic aorta, femoral and mesenteric arteries of rats at 2 h and 6 h post-intratracheal instillation of a single DEP dose (0.5 mg) [156]. While the contractile response to PE in femoral and mesenteric arteries was similar between DEP-exposed and control animals, a significantly greater response was observed in the aorta at 6 h post-exposure. No significant effects of DEP on ACh response were detected in any vessel at either time point, though a trend toward DEP-induced ACh hypersensitivity was noted in the mesenteric artery at 6 h post-exposure, similar to our observations. Sensitivity to SNP-induced vasodilation was comparable in aortas and femoral arteries from DEP- and saline-exposed mice, but a significantly greater sensitivity to SNP vasodilation was found in the mesenteric arteries of DEP-exposed mice 6 h post-exposure [156].

5.4.5 Chapter summary

In this study, the effects of chronic pulmonary DEP exposure on the kidney and renal vasculature in healthy mice were explored. In summary, the main findings of this chapter are:

- Chronic DEP exposure induced significant pulmonary inflammation, as evidenced by a marked increase in BALF total cell count and significant neutrophil and macrophage infiltration in the lungs.
- Prolonged DEP exposure had no effect on markers of systemic inflammation.
- No gross morphological abnormalities were observed in renal tissues following chronic DEP exposure. DEP did not affect renal *KIM-1* and *TNF-α* mRNA levels or urinary KIM-1 concentrations.
- DEP exposure lead to a leftward shift in the dose-response curve for endothelium-dependent vasodilation and significantly reduced EC_{50} values suggesting potential hypersensitivity to ACh treatment. No changes were observed for PE-induced vasoconstriction or endothelium-independent vasodilation by SNP.

Chapter 6

The effects of DEP exposure on renal function in a hypertension-induced mouse model of kidney injury

6.1 Introduction

Chapter 4 and Chapter 5 examined the effects of DEP exposure on renal function in healthy mice. The aim of this chapter was to investigate whether DEP would exacerbate renal injury in a mouse model of pre-existing kidney damage. Research in rodent models on the topic is sparse and primarily conducted by Nemmar and colleagues. They have utilised two models: the cisplatin (CP) model of AKI, involving a single *ip* injection of the drug, and the adenine (AD) model of CKD, in which animals were fed an AD-supplemented diet over several weeks. The mechanisms by which these models induce kidney disease are summarised below.

Cisplatin (cis-diamminedichloroplatinum (II)) is a potent platinum-based chemotherapy drug used to treat various malignancies, including breast, cervical, testicular and bladder cancers [220–223]. Its antitumour effects are mediated by DNA crosslinking, which impairs DNA repair mechanisms and leads to cell death. However, its clinical use is limited by severe side effects, particularly nephrotoxicity [224].

Although DNA-damaging agents are typically less toxic to non-proliferating cells, CP selectively damages the proximal tubular cells of the kidney. Approximately 20% of patients receiving high-dose CP develop severe renal dysfunction [225]. The pathogenesis of CP-induced AKI is primarily due to platinum accumulation in renal cells, which increases the production of TNF-α and ROS. These factors stimulate inflammation, OS, vascular injury and apoptosis, leading to renal damage. This results in accumulation of waste products, such as urea, nitrogen and creatinine, and reduced GFR, which are key clinical manifestations of nephrotoxicity [224, 226].

In the AD-induced model of CKD, AD is administered as a dietary supplement over several weeks (0.75% w/w for rats and 0.20% w/w for mice) [227–229]. Adenine, a common dietary component present in foods like meat, fish and legumes, induces renal disease at non-physiologically high concentrations [230, 231]. It is metabolised into the highly insoluble 2,8-dihydroxyadenine, which precipitates and forms crystals in the renal tubules, especially the proximal tubules [232, 233]. These crystals cause

mechanical obstruction and tubular epithelial damage, leading to an inflammatory response, ROS generation and OS [234, 235]. This process results in chronic kidney damage characterised by decreased renal function, increased proteinuria and albuminuria, elevated serum creatinine, tubulointerstitial injury and histological changes, such as interstitial fibrosis and tubular atrophy [236, 237].

Hypertension is a leading cause of kidney disease, affecting over a third of the adult population worldwide, with numbers expected to rise. Exposure to ambient air pollution has been linked to elevated BP in epidemiological and controlled exposure studies [238–241]. Therefore, we utilised a hypertension-induced mouse model of kidney injury by subjecting WT mice to prolonged administration of exogenous angiotensin II combined with a high-salt diet (Ang II+HSD).

6.1.1 Hypothesis and aims

The hypothesis explored in this chapter is:

Chronic exposure to DEP exacerbates pre-existing renal damage in a mouse model of hypertension-induced kidney injury.

Aims:

1. Investigate whether DEP administration amplifies systemic inflammatory markers in a mouse model of renal damage.
2. Evaluate renal function markers to determine if pulmonary DEP exposure exacerbates renal damage in a hypertension-induced model of kidney injury.

6.1.2 Study design

To address the aims of this chapter, a study was conducted in which healthy mice were fed a high-salt diet and administered exogenous Ang II via osmotic minipumps to drive hypertension-induced kidney injury. Concurrently, the mice received either DEP or saline through pulmonary instillation (*it*) twice weekly. The study, initially

planned for 4 weeks, was prematurely terminated after 2.5 weeks (16–18 days) due to spontaneous aortic ruptures in the animals. As a result, the last 5 mice were excluded from the protocol and therefore formed an additional control group, which was fed a normal chow diet, did not receive Ang II and was not instilled with DEP or saline (Table 6.1 outlines the groups and their respective treatments). Mice were culled ~18 h after the last 5th *it* and tissues collected. BALF was collected to assess pulmonary inflammation, blood samples were taken to analyse systemic inflammation and kidneys were harvested to quantify markers of renal injury, inflammation and OS and to examine changes in renal morphology. A diagram of the study design is presented in Figure 6.1.

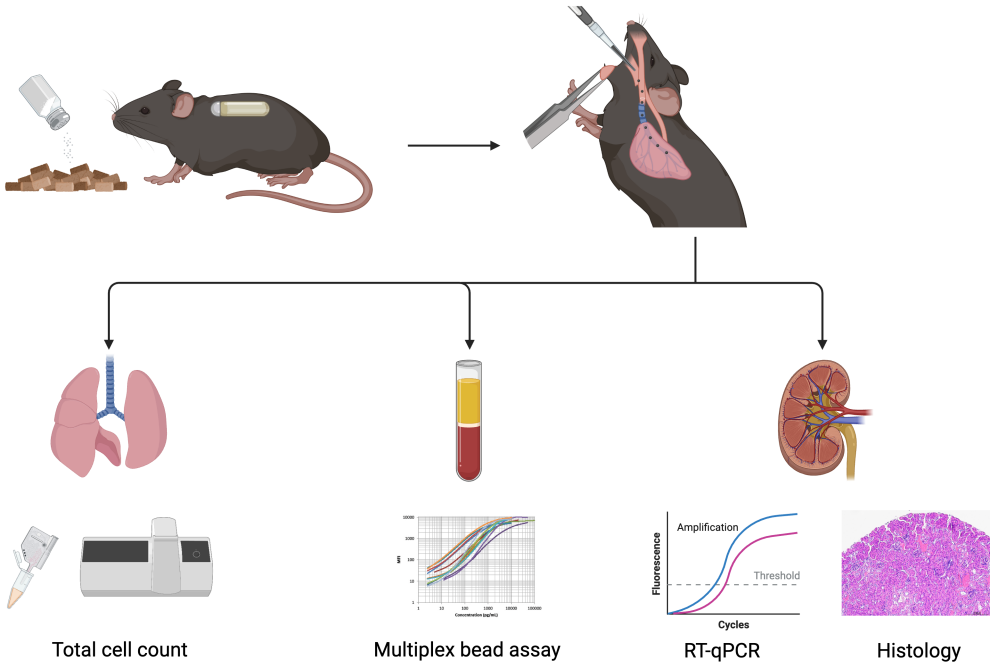

Figure 6.1: Study design of DEP exposure in a hypertension-induced mouse model of kidney injury. Mice were implanted with osmotic minipumps delivering exogenous angiotensin II (500 ng/kg/min) and fed a high-salt diet (3% Na^+) for 2.5 weeks (16–18 days) while simultaneously being administered diesel exhaust particles (DEP, 50 µg) or saline by pulmonary instillation (*it*) twice weekly (total of 5 *it*). A control group was fed normal diet (0.3% Na^+), did not receive angiotensin II and was not instilled. Mice were culled ~18 h after last *it* and various organs collected for measurement of DEP-induced effects on pulmonary and systemic inflammation and markers of renal injury. Figure created by the author using BioRender.

Group	Angiotensin II	High-salt diet	Saline/DEP
Control	-	-	-
Saline	+	+	Saline
DEP	+	+	DEP

Table 6.1: Treatment groups for studying DEP effects in a hypertension-induced mouse model of kidney injury. Angiotensin II-500 ng/kg/min, high-salt diet-3% Na^+, DEP-50 µg, saline-50 µL, "-" indicates the group did not receive angiotensin II, was on a normal-salt diet (0.3% Na^+) and was not instilled.

6.2 Methods

Each procedure performed in this chapter is detailed in the main Materials and Methods chapter. All animal experiments in this chapter were performed on healthy, adult, male C57BL/6J mice, aged 8–10 weeks at the start of the study and maintained under controlled conditions, further detailed in Section 2.1.

6.2.1 Osmotic minipump implantation

Minipump preparation

Minipump preparation was carried out using aseptic techniques to prevent contamination of both the solution and the minipump. Using a syringe and blunt-tipped filling tubes the osmotic minipumps were filled with Ang II at the desired dose of 500 ng/kg/min. This was done slowly to prevent the introduction of bubbles as this can affect pumping rates. Minipumps were then placed in sterile saline and kept at 37°C for 40 h for "priming" as per manufacturer's instructions. This step is essential as all minipumps have a start-up gradient during which they soak up fluid and come to temperature, therefore priming allows immediate pumping when implanted into the animal.

Minipump implantation surgery

Osmotic minipumps were implanted subcutaneously (*s/c*) in mice under isoflurane anaesthesia-4% used for induction in a chamber and 2–3% for maintenance via a nose cone. Prior to surgery animals received a *s/c* injection of Vetergesic analgesic (0.3 mg/mL) and 0.5 mL of 0.9% sterile saline to minimise post-operative pain and facilitate recovery. Hair from the lower cervical area was shaved and cleaned with iodine. A small incision was made at the nape of the neck and a *s/c* pocket was created using tissue separating scissors. The minipump was then placed in the pocket and the incision was closed with a 5-0 absorbable suture. Further detail on the minipump preparation and implantation surgery is outlined in Section 2.7 and a schematic diagram of the

procedure is presented in Figure 2.4. Immediately following surgery, mice were placed on a high-salt diet (3% Na^+; Special Diets Services, Essex, UK).

6.2.2 Particle administration

DEP (SRM 2975, NIST) was suspended in sterile saline (0.9% NaCl) at a concentration of 1 mg/mL and was always sonicated and vortexed prior to administration to avoid particle aggregation. Using the instillation/aspiration method mice were administered DEP twice weekly for 2.5 weeks (16–18 days) at a dose of 50 µg (total of 5 *it*). Briefly, mice were placed under transient isoflurane anaesthesia and following assessment of anaesthesia level, were placed supine on an angled board. Suspension of DEP (or saline-50 µL) was gently positioned at the base of the tongue as to be inhaled as the anaesthesia wore off. DEP was administered at a maximum frequency of once every 72 h and a minimum period of 48 h was allowed between minipump implantation surgery and first instillation. This procedure is detailed in Section 2.2.1.

6.2.3 BALF measurements

BALF collection

To assess pulmonary inflammation in mice following chronic DEP exposure, BALF was collected by lavaging the lungs three times with 0.9% NaCl. Primary lavage was kept separate, secondary and tertiary lavages were combined, now referred to as secondary lavage. BALF was centrifuged, cell pellet from primary lavage was resuspended in 1% BSA and combined with suspension from secondary lavage by gentle pipetting (see Section 2.3.1).

Total cell count

For each sample, 50 µL of cell suspension was mixed with equal volumes of lysis buffer and stabilising buffer, sample was drawn up a NucleoCassette™ and total cell count was established using a NucleoCounter™ (see Section 2.3.2).

6.2.4 Measurement of circulating cytokines using a multiplex assay

Mice were culled by terminal anaesthesia with an *ip* injection of Dolethal. Following assessment of mouse consciousness using the hind limb reflex test, blood was collected by cardiac puncture (syringe was pre-coated with citrate 3.8%), placed in an EDTA-coated tube and kept on ice. Within 30 min of collection, blood was centrifuged for 20 min at 1,000 × g, plasma was separated, placed in a fresh Eppendorf tube and stored at -80°C until further processing.

Cytokine levels were measured in plasma using the LEGENDplex™ Multi-Analyte Flow Assay Kit (Mouse Macrophage/Microglia Panel (13-plex); Biolegend®). Plasma samples were diluted 2-fold with Assay Buffer and run in singles. An 8-point standard curve was generated by making 1:4 serial dilutions from the stock standard provided (10,000 pg/mL). The final point of the standard was used as a blank (Assay Buffer only). Each standard was run in technical duplicates.

Samples were mixed with beads and either matrix C (for standards) or Assay Buffer (for plasma samples) and loaded onto a V-bottom 96-well plate. The samples and beads were mixed for 2 h at room temperature on a plate shaker, protected from light. Following incubation, the plate was centrifuged for 5 min and supernatant discarded. The plate was washed by dispensing 200 µL Wash Buffer into each well, incubating it for 1 min, centrifuging again for 5 min and finally discarding the Wash Buffer. This wash step was repeated twice. Samples were then incubated with Detection Antibodies for 1 h at room temperature on a plate shaker, protected from light. Streptavidin-phycoerythrin (SA-PE) was then added directly and allowed to incubate with the samples for 30 min at room temperature on a plate shaker, protected from light. The plate was centrifuged, supernatant discarded and plate washed as previously described, forming a bead pellet at the bottom of the plate at the end. Finally, the beads were resuspended in Wash Buffer by gentle pipetting. Samples were then read on a flow cytometer. A diagram detailing the underlying assay principle is presented in Figure 2.3 and a more comprehensive procedural outline is provided in Section 2.4.2.

6.2.5 Measuring mRNA levels in renal tissue by RT-qPCR

Tissue harvest

Mice were culled ~18 h after final 8th instillation by terminal anaesthesia with *ip* injection of Dolethal. Kidneys were dissected and the capsule removed. The left kidney was cut longitudinally and one half further cut horizontally into two. A quarter of each kidney was placed in RNA*later*™ solution for 24 h at 4°C, then stored at -80°C for further processing.

RNA extraction

Immediately prior to RNA extraction the quarter of mouse kidney was split into cortex and medulla, placed in QIAzol™ lysis reagent and homogenised using a tissue lyser. RNA was isolated using a commercial kit following manufacturer's instructions and RNA concentration was quantified using a spectrophotometer (see Section 2.5.2).

RT-qPCR

cDNA was synthesised using a commercial kit and following manufacturer's instructions. Briefly, for each RT reaction an RNA extract volume corresponding to 2,000 ng of diluted RNA was mixed with enzyme mix and RT buffer. Negative controls were also included, where RT enzyme or RNA were replaced with an equal volume of water. Samples were reverse transcribed on a Thermal Cycler and the cDNA generated was stored at -20°C until further processing.

The cDNA generated from the RT reaction was amplified and quantified using qPCR. An 8-point standard curve was constructed by pooling an equal volume from each cDNA sample and performing a 1:4 dilution for the first point and serial 1:2 dilutions for points 2–7. The final point of the standard was used as a blank (nuclease-free water only). The remaining cDNA was diluted 1:40 (2.5 ng/µL) to fall within the middle of the standard curve. For each reaction (run in technical triplicates) cDNA was mixed with master mix. Negative controls, as described above, were also added.

Reactions were run on a LightCycler instrument and quantification data were accepted if standard curve was satisfactory. Results were normalised against the average Cp value of the housekeeping gene GAPDH. Further details on the RT-qPCR protocol, master mix components, cycling conditions and primer sequences are outlined in Section 2.5.3.

6.2.6 Histology

Dissected mouse kidneys were place in 10% formalin for 24 h at room temperature before being transferred to 70% ethanol long-term. Samples were dehydrated up an ethanol gradient (70%, 80%, 95% and 100%) and xylene before embedding in paraffin blocks. Sections of fixed kidneys were cut (5 µm), stained with haematoxylin and eosin (H&E) and assessed for morphological abnormalities using light microscopy.

Haematoxylin and eosin staining

Kidney sections were deparaffinised in xylene and passed down an ethanol gradient for rehydration. After staining for 5 min with Harris modified Haematoxylin, sections were sequentially placed in acid alcohol, Scott's Tap Water Substitute and eosin. Slides were then taken back up the ethanol gradient and xylene and mounted with DPX. A more comprehensive staining protocol is detailed in Section 2.6.

6.3 Results

6.3.1 DEP exposure does not induce significant pulmonary inflammation in a hypertension-induced mouse model of kidney injury

Both saline and DEP treatment groups exhibited a tendency toward increased BALF TCC compared to untreated controls, however, these increases were not statistically significant (p=0.4351 and p=0.1573, respectively; Figure 6.2). Pulmonary instillation with DEP for 2.5 weeks did not result in a significant increase in BALF TCC compared to saline (p=0.5379), although a trend was noted. Due to the low number of replicates, these findings should be interpreted with caution.

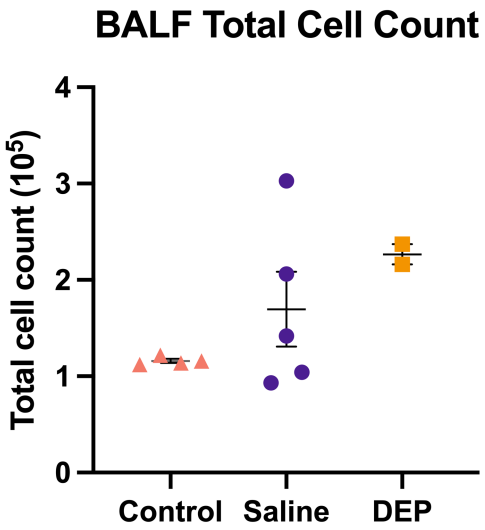

Figure 6.2: Effects of pulmonary DEP exposure on lung inflammation in a mouse model of hypertension. Mice were implanted with osmotic minipumps delivering exogenous angiotensin II (500 ng/kg/min) and fed a high-salt diet (3% Na^+) for 2.5 weeks (16–18 days) while simultaneously being administered diesel exhaust particles (DEP, 50 µg) or saline by pulmonary instillation (*it*) twice weekly (total of 5 *it*). Control group was fed normal diet (0.3% Na^+), did not receive angiotensin II and was not instilled. Mice were culled ~18 h after last *it*, bronchoalveolar lavage fluid (BALF) collected and analysed for total cell count. Data presented as Mean ± SEM (ordinary One-way ANOVA followed by Tukey's multiple comparisons test).

6.3.2 Pulmonary DEP exposure does not induce significant systemic inflammation in a hypertension-induced mouse model of kidney injury

Data from a multiplex assay indicated that combined Ang II+HSD treatment in mice resulted in a slight but statistically insignificant increase in some markers of systemic inflammation, which was not exacerbated by DEP exposure (Figure 6.3). Significant variance was observed within groups for most markers, which was accounted for in the statistical analysis. However, this and the low number of replicates require cautious interpretation of these findings.

A trend towards increased plasma CCL22 (MDC) levels was observed in both saline and DEP groups compared to controls, with mean values of 264, 369 and 45 pg/mL, respectively. DEP treatment did not significantly amplify the Ang II+HSD-induced increase (p=0.7131; Figure 6.3D). Concentrations of plasma CXCL were similar between control and saline groups (mean concentration ~120 pg/mL), but the DEP group exhibited a two-fold higher mean concentration (258 pg/mL; p=0.4052 and p=0.3592 compared to control and saline, respectively). Notably, most data points from the DEP group fell within the range of the control and saline groups (Figure 6.3A). A similar pattern was observed for IL-18 levels (Figure 6.3B).

A decrease in plasma G-CSF levels was noted in both saline- and DEP-treated animals compared to controls (p=0.0952 and p=0.1247, respectively), with no significant changes due to DEP exposure (Figure 6.3F). Concentrations of IL-23, IL-12p70 and IL-1β were generally at the limit of detection (LOD=0.24 pg/mL; Figures 6.3C, 6.3E and 6.3G).

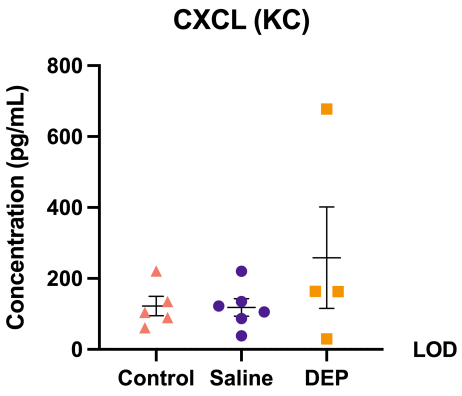
CXCL (KC)
Concentration (pg/mL)
800
600
400
200
0
Control
Saline
DEP
LOD

(A)

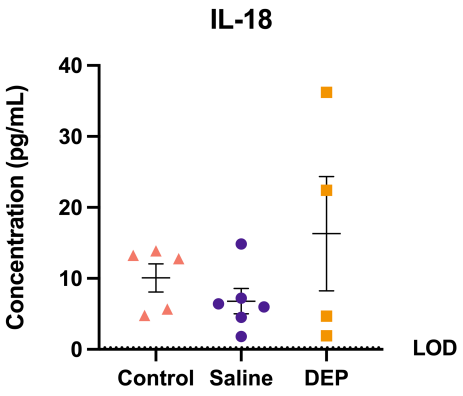
IL-18
Concentration (pg/mL)
40
30
20
10
0
Control
Saline
DEP
LOD

(B)

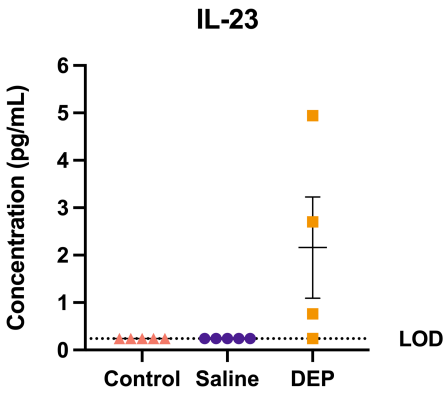
IL-23
Concentration (pg/mL)
6
5
4
3
2
1
0
Control
Saline
DEP
LOD

(C)

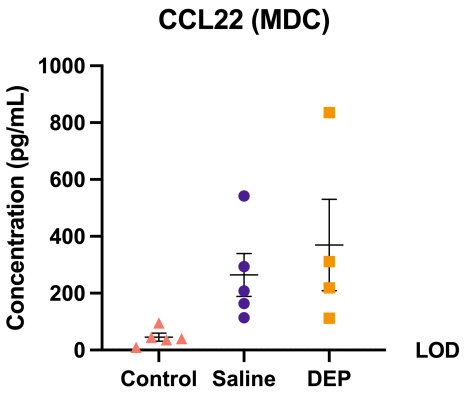
CCL22 (MDC)
Concentration (pg/mL)
1000
800
600
400
200
0
Control
Saline
DEP
LOD

(D)

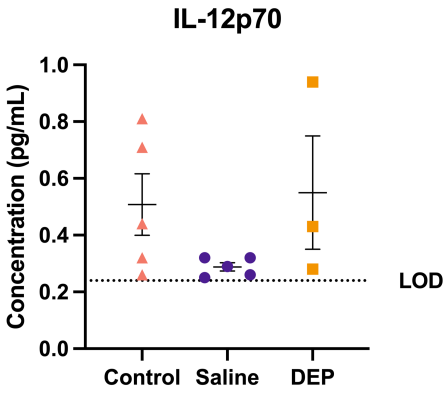
IL-12p70
Concentration (pg/mL)
1.0
0.8
0.6
0.4
0.2
0.0
Control
Saline
DEP
LOD

(E)

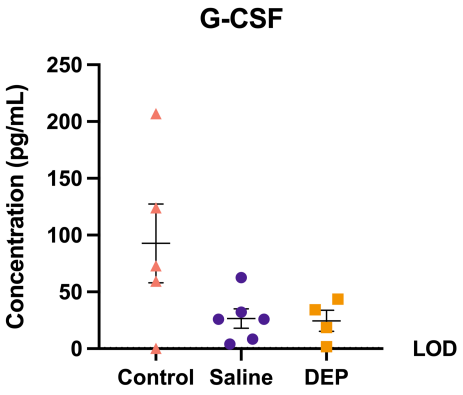
G-CSF
Concentration (pg/mL)
250
200
150
100
50
0
Control
Saline
DEP
LOD

(F)

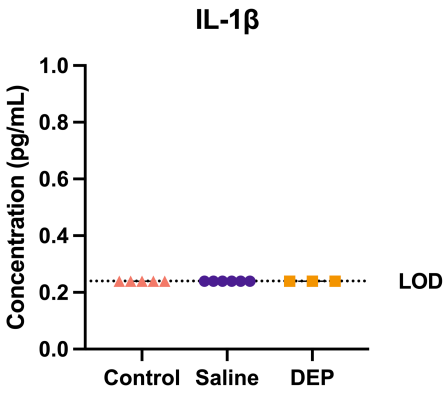

(G)

Figure 6.3: Effects of pulmonary DEP exposure on markers of systemic inflammation in a mouse model of hypertension. Mice were implanted with osmotic minipumps delivering exogenous angiotensin II (500 ng/kg/min) and fed a high-salt diet (3% Na^+) for 2.5 weeks (16–18 days) while simultaneously being administered diesel exhaust particles (DEP, 50 µg) or saline by pulmonary instillation (*it*) twice weekly (total of 5 *it*). Control group was fed normal diet (0.3% Na^+), did not receive angiotensin II and was not instilled. Mice were culled ~18 h after last *it*, blood collected by cardiac puncture, centrifuged and levels of various markers of systemic inflammation measured in plasma using a multiplex bead assay. Each dot represents an animal. Data presented as Mean ± SEM (ordinary One-way ANOVA followed by Tukey's multiple comparisons test). KC-keratinocyte chemoattractant, IL-interleukin, MDC-macrophage-derived chemokine, G-CSF-granulocyte colony-stimulating factor, LOD-limit of detection.

6.3.3 Pulmonary DEP exposure does not promote renal morphological changes in a hypertension-induced mouse model of kidney injury

To determine whether pulmonary DEP exposure exacerbates renal damage in mice with pre-existing kidney injury, histological evaluation was performed on kidney sections from mice administered Ang II and fed a high-salt diet, followed by instillation with saline or DEP. Mice in the control group received no treatment. H&E staining showed that Ang II+HSD treatment for 2.5 weeks did not cause gross abnormalities compared to control mice (Figure 6.4). DEP administration also did not induce morphological changes. No signs of tubular or interstitial damage were observed, such as loss of tubular cell nuclei, interstitial thickening or oedema.

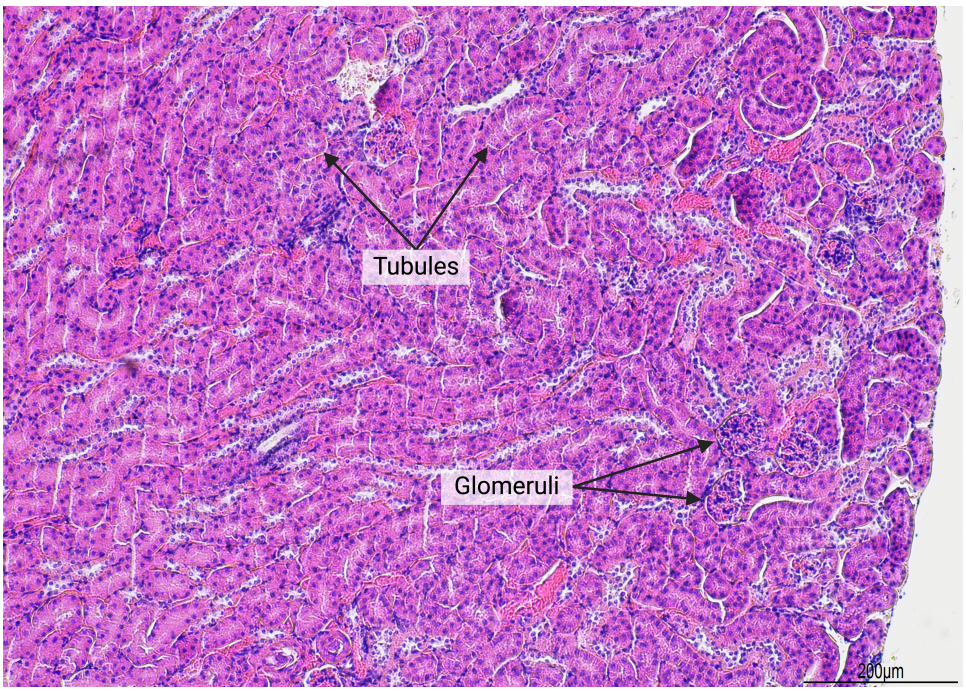

(A) Control

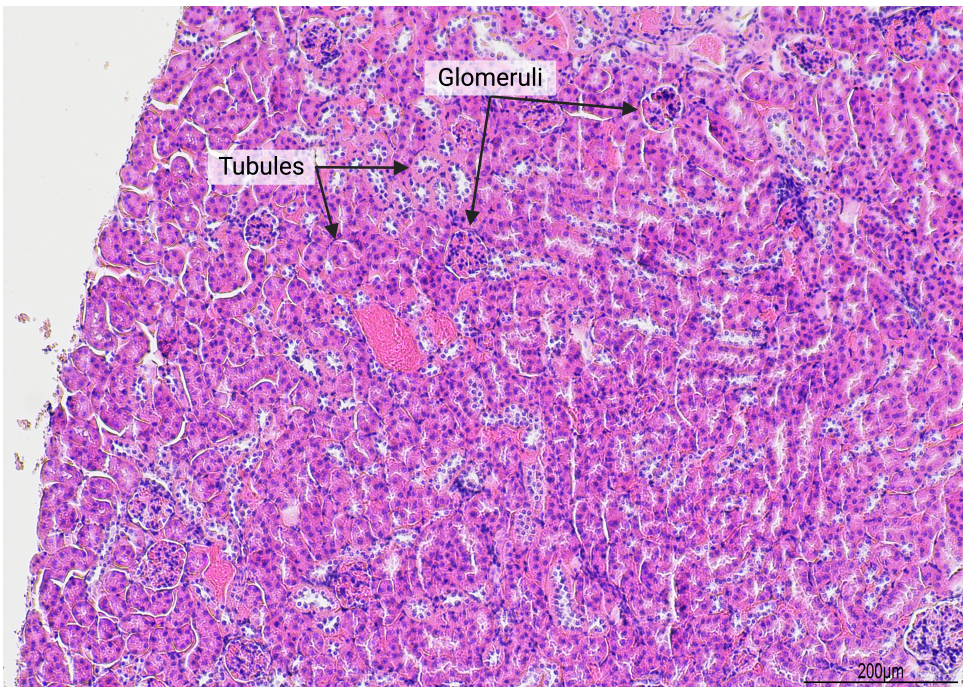

(B) Saline

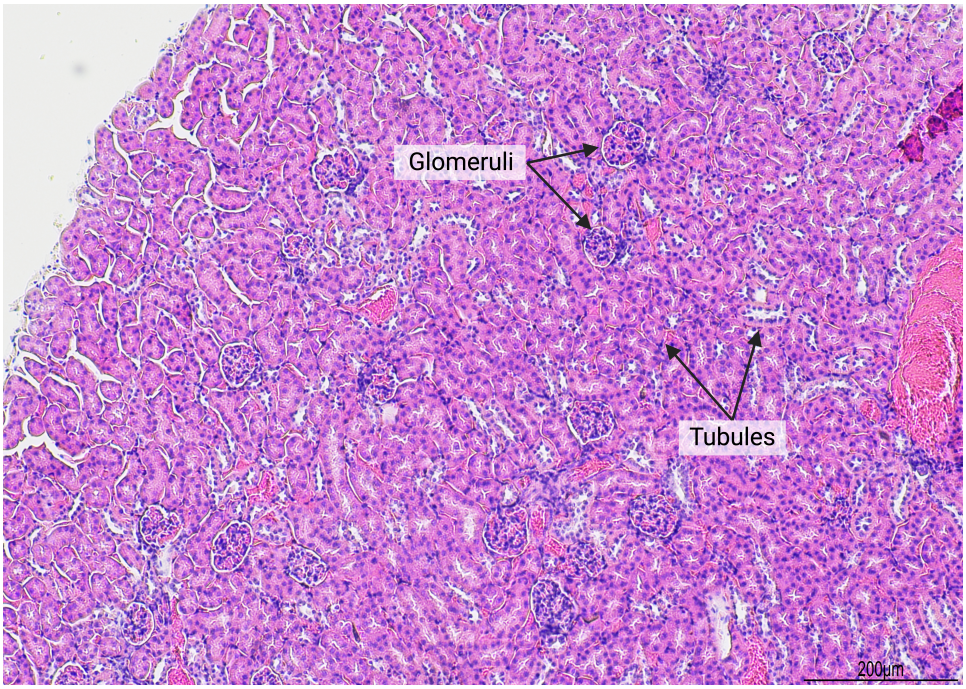

(C) DEP

Figure 6.4: Effects of pulmonary DEP exposure on renal morphology in a mouse model of hypertension-induced kidney injury. Mice were implanted with osmotic minipumps delivering exogenous angiotensin II (500 ng/kg/min) and fed a high-salt diet (3% Na^+) for 2.5 weeks (16–18 days) while simultaneously being administered diesel exhaust particles (DEP, 50 µg) or saline by pulmonary instillation (*it*) twice weekly (total of 5 *it*). A control group was fed normal diet (0.3% Na^+), did not receive angiotensin II and was not instilled. Mice were culled ~18 h after last *it*. Representative light microscopy images of haematoxylin and eosin (H&E)-stained kidney sections (5 µm) from (**A**) control, (**B**) saline and (**C**) DEP mice. Scale bar 200 µm.

6.3.4 DEP exposure may upregulate renal RAAS and OS genes in a mouse model of hypertension-induced kidney damage

The impact of DEP on exacerbating kidney damage in mice receiving pro-hypertensive treatment was evaluated by measuring mRNA levels of markers related to renal injury, inflammation, fibrosis, oxidative stress and genes involved in the RAAS (Figure 6.5). Significant variability was observed in some markers across groups, which was accounted for in the statistical analysis.

Compared to controls, Ang II+HSD treatment lead to a significant reduction in cortical *KIM-1* levels in both the saline and DEP groups (p<0.0001 and p=0.0062, respectively; Figure 6.5A). Medullary *KIM-1* levels in the saline group were slightly reduced compared to controls (p=0.0498). No increase in renal *TNF-*α mRNA was observed following Ang II+HSD treatment, with or without DEP exposure (Figure 6.5B).

Administration of Ang II+HSD, with or without DEP exposure, did not upregulate renal *Renin* expression (Figure 6.5C). However, a significant increase in Ang II receptor type 1A ($AT1_AR$) mRNA was observed in both hypertension-induced groups compared to controls (p=0.0114 saline, p=0.0030 DEP). Although not statistically significant, there was a trend towards higher cortical $AT1_AR$ levels following DEP exposure (Figure 6.5D).

A significant increase in cortical endothelial nitric oxide synthase (*eNOS*) and *SOD3* mRNA levels was observed in both Ang II+HSD-treated groups when compared to untreated controls (Figures 6.5E and 6.5F). While the Ang II+HSD-induced rise in *eNOS* was not amplified by DEP exposure, there was a trend towards higher renal *SOD3* levels in the DEP group compared to saline. Neither Ang II+HSD alone nor combined with DEP exposure altered *COL1A1* mRNA expression in renal tissue (Figure 6.5G). Raw cycle threshold (Ct) values for each gene and treatment group are presented in Table 6.2.

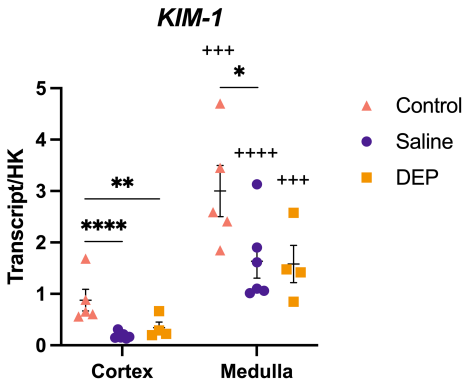
KIM-1
Transcript/HK
Cortex
Medulla
Control
Saline
DEP

(A)

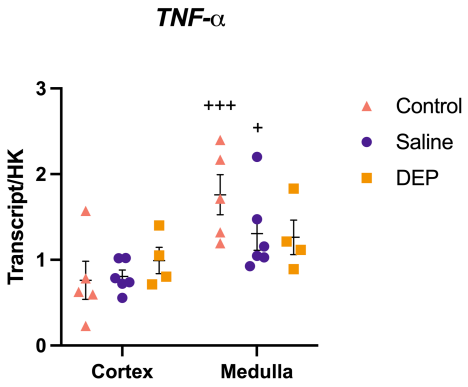
TNF-α
Transcript/HK
Cortex
Medulla
Control
Saline
DEP

(B)

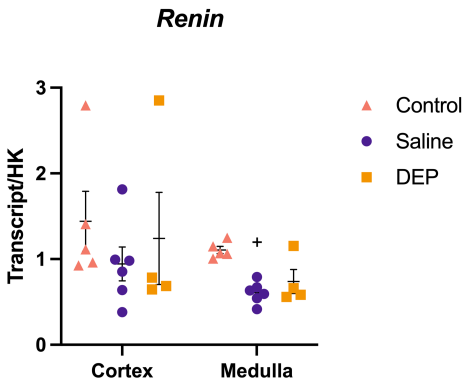
Renin
Transcript/HK
Cortex
Medulla
Control
Saline
DEP

(C)

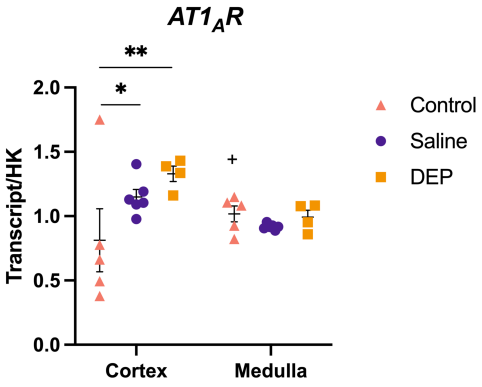
AT1AR
Transcript/HK
Cortex
Medulla
Control
Saline
DEP

(D)

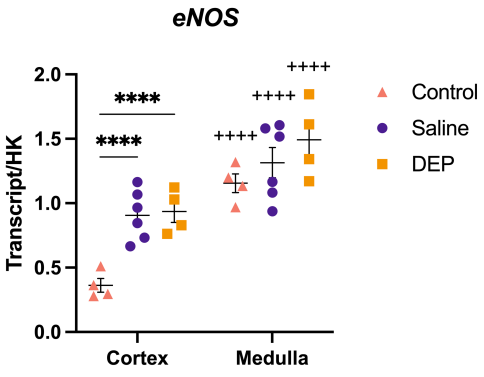
eNOS
Transcript/HK
Cortex
Medulla
Control
Saline
DEP

(E)

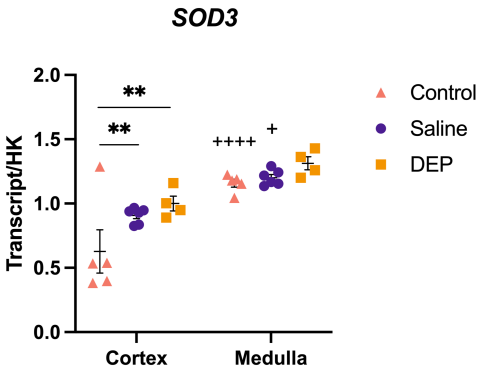
SOD3
Transcript/HK
Cortex
Medulla
Control
Saline
DEP

(F)

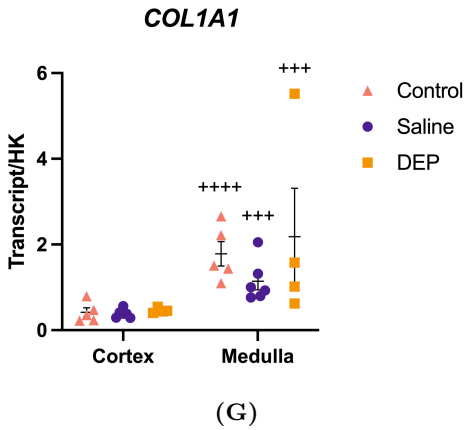

Figure 6.5: Effects of pulmonary DEP exposure on transcript levels of biomarkers of kidney injury and inflammation in a hypertension-induced mouse model of kidney injury. Mice were implanted with osmotic minipumps delivering exogenous angiotensin II (500 ng/kg/min) and fed a high-salt diet (3% Na^+) for 2.5 weeks (16–18 days) while simultaneously being administered diesel exhaust particles (DEP, 50 µg) or saline by pulmonary instillation (*it*) twice weekly (total of 5 *it*). A control group was fed normal diet (0.3% Na^+), did not receive angiotensin II and was not instilled. Mice were culled ~18 h after last *it*, kidneys collected and renal mRNA levels of (**A**) kidney injury molecule-1 (*KIM-1*), (**B**) tomour necrosis factor-alpha (*TNF-α*), (**C**) *Renin*, (**D**) angiotensin II receptor type 1A ($AT1_AR$), (**E**) endothelial nitric oxide synthase (*eNOS*), (**F**) superoxide dismutase 3 (*SOD3*) and (**G**) collagen type I alpha 1 (*COL1A1*) were measured by RT-qPCR (each dot indicates an animal). Results are normalised to the housekeeping (HK) gene glyceraldehyde 3-phosphate dehydrogenase (GAPDH) and data presented as Mean ± SEM. Comparisons between treatment groups within the same kidney region are indicated by *, whereas comparisons between kidney regions within the same treatment group are indicated by $^+$; $*/^+p \leq 0.05$, $**/^{++}p \leq 0.01$, $***/^{+++}p \leq 0.001$, $****/^{++++}p \leq 0.0001$ (Two-way ANOVA with a mixed-effects model fitted on log-transformed data followed by Tukey's multiple comparisons test).

		Control	Saline	DEP
GAPDH	Cortex	17.52 ± 0.34	17.93 ± 0.05	18.04 ± 0.12
	Medulla	18.60 ± 0.18	18.19 ± 0.11	18.31 ± 0.08
KIM-1	Cortex	27.63 ± 0.51	30.12 ± 0.17	29.50 ± 0.44
	Medulla	26.92 ± 0.36	27.42 ± 0.30	27.57 ± 0.30
TNF-α	Cortex	32.66 ± 0.39	32.77 ± 0.18	32.60 ± 0.33
	Medulla	32.34 ± 0.33	32.37 ± 0.22	32.53 ± 0.23
Renin	Cortex	24.86 ± 0.13	25.94 ± 0.31	25.82 ± 0.59
	Medulla	26.26 ± 0.20	26.74 ± 0.17	26.62 ± 0.24
$AT1_AR$	Cortex	24.65 ± 0.22	24.36 ± 0.07	24.26 ± 0.09
	Medulla	25.23 ± 0.21	24.95 ± 0.11	24.97 ± 0.07
eNOS	Cortex	28.50 ± 0.22	27.90 ± 0.09	27.96 ± 0.21
	Medulla	28.22 ± 0.20	27.63 ± 0.08	27.56 ± 0.22
SOD3	Cortex	20.42 ± 0.15	20.14 ± 0.04	20.12 ± 0.15
	Medulla	20.49 ± 0.16	20.00 ± 0.10	20.00 ± 0.13
COL1A1	Cortex	28.39 ± 0.21	28.76 ± 0.11	28.61 ± 0.20
	Medulla	27.34 ± 0.19	27.58 ± 0.19	27.20 ± 0.73

Table 6.2: Raw Ct values of renal transcript levels following DEP exposure in a hypertension-induced mouse model of kidney injury. Mice were implanted with osmotic minipumps delivering exogenous angiotensin II (500 ng/kg/min) and fed a high-salt diet (3% Na^+) for 2.5 weeks (16–18 days) while simultaneously being administered diesel exhaust particles (DEP, 50 µg) or saline by pulmonary instillation (*it*) twice weekly (total of 5 *it*). A control group was fed normal diet (0.3% Na^+), did not receive angiotensin II and was not instilled. Mice were culled ~18 h after last *it*, kidneys collected and renal mRNA levels of kidney injury molecule-1 (*KIM-1*), tomour necrosis factor-alpha (*TNF-α*), *Renin*, angiotensin II receptor type 1A ($AT1_AR$), endothelial nitric oxide synthase (*eNOS*), superoxide dismutase 3 (*SOD3*) and collagen type I alpha 1 (*COL1A1*) were measured by RT-qPCR (glyceraldehyde 3-phosphate dehydrogenase (*GAPDH*) served as housekeeping gene). Raw cycle threshold (Ct) values are presented for each treatment group as Mean ± SEM.

6.4 Discussion

6.4.1 Aortic aneurysms in mice induced by Ang II+HSD treatment

This study employed a hypertension-induced model of kidney injury. The experimental design involved inducing hypertension in mice via osmotic minipumps delivering Ang II combined with a high-salt diet. The mice were then randomly assigned to two groups and instilled with either saline or DEP. The Ang II dose was selected based on previous studies in the group, as we hypothesised it would be sufficient to induce renal injury without obscuring any DEP-induced exacerbation of renal damage [242].

Due to the sudden deaths of mice, the study was prematurely terminated after 2.5 weeks and mice were culled ~18 h after the 5^{th} instillation. Consequently, the last 5 animals in the study, unable to be put on the protocol, served as untreated controls. Among the 15 mice that started the protocol, 4 (27%) were found dead: 3 from the DEP group (on days 7, 8 and 10) and 1 from the saline group (on day 11). Post-mortem examinations indicated that deaths were caused by thrombosis in the cardiac area or thoracic/abdominal haemorrhages. The surgical procedure of minipump implantation was ruled out as a cause, as there were no thrombi around the surgical site and the sutures were intact. In another study conducted by a colleague, administration of the same Ang II dose to WT mice resulted in 2 deaths at a similar time point (days 7–8, death rate 8%), with the remaining 23 mice successfully completing the experimental protocol (personal communication).

While DEP has not previously been used in this Ang II+HSD model, our group has not observed adverse or pro-thrombotic effects with similar DEP exposure protocols in WT and $ApoE^{-/-}$ knockout atherosclerotic mice [157, 243]. Additionally, other groups have studied prolonged DEP exposure in drug-induced kidney injury models without reporting adverse effects. Examination at the end of the study revealed aneurysms in ~60% of the mice, evenly distributed between both treatment groups, suggesting that these adverse effects are likely due to Ang II (Supplementary Figure S.1 shows a

representative image of vessel bulging observed at tissue collection).

The impact of air pollution on aortic aneurysm formation has previously been studied in mice. Jun *et al.* investigated the effect of $PM_{2.5}$ on the development of abdominal aortic aneurysm (AAA) in $ApoE^{-/-}$ mice treated with Ang II. Mice were infused with Ang II (1,000 ng/kg/min) or saline for 4 weeks using osmotic minipumps (Ang II treatment was combined with a high-fat diet) [244]. During this period, mice were administered $PM_{2.5}$ (10 µg) or saline intranasally twice weekly. Results demonstrated that while saline infusion did not induce AAA formation in either group, Ang II infusion significantly increased AAA incidence in both saline- (58%) and $PM_{2.5}$-treated (94%) mice. Notably, 31% of mice in the Ang II+$PM_{2.5}$ group suffered aortic rupture, with deaths occurring every 3–4 days between weeks 1 and 3, whereas only 5% of mice in the Ang II+saline group died (1 mouse on day 9). The authors suggest that $PM_{2.5}$ exposure significantly increases the incidence of Ang II-induced AAA by promoting cellular senescence, with a significant increase in the expression of senescence markers observed at the 3 week time point [244].

In a recent study, Ming *et al.* investigated the impact of DEP on thoracic aortic aneurysm (TAA) progression in a β-aminopropionitrile (BAPN)-induced mouse model [245]. Three-week-old male C57BL/6J mice, either healthy or treated with BAPN, were administered DEP (10 µg, SRM 2975) or phosphate-buffered saline (PBS) for 2, 4 or 6 weeks. After 6 weeks, there were no significant differences in thoracic aorta diameter or the incidence of TAA and aortic dissection (AD) between the DEP and control groups. However, in BAPN-treated mice, DEP significantly increased AD incidence (40% vs 17%) and the thoracic aorta diameter. These effects were not observed at the 2- and 4-week time points. Additionally, mortality due to aortic rupture increased from 20% in the BAPN group to 38% in the BAPN+DEP group. The authors concluded that DEP exacerbated TAA and AD progression, potentially through enhanced apoptosis via the ERK1/2 MAPK signalling pathway [245].

These studies collectively indicate that prolonged particulate exposure (4–6 weeks) may exacerbate aortic aneurysm formation. Consistent with the present

experiment, both studies reported increased mortality in particle-treated mice due to aortic ruptures. However, in the current study, although 75% of deaths occurred in the DEP group, the small sample size and the equal distribution of aneurysms between saline- and DEP-treated mice at the time of tissue collection prevent drawing definitive conclusions about DEP's role in increasing aneurysm rupture risk.

6.4.2 The role of DEP in lung inflammation in a hypertension model of kidney injury

In the current study, BALF TCC was measured as an indicator of pulmonary inflammation following DEP exposure in mice treated with exogenous Ang II and fed a high-salt diet. Our data indicated a trend towards increased BALF TCC in Ang II+HSD mice compared to untreated controls, with DEP exposure appearing to further elevate BALF TCC. However, these differences were not statistically significant.

Ang II is implicated in respiratory diseases, including the pathogenesis of acute respiratory distress syndrome and its milder form-acute lung injury. Animal studies have shown that exogenous Ang II administration can induce lung injury, manifested by pulmonary oedema and alveolar filling, due to inhibition of alveolar fluid clearance [246]. Additionally, Ang II is associated with lung fibrosis. Studies in rodents suggest that angiotensin-converting enzyme 2 (ACE2) may have a protective role against Ang II-induced lung injury by converting Ang II to Ang 1-7. ACE2-deficient mice experience greater lung injury compared to WT mice, while recombinant ACE2 and Ang 1-7 treatment mitigate lung injury [247].

The pulmonary inflammatory potential of DEP is well documented in the literature and in the studies discussed in Chapter 4 and Chapter 5 of this thesis. The lack of significant increases in TCC following Ang II administration or DEP exposure in this study could be attributed to the small sample sizes (4, 5 and 2 mice in control, saline and DEP group, respectively). To obtain conclusive results, the experiment should be repeated with larger sample sizes.

6.4.3 Impact of Ang II+HSD on markers of inflammation, oxidative stress and renal injury in a mouse model of hypertension

In the current study, macrophage inflammatory markers were measured in plasma and renal tissue in a mouse model of hypertension. Our results indicated that Ang II+HSD treatment did not alter levels of circulating cytokines or renal *TNF-α* expression, which contradicts existing literature on the immune system's role in hypertension.

Myeloid cells, including macrophages and monocytes, are increasingly recognised as key players in the onset of hypertension [248]. Ang II-induced hypertension and subsequent organ damage are associated with increased proliferation and differentiation of hematopoietic stem cells into pro-inflammatory monocytes within the bone marrow [249]. In hypertension, activation of AT1R results in significant monocyte infiltration into the kidneys, where they further differentiate into macrophages [250]. Owing to the challenges associated with investigating organ macrophage infiltration in hypertensive individuals, majority of human studies concentrate on peripheral blood monocytes instead. Circulating monocytes in hypertensive patients show increased secretion of pro-inflammatory cytokines, such as IL-1β and TGF-β [251, 252]. Animal studies have shown that Ang II-induced hypertension raises BP, increases macrophage infiltration in renal tissue and induces fibrosis [253, 254]. Macrophages are critical in mediating BP elevation, OS and renal damage, as evidenced by significant reductions in these effects following macrophage depletion (prior to renal damage) or deficiencies in macrophage colony-stimulating factor (M-CSF)-important in macrophage differentiation, or CC chemokine receptor 2 (CCR2)-essential for macrophage recruitment [253, 255–257].

High-salt intake also promotes a pro-inflammatory macrophage phenotype. Studies in humans have shown that short-term increases in dietary salt intake elevate circulating pro-inflammatory monocytes [258]. *In vitro* studies on human monocyte-derived macrophages and mouse bone marrow-derived macrophages have demonstrated that increasing the NaCl content in the culture medium significantly

upregulates pro-inflammatory gene expression and downregulates anti-inflammatory gene expression [259].

In this study, renal inflammation was assessed by measuring *TNF-α* mRNA levels, which remained unchanged following Ang II treatment. These results differ from Guyonnet *et al.*, who reported a 3-fold increase in *TNF-α* mRNA in mice treated with Ang II+HSD compared to controls [242]. The discrepancy may be attributed to the longer infusion duration (6 weeks vs 2.5 weeks in our study) and the higher dose (1,000 ng/kg/min vs 500 ng/kg/min in our study).

In our model, a 2-week Ang II+HSD treatment did not increase renal *Renin* expression, consistent with the inhibitory effect of high Ang II levels on Renin release [260]. This aligns with previous studies in rats, where chronic Ang II infusion (6 weeks, 200 ng/kg/min) had no impact on intra-renal *Renin* expression [261]. However, another study reported a significant reduction in *Renin* levels following a 7-day Ang II infusion compared to the vehicle group. Similarly, rats on a high-salt diet (7.5% NaCl, 7 days) exhibited lower *Renin* levels than those on a normal-salt diet (0.3% NaCl), with the highest levels observed in low-salt conditions (0.07% NaCl) [262]. In the current study, $AT1_AR$ levels were significantly elevated in the Ang II+HSD group. Studies in rats have shown a slight but insignificant elevation in renal $AT1_AR$ expression after short term (7 days, 200 ng/kg/min) and chronic (6 weeks, 200 ng/kg/min) Ang II treatment [261, 262] or no change in receptor expression (13 days, 80 ng/min) [263]. Interestingly, however, feeding rats high-salt diet alone has been shown to significantly increase renal $AT1_AR$ expression [262]. Given the role of $AT1_AR$ in mediating Ang II-induced macrophage recruitment to the kidney, I began optimising an IHC protocol for the macrophage marker F4/80 in renal sections which was not completed due to time constraints. Completing the IHC staining and measuring additional inflammatory markers, such as IL-6 and TGF-β, which have been shown to be elevated following Ang II infusion [242, 261], could provide crucial insights into the kidney's inflammatory response in this model.

The kidney's high metabolic activity makes it particularly vulnerable to OS-a

critical pathway for organ damage in Ang II-induced hypertension. Our findings indicate that Ang II+HSD treatment significantly increases renal *eNOS* mRNA levels. Tojo *et al.* demonstrated that in rats, concomitant high-salt (HS) diet (6% NaCl) and Ang II infusion (6 days, 200 ng/kg/min) resulted in greater cortical eNOS expression compared to the HS diet alone, as shown by immunohistochemistry. Although eNOS protein levels were also elevated, the increase did not reach statistical significance [264]. Another study found no changes in renal *eNOS* mRNA levels following a 28-day Ang II infusion (1,000 ng/kg/min) compared to saline-infused controls (minipumps implanted on day 10 after unilateral nephrectomy) [265]. NO is a key signalling molecule in BP regulation and cardiovascular function. In the vasculature, eNOS synthesises NO from L-arginine. However, increased vascular OS, as seen in hypertension, can lead to eNOS uncoupling, causing it to produce O_2^- instead of NO. This shift generates free radicals and exacerbates OS.

Superoxide dismutases (SOD) are a family of antioxidant enzymes which convert O_2^- into H_2O_2 and O_2. Mammals have three SOD isoforms: intracellular SOD1, mitochondrial SOD2 and extracellular SOD3. Rodent studies have highlighted the protective role of SOD3 in renal disease and our study demonstrated that Ang II+HSD treatment results in significant increase in *SOD3* mRNA levels. Schneider *et al.* demonstrated that SOD3 deletion increased OS and kidney injury following ischaemia/reperfusion injury [266]. Guo *et al.* found that while $SOD3^{-/-}$ rats were phenotypically identical to WT rats up to 8 weeks of age, they developed severe CKD, characterised by interstitial fibrosis, tubular dilatation, hypertension and renal failure by 21 weeks [267].

Our findings suggest that Ang II+HSD treatment may induce eNOS uncoupling, leading to increased O_2^- production and a subsequent rise in *SOD3* expression as a compensatory mechanism to reduce OS. Since eNOS-derived NO is rapidly converted to nitrite (NO_2^-) and nitrate (NO_3^-), a nitrite/nitrate assay could determine if eNOS uncoupling is a mechanism for OS in our model. Reduced levels of these metabolites would suggest eNOS uncoupling.

In rodent models, Ang II infusion is known to cause renal fibrosis and excessive extracellular matrix (ECM) deposition. However, in our Ang II+HSD model, examination of H&E-stained renal tissue sections revealed no gross abnormalities in kidney morphology. Furthermore, the expression levels of *COL1A1*, which encodes the α-1 subunit of type I collagen (Col I), were comparable across treatment groups and untreated controls.

A previous study by Casare *et al.* demonstrated that compared to controls, Wistar rats treated with Ang II (200 ng/kg/min) for 6 weeks exhibited gross morphological changes in the kidney, including perivascular and tubulointerstitial fibrosis, along with elevated *Col III* transcript levels [261]. Similarly, Ang II treatment in mice significantly increased renal *Col I* and *Col IV* mRNA levels and intensified Col IV IHC staining in kidney sections [268]. The discrepancy between these findings and our results may be attributed to differences in the length of infusion (4 weeks vs 2.5 weeks in our study) and/or the Ang II dose (1 mg/kg/day, equivalent to 694 ng/kg/min, vs 500 ng/kg/min in our study).

6.4.4 The role of DEP in exacerbating systemic and renal effects following Ang II+HSD treatment

Comparing exposure studies is challenging due to differences in animal models of renal damage and variations in pollutant source, exposure duration, frequency and dose and rodent type and strain.

In our study, 2.5 weeks of pulmonary DEP exposure did not elevate markers of inflammation or OS in the circulation and kidney. Given the length and frequency of exposure, these findings align with data from other groups. In a rat CP model of AKI, a single DEP instillation slightly increased plasma IL-6 levels but did not alter other inflammation or OS markers, including plasma CRP and TAC [151, 152]. Conversely, in an AD model of CKD, prolonged DEP exposure over 4 weeks significantly raised renal TNF-α protein levels, increased ROS production, induced DNA damage and reduced renal catalase levels [153, 154].

Measurement of *KIM-1* mRNA indicated that DEP did not induce proximal tubular injury in our hypertension model, differing from findings in CP models of kidney disease. In a rat AKI model, a single DEP exposure did not exacerbate CP-induced changes in renal injury markers, such as renal GSH, urinary NAG, plasma NGAL and serum urea and creatinine [151, 152]. DEP only aggravated CP-induced changes when the dose was doubled to 1 mg/kg [152]. However, more frequent DEP exposure (instillation every 2nd day for 8 days) significantly increased plasma urea, renal NGAL and urinary albumin and GGT compared to CP treatment alone [153]. Furthermore, in our hypertension model, DEP exposure did not result in significant renal structural abnormalities or changes in collagen mRNA levels. This contrasts with findings in an AD model of CKD, where DEP instillation every 2nd day for 4 weeks lead to notable renal damage, characterised by necrosis, tubular dilation and cast formation [155].

These results suggest that prolonged exposure and/or higher DEP doses are required to exacerbate renal damage in these models. Future studies could involve infusing mice with a lower Ang II dose over a longer period (6 weeks) to enhance survival and allow for an extended DEP exposure protocol to be employed. Our data indicated that DEP did not induce tubular injury in this hypertension model, however, future experiments should evaluate markers of glomerular and/or tubulointerstitial damage.

6.4.5 Chapter summary

This study explored the potential of DEP to exacerbate renal damage in a mouse model of hypertension. In summary, the main findings of this chapter are:

- Ang II infusion, combined with a high-salt diet for 2.5 weeks, lead to aortic rupture in mice, likely as a result of aortic aneurysm.
- BALF TCC was slightly elevated in the hypertension model, with pulmonary DEP exposure showing a non-significant trend towards further increase.

- Ang II+HSD treatment significantly increased oxidative stress markers in the kidney without inducing systemic or renal inflammation and DEP exposure did not exacerbate these effects significantly.
- Ang II+HSD treatment had no effect on *Renin* mRNA levels, but notably increased $AT1_AR$ transcripts, with concomitant DEP exposure showing a non-significant trend towards further increase.
- Following Ang II+HSD treatment, *KIM-1* mRNA levels were markedly reduced, irrespective of DEP exposure.
- No morphological abnormalities or changes in *COL1A1* mRNA expression were observed in renal tissues from the hypertension mouse model, regardless of DEP exposure.

Chapter 7

Discussion

7.1 Summary of findings

The central hypothesis of this thesis is that inhaled diesel exhaust particles can cross the alveolar-capillary barrier, enter the bloodstream and reach distant organs, including the kidneys, where they accumulate, leading to direct impairment of renal function and the induction of renal vascular dysfunction. Additionally, I hypothesised that DEP-induced renal effects will be exacerbated in a mouse model of hypertension-induced renal injury.

Currently, it is not possible to track diesel exhaust particles in the body, therefore, gold nanoparticles were used as a model. To test these hypotheses, mice were first exposed to synthetically produced gold nanoparticles of varying sizes and their biodistribution was tracked through the circulation, kidneys and urine using the highly sensitive inductively coupled plasma mass spectrometry (ICP-MS) technique. Subsequently, standardised diesel particles were used to assess their effects on renal function in healthy mice under both acute and chronic exposure conditions. The impact of translocated DEP on vascular function was initially investigated by *in vitro* exposure of isolated renal arteries from healthy mice to DEP, followed by analysis of renal vascular function of renal arteries isolated from mice chronically exposed to DEP. Finally, a chronic angiotensin II infusion combined with a high-salt diet was used to model hypertension-induced renal injury and evaluate whether DEP exposure exacerbates renal impairment in this context.

The key findings of this thesis are:

- Inhaled nanoparticles translocated to the circulation in a size-dependent manner, with particles <7 nm accumulating in the kidneys.
- In healthy mice both acute and chronic DEP exposure induced pulmonary inflammation with significant inflammatory cell infiltration to the lungs.
- DEP had no substantial effects on markers of systemic inflammation either in healthy mice, or in our hypertension model.

- In healthy mice, DEP exposure did not cause gross abnormalities in renal tissue or affect the expression of kidney markers associated with inflammation and injury.
- DEP exposure impaired NO-dependent vasodilation in renal arteries *in vitro* and chronic DEP exposure in healthy mice suggested a potential hypersensitivity to endothelium-dependent vasodilation *ex vivo*.
- Angiotensin II infusion and a high-salt diet significantly increased expression of oxidative stress markers and RAAS components in the kidney. Although not statistically significant, DEP exposure showed a trend toward increased expression of some of these markers without affecting markers of renal injury or leading to gross morphological abnormalities.

7.2 Nanoparticle translocation as a mechanism for DEP effects

The first experiment in this thesis aimed to investigate particle translocation as a mechanism underlying the extrapulmonary effects of DEP exposure. Combustion-derived particles typically consist of a carbon core with surface-bound toxic compounds, including transition metals and organic chemicals, such as quinones and polycyclic aromatic hydrocarbons [97, 126]. Although previous studies have shown that inhaled DEP can harm biological tissues, including the kidneys, they have not conclusively demonstrated direct DEP translocation to extrapulmonary organs. This limitation is likely due to the carbon-based structure of the particles which are difficult to quantify and visualise from biological carbon and the extremely low concentrations reaching secondary target organs (estimated at <1–2% [171, 175]).

To address this challenge, various radiolabelled particles have been developed to simulate diesel exhaust particles and study their translocation. For instance, translocation of radiolabelled polystyrene ultrafine particles to the circulation and organs was observed in rats following instillation, with significantly greater

translocation in rats pre-treated with lipopolysaccharide, suggesting that lung inflammation increases alveolar permeability, facilitating particle movement into the circulation [269]. In humans, radiolabelled carbon particles (technetium-99m (^{99m}Tc)-labelled, primary particle size 5–10 nm) were used to demonstrate particle translocation to the blood as early as 1 min after exposure, and to the bladder and liver within 5 min [96]. However, a subsequent study using the same radiolabelled particles did not replicate these findings in healthy volunteers and suggested that the observed radioactivity in the previous study may have been due to the dissociation of the radiolabels from the particles before entering the circulation [270].

To directly measure particle translocation and concentration in the blood, urine and kidneys, we employed gold nanoparticles and used ICP-MS for quantification. This approach successfully demonstrated the accumulation of ultrafine particles in renal tissues following chronic exposure. As discussed in Chapter 3, future research could further investigate nanoparticle translocation by Raman spectroscopy to determine whether nanoparticles preferentially deposit in specific renal regions and whether such deposition is size-dependent. This would have a number of advantages including: (1) Raman can be used for quantification of the levels of gold, not in real concentration terms, but in a semi-quantitative manner between groups. This would provide a back-up measure to the ICP-MS, (2) Raman can be used to generate a visual map of gold localisation across tissue sections (albeit without the structural resolution of electron microscopy), and (3) Raman detects the vibration of molecules in non-ion form, as opposed to ICP-MS, which does not distinguish between soluble and insoluble gold, therefore, using Raman will serve as confirmation that the gold detected was in a particulate form.

Recent research has increasingly focused on the potential application of gold nanoparticles in the diagnosis and treatment of kidney disease. Intravenous administration of renal clearable, near infrared-emitting glutathione-coated gold nanoparticles, followed by fluorescent imaging, has been successfully tested as a non-invasive method for detecting kidney dysfunction in a mouse model of unilateral

obstructive nephropathy [271]. Additionally, the potential of intra-arterial injection of gold nanoparticles conjugated with an anti-collagen-I antibody, followed by computed tomography, has been explored as a non-invasive alternative to renal biopsy for assessing renal fibrosis in a mouse model of unilateral renal artery stenosis [272]. Furthermore, studies are investigating the use of gold nanoparticles as drug delivery agents to achieve more targeted therapeutic interventions in the kidneys [273–276].

7.3 DEP exposure model

In experimental research, various methodologies are employed to expose humans and animals to particulate matter. In human studies, inhalation is the preferred method as it closely mimics real-world exposure, often utilising specialised exposure chambers for controlled environments [116, 118, 277, 278]. Similarly, inhalation is considered the most physiological approach for animal studies and is employed particularly in studies using PM collected from urban environments [148, 215]. However, this method presents challenges, especially in rodents, which are obligate nose breathers with intricate nasal passages. These anatomical features, including nasal hairs and cilia, significantly filter inhaled particles before they reach the lungs [126, 279]. Additionally, whole-body exposure chambers pose a risk of particles adhering to the animal's fur, further complicating accurate dose calculations [279]. Moreover, the use of specialised equipment required for this technique is not always feasible and prolonged confinement of mice in inhalation tubes for several hours each day may raise ethical concerns due to potential stress and discomfort experienced by the animals. As an alternative, instillation methods are widely used for pulmonary exposure to particulate matter (in the absence of gas). Intratracheal and oropharyngeal aspiration instillation (the latter being utilised for DEP exposure in this thesis) are two commonly employed techniques. These almost identical methods are highly effective in delivering and dispersing particles uniformly across the alveoli and have been shown to produce similar deposition and clearance profiles [280–282].

As detailed in Section 1.2.3, ultrafine particles in air pollution are recognised as the

most harmful to human health, with diesel engine exhaust being a significant source of these nanoparticles. DEPs are therefore likely to play a major role in the health risks associated with exposure to particulate matter in urban environments. For all DEP exposure studies conducted, a standard reference material (SRM 2975) was used [283]. This material, derived from a diesel engine of an industrial forklift, is commonly used in research, enabling direct comparisons across the literature in the field. Additionally, its capacity to generate superoxides is well documented [123, 284]. Due to the challenges and limitations of chronic exposure protocols, very high DEP doses are often employed in animal studies. In this thesis, a 50 µg dose was used in most experiments, which is a common dose used in similar research. The 24 h instilled dose used here is estimated to be 30–40 times higher than the equivalent alveolar deposition from a 24 h inhalation of 100 µg/m^3 in humans (adjusted for mice using the MPPD model) [156, 157, 285].

7.4 Inflammatory response to DEP exposure in the lungs and circulation

In accordance with our hypothesis of particles translocating from the lungs, through the circulation and ultimately sequestering in the kidney, in every experiment the effects of DEP was investigated in each of these sites. Both acute and chronic DEP exposures resulted in pulmonary inflammation, evidenced by increased TCC in BALF and significant immune cell infiltration in the lungs. When employing the acute exposure protocol, lung inflammation was observed only at 18 h post instillation. However, at 16 h and in our hypertension model, a trend towards increased BALF TCC was observed in the DEP group, however, as previously discussed, the low sample size prevents definitive conclusions from being drawn (16 h saline group n=3, Ang II+HSD DEP group n=2). The presence of diesel particles in BALF after lung washout further confirmed particles were effectively deposited in the lungs, rather than being misdirected to the oesophagus. Given that examining pulmonary inflammation was not the primary focus of this thesis, cytokine release in BALF was not measured, as this has already been well documented by others

[156, 189]. Additionally, previous studies have shown that saline instillation does not induce pulmonary or systemic inflammation when compared to untreated controls, eliminating the need for a non-instilled control group in our experiments [156].

When investigating the systemic effects of DEP exposure in rodents, most studies focus on measuring three markers-IL-6, TNF-α and CRP-with inconsistent results, highlighting the need for a broader panel of markers. To address this, we employed a multiplex bead assay, which combines sandwich ELISA with flow cytometry, enabling the simultaneous measurement of multiple macrophage markers using a smaller blood volume than traditional ELISA (assay details in Section 2.4.2). Our results demonstrated that DEP significantly elevated plasma levels of IL-18 and CCL22 (MDC) at 6 h post-instillation, but this inflammatory response was largely resolved by 16 h. Prolonged exposure did not significantly alter plasma inflammatory markers in either healthy mice, or our hypertension model. Notably, 18 h after DEP exposure a slight decrease in plasma levels of IL-6 (following a single instillation), CCL22 (MDC), CXCL (KC) and G-CSF (after chronic exposure) was observed. Interestingly, a recent study also found that *in vitro* exposure of normal human bronchoepithelial cells to SRM 2585 (a model of settled indoor dust) significantly reduced IL-1β and to a lesser degree IL-6 production compared to the negative control [286]. In our analysis, cytokines with an R^2 value <0.9 were excluded from analysis as values below this threshold indicated a poor fit of the standard curve to the data, suggesting that the relationship between the known concentrations and the corresponding readings is not sufficiently reliable, potentially leading to inaccurate quantification of cytokine concentrations in the samples. Additionally, as samples were run in technical singles, further optimisation is needed and future studies should employ triplicate measurements to enhance reliability.

7.5 The impact of DEP on renal vascular function

To assess the effects of DEP exposure on vascular function, two experiments were conducted. The first was a proof-of-concept study designed to mimic particle

translocation to the circulation. Our findings revealed that *in vitro* application of DEP directly to renal arteries isolated from healthy mice impaired their response to ACh and SNP, as indicated by a rightward shift in the dose-response curves (see Chapter 3). In the second study, vascular reactivity was evaluated in renal arteries isolated from healthy mice after 4 weeks of pulmonary DEP exposure. Interestingly, while prolonged DEP exposure did not affect SNP-induced vasorelaxation, a leftward shift was observed in the ACh dose-response curve (see Chapter 5).

The discrepancy between these studies reflects differences between acute direct exposure and chronic pulmonary exposure. In the *in vitro* model, arteries were exposed to a high concentration of DEP in an isolated system, where particles could directly scavenge NO via particle-derived superoxide. This may result in an acute impairment of NO-mediated vasodilation, indicated by the rightward shift in the dose-response curve. The short exposure duration limits the adaptive endothelial responses that could counteract the effects of oxidative stress, resulting in a vasodilatory dysfunction.

In contrast, arteries isolated from mice subjected to chronic pulmonary DEP exposure displayed a hypersensitised vasodilatory response, evidenced by the leftward shift in the ACh dose-response curve. This suggests that chronic exposure may induce compensatory adaptations rather than immediate functional impairment. Over time, persistent low-grade exposure to DEP may trigger endothelial adaptations, such as upregulation of endothelial nitric oxide synthase (eNOS), increased antioxidant defences or heightened receptor sensitivity to ACh. Additionally, systemic inflammation arising from pulmonary DEP exposure could contribute to endothelial dysfunction and vascular remodelling. Circulating inflammatory mediators, such as cytokines and ROS, may modulate vascular tone, promoting a state of enhanced endothelial sensitivity rather than impairment.

Another key difference is the route of exposure. While *in vitro* DEP treatment directly impacts the vasculature, pulmonary exposure to DEP *in vivo* induces a broader systemic response, involving the immune system, inflammatory signalling pathways and neurohumoral regulation. This chronic inflammatory environment could contribute

to the observed hypersensitivity by altering endothelial function through both direct (receptor upregulation) and indirect (circulating mediators) mechanisms.

Collectively, these findings highlight the importance of exposure dynamics in determining vascular outcomes. Acute, direct exposure leads to oxidative stress-driven NO depletion and impaired vasodilation, whereas chronic exposure allows for compensatory adaptations that result in heightened endothelial responsiveness. Further studies are required to elucidate the precise molecular pathways underlying these effects (see Chapter 5).

7.6 DEP and the kidney in health and disease

The data presented in this thesis demonstrated that DEP, under both acute and chronic exposure conditions, did not cause significant morphological changes in the kidneys. In healthy mice, these findings suggest that the exposure duration and/or frequency may have been insufficient to elicit detectable alterations in renal tissue, or that the healthy mice were not susceptible to such changes. Similarly, in the hypertension model, renal structure remained unaffected, regardless of DEP exposure. Although vascular effects were evident in this model, the early termination of the study limited the investigation of the full impact of Ang II+HSD alone and the potential exacerbating effects of DEP.

To investigate more subtle renal changes, *KIM-1* mRNA levels were measured, as it is a sensitive early marker of renal injury. Significant upregulation of KIM-1 has been well-documented across various kidney injury models, including ischaemia-reperfusion injury (IRI) and CP-induced AKI, and hypertension models, such as the two-kidney one-clip and Ang II infusion models [198, 242, 287–290]. For instance, IRI in WT mice lead to a 1,200-fold increase in urinary KIM-1 1 day post-surgery and a 100-fold increase in renal transcripts 23 days post-IRI, while 6 weeks of Ang II infusion resulted in a 1,500-fold increase in renal *KIM-1* mRNA levels [242, 288]. In contrast, in this study, renal *KIM-1* transcripts were unchanged at 6 h and 16 h after acute DEP exposure but were significantly reduced at 18 h compared to controls. Four

weeks of DEP exposure had no effect on *KIM-1* levels in either the kidney or urine. Notably, in the hypertension model, *KIM-1* expression was downregulated compared to controls, independent of DEP exposure. Since *KIM-1* is usually expressed at very low levels in healthy kidneys, this downregulation is unexpected and may indicate adaptive or compensatory mechanisms that reduce *KIM-1* expression as a protective response to sustained stress, potentially involving anti-apoptotic pathways. Further research, including time-course studies, is necessary to elucidate the underlying mechanisms.

Inflammation and OS are key contributors to the pathogenesis of various diseases and are believed to play a central role in the adverse effects associated with DEP exposure. TNF-α, a critical mediator of renal inflammatory responses following injury, is predominantly produced by macrophages, with additional contributions from mesangial and tubular epithelial cells [291, 292]. Elevated levels of TNF-α in both renal tissue and serum have been documented in human CKD and in animal models of renal injury, including IRI, CP-induced nephrotoxicity and unilateral ureteral obstruction with severity of renal injury positively correlating with serum cytokine levels [292–294]. TNF-α also plays a role in renal injury associated with Ang II-induced hypertension [295, 296]. Genetic and pharmacological inhibition of TNF-α have been shown to ameliorate kidney injury in models of renal damage, such as IRI and diabetic nephropathy, where inflammation is a critical part of the pathogenesis [297–299]. In our studies, however, DEP exposure did not significantly alter *TNF-α* expression in either healthy mice or in the hypertension model. Nonetheless, a modest trend towards increased *SOD3* and $AT1_AR$ mRNA levels was observed in DEP-exposed mice subjected to Ang II and a high-salt diet. These findings suggest a potential role for DEP in exacerbating OS and RAAS activation in the context of hypertension, which warrants further investigation in future studies.

7.7 Broader implications

The findings of this thesis have significant implications for public health and policy, especially in light of the widespread exposure to air pollution and the rapid

growth of nanoparticle technology. The number of vehicles on the road has increased dramatically over the past several decades, with licensed vehicles in the UK rising from 4 million in 1950 to over 34 million in 2010. This surge has lead to the implementation of regulations to control exposure levels. PM levels are typically measured by the mass of particles per unit volume of air, reflecting their total weight. Although regulatory measures have reduced exposure to large particle mass, there has been a shift in exposure toward a higher number of traffic-derived UFPs. In urban areas, UFPs constitute the predominant form of particulate exposure by particle number.

Several factors underscore the critical need to study the health impacts of air pollution exposure. Air pollution is a widespread issue that affects people in all demographics-age, gender, socioeconomic status and health condition. It is estimated that approximately 90% of the global population lives in areas where air pollution levels exceed recommended limits. These levels continue to rise worldwide, with particularly rapid increases in developing countries. Importantly, no level of exposure can be considered 'safe'-even low levels of air pollution can be harmful, particularly with prolonged exposure.

This study demonstrates that inhaled nanoparticles can translocate into the bloodstream and accumulate in organs such as the kidneys. Furthermore, exposure to DEP, which is rich in nanoparticles, was found to impair renal vascular function in healthy mice. These findings underscore the need for stricter regulations specifically addressing UFPs in the environment. Current air quality standards focus mainly on larger particulate matter ($PM_{2.5}$ and PM_{10}), but this research suggests that UFPs pose a distinct risk due to their ability to enter the systemic circulation and accumulate in sensitive organs. Policymakers should consider revising air quality standards to include limits on UFPs concentrations. Furthermore, these studies highlight the importance of raising public awareness about the health risks associated with air pollution exposure.

7.8 Future studies

- **Particle localisation in renal tissue**:

  Conduct Raman spectroscopy and TEM analysis on renal sections from mice administered gold nanoparticles to determine if size of translocated particles influences their localisation within specific kidney regions.

- **Immune cell infiltration**:

  Optimise IHC staining to evaluate immune cell infiltration in the kidneys following chronic DEP exposure in both healthy mice and the Ang II+HSD hypertension model.

- **Expand injury marker panel**:

  Broaden the range of injury markers assessed in these studies to include additional biomarkers, such as NAG and NGAL.

- **Chronic DEP exposure in a mouse model of hypertension**:

  Investigate the effects of chronic DEP exposure in a hypertension model by reducing the Ang II dose and extending exposure duration to 6 weeks. This may require optimisation to ensure mouse survival throughout the protocol.

- **Mechanisms for vascular hypersensitivity following DEP exposure**:

  Further explore the mechanisms underlying DEP-induced hypersensitivity to endothelium-dependent vasodilation under chronic exposure conditions. Extend this study to assess renal vascular function in response to chronic DEP exposure in both healthy mice and those administered Ang II+HSD.

Bibliography

[1] Ravi Thadhani, Manuel Pascual, and Joseph V. Bonventre. Acute renal failure. *New England Journal of Medicine*, 334(22):1448–1460, 1996.

[2] David P Basile, Melissa D Anderson, and Timothy A Sutton. Pathophysiology of acute kidney injury. *Comprehensive Physiology*, 2(2):1303, 2012.

[3] Konstantinos Makris and Loukia Spanou. Acute kidney injury: definition, pathophysiology and clinical phenotypes. *The Clinical Biochemist Reviews*, 37 (2):85, 2016.

[4] Ravindra L Mehta, Jorge Cerdá, Emmanuel A Burdmann, Marcello Tonelli, Guillermo García-García, Vivekanand Jha, Paweena Susantitaphong, Michael Rocco, Raymond Vanholder, Mehmet Sukru Sever, et al. International society of nephrology's 0by25 initiative for acute kidney injury (zero preventable deaths by 2025): a human rights case for nephrology. *The Lancet*, 385(9987):2616–2643, 2015.

[5] Andrew JP Lewington, Jorge Cerdá, and Ravindra L Mehta. Raising awareness of acute kidney injury: a global perspective of a silent killer. *Kidney International*, 84(3):457–467, 2013.

[6] Abinet Abebe, Kabaye Kumela, Maekel Belay, Bezie Kebede, and Yohannes Wobie. Mortality and predictors of acute kidney injury in adults: a hospital-based prospective observational study. *Scientific Reports*, 11(1):15672, 2021.

[7] Paweena Susantitaphong, Dinna N Cruz, Jorge Cerda, Maher Abulfaraj, Fahad Alqahtani, Ioannis Koulouridis, and Bertrand L Jaber. World incidence of AKI: a meta-analysis. *Clinical journal of the American Society of Nephrology*, 8(9): 1482–1493, 2013.

[8] John A Kellum, Paola Romagnani, Gloria Ashuntantang, Claudio Ronco, Alexander Zarbock, and Hans-Joachim Anders. Acute kidney injury. *Nature Reviews Disease Primers*, 7(1):1–17, 2021.

[9] Eric AJ Hoste, Sean M Bagshaw, Rinaldo Bellomo, Cynthia M Cely, Roos Colman, Dinna N Cruz, Kyriakos Edipidis, Lui G Forni, Charles D Gomersall, Deepak Govil, et al. Epidemiology of acute kidney injury in critically ill patients: the multinational AKI-EPI study. *Intensive Care Medicine*, 41:1411–1423, 2015.

[10] Mayer Brezis and Seymour Rosen. Hypoxia of the renal medulla-its implications for disease. *New England Journal of Medicine*, 332(10):647–655, 1995.

[11] Roland C Blantz. Pathophysiology of pre-renal azotemia. *Kidney International*, 53(2):512–523, 1998.

[12] RW Norman, FG Mack, SA Awad, P Belitsky, RD Schwarz, and SG Lannon. Acute renal failure secondary to bilateral ureteric obstruction: review of 50 cases. *Canadian Medical Association Journal*, 127(7):601, 1982.

[13] KDIGO Working Group et al. Chapter 1: Definition and classification of CKD. *Kidney International Supplements*, 3:19–62, 2013.

[14] Andrew S Levey, Josef Coresh, Ethan Balk, Annamaria T Kausz, Adeera Levin, Michael W Steffes, Ronald J Hogg, Ronald D Perrone, Joseph Lau, and Garabed Eknoyan. National kidney foundation practice guidelines for chronic kidney disease: evaluation, classification, and stratification. *Annals of Internal Medicine*, 139(2):137–147, 2003.

[15] Nathan R Hill, Samuel T Fatoba, Jason L Oke, Jennifer A Hirst, Christopher A O'Callaghan, Daniel S Lasserson, and FD Richard Hobbs. Global prevalence of chronic kidney disease–a systematic review and meta-analysis. *PloS One*, 11(7): e0158765, 2016.

[16] Qiu-Li Zhang and Dietrich Rothenbacher. Prevalence of chronic kidney disease in population-based studies: systematic review. *BMC Public Health*, 8:1–13, 2008.

[17] Mohsen Naghavi, Amanuel Alemu Abajobir, Cristiana Abbafati, Kaja M Abbas, Foad Abd-Allah, Semaw Ferede Abera, Victor Aboyans, Olatunji Adetokunboh, Ashkan Afshin, Anurag Agrawal, et al. Global, regional, and national age-sex specific mortality for 264 causes of death, 1980–2016: a systematic analysis for the global burden of disease study 2016. *The Lancet*, 390(10100):1151–1210, 2017.

[18] Kyle J Foreman, Neal Marquez, Andrew Dolgert, Kai Fukutaki, Nancy Fullman, Madeline McGaughey, Martin A Pletcher, Amanda E Smith, Kendrick Tang, Chun-Wei Yuan, et al. Forecasting life expectancy, years of life lost, and all-cause and cause-specific mortality for 250 causes of death: reference and alternative scenarios for 2016–40 for 195 countries and territories. *The Lancet*, 392(10159): 2052–2090, 2018.

[19] Adeera Levin, Paul E Stevens, Rudy W Bilous, Josef Coresh, Angel LM De Francisco, Paul E De Jong, Kathryn E Griffith, Brenda R Hemmelgarn, Kunitoshi Iseki, Edmund J Lamb, et al. Kidney disease: Improving global outcomes (KDIGO) CKD work group. KDIGO 2012 clinical practice guideline for the evaluation and management of chronic kidney disease. *Kidney International Supplements*, 3(1):1–150, 2013.

[20] Angela C Webster, Evi V Nagler, Rachael L Morton, and Philip Masson. Chronic kidney disease. *The Lancet*, 389(10075):1238–1252, 2017.

[21] Ron T Gansevoort, Ricardo Correa-Rotter, Brenda R Hemmelgarn, Tazeen H Jafar, Hiddo J Lambers Heerspink, Johannes F Mann, Kunihiro Matsushita, and Chi Pang Wen. Chronic kidney disease and cardiovascular risk: epidemiology, mechanisms, and prevention. *The Lancet*, 382(9889):339–352, 2013.

[22] Anna Kottgen, Stuart D Russell, Laura R Loehr, Ciprian M Crainiceanu, Wayne D Rosamond, Patricia P Chang, Lloyd E Chambless, and Josef Coresh. Reduced kidney function as a risk factor for incident heart failure: the atherosclerosis risk in communities (ARIC) study. *Journal of the American Society of Nephrology*, 18(4):1307–1315, 2007.

[23] Keattiyoat Wattanakit, Aaron R Folsom, Elizabeth Selvin, Josef Coresh, Alan T Hirsch, and Beth D Weatherley. Kidney function and risk of peripheral arterial disease: results from the atherosclerosis risk in communities (ARIC) study. *Journal of the American Society of Nephrology*, 18(2):629–636, 2007.

[24] Jerome L Abramson, Claudine T Jurkovitz, Viola Vaccarino, William S Weintraub, and William Mcclellan. Chronic kidney disease, anemia, and incident stroke in a middle-aged, community-based population: the ARIC study. *Kidney International*, 64(2):610–615, 2003.

[25] Alan S Go, Glenn M Chertow, Dongjie Fan, Charles E McCulloch, and Chi-yuan Hsu. Chronic kidney disease and the risks of death, cardiovascular events, and hospitalization. *New England Journal of Medicine*, 351(13):1296–1305, 2004.

[26] Andrew S Levey, Judith A Beto, BE Coronado, G Eknoyan, RN Foley, BL Kasiske, MJ Klag, LU Mailloux, CL Manske, KB Meyer, et al. Controlling the epidemic of cardiovascular disease in chronic renal disease: What do we know? What do we need to learn? Where do we go from here? *American Journal of Kidney Diseases*, 32(5):853–906, 1998.

[27] Nagesh S Anavekar, John JV McMurray, Eric J Velazquez, Scott D Solomon, Lars Kober, Jean-Lucien Rouleau, Harvey D White, Rolf Nordlander, Aldo Maggioni, Kenneth Dickstein, et al. Relation between renal dysfunction and cardiovascular outcomes after myocardial infarction. *New England Journal of Medicine*, 351(13): 1285–1295, 2004.

[28] Pantelis A Sarafidis, Suying Li, Shu-Cheng Chen, Allan J Collins, Wendy W Brown, Michael J Klag, and George L Bakris. Hypertension awareness, treatment, and control in chronic kidney disease. *The American Journal of Medicine*, 121 (4):332–340, 2008.

[29] Gianfranco Parati, Juan Eugenio Ochoa, Grzegorz Bilo, Rajiv Agarwal, Adrian Covic, Friedo W Dekker, Danilo Fliser, Gunnar H Heine, Kitty J Jager, Luna Gargani, et al. Hypertension in chronic kidney disease part 1: out-of-office blood pressure monitoring: methods, thresholds, and patterns. *Hypertension*, 67(6): 1093–1101, 2016.

[30] Lakhmir S Chawla, Paul W Eggers, Robert A Star, and Paul L Kimmel. Acute kidney injury and chronic kidney disease as interconnected syndromes. *New England Journal of Medicine*, 371(1):58–66, 2014.

[31] Steven G Coca, Swathi Singanamala, and Chirag R Parikh. Chronic kidney disease after acute kidney injury: a systematic review and meta-analysis. *Kidney International*, 81(5):442–448, 2012.

[32] Xiao-Ming Meng, David J Nikolic-Paterson, and Hui Yao Lan. Inflammatory processes in renal fibrosis. *Nature Reviews Nephrology*, 10(9):493–503, 2014.

[33] Zhiwen Wang and Chun Zhang. From AKI to CKD: Maladaptive repair and the underlying mechanisms. *International Journal of Molecular Sciences*, 23(18): 10880, 2022.

[34] Li Yang, Tatiana Y Besschetnova, Craig R Brooks, Jagesh V Shah, and Joseph V Bonventre. Epithelial cell cycle arrest in G2/M mediates kidney fibrosis after injury. *Nature Medicine*, 16(5):535–543, 2010.

[35] CY Hsu, JD Ordonez, GM Chertow, D Fan, CE McCulloch, and AS Go. The risk of acute renal failure in patients with chronic kidney disease. *Kidney International*, 74(1):101–107, 2008.

[36] Liyu He, Qingqing Wei, Jing Liu, Mixuan Yi, Yu Liu, Hong Liu, Lin Sun, Youming Peng, Fuyou Liu, Manjeri A Venkatachalam, et al. AKI on CKD: heightened injury, suppressed repair, and the underlying mechanisms. *Kidney International*, 92(5):1071–1083, 2017.

[37] Fitzsimons JT. Angiotensin, thirst, and sodium appetite. *Physiological reviews*, 78(3):583–686, 1998.

[38] Bryan Williams, Giuseppe Mancia, Wilko Spiering, Enrico Agabiti Rosei, Michel Azizi, Michel Burnier, Denis L Clement, Antonio Coca, Giovanni De Simone, Anna Dominiczak, et al. 2018 ESC/ESH guidelines for the management of arterial hypertension: The Task Force for the management of arterial hypertension of the european society of cardiology (ESC) and the european society of hypertension (ESH). *European Heart Journal*, 39(33):3021–3104, 2018.

[39] Katherine T Mills, Joshua D Bundy, Tanika N Kelly, Jennifer E Reed, Patricia M Kearney, Kristi Reynolds, Jing Chen, and Jiang He. Global disparities of hypertension prevalence and control: a systematic analysis of population-based studies from 90 countries. *Circulation*, 134(6):441–450, 2016.

[40] GBD 2013 Risk Factors Collaborators et al. Global, regional, and national comparative risk assessment of 79 behavioural, environmental and occupational, and metabolic risks or clusters of risks in 188 countries, 1990–2013: a systematic analysis for the global burden of disease study 2013. *The Lancet*, 386(10010): 2287, 2015.

[41] Katherine T Mills, Andrei Stefanescu, and Jiang He. The global epidemiology of hypertension. *Nature Reviews Nephrology*, 16(4):223–237, 2020.

[42] Theodore A Kotchen, Allen W Cowley Jr, and Edward D Frohlich. Salt in health and disease—a delicate balance. *New England Journal of Medicine*, 368(13): 1229–1237, 2013.

[43] Aaron M Lucko, Chelsea Doktorchik, Mark Woodward, Mary Cogswell, Bruce Neal, Doreen Rabi, Cheryl Anderson, Feng J He, Graham A MacGregor, Mary L'Abbe, et al. Percentage of ingested sodium excreted in 24-hour urine collections: a systematic review and meta-analysis. *The Journal of Clinical Hypertension*, 20 (9):1220–1229, 2018.

[44] World Health Organization. *WHO global report on sodium intake reduction.* World Health Organization, 2023.

[45] Xiangbo Chen, Jianqiang Du, Xiaoming Wu, Wangnan Cao, and Shengzhi Sun. Global burden attributable to high sodium intake from 1990 to 2019. *Nutrition, Metabolism and Cardiovascular Diseases*, 31(12):3314–3321, 2021.

[46] Lewis K Dahl. Possible role of chronic excess salt consumption in the pathogenesis of essential hypertension. *The American Journal of Cardiology*, 8(4):571–575, 1961.

[47] FC Luft, LI Rankin, R Bloch, AE Weyman, LR Willis, RH Murray, CE Grim, and

MH Weinberger. Cardiovascular and humoral responses to extremes of sodium intake in normal black and white men. *Circulation*, 60(3):697–706, 1979.

[48] Jian-Wei Gu, Amelia P Bailey, Wei Tan, Megan Shparago, and Emily Young. Long-term high-salt diet causes hypertension and decreases renal expression of vascular endothelial growth factor in sprague-dawley rats. *Journal of the American Society of Hypertension*, 2(4):275–285, 2008.

[49] JW Gu, Emily Young, ZJ Pan, Kevan B Tucker, Megan Shparago, Min Huang, and Amelia Purser Bailey. Long-term high salt diet causes hypertension and alters renal cytokine gene expression profiles in sprague-dawley rats. *Journal of Peking University. Health sciences*, 41(5):505–515, 2009.

[50] Andrew Mente, Martin J O'Donnell, Sumathy Rangarajan, Matthew J McQueen, Paul Poirier, Andreas Wielgosz, Howard Morrison, Wei Li, Xingyu Wang, Chen Di, et al. Association of urinary sodium and potassium excretion with blood pressure. *New england journal of medicine*, 371(7):601–611, 2014.

[51] Feng J He, Jiafu Li, and Graham A MacGregor. Effect of longer term modest salt reduction on blood pressure: Cochrane systematic review and meta-analysis of randomised trials. *Bmj*, 346, 2013.

[52] Lawrence J Appel, Mark A Espeland, Linda Easter, Alan C Wilson, Steven Folmar, and Clifton R Lacy. Effects of reduced sodium intake on hypertension control in older individuals: results from the trial of nonpharmacologic interventions in the elderly (TONE). *Archives of internal medicine*, 161(5):685–693, 2001.

[53] JJ Carvalho, Roberto G Baruzzi, Peter F Howard, Neil Poulter, Michael P Alpers, Laercio J Franco, Luiz F Marcopito, Veronica J Spooner, Alan R Dyer, and Paul Elliott. Blood pressure in four remote populations in the intersalt study. *Hypertension*, 14(3):238–246, 1989.

[54] Boris Z Simkhovich, Michael T Kleinman, and Robert A Kloner. Air pollution and cardiovascular injury: epidemiology, toxicology, and mechanisms. *Journal of the American College of Cardiology*, 52(9):719–726, 2008.

[55] Benoit Nemery, Peter HM Hoet, and Abderrahim Nemmar. The Meuse Valley fog of 1930: an air pollution disaster. *The Lancet*, 357(9257):704–708, 2001.

[56] William H Helfand, Jan Lazarus, and Paul Theerman. Donora, Pennsylvania: an environmental disaster of the 20th century. *American Journal of Public Health*, 91(4):553, 2001.

[57] Elizabeth T Jacobs, Jefferey L Burgess, and Mark B Abbott. The Donora smog revisited: 70 years after the event that inspired the clean air act. *American Journal of Public Health*, 108(S2):S85–S88, 2018.

[58] Devra L Davis. A look back at the London smog of 1952 and the half century since. *Environmental Health Perspectives*, 110(12):A734–A735, 2002.

[59] Barbara J Polivka. The great London smog of 1952. *AJN The American Journal of Nursing*, 118(4):57–61, 2018.

[60] ET Wilkins. Air pollution and the London fog of december, 1952. *Journal of the Royal Sanitary Institute*, 74(1):1–21, 1954.

[61] Michelle L Bell and Devra Lee Davis. Reassessment of the lethal London fog of 1952: novel indicators of acute and chronic consequences of acute exposure to air pollution. *Environmental Health Perspectives*, 109(suppl 3):389–394, 2001.

[62] Erin Dooley. Clearing the air over the London fog. *Environmental Health Perspectives*, 110(12):A748–A749, 2002.

[63] King's College London. London average air quality levels, 2019. `https://data.london.gov.uk/dataset/london-average-air-quality-levels`.

[64] Department for Environment Food & Rural Affairs. Air pollution forecast, 2023. `https://uk-air.defra.gov.uk/`.

[65] Aaron J Cohen, Michael Brauer, Richard Burnett, H Ross Anderson, Joseph Frostad, Kara Estep, Kalpana Balakrishnan, Bert Brunekreef, Lalit Dandona, Rakhi Dandona, et al. Estimates and 25-year trends of the global burden of disease attributable to ambient air pollution: an analysis of data from the global burden of diseases study 2015. *The Lancet*, 389(10082):1907–1918, 2017.

[66] Jos Lelieveld, Klaus Klingmüller, Andrea Pozzer, Ulrich Pöschl, Mohammed Fnais, Andreas Daiber, and Thomas Münzel. Cardiovascular disease burden from ambient air pollution in Europe reassessed using novel hazard ratio functions. *European Heart Journal*, 40(20):1590–1596, 2019.

[67] Richard Burnett, Hong Chen, Mieczysław Szyszkowicz, Neal Fann, Bryan Hubbell, C Arden Pope III, Joshua S Apte, Michael Brauer, Aaron Cohen, Scott Weichenthal, et al. Global estimates of mortality associated with long-term exposure to outdoor fine particulate matter. *Proceedings of the National Academy of Sciences*, 115(38):9592–9597, 2018.

[68] Mohsen Abbasi-Kangevari, Mohammad-Reza Malekpour, Masoud Masinaei, Sahar Saeedi Moghaddam, Seyyed-Hadi Ghamari, Zeinab Abbasi-Kangevari, Negar Rezaei, Nazila Rezaei, Ali H Mokdad, Mohsen Naghavi, et al. Effect of air pollution on disease burden, mortality, and life expectancy in North Africa and the Middle East: a systematic analysis for the global burden of disease study 2019. *The Lancet Planetary Health*, 7(5):e358–e369, 2023.

[69] OECD. *The Economic Consequences of Outdoor Air Pollution*. The Organisation for Economic Co-operation and Development, 2016. doi: https://doi.org/https://doi.org/10.1787/9789264257474-en. URL `https://www.oecd-ilibrary.org/content/publication/9789264257474-en`.

[70] Elisa Lanzi, Rob Dellink, and Jean Chateau. The sectoral and regional economic consequences of outdoor air pollution to 2060. *Energy Economics*, 71:89–113, 2018.

[71] World Health Organization. *WHO global air quality guidelines: particulate matter ($PM_{2.5}$ and PM_{10}), ozone, nitrogen dioxide, sulfur dioxide and carbon monoxide.* World Health Organization, 2021.

[72] Joshua S Apte, Michael Brauer, Aaron J Cohen, Majid Ezzati, and C Arden Pope III. Ambient $PM_{2.5}$ reduces global and regional life expectancy. *Environmental Science & Technology Letters*, 5(9):546–551, 2018.

[73] Robert D Brook, Sanjay Rajagopalan, C Arden Pope III, Jeffrey R Brook,

Aruni Bhatnagar, Ana V Diez-Roux, Fernando Holguin, Yuling Hong, Russell V Luepker, Murray A Mittleman, et al. Particulate matter air pollution and cardiovascular disease: an update to the scientific statement from the american heart association. *Circulation*, 121(21):2331–2378, 2010.

[74] Ioannis Manisalidis, Elisavet Stavropoulou, Agathangelos Stavropoulos, and Eugenia Bezirtzoglou. Environmental and health impacts of air pollution: a review. *Frontiers in Public Health*, page 14, 2020.

[75] Roya Kelishadi and Parinaz Poursafa. Air pollution and non-respiratory health hazards for children. *Archives of Medical Science*, 6(4):483–495, 2010.

[76] JP Langrish, Jenny Bosson, Jon Unosson, Ala Muala, DE Newby, NL Mills, Anders Blomberg, and Thomas Sandström. Cardiovascular effects of particulate air pollution exposure: time course and underlying mechanisms. *Journal of Internal Medicine*, 272(3):224–239, 2012.

[77] Kenneth Donaldson, Vicky Stone, Anna Clouter, Louise Renwick, and William MacNee. Ultrafine particles. *Occupational and Environmental Medicine*, 58(3): 211–216, 2001.

[78] Robert D Brook, Barry Franklin, Wayne Cascio, Yuling Hong, George Howard, Michael Lipsett, Russell Luepker, Murray Mittleman, Jonathan Samet, Sidney C Smith Jr, et al. Air pollution and cardiovascular disease: a statement for healthcare professionals from the expert panel on population and prevention science of the american heart association. *Circulation*, 109(21):2655–2671, 2004.

[79] Davin K Quinn, Shunda M McGahee, Laura C Politte, Gina N Duncan, Cristina Cusin, Christopher J Hopwood, and Theodore A Stern. Complications of carbon monoxide poisoning: a case discussion and review of the literature. *Primary Care Companion to the Journal of Clinical Psychiatry*, 11(2):74, 2009.

[80] CL Townsend and Robert L Maynard. Effects on health of prolonged exposure to low concentrations of carbon monoxide. *Occupational and Environmental Medicine*, 59(10):708–711, 2002.

[81] Michelle C Turner, Daniel Krewski, W Ryan Diver, C Arden Pope III, Richard T Burnett, Michael Jerrett, Julian D Marshall, and Susan M Gapstur. Ambient air pollution and cancer mortality in the cancer prevention study II. *Environmental Health Perspectives*, 125(8):087013, 2017.

[82] Shiwen Huang, Haomin Li, Mingrui Wang, Yaoyao Qian, Kyle Steenland, William Michael Caudle, Yang Liu, Jeremy Sarnat, Stefania Papatheodorou, and Liuhua Shi. Long-term exposure to nitrogen dioxide and mortality: a systematic review and meta-analysis. *Science of The Total Environment*, 776:145968, 2021.

[83] Xinyi Fang, Suijie Huang, Yixiang Zhu, Jian Lei, Yanyi Xu, Yue Niu, and Renjie Chen. Short-term exposure to ozone and asthma exacerbation in adults: A longitudinal study in China. *Frontiers in Public Health*, 10, 2022.

[84] Yue Niu, Yuchang Zhou, Renjie Chen, Peng Yin, Xia Meng, Weidong Wang, Cong Liu, John S Ji, Yang Qiu, Haidong Kan, et al. Long-term exposure to ozone and cardiovascular mortality in China: a nationwide cohort study. *The Lancet Planetary Health*, 6(6):e496–e503, 2022.

[85] Michael Jerrett, Richard T Burnett, C Arden Pope III, Kazuhiko Ito, George Thurston, Daniel Krewski, Yuanli Shi, Eugenia Calle, and Michael Thun. Long-term ozone exposure and mortality. *New England Journal of Medicine*, 360(11): 1085–1095, 2009.

[86] Pablo Orellano, Julieta Reynoso, and Nancy Quaranta. Short-term exposure to sulphur dioxide (SO_2) and all-cause and respiratory mortality: A systematic review and meta-analysis. *Environment International*, 150:106434, 2021.

[87] Anita L Reno, Edward G Brooks, and Bill T Ameredes. Mechanisms of heightened airway sensitivity and responses to inhaled SO_2 in asthmatics. *Environmental Health Insights*, 9:EHI–S15671, 2015.

[88] Kenichi Azuma, Naoki Kagi, U Yanagi, and Haruki Osawa. Effects of low-level inhalation exposure to carbon dioxide in indoor environments: A short review on human health and psychomotor performance. *Environment International*, 121: 51–56, 2018.

[89] Tyler A Jacobson, Jasdeep S Kler, Michael T Hernke, Rudolf K Braun, Keith C Meyer, and William E Funk. Direct human health risks of increased atmospheric carbon dioxide. *Nature Sustainability*, 2(8):691–701, 2019.

[90] World Health Organization (WHO) et al. Environmental criteria 150: Benzene. Geneva: International Programme on Chemical Safety (IPCS), WHO/United Nations Environment Programme. *International Labour Organisation*, 1993.

[91] Dana Loomis, Kathryn Z Guyton, Yann Grosse, Fatiha El Ghissassi, Véronique Bouvard, Lamia Benbrahim-Tallaa, Neela Guha, Nadia Vilahur, Heidi Mattock, and Kurt Straif. Carcinogenicity of benzene. *The Lancet Oncology*, 18(12):1574–1575, 2017.

[92] World Health Organization et al. Human health effects of polycyclic aromatic hydrocarbons as ambient air pollutants: report of the working group on polycyclic aromatic hydrocarbons of the joint task force on the health aspects of air pollution. In *Human health effects of polycyclic aromatic hydrocarbons as ambient air pollutants: report of the Working Group on Polycyclic Aromatic Hydrocarbons of the Joint Task Force on the Health Aspects of Air Pollution*. World Health Organization. Regional Office for Europe, 2021.

[93] Manthar Ali Mallah, Li Changxing, Mukhtiar Ali Mallah, Sobia Noreen, Yang Liu, Muhammad Saeed, He Xi, Bilal Ahmed, Feifei Feng, Ali Asghar Mirjat, et al. Polycyclic aromatic hydrocarbon and its effects on human health: an updated review. *Chemosphere*, page 133948, 2022.

[94] Roy M Harrison and Jianxin Yin. Particulate matter in the atmosphere: which particle properties are important for its effects on health? *Science of the Total Environment*, 249(1-3):85–101, 2000.

[95] Yixing Du, Xiaohan Xu, Ming Chu, Yan Guo, and Junhong Wang. Air particulate matter and cardiovascular disease: the epidemiological, biomedical and clinical evidence. *Journal of Thoracic Disease*, 8(1):E8, 2016.

[96] Abderrahim Nemmar, PH Mq Hoet, B Vanquickenborne, D Dinsdale, Maarten Thomeer, MF Hoylaerts, H Vanbilloen, Luc Mortelmans, and Benoit Nemery.

Passage of inhaled particles into the blood circulation in humans. *Circulation*, 105(4):411–414, 2002.

[97] Ken Donaldson, Lang Tran, Luis Albert Jimenez, Rodger Duffin, David E Newby, Nicholas Mills, William MacNee, and Vicki Stone. Combustion-derived nanoparticles: a review of their toxicology following inhalation exposure. *Particle and Fibre Toxicology*, 2(1):1–14, 2005.

[98] Ken Donaldson, Rodger Duffin, Jeremy P Langrish, Mark R Miller, Nicholas L Mills, Craig A Poland, Jennifer Raftis, Anoop Shah, Catherine A Shaw, and David E Newby. Nanoparticles and the cardiovascular system: a critical review. *Nanomedicine*, 8(3):403–423, 2013.

[99] Mark R Miller and David E Newby. Air pollution and cardiovascular disease: car sick. *Cardiovascular Research*, 116(2):279–294, 2019.

[100] Roy M Harrison. Airborne particulate matter. *Philosophical Transactions of the Royal Society A*, 378(2183):20190319, 2020.

[101] United States Environmental Protection Agency. Particulate matter (PM) basics, 2022. `https://www.epa.gov/pm-pollution/particulate-matter-pm-basics#PM`.

[102] Gregory M Rowangould. A census of the US near-roadway population: Public health and environmental justice considerations. *Transportation Research Part D: Transport and Environment*, 25:59–67, 2013.

[103] Junfeng Jim Zhang and Lidia Morawska. Combustion sources of particles: 2. emission factors and measurement methods. *Chemosphere*, 49(9):1059–1074, 2002.

[104] Davaasambuu Enkhmaa, Nicole Warburton, Badrakh Javzandulam, Jadambajav Uyanga, Yarinpil Khishigsuren, Sereeter Lodoysamba, Shonkuuz Enkhtur, and David Warburton. Seasonal ambient air pollution correlates strongly with spontaneous abortion in mongolia. *BMC Pregnancy and Childbirth*, 14(1):1–7, 2014.

[105] Niya Zhou, Zhihong Cui, Sanming Yang, Xue Han, Gangcai Chen, Ziyuan Zhou, Chongzhi Zhai, Mingfu Ma, Lianbing Li, Min Cai, et al. Air pollution and decreased semen quality: a comparative study of Chongqing urban and rural areas. *Environmental Pollution*, 187:145–152, 2014.

[106] Tom Clemens, Steve Turner, and Chris Dibben. Maternal exposure to ambient air pollution and fetal growth in North-East Scotland: A population-based study using routine ultrasound scans. *Environment International*, 107:216–226, 2017.

[107] Shiliang Liu, Daniel Krewski, Yuanli Shi, Yue Chen, and Richard T Burnett. Association between maternal exposure to ambient air pollutants during pregnancy and fetal growth restriction. *Journal of Exposure Science & Environmental Epidemiology*, 17(5):426–432, 2007.

[108] Jun Wu, Cizao Ren, Ralph J Delfino, Judith Chung, Michelle Wilhelm, and Beate Ritz. Association between local traffic-generated air pollution and preeclampsia and preterm delivery in the south coast air basin of California. *Environmental Health Perspectives*, 117(11):1773–1779, 2009.

[109] Maeve E Wallace, Katherine L Grantz, Danping Liu, Yeyi Zhu, Sung Soo Kim, and Pauline Mendola. Exposure to ambient air pollution and premature rupture of membranes. *American Journal of Epidemiology*, 183(12):1114–1121, 2016.

[110] Hong Chen, Jeffrey C Kwong, Ray Copes, Karen Tu, Paul J Villeneuve, Aaron Van Donkelaar, Perry Hystad, Randall V Martin, Brian J Murray, Barry Jessiman, et al. Living near major roads and the incidence of dementia, parkinson's disease, and multiple sclerosis: a population-based cohort study. *The Lancet*, 389(10070):718–726, 2017.

[111] Éric Lavigne, Marc-André Bélair, Minh T Do, David M Stieb, Perry Hystad, Aaron van Donkelaar, Randall V Martin, Daniel L Crouse, Eric Crighton, Hong Chen, et al. Maternal exposure to ambient air pollution and risk of early childhood cancers: a population-based study in Ontario, Canada. *Environment International*, 100:139–147, 2017.

[112] Linda Kachuri, Paul J Villeneuve, Marie-Élise Parent, Kenneth C Johnson, and Shelley A Harris. Workplace exposure to diesel and gasoline engine exhausts and the risk of colorectal cancer in Canadian men. *Environmental Health*, 15(1):1–12, 2016.

[113] Hui-Fen Chiu, Shang-Shyue Tsai, Pei-Shih Chen, Yen-Hsiung Liao, Saou-Hsing Liou, Trong-Neng Wu, and Chun-Yuh Yang. Traffic air pollution and risk of death from gastric cancer in Taiwan: petrol station density as an indicator of air pollutant exposure. *Journal of Toxicology and Environmental Health, Part A*, 74 (18):1215–1224, 2011.

[114] Shang-Shyue Tsai, Mao-Meng Tiao, Hsin-Wei Kuo, Trong-Neng Wu, and Chun-Yuh Yang. Association of bladder cancer with residential exposure to petrochemical air pollutant emissions in Taiwan. *Journal of Toxicology and Environmental Health, Part A*, 72(2):53–59, 2009.

[115] Gemma Castaño-Vinyals, Kenneth P Cantor, Núria Malats, Adonina Tardon, Reina Garcia-Closas, Consol Serra, Alfredo Carrato, Nathaniel Rothman, Roel Vermeulen, Debra Silverman, et al. Air pollution and risk of urinary bladder cancer in a case-control study in Spain. *Occupational and Environmental Medicine*, 65(1):56–60, 2008.

[116] Nicholas L Mills, Hakan Tornqvist, Simon D Robinson, Manuel Gonzalez, Kareen Darnley, William MacNee, Nicholas A Boon, Ken Donaldson, Anders Blomberg, Thomas Sandstrom, et al. Diesel exhaust inhalation causes vascular dysfunction and impaired endogenous fibrinolysis. *Circulation*, 112(25):3930–3936, 2005.

[117] Magnus Lundbäck, Nicholas L Mills, Andrew Lucking, Stefan Barath, Ken Donaldson, David E Newby, Thomas Sandström, and Anders Blomberg. Experimental exposure to diesel exhaust increases arterial stiffness in man. *Particle and Fibre Toxicology*, 6:1–6, 2009.

[118] Andrew J Lucking, Magnus Lundbäck, Nicholas L Mills, Dana Faratian, Stefan L Barath, Jamshid Pourazar, Flemming R Cassee, Kenneth Donaldson, Nicholas A Boon, Juan J Badimon, et al. Diesel exhaust inhalation increases thrombus formation in man. *European Heart Journal*, 29(24):3043–3051, 2008.

[119] Andrew J Lucking, Magnus Lundbäck, Stefan L Barath, Nicholas L Mills,

Manjit K Sidhu, Jeremy P Langrish, Nicholas A Boon, Jamshid Pourazar, Juan J Badimon, Miriam E Gerlofs-Nijland, et al. Particle traps prevent adverse vascular and prothrombotic effects of diesel engine exhaust inhalation in men. *Circulation*, 123(16):1721–1728, 2011.

[120] Nicholas L Mills, Mark R Miller, Andrew J Lucking, Jon Beveridge, Laura Flint, A John F Boere, Paul H Fokkens, Nicholas A Boon, Thomas Sandstrom, Anders Blomberg, et al. Combustion-derived nanoparticulate induces the adverse vascular effects of diesel exhaust inhalation. *European Heart Journal*, 32(21): 2660–2671, 2011.

[121] Sarah Robertson, Ashleigh L Thomson, Rod Carter, Holly R Stott, Catherine A Shaw, Patrick WF Hadoke, David E Newby, Mark R Miller, and Gillian A Gray. Pulmonary diesel particulate increases susceptibility to myocardial ischemia/reperfusion injury via activation of sensory TRPV1 and $\beta 1$ adrenoreceptors. *Particle and Fibre Toxicology*, 11(1):1–10, 2014.

[122] Caroline M Tabor, Catherine A Shaw, Sarah Robertson, Mark R Miller, Rodger Duffin, Ken Donaldson, David E Newby, and Patrick WF Hadoke. Platelet activation independent of pulmonary inflammation contributes to diesel exhaust particulate-induced promotion of arterial thrombosis. *Particle and Fibre Toxicology*, 13:1–14, 2015.

[123] Mark R Miller, Stephen J Borthwick, Catherine A Shaw, Steven G McLean, Daniel McClure, Nicholas L Mills, Rodger Duffin, Ken Donaldson, Ian L Megson, Patrick WF Hadoke, et al. Direct impairment of vascular function by diesel exhaust particulate through reduced bioavailability of endothelium-derived nitric oxide induced by superoxide free radicals. *Environmental Health Perspectives*, 117(4):611–616, 2009.

[124] Kenneth Donaldson, David M Brown, Colin Mitchell, Miglena Dineva, Paul H Beswick, Peter Gilmour, and William MacNee. Free radical activity of PM_{10}: iron-mediated generation of hydroxyl radicals. *Environmental Health Perspectives*, 105(suppl 5):1285–1289, 1997.

[125] Emma DiStefano, Arantzazu Eiguren-Fernandez, Ralph J Delfino, Constantinos Sioutas, John R Froines, and Arthur K Cho. Determination of metal-based hydroxyl radical generating capacity of ambient and diesel exhaust particles. *Inhalation Toxicology*, 21(9):731–738, 2009.

[126] Mark R Miller, Catherine A Shaw, and Jeremy P Langrish. From particles to patients: oxidative stress and the cardiovascular effects of air pollution. *Future Cardiology*, 8(4):577–602, 2012.

[127] Lotte Risom, Peter Møller, and Steffen Loft. Oxidative stress-induced DNA damage by particulate air pollution. *Mutation Research/Fundamental and Molecular Mechanisms of Mutagenesis*, 592(1-2):119–137, 2005.

[128] Antonella Fiordelisi, Prisco Piscitelli, Bruno Trimarco, Enrico Coscioni, Guido Iaccarino, and Daniela Sorriento. The mechanisms of air pollution and particulate matter in cardiovascular diseases. *Heart Failure Reviews*, 22:337–347, 2017.

[129] Anthony Seaton, D Godden, W MacNee, and K Donaldson. Particulate air pollution and acute health effects. *The Lancet*, 345(8943):176–178, 1995.

[130] Urmila P Kodavanti. Stretching the stress boundary: Linking air pollution health effects to a neurohormonal stress response. *Biochimica et Biophysica Acta (BBA)-General Subjects*, 1860(12):2880–2890, 2016.

[131] Christina M Perez, Mehdi S Hazari, and Aimen K Farraj. Role of autonomic reflex arcs in cardiovascular responses to air pollution exposure. *Cardiovascular Toxicology*, 15:69–78, 2015.

[132] Mehdi S Hazari, Najwa Haykal-Coates, Darrell W Winsett, Q Todd Krantz, Charly King, Daniel L Costa, and Aimen K Farraj. TRPA1 and sympathetic activation contribute to increased risk of triggered cardiac arrhythmias in hypertensive rats exposed to diesel exhaust. *Environmental Health Perspectives*, 119(7):951–957, 2011.

[133] Bin Pan, Minjie Chen, Xuan Zhang, Shuai Liang, Xiaobo Qin, Lianglin Qiu, Qi Cao, Renzhen Peng, Shimin Tao, Zhouzhou Li, et al. Hypothalamic-pituitary-adrenal axis mediates ambient $PM_{2.5}$ exposure-induced pulmonary inflammation. *Ecotoxicology and Environmental Safety*, 208:111464, 2021.

[134] Yue Niu, Renjie Chen, Yongjie Xia, Jing Cai, Zhekang Ying, Zhijing Lin, Cong Liu, Chen Chen, Li Peng, Zhuohui Zhao, et al. Fine particulate matter constituents and stress hormones in the hypothalamus–pituitary–adrenal axis. *Environment International*, 119:186–192, 2018.

[135] Mainul Husain, Dongmei Wu, Anne T Saber, Nathalie Decan, Nicklas R Jacobsen, Andrew Williams, Carole L Yauk, Hakan Wallin, Ulla Vogel, and Sabina Halappanavar. Intratracheally instilled titanium dioxide nanoparticles translocate to heart and liver and activate complement cascade in the heart of C57BL/6 mice. *Nanotoxicology*, 9(8):1013–1022, 2015.

[136] Günther Oberdörster, Zachary Sharp, Viorel Atudorei, Alison Elder, Robert Gelein, Wolfgang Kreyling, and Christopher Cox. Translocation of inhaled ultrafine particles to the brain. *Inhalation Toxicology*, 16(6-7):437–445, 2004.

[137] Lilian Calderón-Garcidueñas, Anna C Solt, Carlos Henríquez-Roldán, Ricardo Torres-Jardón, Bryan Nuse, Lou Herritt, Rafael Villarreal-Calderón, Norma Osnaya, Ida Stone, Raquel García, et al. Long-term air pollution exposure is associated with neuroinflammation, an altered innate immune response, disruption of the blood-brain barrier, ultrafine particulate deposition, and accumulation of amyloid β-42 and α-synuclein in children and young adults. *Toxicologic Pathology*, 36(2):289–310, 2008.

[138] Mark R Miller, Jennifer B Raftis, Jeremy P Langrish, Steven G McLean, Pawitrabhorn Samutrtai, Shea P Connell, Simon Wilson, Alex T Vesey, Paul HB Fokkens, A John F Boere, et al. Inhaled nanoparticles accumulate at sites of vascular disease. *ACS nano*, 11(5):4542–4552, 2017.

[139] Benjamin Bowe, Yan Xie, Tingting Li, Yan Yan, Hong Xian, and Ziyad Al-Aly. Particulate matter air pollution and the risk of incident CKD and progression to ESRD. *Journal of the American Society of Nephrology*, 29(1):218–230, 2018.

[140] Matthew F Blum, Aditya Surapaneni, James D Stewart, Duanping Liao, Jeff D Yanosky, Eric A Whitsel, Melinda C Power, and Morgan E Grams. Particulate

matter and albuminuria, glomerular filtration rate, and incident CKD. *Clinical Journal of the American Society of Nephrology*, 15(3):311–319, 2020.

[141] Jennifer Bragg-Gresham, Hal Morgenstern, William McClellan, Sharon Saydah, Meda Pavkov, Desmond Williams, Neil Powe, Delphine Tuot, Raymond Hsu, Rajiv Saran, et al. County-level air quality and the prevalence of diagnosed chronic kidney disease in the US Medicare population. *PloS One*, 13(7):e0200612, 2018.

[142] Amar J Mehta, Antonella Zanobetti, Marie-Abele C Bind, Itai Kloog, Petros Koutrakis, David Sparrow, Pantel S Vokonas, and Joel D Schwartz. Long-term exposure to ambient fine particulate matter and renal function in older men: the veterans administration normative aging study. *Environmental Health Perspectives*, 124(9):1353–1360, 2016.

[143] Shih-Yi Lin, Shu-Woei Ju, Cheng Li Lin, Wu-Huei Hsu, Cheng-Chieh Lin, I-Wen Ting, and Chia-Hung Kao. Air pollutants and subsequent risk of chronic kidney disease and end-stage renal disease: A population-based cohort study. *Environmental Pollution*, 261:114154, 2020.

[144] Ta-Chien Chan, Zilong Zhang, Bo-Cheng Lin, Changqing Lin, Han-Bing Deng, Yuan Chieh Chuang, Jimmy WM Chan, Wun Kai Jiang, Tony Tam, Ly-yun Chang, et al. Long-term exposure to ambient fine particulate matter and chronic kidney disease: a cohort study. *Environmental Health Perspectives*, 126(10): 107002, 2018.

[145] Ya-Ru Yang, Yung-Ming Chen, Szu-Ying Chen, and Chang-Chuan Chan. Associations between long-term particulate matter exposure and adult renal function in the Taipei metropolis. *Environmental Health Perspectives*, 125(4): 602–607, 2017.

[146] Szu-Ying Chen, Da-Chen Chu, Jui-Huan Lee, Ya-Ru Yang, and Chang-Chuan Chan. Traffic-related air pollution associated with chronic kidney disease among elderly residents in Taipei City. *Environmental Pollution*, 234:838–845, 2018.

[147] Yining Zhang, Qiujuan Li, Mengxiong Fang, Yanmin Ma, Na Liu, Xiaomei Yan, Jie Zhou, and Fasheng Li. The kidney injury induced by short-term $PM_{2.5}$ exposure and the prophylactic treatment of essential oils in BALB/c mice. *Oxidative Medicine and Cellular Longevity*, 2018, 2018.

[148] OG Aztatzi-Aguilar, M Uribe-Ramírez, J Narváez-Morales, A De Vizcaya-Ruiz, and O Barbier. Early kidney damage induced by subchronic exposure to $PM_{2.5}$ in rats. *Particle and Fibre Toxicology*, 13:1–20, 2016.

[149] Xi Lu, Zhengmeng Ye, Shuo Zheng, Hongmei Ren, Jing Zeng, Xinquan Wang, Pedro A Jose, Ken Chen, and Chunyu Zeng. Long-term exposure of fine particulate matter causes hypertension by impaired renal D1 receptor-mediated sodium excretion via upregulation of G-protein-coupled receptor kinase type 4 expression in sprague-dawley rats. *Journal of the American Heart Association*, 7 (1):e007185, 2018.

[150] Zhengmeng Ye, Xi Lu, Yi Deng, Xinquan Wang, Shuo Zheng, Hongmei Ren, Miao Zhang, Tingting Chen, Pedro A Jose, Jian Yang, et al. In utero exposure to fine particulate matter causes hypertension due to impaired renal dopamine

D1 receptor in offspring. *Cellular Physiology and Biochemistry*, 46(1):148–159, 2018.

[151] Badreldin H Ali, Mohammed Al Za'abi, Asem Shalaby, Priyadarsini Manoj, Mostafa I Waly, Javed Yasin, Mohamed Fahim, and Abderrahim Nemmar. The effect of thymoquinone treatment on the combined renal and pulmonary toxicity of cisplatin and diesel exhaust particles. *Experimental Biology and Medicine*, 240 (12):1698–1707, 2015.

[152] Abderrahim Nemmar, Suhail Al-Salam, Shaheen Zia, Javed Yasin, Isehaq Al Husseni, and Badreldin H Ali. Diesel exhaust particles in the lung aggravate experimental acute renal failure. *Toxicological Sciences*, 113(1):267–277, 2010.

[153] Abderrahim Nemmar, Sumaya Beegam, Priya Yuvaraju, Javed Yasin, Mohamed A Fahim, Elsadig E Kazzam, Ibrahim Alhaddabi, and Badreldin H Ali. Potentiation of cisplatin-induced nephrotoxicity by repeated exposure to diesel exhaust particles: An experimental study in rats. *Experimental Biology and Medicine*, 239(8):1036–1044, 2014.

[154] Abderrahim Nemmar, Turan Karaca, Sumaya Beegam, Priya Yuvaraju, Javed Yasin, Naserddine Kamel Hamadi, and Badreldin H Ali. Prolonged pulmonary exposure to diesel exhaust particles exacerbates renal oxidative stress, inflammation and DNA damage in mice with adenine-induced chronic renal failure. *Cellular Physiology and Biochemistry*, 38(5):1703–1713, 2016.

[155] Yousuf M Al Suleimani, Ahmed S Al Mahruqi, M Al Za'abi, A Shalaby, Mohammed Ashique, A Nemmar, and BH Ali. Effect of diesel exhaust particles on renal vascular responses in rats with chronic kidney disease. *Environmental Toxicology*, 32(2):541–549, 2017.

[156] Sarah Robertson, Gillian A Gray, Rodger Duffin, Steven G McLean, Catherine A Shaw, Patrick WF Hadoke, David E Newby, and Mark R Miller. Diesel exhaust particulate induces pulmonary and systemic inflammation in rats without impairing endothelial function *ex vivo* or *in vivo*. *Particle and Fibre Toxicology*, 9:1–13, 2012.

[157] Mark R Miller, Steven G McLean, Rodger Duffin, Akeem O Lawal, Jesus A Araujo, Catherine A Shaw, Nicholas L Mills, Ken Donaldson, David E Newby, and Patrick WF Hadoke. Diesel exhaust particulate increases the size and complexity of lesions in atherosclerotic mice. *Particle and Fibre Toxicology*, 10:1–12, 2013.

[158] Viroj Wiwanitkit. Glomerular pore size corresponding to albumin molecular size, an explanation for underlying structural pathology leading to albuminuria at nanolevel. *Renal Failure*, 28(1):101–101, 2006.

[159] U Börner, G Szasz, W Bablok, and EW Busch. A specific fully enzymatic method for creatinine: reference values in serum (author's transl). *Journal of Clinical Chemistry and Clinical Biochemistry*, 17(11):679–682, 1979.

[160] Yushi Bai, Akira K Suzuki, and Masaru Sagai. The cytotoxic effects of diesel exhaust particles on human pulmonary artery endothelial cells in vitro: role of active oxygen species. *Free Radical Biology and Medicine*, 30(5):555–562, 2001.

[161] Richard Fuller, Philip J Landrigan, Kalpana Balakrishnan, Glynda Bathan, Stephan Bose-O'Reilly, Michael Brauer, Jack Caravanos, Tom Chiles, Aaron

Cohen, Lilian Corra, et al. Pollution and health: a progress update. *The Lancet Planetary Health*, 6(6):e535–e547, 2022.

[162] World Health Organization. 7 million premature deaths annually linked to air pollution, 2014. `https://www.who.int/news/item/25-03-2014-7-million-premature-deaths-annually-linked-to-air-pollution"`.

[163] Dean E Schraufnagel, John R Balmes, Clayton T Cowl, Sara De Matteis, Soon-Hee Jung, Kevin Mortimer, Rogelio Perez-Padilla, Mary B Rice, Horacio Riojas-Rodriguez, Akshay Sood, et al. Air pollution and noncommunicable diseases: A review by the forum of international respiratory societies' environmental committee, part 2: Air pollution and organ systems. *Chest*, 155(2):417–426, 2019.

[164] Leen Rasking, Kenneth Vanbrabant, Hannelore Bové, Michelle Plusquin, Katrien De Vusser, Harry A Roels, and Tim S Nawrot. Adverse effects of fine particulate matter on human kidney functioning: a systematic review. *Environmental Health*, 21(1):1–24, 2022.

[165] Xin Xu, Sheng Nie, Hanying Ding, and Fan Fan Hou. Environmental pollution and kidney diseases. *Nature Reviews Nephrology*, 14(5):313–324, 2018.

[166] Jennifer B Raftis and Mark R Miller. Nanoparticle translocation and multi-organ toxicity: a particularly small problem. *Nano Today*, 26:8–12, 2019.

[167] Wolfgang G Kreyling, Manuela Semmler-Behnke, Shinji Takenaka, and Winfried Moller. Differences in the biokinetics of inhaled nano-versus micrometer-sized particles. *Accounts of Chemical Research*, 46(3):714–722, 2013.

[168] Wolfgang G Kreyling, Stephanie Hirn, Winfried Moller, Carsten Schleh, Alexander Wenk, Gulnaz Celik, Jens Lipka, Martin Schaffler, Nadine Haberl, Blair D Johnston, et al. Air–blood barrier translocation of tracheally instilled gold nanoparticles inversely depends on particle size. *ACS nano*, 8(1):222–233, 2014.

[169] Manuela Semmler-Behnke, Wolfgang G Kreyling, Jens Lipka, Stefanie Fertsch, Alexander Wenk, Shinji Takenaka, Gunter Schmid, and Wolfgang Brandau. Biodistribution of 1.4- and 18-nm gold particles in rats. *Small*, 4(12):2108–2111, 2008.

[170] Stephanie Hirn, Manuela Semmler-Behnke, Carsten Schleh, Alexander Wenk, Jens Lipka, Martin Schaffler, Shinji Takenaka, Winfried Moller, Gunter Schmid, Ulrich Simon, et al. Particle size-dependent and surface charge-dependent biodistribution of gold nanoparticles after intravenous administration. *European Journal of Pharmaceutics and Biopharmaceutics*, 77(3):407–416, 2011.

[171] Wolfgang G Kreyling, Manuela Semmler-Behnke, Jurgen Seitz, Wilfried Scymczak, Alexander Wenk, Paula Mayer, Shinji Takenaka, and Günther Oberdörster. Size dependence of the translocation of inhaled iridium and carbon nanoparticle aggregates from the lung of rats to the blood and secondary target organs. *Inhalation Toxicology*, 21(sup1):55–60, 2009.

[172] Lajos Balogh, Shraddha S Nigavekar, Bindu M Nair, Wojciech Lesniak, Chunxin Zhang, Lok Yun Sung, Muhammed ST Kariapper, Areej El-Jawahri, Mikel Llanes, Brian Bolton, et al. Significant effect of size on the *in vivo* biodistribution

of gold composite nanodevices in mouse tumor models. *Nanomedicine: Nanotechnology, Biology and Medicine*, 3(4):281–296, 2007.

[173] Ghazal Bashiri, Marshall S Padilla, Kelsey L Swingle, Sarah J Shepherd, Michael J Mitchell, and Karin Wang. Nanoparticle protein corona: from structure and function to therapeutic targeting. *Lab on a Chip*, 23(6):1432–1466, 2023.

[174] Wolfgang G Kreyling, Stefanie Fertsch-Gapp, Martin Schäffler, Blair D Johnston, Nadine Haberl, Christian Pfeiffer, Jörg Diendorf, Carsten Schleh, Stephanie Hirn, Manuela Semmler-Behnke, et al. In vitro and in vivo interactions of selected nanoparticles with rodent serum proteins and their consequences in biokinetics. *Beilstein Journal of Nanotechnology*, 5(1):1699–1711, 2014.

[175] Mark R Miller, Jennifer B Raftis, Jeremy P Langrish, Steven G McLean, Pawitrabhorn Samutrtai, Shea P Connell, Simon Wilson, Alex T Vesey, Paul HB Fokkens, A John F Boere, et al. Correction to "inhaled nanoparticles accumulate at sites of vascular disease". *ACS nano*, 11(10):10623–10624, 2017.

[176] Wolfgang G Kreyling, Winfried Moller, Uwe Holzwarth, Stephanie Hirn, Alexander Wenk, Carsten Schleh, Martin Schaffler, Nadine Haberl, Neil Gibson, and Johannes C Schittny. Age-dependent rat lung deposition patterns of inhaled 20 nanometer gold nanoparticles and their quantitative biokinetics in adult rats. *ACS nano*, 12(8):7771–7790, 2018.

[177] Akiko Furuyama, Sanae Kanno, Takahiro Kobayashi, and Seishiro Hirano. Extrapulmonary translocation of intratracheally instilled fine and ultrafine particles via direct and alveolar macrophage-associated routes. *Archives of Toxicology*, 83:429–437, 2009.

[178] Manuela Semmler, J Seitz, F Erbe, P Mayer, J Heyder, G Oberdörster, and WG Kreyling. Long-term clearance kinetics of inhaled ultrafine insoluble iridium particles from the rat lung, including transient translocation into secondary organs. *Inhalation Toxicology*, 16(6-7):453–459, 2004.

[179] Gustaf Grande, Catarina Rippe, Anna Rippe, Awahan Rahman, Karl Sward, and Bengt Rippe. Unaltered size selectivity of the glomerular filtration barrier in caveolin-1 knockout mice. *American Journal of Physiology-Renal Physiology*, 297(2):F257–F262, 2009.

[180] Marie Jeansson et al. Glomerular size and charge selectivity in the mouse after exposure to glucosaminoglycan-degrading enzymes. *Journal of the American Society of Nephrology*, 14(7):1756–1765, 2003.

[181] Elena Gagliardini, Sara Conti, Ariela Benigni, Giuseppe Remuzzi, and Andrea Remuzzi. Imaging of the porous ultrastructure of the glomerular epithelial filtration slit. *Journal of the American Society of Nephrology*, 21(12):2081–2089, 2010.

[182] Christophorus F Adhipandito, Siu-Hung Cheung, Yu-Han Lin, and Si-Han Wu. Atypical renal clearance of nanoparticles larger than the kidney filtration threshold. *International Journal of Molecular Sciences*, 22(20):11182, 2021.

[183] Chung Hang J Choi, Jonathan E Zuckerman, Paul Webster, and Mark E Davis. Targeting kidney mesangium by nanoparticles of defined size. *Proceedings of the National Academy of Sciences*, 108(16):6656–6661, 2011.

[184] Graham Patrick and Christine Stirling. Transport of particles of colloidal gold within and from rat lung after local deposition by alveolar microinjection. *Environmental Health Perspectives*, 97:47–51, 1992.

[185] Håkan Törnqvist, Nicholas L Mills, Manuel Gonzalez, Mark R Miller, Simon D Robinson, Ian L Megson, William MacNee, Ken Donaldson, Stefan Söderberg, David E Newby, et al. Persistent endothelial dysfunction in humans after diesel exhaust inhalation. *American Journal of Respiratory and Critical Care Medicine*, 176(4):395–400, 2007.

[186] RJ Gryglewski, RMJ Palmer, and S Moncada. Superoxide anion is involved in the breakdown of endothelium-derived vascular relaxing factor. *Nature*, 320(6061): 454–456, 1986.

[187] Christian S Hansen, Majid Sheykhzade, Peter Møller, Janne Kjærgaard Folkmann, Ole Amtorp, Thomas Jonassen, and Steffen Loft. Diesel exhaust particles induce endothelial dysfunction in ApoE$^{-/-}$ mice. *Toxicology and Applied Pharmacology*, 219(1):24–32, 2007.

[188] Abderrahim Nemmar, Marc F Hoylaerts, Peter HM Hoet, and Benoit Nemery. Possible mechanisms of the cardiovascular effects of inhaled particles: systemic translocation and prothrombotic effects. *Toxicology Letters*, 149(1-3):243–253, 2004.

[189] Abderrahim Nemmar, Sultan Al-Maskari, Badreldin H Ali, and Issa S Al-Amri. Cardiovascular and lung inflammatory effects induced by systemically administered diesel exhaust particles in rats. *American Journal of Physiology-Lung Cellular and Molecular Physiology*, 292(3):L664–L670, 2007.

[190] Pramila Singh, David M DeMarini, Colin AJ Dick, Dennis G Tabor, Jeff V Ryan, William P Linak, Takahiro Kobayashi, and M Ian Gilmour. Sample characterization of automobile and forklift diesel exhaust particles and comparative pulmonary toxicity in mice. *Environmental Health Perspectives*, 112 (8):820–825, 2004.

[191] Abderrahim Nemmar, Suhail Al-Salam, Subramanian Dhanasekaran, Manjusha Sudhadevi, and Badreldin H Ali. Pulmonary exposure to diesel exhaust particles promotes cerebral microvessel thrombosis: protective effect of a cysteine prodrug l-2-oxothiazolidine-4-carboxylic acid. *Toxicology*, 263(2-3):84–92, 2009.

[192] Pascal Detampel, Anutosh Ganguly, Sara Tehranian, Francis Green, Santiswarup Singha, Pere Santamaria, Ayodeji A Jeje, Clifford S Cho, Björn Petri, and Matthias W Amrein. In vivo clearance of nanoparticles by transcytosis across alveolar epithelial cells. *PLoS One*, 14(9):e0223339, 2019.

[193] Christian A Ruge, Julian Kirch, Olga Cañadas, Marc Schneider, Jesus Perez-Gil, Ulrich F Schaefer, Cristina Casals, and Claus-Michael Lehr. Uptake of nanoparticles by alveolar macrophages is triggered by surfactant protein A. *Nanomedicine: Nanotechnology, Biology and Medicine*, 7(6):690–693, 2011.

[194] Jessica Hoppstädter, Michelle Seif, Anna Dembek, Christian Cavelius, Hanno Huwer, Annette Kraegeloh, and Alexandra K Kiemer. M2 polarization enhances silica nanoparticle uptake by macrophages. *Frontiers in Pharmacology*, 6:129823, 2015.

[195] Abderrahim Nemmar, Shaheen Zia, Deepa Subramaniyan, Mohamed A Fahim, and Badreldin H Ali. Exacerbation of thrombotic events by diesel exhaust particle in mouse model of hypertension. *Toxicology*, 285(1-2):39–45, 2011.

[196] Yuanting Xie, Shimin Tao, Bin Pan, Wenhui Yang, Wenpu Shao, Xinyi Fang, Dongyang Han, Jingyu Li, Yubin Zhang, Renjie Chen, et al. Cholinergic anti-inflammatory pathway mediates diesel exhaust $PM_{2.5}$-induced pulmonary and systemic inflammation. *Journal of Hazardous Materials*, 458:131951, 2023.

[197] Swapna Upadhyay, Koustav Ganguly, Tobias Stoeger, Manuela Semmler-Bhenke, Shinji Takenaka, Wolfgang G Kreyling, Mike Pitz, Peter Reitmeir, Annette Peters, Oliver Eickelberg, et al. Cardiovascular and inflammatory effects of intratracheally instilled ambient dust from Augsburg, Germany, in spontaneously hypertensive rats (SHRs). *Particle and Fibre Toxicology*, 7:1–20, 2010.

[198] Takaharu Ichimura, Joseph V Bonventre, Véronique Bailly, Henry Wei, Catherine A Hession, Richard L Cate, and Michele Sanicola. Kidney injury molecule-1 (KIM-1), a putative epithelial cell adhesion molecule containing a novel immunoglobulin domain, is up-regulated in renal cells after injury. *Journal of Biological Chemistry*, 273(7):4135–4142, 1998.

[199] Benjamin D Humphreys, Fengfeng Xu, Venkata Sabbisetti, Ivica Grgic, Said Movahedi Naini, Ningning Wang, Guochun Chen, Sheng Xiao, Dhruti Patel, Joel M Henderson, et al. Chronic epithelial kidney injury molecule-1 expression causes murine kidney fibrosis. *The Journal of Clinical Investigation*, 123(9):4023–4035, 2013.

[200] Li Yang, Craig R Brooks, Sheng Xiao, Venkata Sabbisetti, Melissa Y Yeung, Li-Li Hsiao, Takaharu Ichimura, Vijay Kuchroo, Joseph V Bonventre, et al. KIM-1-mediated phagocytosis reduces acute injury to the kidney. *The Journal of Clinical Investigation*, 125(4):1620–1636, 2015.

[201] Véronique Bailly, Zhiwei Zhang, Werner Meier, Richard Cate, Michele Sanicola, and Joseph V Bonventre. Shedding of kidney injury molecule-1, a putative adhesion protein involved in renal regeneration. *Journal of Biological Chemistry*, 277(42):39739–39748, 2002.

[202] Yuanyuan Zhang, Aiju Li, Jiliang Wen, Junhui Zhen, Qiufa Hao, Yidan Zhang, Zhao Hu, and Xiaoyan Xiao. Kidney injury molecule-1 level is associated with the severity of renal interstitial injury and prognosis in adult henoch–schönlein purpura nephritis. *Archives of Medical Research*, 48(5):449–458, 2017.

[203] Won K Han, Veronique Bailly, Rekha Abichandani, Ravi Thadhani, and Joseph V Bonventre. Kidney injury molecule-1 (KIM-1): a novel biomarker for human renal proximal tubule injury. *Kidney International*, 62(1):237–244, 2002.

[204] Prasad Devarajan. Emerging urinary biomarkers in the diagnosis of acute kidney injury. *Expert Opinion on Medical Diagnostics*, 2(4):387–398, 2008.

[205] Kianoush Kashani, Wisit Cheungpasitporn, and Claudio Ronco. Biomarkers of acute kidney injury: the pathway from discovery to clinical adoption. *Clinical Chemistry and Laboratory Medicine (CCLM)*, 55(8):1074–1089, 2017.

[206] Venkata S Sabbisetti, Sushrut S Waikar, Daniel J Antoine, Adam Smiles, Chang Wang, Abinaya Ravisankar, Kazumi Ito, Sahil Sharma, Swetha Ramadesikan,

Michelle Lee, et al. Blood kidney injury molecule-1 is a biomarker of acute and chronic kidney injury and predicts progression to ESRD in type I diabetes. *Journal of the American Society of Nephrology*, 25(10):2177–2186, 2014.

[207] Takaharu Ichimura, Cheng Chieh Hung, Soon Ae Yang, James L Stevens, and Joseph V Bonventre. Kidney injury molecule-1: a tissue and urinary biomarker for nephrotoxicant-induced renal injury. *American Journal of Physiology-Renal Physiology*, 286(3):F552–F563, 2004.

[208] Sunyoung Jeong, Jong-Hwa Lee, Jung-Heun Ha, Jinhee Kim, Inyong Kim, and Sungryong Bae. An exploratory study of the relationships between diesel engine exhaust particle inhalation, pulmonary inflammation and anxious behavior. *International Journal of Environmental Research and Public Health*, 18(3):1166, 2021.

[209] Abderrahim Nemmar, Deepa Subramaniyan, and Badreldin H Ali. Protective effect of curcumin on pulmonary and cardiovascular effects induced by repeated exposure to diesel exhaust particles in mice. *PLoS One*, 7(6):e39554, 2012.

[210] Dong Im Kim, Mi-Kyung Song, Seon-Hee Kim, Chan Young Park, and Kyuhong Lee. TF-343 alleviates diesel exhaust particulate-induced lung inflammation via modulation of nuclear factor-κb signaling. *Journal of Immunology Research*, 2019 (1):8315845, 2019.

[211] Sharen Provoost, Tania Maes, Monique AM Willart, Guy F Joos, Bart N Lambrecht, and Kurt G Tournoy. Diesel exhaust particles stimulate adaptive immunity by acting on pulmonary dendritic cells. *The Journal of Immunology*, 184(1):426–432, 2010.

[212] Dong Im Kim, Mi-Kyung Song, Ji Eun Yuk, Hyeon Jin Seo, and Kyuhong Lee. Establishment of an artificial particulate matter-induced lung disease model through analyzing pathological changes and transcriptomic profiles in mice. *Scientific Reports*, 13(1):5955, 2023.

[213] Jinzhuo Zhao, Yuquan Xie, Xiaolin Qian, Rongfang Jiang, and Weimin Song. Acute effects of fine particles on cardiovascular system: differences between the spontaneously hypertensive rats and wistar kyoto rats. *Toxicology Letters*, 193 (1):50–60, 2010.

[214] C Arden Pope III, Aruni Bhatnagar, James P McCracken, Wesley Abplanalp, Daniel J Conklin, and Timothy O'Toole. Exposure to fine particulate air pollution is associated with endothelial injury and systemic inflammation. *Circulation Research*, 119(11):1204–1214, 2016.

[215] Xiaoliu Huang, Zhitong Zhou, Xinwen Liu, Jue Li, and Lijuan Zhang. $PM_{2.5}$ exposure induced renal injury via the activation of the autophagic pathway in the rat and HK-2 cell. *Environmental Sciences Europe*, 32:1–13, 2020.

[216] Adrian Gericke, Andreas Steege, Caroline Manicam, Tobias Böhmer, Jürgen Wess, and Norbert Pfeiffer. Role of the M3 muscarinic acetylcholine receptor subtype in murine ophthalmic arteries after endothelial removal. *Investigative Ophthalmology & Visual Science*, 55(1):625–631, 2014.

[217] Yingzi Zhao, Paul M Vanhoutte, and Susan WS Leung. Vascular nitric oxide: Beyond eNOS. *Journal of Pharmacological Sciences*, 129(2):83–94, 2015.

[218] Panot Tangsucharit, Shingo Takatori, Yoshito Zamami, Mitsuhiro Goda, Poungrat Pakdeechote, Hiromu Kawasaki, and Fusako Takayama. Muscarinic acetylcholine receptor M1 and M3 subtypes mediate acetylcholine-induced endothelium-independent vasodilatation in rat mesenteric arteries. *Journal of Pharmacological Sciences*, 130(1):24–32, 2016.

[219] Ziqiang Wu, Huan Yao, Huan Xu, Yang Wang, Wangming Hu, Guanhua Lou, Lingling Zhang, Cong Huang, Cen Jiang, Shiyi Zhou, et al. Inhibition of eNOS by L-NAME resulting in rat hind limb developmental defects through PFKFB3 mediated angiogenetic pathway. *Scientific Reports*, 10(1):16754, 2020.

[220] Shaojia Wang, Jie Xie, Jiajia Li, Fei Liu, Xiaohua Wu, and Ziliang Wang. Cisplatin suppresses the growth and proliferation of breast and cervical cancer cell lines by inhibiting integrin β5-mediated glycolysis. *American Journal of Cancer Research*, 6(5):1108, 2016.

[221] Lawrence H Einhorn and John Donohue. Cis-diamminedichloroplatinum, vinblastine, and bleomycin combination chemotherapy in disseminated testicular cancer. *Annals of Internal Medicine*, 87(3):293–298, 1977.

[222] Matthew D Galsky, Siamak Daneshmand, Sudeh Izadmehr, Edgar Gonzalez-Kozlova, Kevin G Chan, Sara Lewis, Bassam El Achkar, Tanya B Dorff, Jeremy Paul Cetnar, Brock O Neil, et al. Gemcitabine and cisplatin plus nivolumab as organ-sparing treatment for muscle-invasive bladder cancer: a phase 2 trial. *Nature Medicine*, 29(11):2825–2834, 2023.

[223] SA Hussain, DH Palmer, B Lloyd, SI Collins, Darren Barton, J Ansari, and Nicholas D James. A study of split-dose cisplatin-based neo-adjuvant chemotherapy in muscle-invasive bladder cancer. *Oncology Letters*, 3(4):855–859, 2012.

[224] Kristen Renee McSweeney, Laura Kate Gadanec, Tawar Qaradakhi, Benazir Ashiana Ali, Anthony Zulli, and Vasso Apostolopoulos. Mechanisms of cisplatin-induced acute kidney injury: pathological mechanisms, pharmacological interventions, and genetic mitigations. *Cancers*, 13(7):1572, 2021.

[225] Xin Yao, Kessarin Panichpisal, Neil Kurtzman, and Kenneth Nugent. Cisplatin nephrotoxicity: a review. *The American Journal of the Medical Sciences*, 334(2): 115–124, 2007.

[226] Gi-Su Oh, Hyung-Jin Kim, AiHua Shen, Su Bin Lee, Dipendra Khadka, Arpana Pandit, and Hong-Seob So. Cisplatin-induced kidney dysfunction and perspectives on improving treatment strategies. *Electrolytes & Blood Pressure: E & BP*, 12(2):55, 2014.

[227] Qiao Yang, Songya Su, Nan Luo, and Gang Cao. Adenine-induced animal model of chronic kidney disease: current applications and future perspectives. *Renal Failure*, 46(1):2336128, 2024.

[228] Ting Jia, Hannes Olauson, Karolina Lindberg, Risul Amin, Karin Edvardsson, Bengt Lindholm, Göran Andersson, Annika Wernerson, Yves Sabbagh, Susan Schiavi, et al. A novel model of adenine-induced tubulointerstitial nephropathy in mice. *BMC Nephrology*, 14:1–8, 2013.

[229] Badreldin H Ali, Suhail Al-Salam, Mohammed Al Za'abi, Mostafa I Waly, Aishwarya Ramkumar, Sumyia Beegam, Intisar Al-Lawati, Sirin A Adham, and Abderrahim Nemmar. New model for adenine-induced chronic renal failure in mice, and the effect of gum acacia treatment thereon: comparison with rats. *Journal of Pharmacological and Toxicological Methods*, 68(3):384–393, 2013.

[230] Takako Yokozawa, Hikokichi Oura, and Toshio Okada. Metabolic effects of dietary purine in rats. *Journal of Nutritional Science and Vitaminology*, 28(5): 519–526, 1982.

[231] Takako Yokozawa, Ping Dong Zheng, Hikokichi Oura, and Fumitomo Koizumi. Animal model of adenine-induced chronic renal failure in rats. *Nephron*, 44(3): 230–234, 1986.

[232] James B Wyngaarden and John T Dunn. 8-hydroxyadenine as the intermediate in the oxidation of adenine to 2, 8-dihydroxyadenine by xanthine oxidase. *Archives of Biochemistry and Biophysics*, 70(1):150–156, 1957.

[233] Barbara Mara Klinkhammer, Sonja Djudjaj, Uta Kunter, Runolfur Palsson, Vidar Orn Edvardsson, Thorsten Wiech, Margret Thorsteinsdottir, Sverrir Hardarson, Orestes Foresto-Neto, Shrikant R Mulay, et al. Cellular and molecular mechanisms of kidney injury in 2, 8-dihydroxyadenine nephropathy. *Journal of the American Society of Nephrology*, 31(4):799–816, 2020.

[234] Badreldin H Ali, Isehaq Al-Husseni, Sumyia Beegam, Ahmed Al-Shukaili, Abderrahim Nemmar, Simone Schierling, Nina Queisser, and Nicole Schupp. Effect of gum arabic on oxidative stress and inflammation in adenine–induced chronic renal failure in rats. *PloS One*, 8(2):e55242, 2013.

[235] Vishal Diwan, Lindsay Brown, and Glenda C Gobe. Adenine-induced chronic kidney disease in rats. *Nephrology*, 23(1):5–11, 2018.

[236] Vishal Diwan, David Small, Kate Kauter, Glenda C Gobe, and Lindsay Brown. Gender differences in adenine-induced chronic kidney disease and cardiovascular complications in rats. *American Journal of Physiology-Renal Physiology*, 307(11): F1169–F1178, 2014.

[237] Vishal Diwan, Anand Mistry, Glenda Gobe, and Lindsay Brown. Adenine-induced chronic kidney and cardiovascular damage in rats. *Journal of Pharmacological and Toxicological Methods*, 68(2):197–207, 2013.

[238] Zilong Zhang, Bin Dong, Shanshan Li, Gongbo Chen, Zhaogeng Yang, Yanhui Dong, Zhenghe Wang, Jun Ma, and Yuming Guo. Exposure to ambient particulate matter air pollution, blood pressure and hypertension in children and adolescents: a national cross-sectional study in China. *Environment International*, 128:103–108, 2019.

[239] Licheng Zhang, Ji An, Xue Tian, Mengyang Liu, Lixin Tao, Xiangtong Liu, Xiaonan Wang, Deqiang Zheng, Xiuhua Guo, and Yanxia Luo. Acute effects of ambient particulate matter on blood pressure in office workers. *Environmental Research*, 186:109497, 2020.

[240] J Timothy Dvonch, Srimathi Kannan, Amy J Schulz, Gerald J Keeler, Graciela Mentz, James House, Alison Benjamin, Paul Max, Robert L Bard, and Robert D

Brook. Acute effects of ambient particulate matter on blood pressure: differential effects across urban communities. *Hypertension*, 53(5):853–859, 2009.

[241] Kristen E Cosselman, Ranjini M. Krishnan, Assaf P Oron, Karen Jansen, Alon Peretz, Jeffrey H Sullivan, Timothy V Larson, and Joel D Kaufman. Blood pressure response to controlled diesel exhaust exposure in human subjects. *Hypertension*, 59(5):943–948, 2012.

[242] Léa Guyonnet, Alicja Czopek, Tariq E Farrah, Véronique Baudrie, Philippe Bonnin, Anna Chipont, Olivia Lenoir, Florian Sennlaub, Christophe Roubeix, David J Webb, et al. Deletion of the myeloid endothelin-B receptor confers long-term protection from angiotensin II-mediated kidney, eye and vessel injury. *Kidney International*, 98(5):1193–1209, 2020.

[243] Mark R Miller, Steven G McLean, Rodger Duffin, Catherine A Shaw, Nicholas L Mills, Kenneth Donaldson, David E Newby, and Patrick W Hadoke. Diesel exhaust particles promote atherosclerosis in apolipoprotein E-deficient mice. *Arteriosclerosis, Thrombosis, and Vascular Biology*, 30(11):E292–E293, 2010.

[244] Xie Jun, Geng Jin, Chen Fu, Zhao Jinxuan, Li Xueling, Hu Jiaxin, Qiao Shuaihua, Shan Anqi, Chen Jianzhou, Zhou Lian, et al. $PM_{2.5}$ promotes abdominal aortic aneurysm formation in angiotensin II-infused $ApoE^{-/-}$mice. *Biomedicine & Pharmacotherapy*, 104:550–557, 2018.

[245] Yang Ming, Xiaonan Zhou, Gang Liu, Mieradilijiang Abudupataer, Shichao Zhu, Bitao Xiang, Xiujie Yin, Hao Lai, Yongxin Sun, Chunsheng Wang, et al. $PM_{2.5}$ exposure exacerbates mice thoracic aortic aneurysm and dissection by inducing smooth muscle cell apoptosis via the MAPK pathway. *Chemosphere*, 313:137500, 2023.

[246] Jia Deng, Dao-xin Wang, Wang Deng, Chang-yi Li, Jin Tong, and Hilary Ma. Regulation of alveolar fluid clearance and ENaC expression in lung by exogenous angiotensin II. *Respiratory Physiology & Neurobiology*, 181(1):53–61, 2012.

[247] Yumiko Imai, Keiji Kuba, Shuan Rao, Yi Huan, Feng Guo, Bin Guan, Peng Yang, Renu Sarao, Teiji Wada, Howard Leong-Poi, et al. Angiotensin-converting enzyme 2 protects from severe acute lung failure. *Nature*, 436(7047):112–116, 2005.

[248] Philip Wenzel. Monocytes as immune targets in arterial hypertension. *British Journal of Pharmacology*, 176(12):1966–1977, 2019.

[249] Seungbum Kim, Michael Zingler, Jeffrey K Harrison, Edward W Scott, Christopher R Cogle, Defang Luo, and Mohan K Raizada. Angiotensin II regulation of proliferation, differentiation, and engraftment of hematopoietic stem cells. *Hypertension*, 67(3):574–584, 2016.

[250] Li-Jun Ma, Bridgette A Corsa, Jun Zhou, HaiChun Yang, HaiJing Li, Yi-Wei Tang, Vladimir R Babaev, Amy S Major, MacRae F Linton, Sergio Fazio, et al. Angiotensin type 1 receptor modulates macrophage polarization and renal injury in obesity. *American Journal of Physiology-Renal Physiology*, 300(5):F1203–F1213, 2011.

[251] Yvonne Dörffel, Christoph Lätsch, Bruno Stuhlmüller, Stefan Schreiber, Susann Scholze, Gerd R Burmester, and Jürgen Scholze. Preactivated peripheral blood

monocytes in patients with essential hypertension. *Hypertension*, 34(1):113–117, 1999.

[252] Ettore Porreca, Concetta Di Febbo, Gabriella Mincione, Marcella Reale, Giovanna Baccante, Maria Domenica Guglielmi, Franco Cuccurullo, and Giulia Colletta. Increased transforming growth factor-β production and gene expression by peripheral blood monocytes of hypertensive patients. *Hypertension*, 30(1): 134–139, 1997.

[253] Tang-Dong Liao, Xiao-Ping Yang, Yun-He Liu, Edward G Shesely, Maria A Cavasin, William A Kuziel, Patrick J Pagano, and Oscar A Carretero. Role of inflammation in the development of renal damage and dysfunction in angiotensin II–induced hypertension. *Hypertension*, 52(2):256–263, 2008.

[254] Yuri Ozawa, Hiroyuki Kobori, Yuki Suzaki, and L Gabriel Navar. Sustained renal interstitial macrophage infiltration following chronic angiotensin II infusions. *American Journal of Physiology-Renal Physiology*, 292(1):F330–F339, 2007.

[255] Carolina De Ciuceis, Farhad Amiri, Pascal Brassard, Dierk H Endemann, Rhian M Touyz, and Ernesto L Schiffrin. Reduced vascular remodeling, endothelial dysfunction, and oxidative stress in resistance arteries of angiotensin II-infused macrophage colony-stimulating factor-deficient mice: evidence for a role in inflammation in angiotensin II-induced vascular injury. *Arteriosclerosis, Thrombosis, and Vascular Biology*, 25(10):2106–2113, 2005.

[256] Bibek Poudel, Corbin A Shields, Andrea K Brown, Ubong Ekperikpe, Tyler Johnson, Denise C Cornelius, and Jan M Williams. Depletion of macrophages slows the early progression of renal injury in obese Dahl salt-sensitive leptin receptor mutant rats. *American Journal of Physiology-Renal Physiology*, 318(6): F1489–F1499, 2020.

[257] Tsubasa Mizokami, Michiko Shimada, and Katsuhiko Suzuki. Macrophage depletion attenuates acute renal damage after exhaustive exercise in mice. *International Journal of Sports Medicine*, 43(11):964–970, 2022.

[258] Xin Zhou, Ling Zhang, Wen-Jie Ji, Fei Yuan, Zhao-Zeng Guo, Bo Pang, Tao Luo, Xing Liu, Wen-Cheng Zhang, Tie-Min Jiang, et al. Variation in dietary salt intake induces coordinated dynamics of monocyte subsets and monocyte-platelet aggregates in humans: implications in end organ inflammation. *PloS One*, 8(4): e60332, 2013.

[259] Wu-Chang Zhang, Xiao-Jun Zheng, Lin-Juan Du, Jian-Yong Sun, Zhu-Xia Shen, Chaoji Shi, Shuyang Sun, Zhiyuan Zhang, Xiao-qing Chen, Mu Qin, et al. High salt primes a specific activation state of macrophages, M(Na). *Cell Research*, 25 (8):893–910, 2015.

[260] Rinaldo Bellomo, Lui G Forni, Laurence W Busse, Michael T McCurdy, Kealy R Ham, David W Boldt, Johanna Hästbacka, Ashish K Khanna, Timothy E Albertson, James Tumlin, et al. Renin and survival in patients given angiotensin II for catecholamine-resistant vasodilatory shock. A clinical trial. *American Journal of Respiratory and Critical Care Medicine*, 202(9):1253–1261, 2020.

[261] Fernando Augusto Malavazzi Casare, Karina Thieme, Juliana Martins Costa-Pessoa, Luciana Venturini Rossoni, Gisele Kruger Couto, Fernanda Barrinha

Fernandes, Dulce Elena Casarini, and Maria Oliveira-Souza. Renovascular remodeling and renal injury after extended angiotensin II infusion. *American Journal of Physiology-Renal Physiology*, 310(11):F1295–F1307, 2016.

[262] Leonardo A Sechi, Chandi A Griffin, Gilberta Giacchetti, Jean-Pierre Valentin, Catherine Llorens-Cortes, Pierre Corvol, and Morris Schambelan. Tissue-specific regulation of type 1 angiotensin II receptor mRNA levels in the rat. *Hypertension*, 28(3):403–408, 1996.

[263] Lisa M Harrison-Bernard, Samir S El-Dahr, Denise F O'Leary, and L Gabriel Navar. Regulation of angiotensin II type 1 receptor mRNA and protein in angiotensin II-induced hypertension. *Hypertension*, 33(1):340–346, 1999.

[264] Akihiro Tojo, Masumi Kimoto, and Christopher S Wilcox. Renal expression of constitutive NOS and DDAH: Separate effects of salt intake and angiotensin. *Kidney International*, 58(5):2075–2083, 2000.

[265] Steven D Crowley, Young-Soo Song, Eugene E Lin, Robert Griffiths, Hyung-Suk Kim, and Phillip Ruiz. Lymphocyte responses exacerbate angiotensin II-dependent hypertension. *American Journal of Physiology-Regulatory, Integrative and Comparative Physiology*, 298(4):R1089–R1097, 2010.

[266] Markus P Schneider, Jennifer C Sullivan, Paul F Wach, Erika I Boesen, Tatsuo Yamamoto, Tohru Fukai, David G Harrison, David M Pollock, and Jennifer S Pollock. Protective role of extracellular superoxide dismutase in renal ischemia/reperfusion injury. *Kidney International*, 78(4):374–381, 2010.

[267] Haipeng Guo, Dachun Xu, Marcos Kuroki, Zhongbing Lu, Xin Xu, Aron Geurts, John W Osborn, and Yingjie Chen. Kidney failure, arterial hypertension and left ventricular hypertrophy in rats with loss of function mutation of SOD3. *Free Radical Biology and Medicine*, 152:787–796, 2020.

[268] Qiulun Lu, Zejun Ma, YE Ding, Tatiana Bedarida, Liming Chen, Zhonglin Xie, Ping Song, and Ming-Hui Zou. Circulating miR-103a-3p contributes to angiotensin II-induced renal inflammation and fibrosis via a SNRK/NF-κB/p65 regulatory axis. *Nature communications*, 10(1):2145, 2019.

[269] Jianmin Chen, Mingguang Tan, Abderrahim Nemmar, Weiming Song, Mo Dong, Guilin Zhang, and Yan Li. Quantification of extrapulmonary translocation of intratracheal-instilled particles in vivo in rats: Effect of lipopolysaccharide. *Toxicology*, 222(3):195–201, 2006.

[270] Nicholas L Mills, Nadia Amin, Simon D Robinson, Atul Anand, John Davies, Dilip Patel, Jesus M de la Fuente, Flemming R Cassee, Nicholas A Boon, William MacNee, et al. Do inhaled carbon nanoparticles translocate directly into the circulation in humans? *American Journal of Respiratory and Critical Care Medicine*, 173(4):426–431, 2006.

[271] Mengxiao Yu, Jiancheng Zhou, Bujie Du, Xuhui Ning, Craig Authement, Leah Gandee, Payal Kapur, Jer-Tsong Hsieh, and Jie Zheng. Noninvasive staging of kidney dysfunction enabled by renal-clearable luminescent gold nanoparticles. *Angewandte Chemie*, 128(8):2837–2841, 2016.

[272] Xiang-Yang Zhu, Xiangyu Zou, Rahul Mukherjee, Zhicong Yu, Christopher M Ferguson, Wei Zhou, Cynthia H McCollough, and Lilach O Lerman. Targeted

imaging of renal fibrosis using antibody-conjugated gold nanoparticles in renal artery stenosis. *Investigative Radiology*, 53(10):623–628, 2018.

[273] Kaibi Yang, Yiwei Shang, Nan Yang, Shujun Pan, Juan Jin, and Qiang He. Application of nanoparticles in the diagnosis and treatment of chronic kidney disease. *Frontiers in Medicine*, 10:1132355, 2023.

[274] Cecilia Ka Wing Chan, Cheuk Chun Szeto, Leo Kit Cheung Lee, Yu Xiao, Bohan Yin, Xiaofan Ding, Thomas Wai Yip Lee, James Yun Wong Lau, and Chung Hang Jonathan Choi. A sub-10-nm, folic acid-conjugated gold nanoparticle as self-therapeutic treatment of tubulointerstitial fibrosis. *Proceedings of the National Academy of Sciences*, 120(42):e2305662120, 2023.

[275] Ruolin Wu, Keshan Wang, Yongkang Gai, Mengting Li, Jingjing Wang, Chenyang Wang, Yajing Zhang, Zhiwei Xiao, Dawei Jiang, Zairong Gao, et al. Nanomedicine for renal cell carcinoma: imaging, treatment and beyond. *Journal of Nanobiotechnology*, 21(1):3, 2023.

[276] Habeeb Mohammad, Huay Woon You, Smita Tukaram Kumbhar, Kiran Balasaheb Aher, Girija Balasaheb Bhavar, Hariharan Thirumalai Vengateswaran, et al. Targeted nanomedicine modulating intercellular communications to arrest renal cell carcinoma progression. *Journal of Drug Delivery Science and Technology*, page 105983, 2024.

[277] Nicholas L Mills, Håkan Törnqvist, Manuel C Gonzalez, Elen Vink, Simon D Robinson, Stefan Söderberg, Nicholas A Boon, Ken Donaldson, Thomas Sandström, Anders Blomberg, et al. Ischemic and thrombotic effects of dilute diesel-exhaust inhalation in men with coronary heart disease. *New England Journal of Medicine*, 357(11):1075–1082, 2007.

[278] Nicholas L Mills, Simon D Robinson, Paul HB Fokkens, Daan LAC Leseman, Mark R Miller, David Anderson, Evelyn J Freney, Mathew R Heal, Robert J Donovan, Anders Blomberg, et al. Exposure to concentrated ambient particles does not affect vascular function in patients with coronary heart disease. *Environmental Health Perspectives*, 116(6):709–715, 2008.

[279] Kevin T Morgan and Thomas M Monticello. Airflow, gas deposition, and lesion distribution in the nasal passages. *Environmental Health Perspectives*, 85:209–218, 1990.

[280] Heather F Lakatos, Heather A Burgess, Thomas H Thatcher, Michelle R Redonnet, Eric Hernady, Jacqueline P Williams, and Patricia J Sime. Oropharyngeal aspiration of a silica suspension produces a superior model of silicosis in the mouse when compared to intratracheal instillation. *Experimental Lung Research*, 32(5):181–199, 2006.

[281] GVS Rao, Sally Tinkle, David Weissman, James Antonini, Michael Kashon, Rebecca Salmen, Lori Battelli, Patsy Willard, Ann Hubbs, and Mark Hoover. Efficacy of a technique for exposing the mouse lung to particles aspirated from the pharynx. *Journal of Toxicology and Environmental Health, Part A*, 66(15-16): 1441–1452, 2003.

[282] W Michael Foster, Dianne M Walters, Malinda Longphre, Kristin Macri, and

Laura M Miller. Methodology for the measurement of mucociliary function in the mouse by scintigraphy. *Journal of Applied Physiology*, 90(3):1111–1118, 2001.

[283] National Institute of Standards & Technology. Certificate of Analysis-Standard Reference Material 2975-Diesel Particulate Matter (Industrial Forklift), 2000.

[284] Masaru Sagai, Hiroki Saito, Takamichi Ichinose, Masahiko Kodama, and Yoki Mori. Biological effects of diesel exhaust particles. I. In vitro production of superoxide and in vivo toxicity in mouse. *Free Radical Biology and Medicine*, 14(1):37–47, 1993.

[285] Satish Anjilvel and Bahman Asgharian. A multiple-path model of particle deposition in the rat lung. *Fundamental and Applied Toxicology*, 28(1):41–50, 1995.

[286] Carine El Hajjar, Tiphaine Rogez-Florent, Virginie Seguin, Anthony Verdin, David Garon, Ivannah Pottier, and Véronique André. Intrinsic characteristics and biological effects of standard reference indoor dust SRM® 2585 and its inhalable subfractions PM_{10} and $PM_{2.5}$. *Atmosphere*, 13(11):1818, 2022.

[287] Vikash Sinha, Luis M Vence, and Abdulla K Salahudeen. Urinary tubular protein-based biomarkers in the rodent model of cisplatin nephrotoxicity: a comparative analysis of serum creatinine, renal histology, and urinary KIM-1, NGAL, and NAG in the initiation, maintenance, and recovery phases of acute kidney injury. *Journal of Investigative Medicine*, 61(3):564–568, 2013.

[288] Josselin Nespoux, Rohit Patel, Haiyan Zhang, Winnie Huang, Brent Freeman, Paul W Sanders, Young Chul Kim, and Volker Vallon. Gene knockout of the Na^+-glucose cotransporter SGLT2 in a murine model of acute kidney injury induced by ischemia-reperfusion. *American Journal of Physiology-Renal Physiology*, 318 (5):F1100–F1112, 2020.

[289] Laale F Alawi, Sanjeev Dhakal, Sana E Emberesh, Harshal Sawant, Anhar Hosawi, Unmesha Thanekar, Nadja Grobe, and Khalid M Elased. Effects of angiotensin II type 1A receptor on ACE2, neprilysin and KIM-1 in two kidney one clip (2K1C) model of renovascular hypertension. *Frontiers in Pharmacology*, 11:602985, 2021.

[290] Chen Yang, Huidie Xu, Dong Yang, Yunhao Xie, Mingrui Xiong, Yu Fan, XiKai Liu, Yu Zhang, Yushuo Xiao, Yuchen Chen, et al. A renal YY1-KIM1-DR5 axis regulates the progression of acute kidney injury. *Nature Communications*, 14(1): 4261, 2023.

[291] Volker Vielhauer and Tanya N Mayadas. Functions of TNF and its receptors in renal disease: distinct roles in inflammatory tissue injury and immune regulation. *Seminars in Nephrology*, 27(3):286–308, 2007.

[292] Shinya Taguchi, Kengo Azushima, Takahiro Yamaji, Shingo Urate, Toru Suzuki, Eriko Abe, Shohei Tanaka, Shunichiro Tsukamoto, Daisuke Kamimura, Sho Kinguchi, et al. Effects of tumor necrosis factor-α inhibition on kidney fibrosis and inflammation in a mouse model of aristolochic acid nephropathy. *Scientific Reports*, 11(1):23587, 2021.

[293] Simona Mihai, Elena Codrici, Ionela Daniela Popescu, Ana-Maria Enciu, Elena Rusu, Diana Zilisteanu, Radu Albulescu, Gabriela Anton, and Cristiana Tanase.

Proteomic biomarkers panel: new insights in chronic kidney disease. *Disease Markers*, 2016(1):3185232, 2016.

[294] Ganesan Ramesh and W Brian Reeves. TNFR2-mediated apoptosis and necrosis in cisplatin-induced acute renal failure. *American Journal of Physiology-Renal Physiology*, 285(4):F610–F618, 2003.

[295] Marta Ruiz-Ortega, Mónica Ruperez, Oscar Lorenzo, Vanesa Esteban, Julia Blanco, Sergio Mezzano, and Jesus Egido. Angiotensin II regulates the synthesis of proinflammatory cytokines and chemokines in the kidney. *Kidney International*, 62:S12–S22, 2002.

[296] Ahmed A Elmarakby, Jeffrey E Quigley, David M Pollock, and John D Imig. Tumor necrosis factor α blockade increases renal Cyp2c23 expression and slows the progression of renal damage in salt-sensitive hypertension. *Hypertension*, 47 (3):557–562, 2006.

[297] Alaa S Awad, Hanning You, Ting Gao, Timothy K Cooper, Sergei A Nedospasov, Jean Vacher, Patrick F Wilkinson, Francis X Farrell, and W Brian Reeves. Macrophage-derived tumor necrosis factor-α mediates diabetic renal injury. *Kidney International*, 88(4):722–733, 2015.

[298] Keisuke Omote, Tomohito Gohda, Maki Murakoshi, Yu Sasaki, Saiko Kazuno, Tsutomu Fujimura, Masanori Ishizaka, Yuji Sonoda, and Yasuhiko Tomino. Role of the TNF pathway in the progression of diabetic nephropathy in KK-Ay mice. *American Journal of Physiology-Renal Physiology*, 306(11):F1335–F1347, 2014.

[299] DE Choi, JY Jeong, BJ Lim, KR Na, YT Shin, and KW Lee. Pretreatment with the tumor nerosis factor-α blocker etanercept attenuated ischemia-reperfusion renal injury. *Transplantation Proceedings*, 41(9):3590–3596, 2009.

Supplementary data

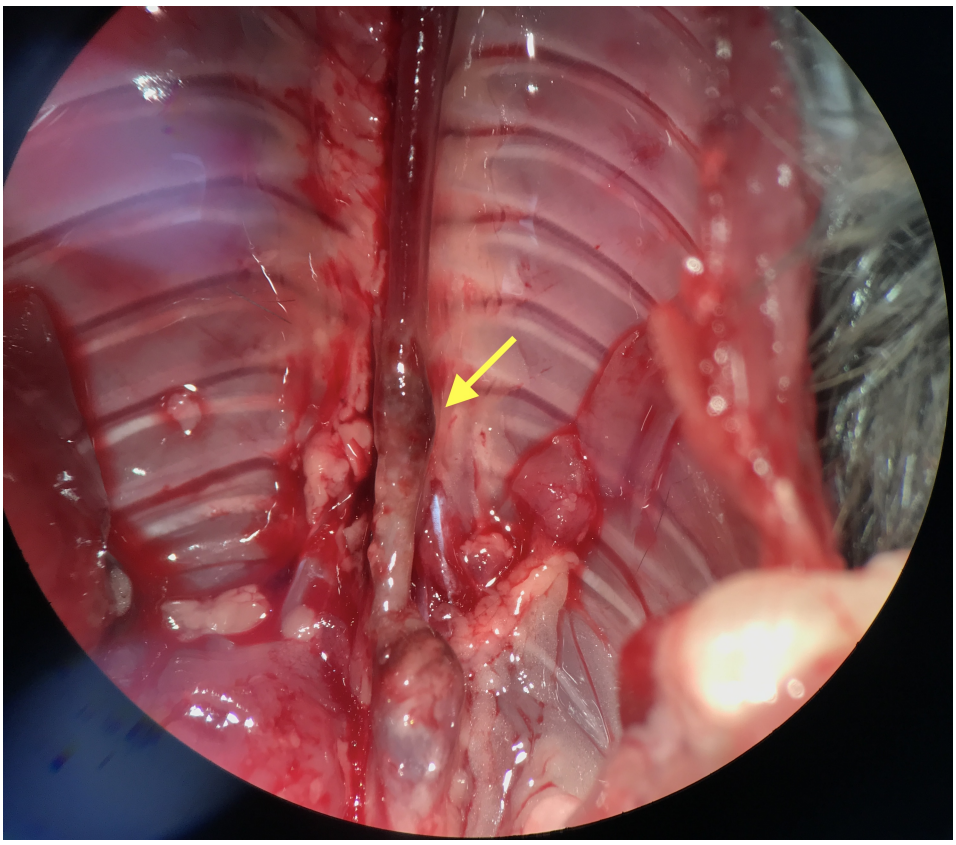

Figure S.1: Representative image of mouse arterial aneurysm following Ang II+HSD treatment. Mice were implanted with an osmotic minipump delivering exogenous Ang II (500 ng/kg/min) combined with a high-salt diet (3% Na) for 2.5 weeks (16–18 days). At tissue collection aortic aneurysms (yellow arrow) were observed in mice from both saline and DEP treatment groups.